



Universität
Basel

BIOZENTRUM

C-di-GMP acts as a cell cycle oscillator to drive chromosome replication

Inauguraldissertation

zur

Erlangung der Würde eines Doktors der Philosophie

vorgelegt der

Philosophisch-Naturwissenschaftlichen Fakultät

der Universität Basel

von

Christian Lori

aus Malans (GR), Schweiz

Basel, 2016

Originaldokument gespeichert auf dem Dokumentenserver der Universität
Basel edoc.unibas.ch

Genehmigt von der Philosophisch-Naturwissenschaftlichen Fakultät auf
Antrag von:

Prof. Dr. Urs Jenal

Prof. Dr. Christoph Dehio

Basel, den 22. März 2016

Prof. Dr. Jörg Schibler

Dekan

Christian Lori: *C-di-GMP acts as a cell cycle oscillator to drive chromosome replication*,
PhD Thesis, 2016

Abstract

Cyclic di-GMP (c-di-GMP) is an omnipresent bacterial second messenger molecule which has been recognized as a central regulator of lifestyle transitions. Generally, high levels of c-di-GMP promote a biofilm associated, surface attached lifestyle, while low levels of c-di-GMP favor a single cell, motile lifestyle. A wide range of c-di-GMP effector proteins are known which control various cellular functions. It has long been assumed that c-di-GMP is involved in the regulation of cell cycle progression. In this work the role of c-di-GMP on the G1-S transition is described in the aquatic bacterium *Caulobacter crescentus*. *C. crescentus* is an ideal model organism since G1-S transition is developmentally linked to the swarmer to stalked cell transition and therefore easily observable. Moreover, c-di-GMP influences several processes at the swarmer to stalked cell transition. Thus, disturbing the c-di-GMP-dependent processes causes specific phenotypes.

In the first part of this work, the effect of c-di-GMP on core components of the *C. crescentus* cell cycle control machinery is assessed. It is described that the essential histidine kinase CckA (Cell cycle kinase A) is regulated by c-di-GMP. Binding of CckA to c-di-GMP activates the phosphatase activity of CckA and leads to dephosphorylation of the transcription factor CtrA (Central transcriptional activator A) which ultimately initiates chromosome replication. Furthermore it is shown that c-di-GMP is required in the predivisional cell to establish a CckA-dependent CtrA phosphorylation gradient.

The second part describes the mechanism by which c-di-GMP activates CckA phosphatase activity. It was possible to isolate several mutations in CckA which specifically target certain activities of CckA and thereby give an insight into the intramolecular signaling mechanisms. Additionally, a recently solved crystal structure of CckA in complex with c-di-GMP will increase our understanding of the activation of phosphatase activity.

The third part of this work deals with the regulation of several histidine kinases by a single domain response regulator. The single domain response Regulator MrrA (Multifunctional response regulator A) is shown to be a central part of the *C. crescentus* stress response pathway. MrrA is phosphorylated by two cognate histidine kinases and additionally acts as a repressor of one of the kinases. The downstream target of MrrA is the histidine kinase LovK which is the main activator of the general stress response. It is demonstrated that phosphorylated MrrA is an allosteric activator of LovK.

Taken together this work increases the understanding of how c-di-GMP regulates cell cycle progression and additionally gives insight into the modes of regulation of histidine kinases.

Contents

Introduction.....	6
C-di-Nucleotide signaling.....	6
Histidine kinases and two-component systems	29
<i>Canlobacter crescentus</i> cell cycle.....	32
CckA controls CtrA phosphorylation	34
The general stress response	36
Aim of the thesis	38
Results	39
Cyclic di-GMP acts as a cell cycle oscillator to drive chromosome replication.....	39
Second messenger enforced bi-functionality of a central cell cycle switch.....	82
Multifunctional single domain response regulator mediates SigT- dependent stress response in <i>canlobacter crescentus</i>	114
Additional results	169
Discussion & Outlook	183
Acknowledgments.....	187
References.....	188
Curriculum vitae.....	215

Introduction

C-di-Nucleotide signaling

The following section on c-di-nucleotide signaling is written to be published as a review in *Nature Reviews Microbiology*. Text is written by Alberto Reinders (cyclases, phosphodiesterases, biofilm and motility) and myself (development, virulence, immunity, methods and “other c-di-nucleotides”).

Abstract

C-di-Nucleotides (cdN) are versatile signaling molecules used by bacterial and eukaryotic cells as second messengers. The best-studied example is bis-(3'-5')-cyclic dimeric GMP (c-di-GMP). Known since the late 1980`s it is now regarded a widespread bacterial second messenger. Recent discoveries, aided by the development of new techniques, shed light on the various processes controlled by c-di-GMP. C-di-GMP effectors display a wide range of targets, ranging from core cell cycle events to biofilm formation, motility and virulence. Here we review the latest discoveries focusing on effector proteins and the output functions controlled by c-di-GMP. We also briefly review the recently emerging second messengers c-di-AMP as well as c-GMP-AMP (cGAMP).

DGCs & PDEs

A planktonic lifestyle is incompatible to a sedentary lifestyle and requires profound reprogramming of cell physiology [1–5]. To trigger the transition and establish the lifestyle the cellular c-di-GMP concentrations have to be precisely set and readily adjusted if the environment requires adaptation. This requisite demands a highly fine-tuned network that can sense a plethora of stimuli to ultimately establish the appropriate c-di-GMP regime. This is achieved through the antagonistic enzyme families, which comprise two of the largest known enzyme families in the bacterial kingdom [6], namely diguanylate cyclases (DGC), which condense two GTP into c-di-GMP [7] and c-di-GMP-specific phosphodiesterases (PDE), which degrade it [8,9]. Diguanylate cyclases are characterized by their consensus GGDEF motif, while c-di-GMP-specific phosphodiesterases either contain an EAL or HD-GYP-motif [10,11]. These proteins either exist as stand-alone proteins or fused to one another to function as so-called “composite proteins”. While composite proteins comprise a large fraction of c-di-GMP-related enzymes and are an avid research target, their function and especially the regulatory mechanisms regulating either of the enzymatic activity still remain elusive. A recurring theme is that most enzymatic domains come along with N-terminally associated accessory domains that in most cases are believed to serve as input domains regulating the enzymatic output domain.

The recent advances in structure and mechanism of c-di-GMP synthesizing and degrading enzymes are centered on the regulatory features of these remarkable enzymes. For nearly a decade, PleD from *C. crescentus* served as a cornerstone in understanding the catalytic and regulatory mechanisms of diguanylate cyclases [12], stating that induced dimerization of the GGDEF-domain drives condensation of c-di-GMP [12]. Moreover, PleD is a precedent in respect to the inherent regulation of catalysis. Most diguanylate cyclases share an allosteric product inhibition site (I-site), most likely to refrain a bacterial cell from excessive GTP consumption or accumulation of unphysiologically high c-di-GMP concentrations [13]. This feature however is not conserved throughout all active diguanylate cyclases.

E.g., structural and biochemical insights into DgcZ (formerly YdeH [14]) from *E. coli* revealed that this particular cyclase does contain an inhibitory I-site, which nevertheless only shows its effect at unphysiologically high c-di-GMP concentrations (ca. 40 μ M) [14]. DgcZ is a constitutive dimer and its enzymatic activity is inhibited through subfemtomolar binding of zinc to the N-terminally

associated chemoreceptor zinc binding (CZB) domain. Mechanistically it was suggested that Zn^{2+} -binding to the CZB arranges the GGDEF-domains of DgcZ such that their mobility is impeded, thereby hindering correct positioning of the substrates [14]. Not only does this study provide a novel activation/inhibition mechanism but is moreover the first diguanylate cyclase crystallized in presence of its cognate regulatory signal.

Although the catalytic mechanisms of c-di-GMP-specific phosphodiesterases are well understood, the mechanisms regulating their activity are not. This is not surprising since we lack knowledge of the input signals that regulate the enzymatic domain. Moreover, it is unclear whether EAL-domains might experience some form of inherent regulation, which could even be uncoupled from their accessory domains. While for cyclases it is clear that two active and GTP-bound monomers have to dimerize in order to condense GTP into c-di-GMP [12,14], dimerization of EAL-domain proteins was readily observed [9,15–17] but its role in enzyme activity remained rather enigmatic. Sundriyal and co-workers recently showed that c-di-GMP concentrations drive dimerization and hence activity of the EAL-domain of PdeL (formerly YahA [18]) from *E. coli* [17]. In fact mutating specific dimerization residues, which are conserved throughout all active EAL-domains, fully abolished substrate-induced dimerization and concomitantly enzyme activity. Noteworthy there is accumulating evidence that PDEs show yet uncharacterized regulatory properties, which appear to be linked to changes in their quaternary structure [9,17]. Investigation of these observations is out for further scrutiny.

A second class of c-di-GMP-specific phosphodiesterases is proteins containing the conserved HD-GYP motif. Although both classes are competent c-di-GMP-specific phosphodiesterases, they are unrelated in terms of structure and their catalytic mechanism. While EAL domain-containing phosphodiesterases degrade c-di-GMP into linear pGpG, HD-GYP domain-containing phosphodiesterases degrade c-di-GMP in a one-step metal-assisted mechanism into two molecules of GMP [11]. Although numerous HD-GYP-domain proteins have been characterized in terms of their biological function [19], it was only in 2014 that the structure of an active HD-GYP-domain protein was solved in presence of its substrate c-di-GMP [11]. This study suggested that HD-GYP-domain proteins can be subdivided in two distinct subgroups with a bi- or tri-nuclear catalytic center and completes the structural picture of all enzyme classes involved in c-di-GMP homeostasis [11].

However for bacteria that lack HD-GYP-domain proteins such as *E. coli* it remained unclear how pGpG is further catabolized into its breakdown product GMP. Although some phosphodiesterases exhibit mild activity to degrade

pGpG into GMP (PDE-B activity) [10], it is unlikely that this mild secondary activity can deplete rapidly accumulating pGpG concentrations e.g. during sessile-motile transitions. Orr and co-workers recently identified and characterized the oligoribonuclease Orn to be specific for degradation of pGpG to GMP, thereby coming full-circle in respect to a complete synthesis and degradation pathway of c-di-GMP [20]. These findings add an important regulatory link to the homeostasis of c-di-GMP and the network regulation as such, namely that certain EAL-domain containing proteins are product inhibited. Moreover we can now assign a regulatory role for a long-thought junk-product of c-di-GMP homeostasis [20,21].

Despite the knowledge we gained in the recent years in terms of structure and function of DGCs and PDEs it remains challenging to unequivocally assign the cognate physiological function of individual DGCs and PDEs under laboratory conditions. In fact, only few input signals have been identified so far [22–28]. To circumvent this issue a genetic study was carried out in *E. coli* that isolated motile suppressors of a non-motile $\Delta pdeH$ (formerly *ybhH*) strain and revealed that – irrespective of the cognate input signal – PDEs can indeed be mutationally activated to exhibit their enzymatic activity [29].

Finally, we would like to highlight, that DGCs and PDEs must be regarded as more than just simple homeostasis elements in the world of c-di-GMP. Rather many of these enzymes engage in further downstream signaling e.g., through protein-protein interactions and by regulation of biological processes in a more localized fashion [22,30]. This observation does not limit to so-called “degenerate proteins”, which have lost their catalytic ability yet maintaining their c-di-GMP-binding properties to function as *bona fide* c-di-GMP effectors [31–34]. Rather examples are emerging of active DGCs and PDEs that act as c-di-GMP sensors to control downstream processes by virtue of their active site [30]. An illustrative example is the PDE PdeR (formerly YciR [18]) from *E. coli*. Lindenberg and co-workers showed that the primary role of PdeR is not to degrade, but sense c-di-GMP and thereby control transcription of amyloid curli fiber genes via its interaction partners DgcM (formerly YdaM [18]) and the transcription factor MlrA [30].

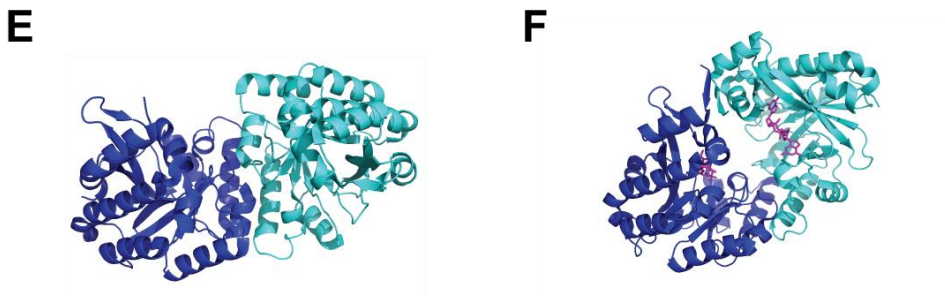
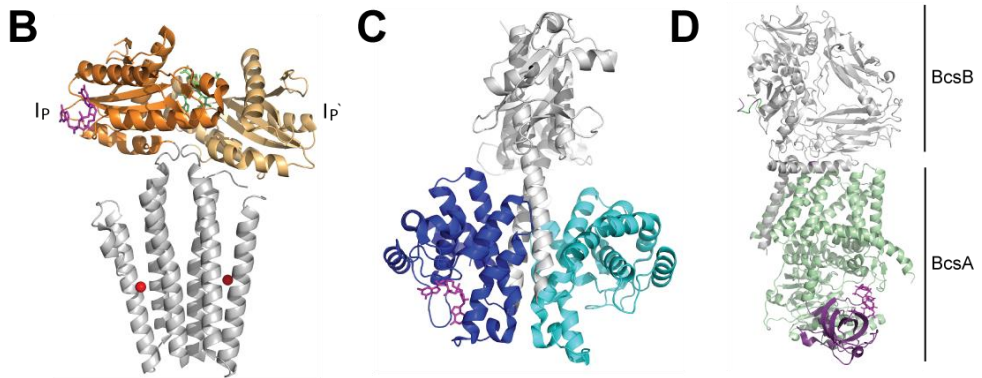
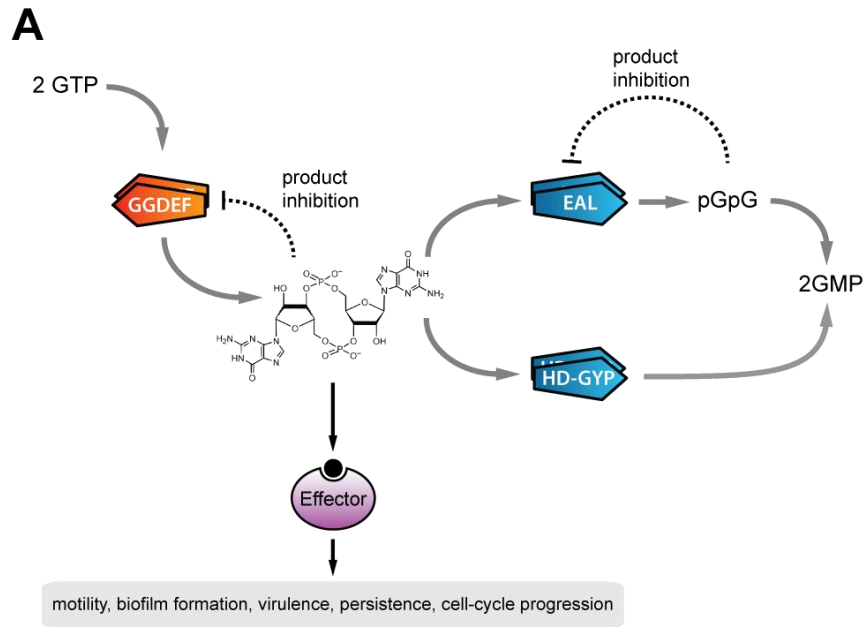


Figure 1: Components of the cyclic di-GMP signaling network. (A) Schematic overview of proteins generating and degrading c-di-GMP as well as exerting effector functions. **(B)** Structure of zinc-binding diguanylate cyclase DgcZ from *E. coli* (PDB-entry: 4H54). GGDEF-domain colored in orange (symmetry mate in light orange). Zinc-binding CZB-domain is shown in grey. C-di-GMP binding to antipodal I-site (I_P & I_P') shown in magenta. Non-hydrolysable GTP α S in active site (A & A') shown in red. **(C)** Crystal structure of a HD-GYP phosphodiesterase PmGH from *Persephonella marina* (PDB-entry: 4MDZ). HD-GYP-domain colored in blue (symmetry mate in light blue). Associated N-terminal GAF domain and α 5-linker helix colored in grey. C-di-GMP bound to active site shown in magenta. **(D)** C-di-GMP effector protein BcsA (green and magenta) (PDB-entry: 4P02). BcsA is a cellulose synthase activated by c-di-GMP. PilZ-domain of BcsA is shown in purple. C-di-GMP shown in magenta. BcsA forms a complex with periplasmatic BcsB shown in grey. **(E, F)** Structure of PdeL_{EAL} phosphodiesterase in relaxed (apo) (PDB-entry: E, 4LYK) and tight conformation (PDB-entry: F, 4LJ3) (c-di-GMP-bound, magenta). EAL-domains shown in blue and light blue for symmetry mate respectively.

Development

C-di-GMP controls *Caulobacter crescentus* cell cycle

C. crescentus has become a widely used model organism to study bacterial growth and development. The *C. crescentus* cell cycle is characterized by a number of developmental stages which are synchronized with chromosome replication [35].

C. crescentus swarmer cells have a single polar flagellum and are motile [35]. In this developmental period, the cells are not able to replicate the chromosome and are therefore blocked in G1 phase. During transformation into stalked cells, the swarmer cells eject the flagellum and produce an extension of the cell wall and membrane at the former site of the flagellum [36]. At the tip of this structure an adhesive compound, the holdfast, is formed which allows the cells to adhere to surfaces. During this developmental transition the cells also start replicating their chromosomes and enter S phase [37]. Next, this predivisional cell elongates and synthesizes a new flagellum at the pole opposite the holdfast. Division of this cell produces two morphologically different daughter cells: one cell still adheres to the surface via the stalk and re-enters S phase, whereas the other cell represents a new swarmer. One cell retains the stalk and immediately

re-enters S phase while the new swarmer cell shows a block in G1 and has to develop into a stalked cell before entering S phase (Fig. 2).

In recent years it has become evident that *C. crescentus* development is tightly linked to the intracellular c-di-GMP levels [7,38]. PleD, the first described GGDEF diguanylate cyclase, turned out to be involved in this process. PleD is a response regulator which harbours a receiver domain and a GGDEF output domain [7,12,39]. Phosphorylation of the receiver domain at the swarmer to stalked cell transition leads to activation of the cyclase activity and recruits the protein to the stalked cell pole [7]. Loss of PleD results in hypermotile cells, inefficient ejection of the flagellum and strongly reduced stalk formation [7]. When c-di-GMP production is abolished completely by deleting all DGCs the phenotypes are more dramatic: The cells lose all polar appendages and are strongly elongated but still retain viability [38]. Since the phenotypes that are regulated by c-di-GMP change throughout the cell cycle, it was suggested that c-di-GMP levels vary in different developmental stages. Indeed, it was reported that c-di-GMP levels are low in swarmer cells and rapidly peak at the swarmer to stalked cell transition resulting in stalked cells with high intracellular c-di-GMP levels [38]. These high levels decrease to intermediate levels as the cell progresses into a predivisional cell. C-di-GMP production by PleD causes the spiking c-di-GMP levels at the swarmer to stalked cell transition [38]. However, PleD is not the only protein contributing to this c-di-GMP peak. Later, degradation of a c-di-GMP-specific phosphodiesterase (PdeA) in the late swarmer cell was found to participate in raising the c-di-GMP levels [40]. High levels of c-di-GMP influence several cellular processes [38]. Once c-di-GMP levels peak a degenerate EAL domain protein, TipF, binds c-di-GMP and is thereby stabilized [36]. As a result, TipF localizes to new swarmer pole and recruits the PflI positioning factor and flagellar switch components to the site where the new flagellum is assembled [36] (Fig. 2A). Since c-di-GMP levels are high at the G1-S transition (swarmer to stalked cell) the question was asked whether c-di-GMP directly controls replication initiation. This connection of c-di-GMP and replication control becomes even more evident if the mechanisms controlling G1-S transition, PleD and PdeA (phosphodiesterase) regulation are compared.

In *C. crescentus*, G1-S transition is highly dependent on the transcription factor CtrA which blocks DNA replication in the swarmer cell by binding to distinct binding sites in the oriC region [41,42]. CtrA activity is tightly controlled by phosphorylation and degradation [43,44]. At the G1-S transition, CtrA is rapidly dephosphorylated by the CckA-ChpT-CtrA phosphorelay and degraded by the ClpXP protease [43]. The phosphodiesterase PdeA is also degraded at

the G1-S transition in a ClpXP dependent manner [40]. Interestingly, the proteins controlling CtrA activity also contribute to c-di-GMP signaling. The diguanylate cyclase PleD is phosphorylated by two histidine kinases known as DivJ and PleC [45]. Notably these are the same histidine kinases that also phosphorylate the single domain response regulator DivK, a protein that activates phosphatase activity of CckA resulting in dephosphorylation of CtrA [46]. Hence, control of cell cycle progression and rise in intracellular c-di-GMP levels are coordinated. High c-di-GMP levels then signal back into cell cycle circuitry. So far two c-di-GMP effector proteins have been characterized that are involved in the control of CtrA activity. As mentioned previously, CtrA must be degraded at the G1-S transition. To allow for rapid degradation the ClpXP protease and CtrA are recruited to the stalked pole before CtrA is being degraded [34]. Localization of CtrA is dependent on the c-di-GMP binding protein PopA. PopA is a PleD homolog but has a degenerate active site and is no longer able to produce c-di-GMP [34,47] (Fig. 2C). Binding of c-di-GMP to the inhibitory site (I-site) is required for sequestration of CtrA to the stalked pole. At the stalked pole PopA acts as an adaptor for the ClpXP protease [48]. Low levels of c-di-GMP or lack of PopA completely abolishes degradation of CtrA. In addition, it has recently been shown that CckA is a c-di-GMP effector protein. C-di-GMP binding to CckA switches its activity from kinase to phosphatase mode thereby driving dephosphorylation of CtrA at the G1-S transition [49]. Additionally, it has been shown that in the predivisional cell, c-di-GMP-dependent regulation of CckA contributes to the establishment of a CtrA phosphorylation gradient priming the two cell poles for their future fate after septation [49] (Fig. 2B, D).

As demonstrated for *C. crescentus* c-di-GMP levels fluctuate during the cell cycle and is tightly associated with the swarmer to stalked cell transition. Also in other bacteria such a behavior was observed [50]. A novel tool allowed measurements of c-di-GMP levels *in vivo*. To do so a c-di-GMP binding protein from *Salmonella enterica* (YcgR) was fused C- and N-terminally to CFP and YFP [50]. Binding of c-di-GMP to this hybrid construct leads to a change in fluorescence resonance energy transfer (FRET) between the fluorophores and this correlates with intracellular c-di-GMP levels. It has been demonstrated that not only *C. crescentus* displays an uneven distribution of c-di-GMP at some point during cell cycle but also *Pseudomonas aeruginosa*, indicating a more general principle. During the *P. aeruginosa* cell cycle overall c-di-GMP levels remain relatively constant. Only during a very short period after cell division one daughter cell (always the one inheriting the polar flagellum) exhibits reduced levels of c-di-GMP [50]. In *P. aeruginosa* the heterogeneity is generated by the phosphodiesterase Pch [51].

Pch localizes to the cell pole which will inherit the flagellum in dependence of the chemotaxis machinery. It is hypothesized that reduction of c-di-GMP levels at this stage promote diversity in the swimming behavior and that this would help to adapt to new environments [51]. Not only the Pch phosphodiesterase is localized but also DGCs and effector proteins localize. Localization of c-di-GMP signaling components raises the question whether gradients, or in the most extreme form, local pools of c-di-GMP exist within single cells. The idea is further substantiated by the findings that c-di-GMP effector proteins and DGCs and PDEs might physically interact to form complexes [52,53]. Such localized centers of c-di-GMP signaling could minimize cross talk with other parts of the c-di-GMP signaling network.

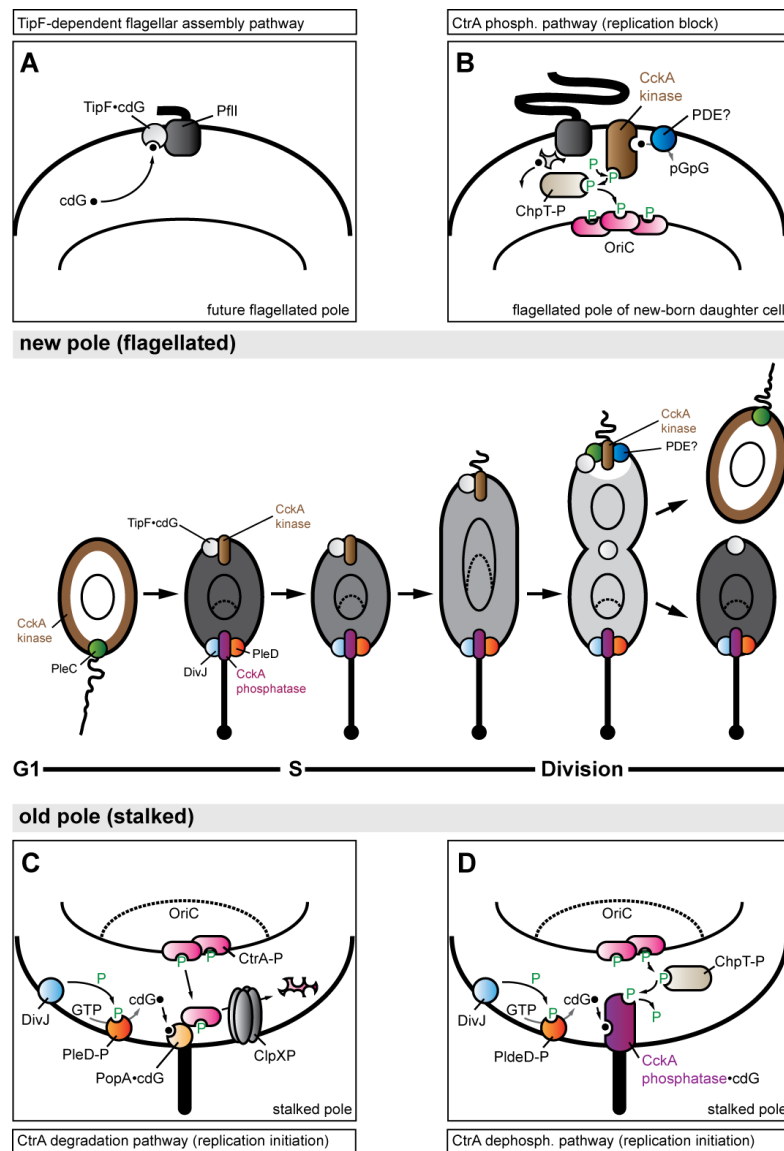


Figure 2: C-di-GMP-dependent cell-cycle control and pole differentiation in *C. crescentus*. *C. crescentus* cell cycle produces two distinct daughter cells (middle panel). A non-replicating, motile swarmer cell and a replicating, sessile and surface-attached stalked cell. Transition from swarmer to stalked cell is c-di-GMP dependent. Throughout the cell cycle many processes are regulated by c-di-GMP. The strong diguanylate cyclase PleD is activated through phosphorylation by the histidine-kinase DivJ and localizes to the stalked pole at the G1-S transition resulting in high c-di-GMP levels (shades of grey in middle panel represent cellular c-di-GMP levels). At the future flagellated pole the c-di-GMP effector TipF binds c-di-GMP thus priming the site for flagellum assembly of the future daughter cell **(A)**. Replication initiation is controlled by two parallel pathways. A proteolytic (C) and a phosphorylation pathway (B, D). Both are c-di-GMP dependent. The c-di-GMP effector PopA localizes CtrA to the ClpXP protease in a c-di-GMP dependent manner resulting in CtrA degradation that initiates chromosome replication **(C)**. In the predivisional cell the cell cycle histidine kinase CckA adopts a bipolar localization. Recent findings suggest that CckA is active as a kinase at the flagellated pole, while it is kept in the phosphatase mode at the stalked pole **(B, D)**. This configuration establishes a CtrA~P gradient across the predivisional cell.

Streptomyces development

Similarly to *C. crescentus*, the *Streptomyces venezuelae* developmental cycle involves clearly distinguishable stages. After spore germination, vegetative hyphae grow into the substrate to scavenge for nutrients. Later, the mycelium enters a reproductive stage, in which aerial hyphae grow out from the mycelium. In these aerial hyphae, spores mature and are released into the environment. The regulation of aerial hyphae growth has been studied in the past. Recently, c-di-GMP was found to play a critical role in the life cycle of *S. venezuelae*. Both, overproduction and depletion of c-di-GMP prevented the formation of aerial hyphae. While overproduction simply blocks development at this step, loss of c-di-GMP causes premature spore production bypassing the formation of aerial hyphae. These observations suggested that c-di-GMP is required for propagating through the reproductive stages.

A similar phenotype (the loss of aerial hyphae) is observed when the master regulator of development in *S. venezuelae*, BldD, is deleted. BldD is a transcription factor regulating more than 100 genes [54]. For a long time, regulation of BldD remained unclear. However recently, it was shown that BldD is a c-di-GMP effector protein [55,56]. This connection was established

by capture compound pulldown experiments and further proven *in vitro*. The crystal structure of BldD bound to c-di-GMP reveals that two BldD molecules bind a c-di-GMP tetramer. Binding of c-di-GMP induces dimerization at low BldD concentrations and enhances DNA binding affinity. Therefore, c-di-GMP binding to BldD is critical for providing the signal to develop aerial hyphae.

So far, c-di-GMP was often described as a central regulator of motile to sessile transitions. The results described for *C. crescentus* and *S. venezuelae* clearly indicate that c-di-GMP is also involved in coordination of core cell and life cycle components.

C-di-GMP controls development of a Eukaryote

For a long time, c-di-GMP was thought to be found only in bacteria. It has now become clear that c-di-GMP is also sensed and produced by eukaryotes. The Amoeba *Dictyostelium discoideum* has been known to be controlled by the cyclic nucleotide cAMP [57]. In an environment with plenty of nutrients, *D. discoideum* replicates and lives as a unicellular amoeba. In case of insufficient nutrient supply, the cells start to aggregate and form a multicellular structure (the slug). This transition is dependent on the secretion of cAMP, which attracts other amoeba to the site where they assemble into the slug [57]. The structure will at some point form a fruiting body that consists of a long stalk and contains spores at the tip that are eventually released.

Recent studies indicated that fruiting body formation is also controlled by another second messenger, c-di-GMP [58]. Bioinformatic searches revealed a gene encoding a GGDEF-domain containing protein. Deletion of this gene (*dgcA*) still allowed the cells to aggregate into multicellular structures but no fruiting body was observed [58]. Fruitification could be restored by expression of DgcA but restoration is dependent on an intact GGDEF domain. Interestingly, fruitification was restored when *dgcA*- strains were mixed with wild type strains indicating that c-di-GMP might be secreted. Indeed, droplets of c-di-GMP were able to restore fruitification of a *dgcA*- strain to normal levels [58].

Initial attempts to clarify the mechanisms of c-di-GMP action involved expression studies of DgcA and developmental genes. Expression of DgcA is restricted to the anterior tip region of the slug, stalk and tip of the fruiting body. Consistent with this, c-di-GMP seems to regulate the expression of genes for stalk and spore biogenesis. Thus, the c-di-GMP signalling pathway in *D. discoideum* are still poorly understood and the downstream targets remain to be discovered.

Motility & Biofilm

C-di-GMP has long been known to be a central regulator of biofilm formation and motility. In *Escherichia coli* there is a strict correlation between cellular c-di-GMP levels and swimming velocity [59]. In fact, during entry into stationary phase, cells experience a c-di-GMP upshift. This upshift is a consequence of downregulation of the FlhDC-coregulated gate-keeper PDE PdeH (formerly YhjH [18]) [59,60]. Thereby c-di-GMP inhibits flagellar rotation through binding of the PilZ-domain protein YcgR to the MotA/FliG interface [59]. Moreover the interaction of YcgR with the flagellar switch complex inhibits the chemotactic behavior through biasing CCW rotations [61]. This interference with the locomotion apparatus was suggested to increase the probability of surface interaction as an initial step towards establishment of a surface-attached lifestyle (Fig. 3A). Interestingly this behavior seems to extend into the gram positive world where it was suggested that the PDE YuxH serves as a PdeH-analogous motility gate-keeper to inhibit flagellar downregulation via interaction of the PilZ-domain protein YpfA with MotA [62,63].

Although it appears to be a common theme to inhibit motility in a c-di-GMP-dependent manner, the strategies are very versatile throughout the bacterial kingdom. In contrast to *E. coli*, *P. aeruginosa* targets flagellar synthesis via the c-di-GMP binding transcription factor and ATPase FleQ [64–66]. C-di-GMP binds to the Walker A motif of FleQ thereby repressing transcription of flagellar genes [65]. ATPases in general appear to be frequently targeted by c-di-GMP and are an emerging field of interest in the c-di-GMP world [65,67]. ATPases and their link to c-di-GMP will be discussed in more detail later in this review.

Apart from regulating flagellar motility, c-di-GMP has extended its control to other locomotion apparatuses such as type-IV pili (T4P). This was recently described for *Myxococcus xanthus* and *Vibrio cholerae* [68,69]. It is noteworthy to mention, that although in both cases c-di-GMP targets pili biogenesis, the mode of action seems to differ. While in *M. xanthus*, c-di-GMP negatively affects transcription of the major pilin (PilA) [68], c-di-GMP positively regulates the synthesis of MshA pili in *V. cholerae* through direct binding to the ATPase MshA [69]. These two examples emphasize the importance of c-di-GMP during the establishment of initial surface contact and raise the awareness that c-di-GMP can be both repressor and activator for motility-dependent processes.

To regulate the maturation of biofilm structures, once bacteria have established surface contact, c-di-GMP exerts its function on all three layers of control (transcriptional [70–72], translational [73–76] and post-translational [77–79]). E.g., in *V. cholerae* roughly 100 motility and biofilm genes are inversely controlled on transcriptional level through c-di-GMP-dependent oligomerization of the transcription factor VpsT [80]. Reminiscent of VpsT the general stress sigma factor σ^S in *E. coli* inversely regulates numerous motility and biofilm associated genes [81] such as amyloid curli fibers. Production of these fibers is regulated via the curli master regulator *csgD* by two parallel transcription-control pathways: (i) directly via σ^S [82,83] and (ii) in a c-di-GMP-dependent manner through a multiprotein signaling unit comprised of the transcription factor MlrA, the DGC DgcM and PDE PdeR [30]. The c-di-GMP-dependent pathway controlling *csgD* expression via MlrA is highly sophisticated and involves a signaling cascade comprised of two c-di-GMP modules. At low intracellular levels trigger-enzyme PdeR inhibits both the cyclase activity of DgcM and transcriptional activity of MlrA (module I). During entry into stationary phase, PdeH is downregulated and the DGC DgcE concomitantly upregulated (module II). Increasing c-di-GMP levels are sensed by PdeR, which by that relieves its inhibiting function on both DgcM and MlrA thus derepressing *csgD* transcription and enabling curli production (Fig. 3C) [30].

This circuit demonstrates the intricate connectivity within the c-di-GMP network, since CsgD further activates the cyclase DgcC [82]. C-di-GMP produced by this cyclase is a potent activator for the PilZ-domain containing cellulose synthase BcsB. From a historic standpoint it is noteworthy to mention that only last year – 28 years post discovery [84] – the structure of c-di-GMP-activated BcsAB complex was solved [75,85] (Fig. 1C). Numerous biofilm-associated processes rely on post-translational regulation by c-di-GMP [73,86] and extends to targets other than PilZ domain-containing proteins. In 2013 Steiner and co-workers identified that activation of the poly-beta-1,6-N-acetylglucosamine (poly-GlcNAc)-synthesizing Pga machinery depends on c-di-GMP-facilitated protein-protein interaction between PgaC and D [73](Fig. 3D). While for many bacteria the processes driving the motile-sessile switch are fairly well understood, the mechanisms underlying dispersal of single cells from a mature biofilm are not. Newell and co-workers however identified an active biofilm escape mechanism in *Pseudomonas fluorescens* [31,32,87]. Here c-di-GMP regulates the proteolytic degradation of an outer membrane adhesine and allows cells to escape a mature biofilm under phosphate starvation conditions. This example nicely illustrates how GGDEF and EAL-domain proteins can

engage in inside-out signaling, thereby regulating sessile-motile transitions (Fig. 3B).

C-di-GMP regulates these two opposing lifestyles by targeting processes on all layers of control. The opportunistic pathogen *P. aeruginosa* involves a highly complex c-di-GMP network to carefully control the c-di-GMP levels during development [51] and lifestyle transitions [32,69,86,88]. Nevertheless depending on the niche it resides in it readily engages in “ping-pong”-mutations that allow it to recurrently alternate its c-di-GMP regimes thereby stabilizing a beneficial lifestyle [89,90]. This happens on the basis of strong selective pressure (e.g., in the lung of cystic-fibrosis patients) and converges to affect c-di-GMP-levels.

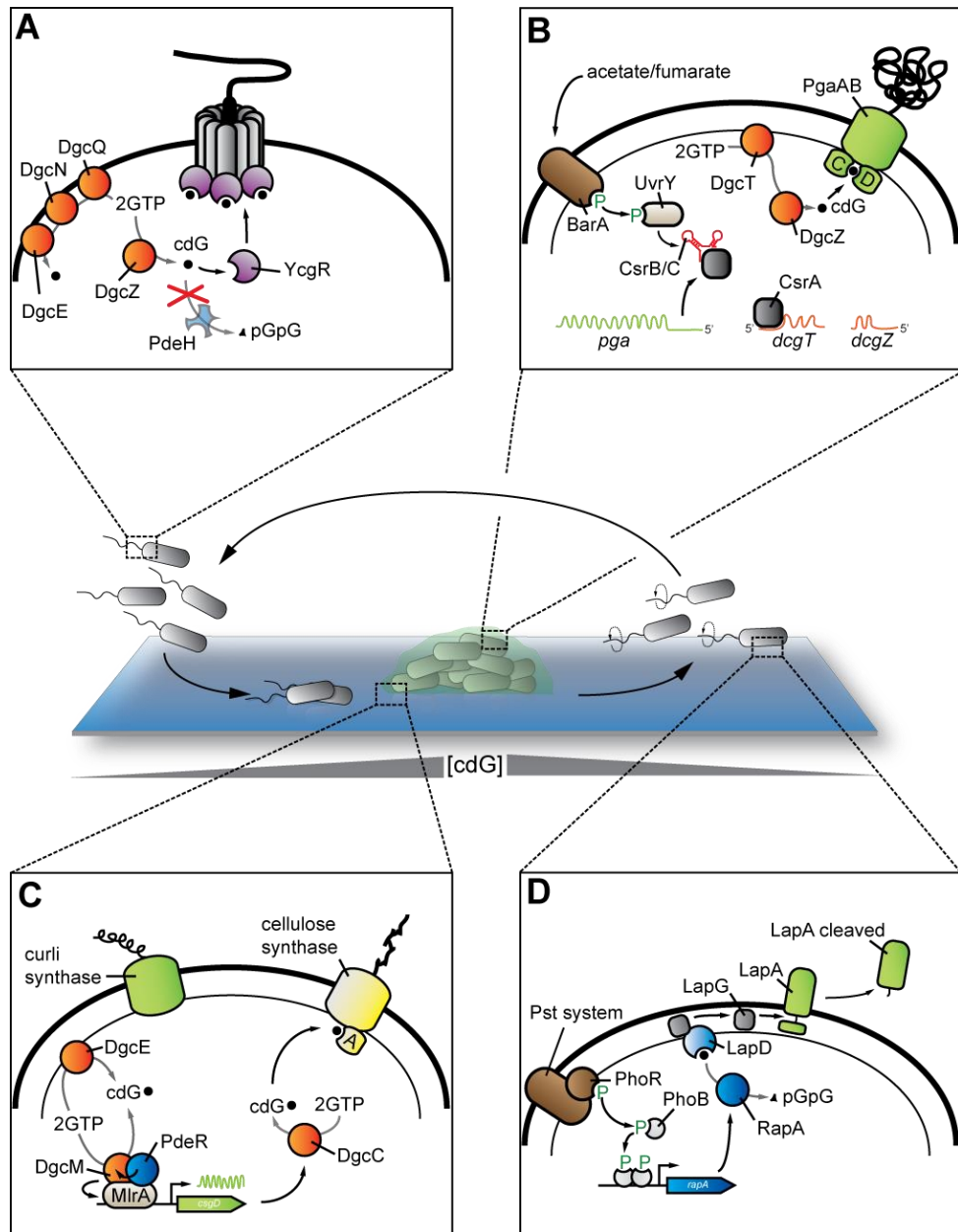


Figure 3: Overview showing the involvement of c-di-GMP in biofilm formation and dispersal. (A) During entry into stationary phase *pdeH* (blue) is downregulated. Increasing c-di-GMP levels curb motor rotation through interaction of c-di-GMP-bound YcgR (purple) to the MotA/FliG interface. Under laboratory conditions, four cyclases (depicted in orange) contribute to the global pool of c-di-GMP. **(B)** Activation of the BarA/UvrY system through fumarate/acetate activates small RNAs CsrB/C (red), which deplete CsrA from target mRNAs. Derepression of target mRNAs leads to translation of the Pga system as well as two cyclases DgcT and DgcZ. C-di-GMP post-translationally activates the Pga machinery. **(C)** C-di-GMP-dependent production of amyloid curli fibers and cellulose. Curli gene expression is transcriptionally activated by c-di-GMP but is under superordinate control of σ^S . C-di-GMP produced by the upstream cyclase DgcE (module I). The DGC/PDE-pair DgcM/PdeR form a complex with the transcription factor MlrA. C-di-GMP is sensed by the trigger enzyme PdeR, leading to activation of DgcM. DgcM activates MlrA thus enabling expression of the curli master regulator CsgD. CsgD activates DgcC (formerly: YaiC), which provides c-di-GMP to post-translationally activate cellulose synthase. **(D)** Biofilm escape mechanism as described in *P. fluorescens* Pf0-1. Under phosphate starvation condition the Pst system activates a phosphorylation cascade, leading to PhoB-activated expression of the PDE RapA (blue). RapA depletes c-di-GMP from active site of the degenerate EAL-domain protein LapD (light blue). C-di-GMP-free LapD activates the periplasmic protease LapG, which in turn cleaves the outer-membrane adhesine LapA.

C-di-GMP in virulence and immune system

The widespread occurrence of c-di-GMP amongst many bacterial species and the diversity of controlled targets raised the question if c-di-GMP is an important virulence factor. An interesting example providing evidence is the 2011 German outbreak of *E. coli* O104:H4. The strain caused an unusually high incidence of haemolytic uraemic syndrome (HUS) [91]. The genome of the causative strain has been sequenced and contains elements of enterohaemorrhagic *E. coli* (EHEC) and enteroaggregative *E. coli* (EAEC) [92]. Interestingly the genome sequence revealed the presence of one additional diguanylate cyclase (*dgcX*) [93]. DgcX is only present in *E. coli* O104H:H4 and closely related strains. This protein is strongly expressed and has an intact active (GGDEF) and inhibitory (RXXD) site [93]. It is usually inserted at the *attB* locus and flanked by prophage elements and is therefore thought to be acquired by horizontal gene transfer. A second c-di-GMP related mutation is an

insertion into the diguanylate cyclase *yedT* [93]. This insertion decreases expression of YcdT [93]. *yedT* is located divergently to the *pgaABCD* operon and in some strains contains an additional IS1 element with the promoter presumably activating transcription of the *pgaABCD* operon [93–96]. Notably the PGA machinery has been shown to be activated by c-di-GMP [73]. Upregulation of c-di-GMP and the PGA machinery could therefore help the strain to form the strong biofilms that are observed.

Another example for the importance of c-di-GMP in virulence is *Clostridium difficile*. In the course of *C. difficile* infections the bacteria adhere to the gut mucosa [97]. Clinical symptoms usually arise when the cells start expressing the two toxins TcdA and TcdB [98]. Interestingly, TcdA and TcdB are controlled by a c-di-GMP responsive riboswitch [99,100]. Not only the toxins are under c-di-GMP control. In the genome of *C. difficile* a total of 16 c-di-GMP responsive riboswitches were predicted [100]. These riboswitches are found upstream of flagellar and pili-related genes and the protease Zmp1 which is important in cleaving the fibronectin network of fibroblasts [97,100] (Fig. 4). Taken together, c-di-GMP appears to be important for several bacteria to deploy their virulence potential. However, production of c-di-GMP is noticed by host cells. The innate immune system is designed to rapidly detect pathogens and stage appropriate responses. While the adaptive immune system requires exposure to specific antigens to produce specific antibodies, the innate immune system recognizes certain structures of entering pathogens, so called pathogen associated molecular patterns (PAMPs), without the need for pre-exposure. Dedicated pattern recognition receptors (PRR) bind specific PAMPs and in response trigger inflammation and activate the complement cascade. Typical bacterial PAMPs that are recognized are flagellins, bacterial DNA, lipopolysaccharides and peptidoglycan. In the past few years it became evident, that cyclic dinucleotides such as c-di-GMP, c-di-AMP and cGAMP are also sensed by the mammalian innate immune system [101]. Recognition of c-di-GMP in the cytosol of human macrophages leads to strong upregulation of interferon 1 production, a hallmark of activation of the innate immune system which then allows the detection of many bacterial species [102]. While the response to c-di-GMP shows a pattern similar to the response elicited by foreign DNA, it does not depend on the same Toll-like receptors. Rather, c-di-GMP binds to an adaptor protein called STING (stimulator of interferon genes) resulting in its dimerization [103] (Fig. 4). STING dimerization causes re-localization of the receptor from its initial endoplasmic reticulum associated position to perinuclear microsomal compartments [103–105]. There, STING

interacts with TBK1 (TANK binding kinase 1) leading to phosphorylation and translocation of the transcription factor IRF3 (interferon regulatory factor 3) into the nucleus and to the induction of innate immune response genes (Fig. 4).

STING is not only important for c-di-GMP detection but appears to be a central sensor of c-di-nucleotides [106]. C-di-AMP as well C-GMP-AMP (cGAMP) induce a STING-dependent host cell response [107].

Intriguingly, cyclic dinucleotides are not only recognized by STING, but also by the DEAD-box helicase DDX41, an alternative protein involved in type I interferon response [108]. Both, DDX41 and STING, are necessary to stimulate the immune response in the presence of c-di-NMPs. The authors of this work propose that DDX41 binds c-di-GMP and subsequently interacts with STING to activate the downstream cascade (Fig. 4). The reason why two individual c-di-NMP binding proteins in the same pathway are required for efficient activation of the interferon response remains unclear.

Regarding c-di-GMP as a stimulator of innate immunity, the second messenger is used by the host immune system to interfere with the growth of invading pathogens. However, a recent report indicated that c-di-GMP might also take an active role for the benefit of invading bacteria in the host. As bacteria grow inside a host cell, they have to ensure sufficient supply of iron. To scavenge iron, many bacteria secrete ferric siderophores, which bind iron with high affinity and are then re-imported into the cell (Fig. 4). As a part of the immune response, the host cell interferes with this process by releasing siderochalins. Siderochalin (LCN2) binds and sequesters siderophores, thereby reducing iron availability to the bacteria [109]. Li *et al.* identified LCN2 in a bioinformatic screen for specific 3D motifs in proteins, which might fit to bind c-di-GMP. Indeed, when testing their results experimentally, LCN2 specifically bound to c-di-GMP, but not to other c-di-NMPs. Binding of c-di-GMP presumably occurs at the site of siderochalin-siderophore interaction, suggesting that c-di-GMP might free siderophores from their caging by siderochalins thereby increase availability of iron. The authors propose that bacteria might actively secrete c-di-GMP to enhance their iron availability and thereby increasing their growth.

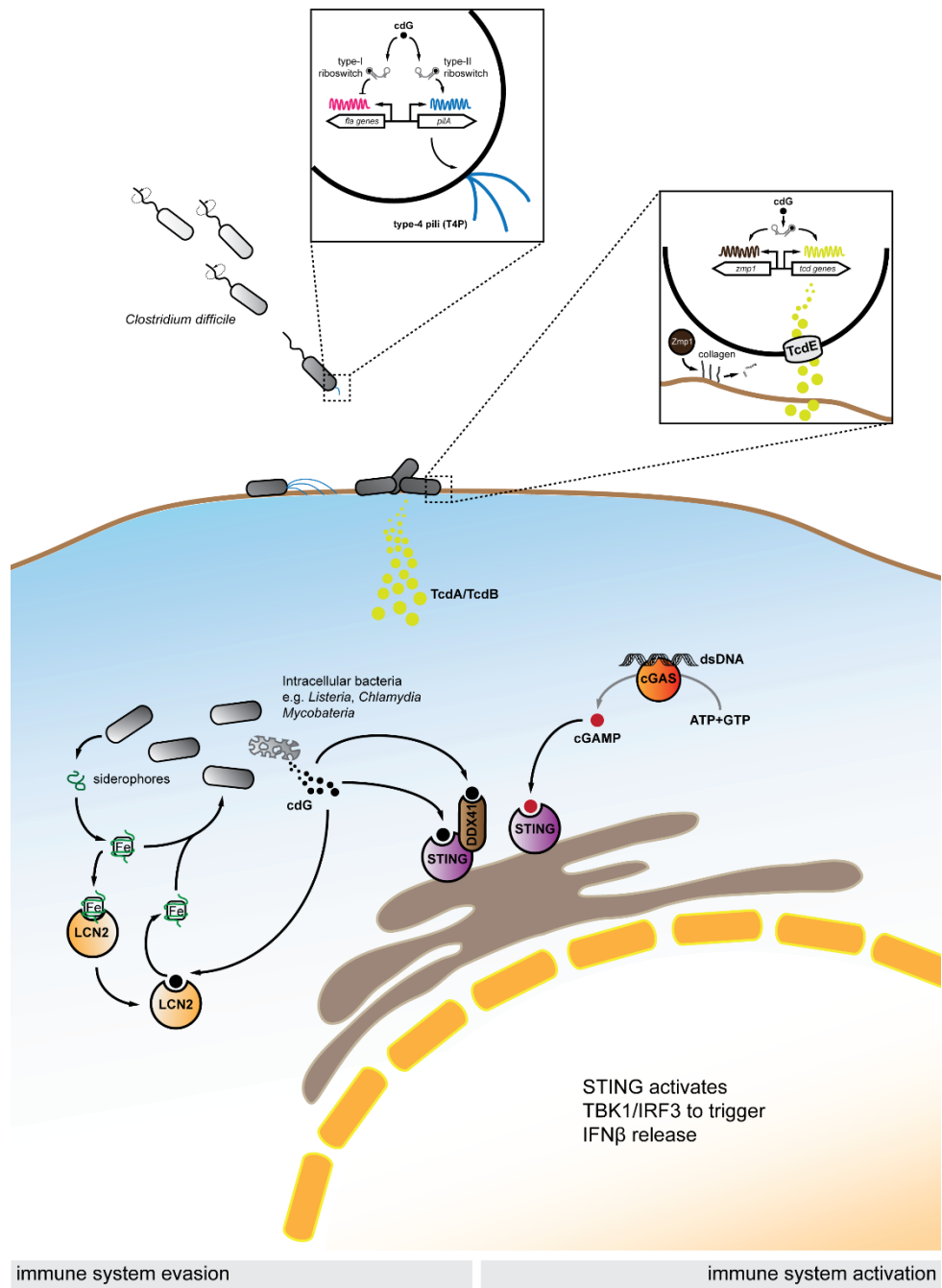


Figure 4: C-di-GMP is a virulence factor. It has been demonstrated that in several bacterial species virulence factors are controlled by c-di-GMP. This figure highlights the virulence factors of *C. difficile*. In the genome of *C. difficile* a total of 16 c-di-GMP responsive riboswitches are found. Two classes of riboswitches have been described. (i) type-I riboswitches, which bind c-di-GMP and repress translation and (ii) type-II riboswitches, which act as translation activators. In *C. difficile* several are positioned upstream of known virulence factors such as flagellar genes, the gene encoding for the major pilin PilA and toxins and proteases. E.g., flagellar and pili genes are inversely regulated to facilitate initial surface contact. Moreover, the secreted zinc-dependent metallo-protease Zmp1 leads to cleavage of collagen on the cell surface, while TcdA/B are glycosyltransferases that target intracellular host-proteins such as small GTPases to disturb signal transduction [110]. C-di-GMP is expressed by many intracellular bacteria and thus is an ideal stimulus for the immune system. Indeed the innate immune system is able to detect c-di-GMP through the two c-di-GMP effectors STING and DDX41, resulting in the upregulation in IFN β release. STING can thereby function as a receptor for other dinucleotides such as cGAMP. The host cell also expresses LCN2, a siderocalin, which is able to bind siderophore-Fe complexes secreted by bacteria to scavenge iron. As a counter-measure, c-di-GMP can bind LCN2 to inhibit siderophore-Fe complexation via LCN2.

Other c-di-nucleotides

Recently c-di-AMP has appeared as another cyclic nucleotide second messenger. When the structure of the DNA damage-sensing protein DisA of *Bacillus subtilis* was solved, the researches unexpectedly identified c-di-AMP to be bound to the N-terminal domain of the protein. Further investigations revealed, that this N-terminal domain produces c-di-AMP and was therefore termed diadenylate cyclase (DAC) domain [111]. Interestingly, c-di-AMP production by DisA strongly depends on the presence of branched DNA and thus, c-di-AMP was proposed to signal DNA damage. Since the initial discovery, different parts of the c-di-AMP network have been studied. Several DACs have been described, some of which are membrane-bound or specific for certain cellular functions, for example sporulation in *B. subtilis* [112,113]. C-di-AMP degrading enzymes have been identified which contain a typical DHH motif that is required for efficient degradation of c-di-AMP to linear pApA or in some cases AMP [114,115]. Notably, c-di-AMP seems to be essential in a variety of different bacteria and any deregulation causes abnormal phenotypes [113]. However, the reason for c-di-AMP essentiality remains unclear. So far,

several c-di-AMP effector proteins have been identified. The first identified receptor was the TetR family transcription factor DarR found in *Mycobacterium smegmatis* [116]. DarR consists of a helix-turn-helix DNA-binding domain and a QacR-like domain. C-di-AMP binds to the QacR domain with high affinity. Although this domain is found in other proteins, it is not a general c-di-AMP-binding domain. Deletion of DarR increases cell size and fatty acid synthesis [116]. In *Staphylococcus aureus* the first comprehensive screen was carried out to isolate several c-di-AMP effectors [117]. The identified effectors seem to be predominantly involved in the regulation of potassium intake on different levels [117]. The *S. aureus* cation-proton antiporter CpaA consists of several transmembrane domains, RCK_N and RCK_C domains. It was shown that c-di-AMP directly binds to the RCK_C domain but it is unclear what the consequences of this interaction are [117,118]. KtrA is a gating component of the KtrB potassium transporter. Like CpaA it harbours a RCK_N and a RCK_C domain and the latter has also been shown to bind c-di-AMP [117,119]. In addition to the Ktr system, the expression of the of the Kdp potassium uptake system is regulated by c-di-AMP. The histidine kinase KdpD has a USP domain which binds c-di-AMP [117,120]. KdpD is part of a two-component system with KdpE as its cognate response regulator. Phosphorylation of KdpE by KdpD results in activation of the *kdpFABC* operon encoding the Kdp potassium transporter components. It has been suggested that c-di-AMP downregulates the activity of the KdpDE two component system although it is unclear how the kinase activity is switched off by c-di-AMP [120]. The mechanistically best understood c-di-AMP effector is the pyruvate carboxylase from *Listeria monocytogenes* (LmPC) [121]. LmPC was identified amongst other effectors of unknown function in a c-di-AMP affinity pulldown [121]. *In vitro* experiments showed that c-di-AMP acts as an allosteric regulator and inhibits the activity of LmPC [121]. The crystal structure of the LmPC tetramer in complex with c-di-AMP revealed that c-di-AMP binding leads to large conformational changes in the protein/oligomer. Based on these findings the authors suggest that c-di-AMP locks LmPC into a conformation that is incapable of catalysis [121]. Until now several components of the c-di-AMP network have been uncovered, yet it is still unclear why the molecule is essential and through which pathway it signals.

The most recently discovered c-di-nucleotide is c-GMP-AMP (cGAMP). cGAMP is of special interest because it is produced by bacterial and eukaryotic cells, [122,123]. Bacterial cGAMP is produced by a cGAMP synthase located on the of the 7th pandemic island of *Vibrio cholerae* [122,124]. The only effector structures found to this date is a riboswitch found in *Geobacter sulfurreducens* and

STING [125–127]. Eucaryotic cGAMP is synthesized by the cGAMP synthase (cGAS) which oligomerizes and is activated in response to dsDNA [123,128,129]. It was also shown that cGAMP produced in immune cells diffuses through gap junctions of neighbouring cells and thereby serves the signal for bystander cell activation [107,130]. Recent reports also suggest, that viral particles pack cGAMP and thereby deliver this second messenger to distant sites where it activates the host immune response [131,132]. Interestingly bacterial and mammalian cGAMP differ in the way the nucleotides are linked [124]. The mechanism by which bacterial and mammalian cGAMP synthase produce the product are different. As a result bacterial cGAMP has two 3'-5' phosphodiester linkages, while mammalian has one 3'-5' and one 2'-5' [133].

Methods for c-di-GMP effector identification

In most organisms loss of c-di-GMP has diverse phenotypes. To assess which processes and pathways are controlled by c-di-GMP an increasing interest in c-di-GMP effector proteins developed during the last years. Already in the early years of c-di-GMP research the PilZ domain has been recognized as a prototypical c-di-GMP binding domain. This domain is present in a variety of different bacteria and is often fused to other domains. Apart from this domain, little was known of other c-di-GMP effector proteins. Lately several approaches were developed to isolate effector proteins on a proteome wide scale. Two approaches involved affinity pulldowns of effector proteins and subsequent mass spectrometry analysis. One method used a so-called capture compound [134,135]. This synthesized compound contains a c-di-GMP moiety to specifically bind effector proteins, a crosslinking domain to covalently link the effector to the compound and biotin to allow for rapid sorting on streptavidin coated magnetic beads. An alternative but very similar approach used c-di-GMP coated sepharose beads for affinity pulldown [136,137]. In both cases the proteins enriched in the pulldown were analyzed using mass spectrometry. These new methods were applied to many bacteria and resulted in discovery of several new c-di-GMP effector proteins in different species like *P. aeruginosa*, *C. crescentus*, *S. venezuelae* and the predatory bacterium *Bdellovibrio bacteriovorus* [55,134,135,138].

Another method aimed at detecting new effector proteins by the expression of the complete ORFeome and subsequent testing of whole cell lysates for binding activity [139,140]. Such a procedure requires a high-throughput binding assay. Hence the DRaCALA (differential radial capillary action of ligand assay)

assay was developed. The idea behind this assay is that proteins and nucleotides (radioactive or fluorescent labelled c-di-GMP, c-di-AMP, etc.) are mixed and placed onto a nitrocellulose membrane. Protein and ligands bound to proteins are immobilized immediately at contact site while free ligand diffuses out. Therefore, if a protein interacts with the nucleotide ligand there will be a strong signal right at the site where it was spotted. If there is no interaction the ligand will diffuse out and result in dispersed signal [117,141].

These new techniques as well as conventional approaches have led to the identification of a plethora of novel effector proteins. It has become evident that c-di-GMP is sensed not only by bacteria but also by eukaryotes. The output functions controlled by c-di-GMP are very diverse and act on transcription, translation and allosterically. One group of effectors that recently has emerged to contain several c-di-GMP effectors are ATPases. The best-studied example is the *P. aeruginosa* transcription factor FleQ consisting of receiver domain, AAA+ and HTH domains. C-di-GMP interacts with the AAA+ domain and reduces its activity thereby decreasing expression of flagellar genes and derepressing EPS biosynthesis [65,142,143]. Interestingly a number of AAA+ ATPases involved in transport across the membrane are subject to c-di-GMP control [67]. FliI was isolated as potential effector in a capture compound pulldown screen in *P. fluorescens*. FliI is part of the soluble components of the flagellum and required for normal flagellum formation [67]. It was shown that binding of c-di-GMP reduces ATPase activity. FliI shares homology with the *P. fluorescens* type III ATPase HrcN and the type VI ATPase ClpB2 and indeed it was demonstrated that also these proteins bind c-di-GMP [67]. In addition *Vibrio cholerae* MhsE is another ATPase that senses c-di-GMP [69,141]. MhsE shares homology with a Type II ATPase but is involved in MhsA pili biogenesis. It was demonstrated that in this case c-di-GMP promotes ATPase activity. The data support a model where MhsE acts as a motor protein to drive pilus elongation [69]. Over-activation of MhsE by c-di-GMP leads to increased surface attachment and reduced motility.

Histidine kinases and two-component systems

In the environment, bacteria encounter diverse stimuli to which they have to respond. Two-component systems and more complicated phosphorelays have evolved to perceive signals and translate them into a cellular response (Fig. 5). The classical two component systems consist of a sensor histidine kinase and a response regulator [144]. The sensory domain of histidine kinases registers a signal which leads to autophosphorylation on a conserved histidine residue. The phosphoryl group on this histidine residue is then transferred on an aspartate residue located in the receiver domain of a response regulator [144]. Usually, response regulators are fused to an output domain. Output domains can regulate transcription or have enzymatic functions (e.g. GGDEF, EAL or Helix-turn-Helix domains) and their activity is regulated by the phosphorylation state of the receiver domain [145–147]. Sometimes, response regulators only have a receiver domain but no output domain [148,149].

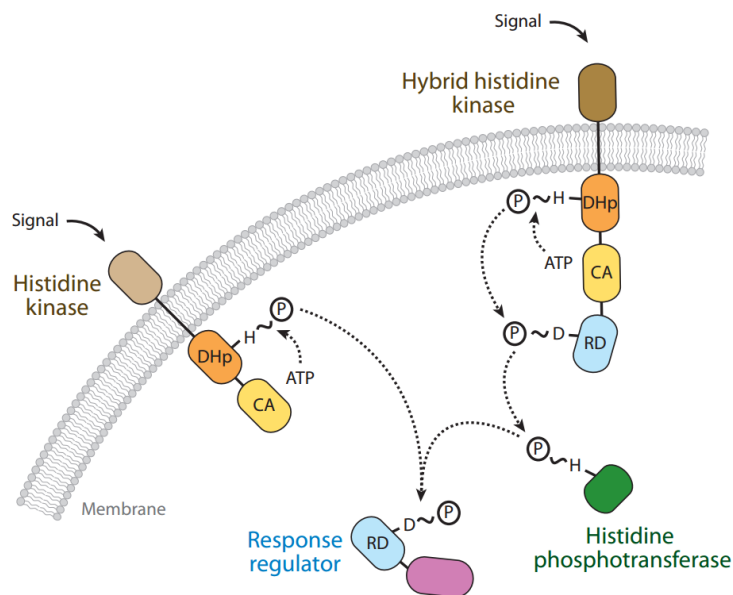


Figure 5: Overview of two-component and phosphorelay systems. The classical two-component system is shown on the left and a phosphorelay on the right. The phosphoryl group is transferred from ATP to a histidine residue in the DHp domain. Subsequently the phosphoryl is moved to a conserved aspartate in the receiver domain. Figure adapted from [150].

These proteins are called single domain response regulators and usually control downstream targets via protein-protein interactions. The best-studied class of single domain response regulators are the CheY proteins involved in chemotaxis [151,152]. Two component systems are modular and can be extended by further signaling components such as phosphotransferases (Fig. 5). Phosphotransferases are proteins which resemble the DHp domain of histidine kinases and offer an additional step in the phosphorylation cascade [153,154]. Such schemes are found in systems where multiple components are integrated into one certain pathway or diverge into different pathways.

The kinase activity of histidine kinases resides in two conserved domains. The catalytic and ATP binding (CA) domain binds ATP and transfers the γ -phosphoryl group of the ATP to a histidine residue within the dimerization and histidine phosphotransfer (DHp) domain (Fig. 6).

A few years ago, the structure of a histidine kinase was solved for the first time [155,156]. The two core kinase domains (DHp and CA) form a homodimer (Fig. 6). The DHp domain consists of two large α -helices which provide the dimerization interface and harbor the acceptor histidine residue [157]. The CA domain shows a classical $\beta\alpha$ Sandwich known as the Bergerat fold [155]. This domain binds the ATP molecule and has ATPase activity. For autophosphorylation, the CA domain has to undergo a conformational change to get in close proximity to the acceptor histidine residue in the DHp domain [158]. Phosphorylation occurs either in *cis* or in *trans* depending on the linker connecting the two α -helices of the DHp domain [159,160]. Once the phosphoryl group is transferred, the CA domain swings out leaving space for a cognate interacting receiver domain.

Since there are many different histidine kinases and response regulators in a cell the risk of nonspecific phosphorylation between histidine kinases and response regulators of otherwise independent TCSs exists. The major mechanism to ensure specific phosphotransfer between a kinase and its corresponding receiver domain is molecular recognition. This means the phosphorylated histidine kinase is able to recognize the cognate response regulator and exclude all noncognate response regulators from interaction [150,161–163]. Several residues in the DHp α -helix and in the receiver domain determine specificity of the histidine kinase-response regulator interaction ensuring correct positioning of the receiver aspartate towards the phosphoryl group residing on the histidine in the Dhp domain [164]. It even has been shown that, by mutating several of these residues responsible for molecular recognition it is possible to rewire non-cognate histidine kinases and receiver domains [160].

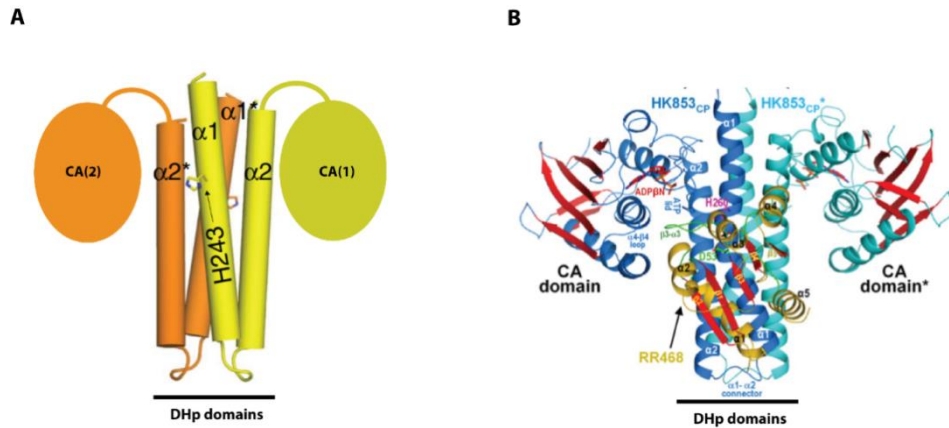


Figure 6: Structural representation of histidine kinases. (A) Schematic drawing of the dimer of the *E. coli* histidine kinase EnvZ. The two protomers are shown in yellow and orange. **(B)** Crystal structure of the *Thermotoga maritima* histidine kinase HK853 in complex with its cognate response regulator RR468. The protomers of the DHp and CA domains are shown in blue and cyan. RR468 is shown in gold and yellow. Figure adapted from [165,166]

In addition it has been shown that histidine kinases not only have kinase activity but most of them also harbour phosphatase activity [167–169]. However, phosphatase activity is not just a reversal of the kinase activity since no backtransfer of the phosphoryl group from the receiver domain aspartate to the histidine residue in the DHp domain takes place [158]. In some cases, the histidine is involved in catalyzing the hydrolysis of the phosphoryl group on the receiver aspartate, but it has been reported, that in some cases the histidine is not necessary for removal of the phosphoryl group [170]. However, it has convincingly been demonstrated that the phosphatase activity is dependent on the DHp domain and that a specific stretch of amino acids next to the acceptor histidine is required for phosphatase function [167,168,171,172]. The signals switching the activities of histidine kinases are poorly understood. It has been shown *in vitro*, that ADP might be an activator of phosphatase activity but *in vivo* evidence is missing.

***Caulobacter crescentus* cell cycle**

To ensure survival of a species, all living organisms have to reproduce. Bacteria usually reproduce by cell division. This highly coordinated process involves cell growth, division and other mechanisms that enable the cell to produce viable offspring. A very useful organism to study the underlying processes of cell cycle progression is *C. crescentus* [35]. In this aquatic bacterium, cell cycle progression is tightly linked to the developmental stages (Fig. 7). One of the stages in the *C. crescentus* cell cycle is represented by the swarmer cell. This cell type typically has one polar flagellum and is therefore motile [173]. However, at this stage the cell is not able to replicate its chromosome [37,174]. After a while, motile swarmer cells transform into stalked cells. During this transition, the flagellum is ejected and at the same pole, an extension of the cell membrane, the stalk, grows [175]. At the tip of the stalk, there is a strongly adhesive compound called the holdfast. The holdfast enables the cells to attach permanently to surfaces. The transition from a motile swarmer cell to a sessile stalked cell temporally coincides with the initiation of chromosome replication [37]. The cell then continues to grow, replicates its chromosome and develops into a predivisional cell. The predivisional cell contains two chromosomes each anchored to the opposing cell poles via the origin of replication [176,177]. The predivisional cell harbours a flagellum at the non-stalked cell pole. Septation finally releases one stalked and one swarmer cell. The stalked cell will immediately restart the next round of replication while the swarmer cell first has to differentiate into a stalked cell. This coupling of development and cell cycle progression has made *C. crescentus* a well-studied model organism.

CtrA – Central transcriptional activator

In *C. crescentus*, chromosome replication at the swarmer to stalked cell transition is initiated by the transcription factor CtrA (central transcriptional activator A)[37,42,44,178]. CtrA consists of a receiver domain and a Helix-turn-Helix DNA binding domain [179]. As a transcription factor, CtrA binds to characteristic CtrA binding boxes which are found all over the chromosome [180]. These binding boxes contain a T⁺TAA-N₇-AATT motif and phosphorylation of the CtrA receiver domain is thought to enhance DNA binding affinity in most cases [41,178]. CtrA controls over 100 promoters, driving the expression of genes involved in a wide variety of cellular processes [178,180]. In addition to its function as a transcription factor, CtrA also blocks replication initiation. The *C. crescentus* origin of replication (oriC) is overlapped by five CtrA binding sites. These sites overlap with binding sites for DnaA, a

protein initiating replication and thereby, occupation by CtrA blocks replication initiation [41].

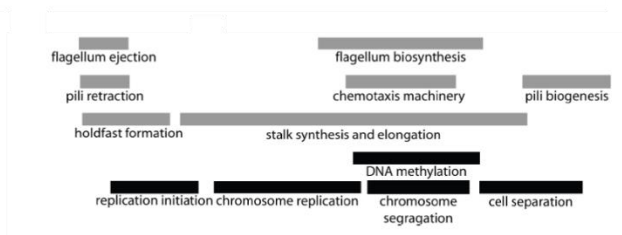
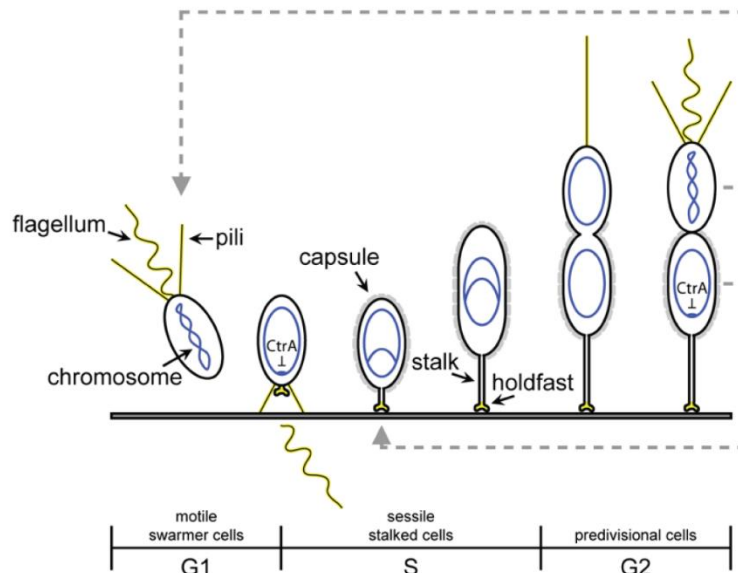


Figure 7: Schematic overview of the *Caulobacter* cell cycle. Chromosomes are depicted in blue and polar appendages in yellow. Black bars represent appearance and duration of cell cycle events while grey bars represent morphogenetic events. Figure was adapted from Sören Abel and [181].

Since CtrA is involved in the control of many essential functions, it is controlled tightly throughout the cell cycle. CtrA transcription is regulated in dependence of the cell cycle [180,182]. CtrA is expressed in the predivisive and swarmer cell and expression is turned off at the swarmer to stalked cell transition (Fig. 7). Once CtrA is expressed, its activity is regulated by protein degradation and the phosphorylation status of the receiver domain [43,178]. At the transition to the stalked cell, the activity of CtrA is reduced. This is achieved by dephosphorylation of the CtrA receiver domain and degradation of CtrA. CtrA is a substrate of the ClpXP protease which gets localized to the stalked pole

during G1-S transition in a CpdR dependent process [178,183]. CtrA also gets localized to the stalked pole where it is degraded by ClpXP [183,184]. Localization of CtrA to the stalked pole depends on PopA [34]. PopA is a PleD homologue with a degenerate GGDEF site which brings CtrA to the stalked pole in a c-di-GMP dependent manner [34,47,185]. The second mechanism to control CtrA activity relies on phosphorylation of the CtrA receiver domain by the CckA-ChpT-CtrA phosphorelay. The phosphorylation status of the CtrA receiver domain is controlled by the CckA-ChpT-CtrA phosphorelay [186–188]. CckA is a histidine kinase which transfers a phosphate from its receiver domain to the phosphotransferase ChpT. ChpT finally transfers the phosphate either to CtrA or CpdR [189].

CckA controls CtrA phosphorylation

CckA is a membrane-bound hybrid histidine kinase consisting of two transmembrane helices, two PAS domains, two core kinase domains (DHP and CA) and a receiver domain [187]. The function of the two PAS domains is unknown. The CA domain binds ATP and transfers the γ -phosphate onto a conserved histidine residue in the DHP domain. The transmembrane domains localize CckA to the cell membrane. In a swarmer cell, CckA is uniformly distributed in the cell membrane and is thought to be active as a kinase. This keeps levels of CtrA~P high thereby blocking replication initiation [187,190,191]. At the swarmer to stalked cell transition, CckA remains uniformly distributed in the membrane but most likely switches its activity from kinase to phosphatase, thereby dephosphorylating CtrA [170] (Fig. 8). In the predivisional cell, CckA localizes to both cell poles and forms distinct foci. At this stage, it was hypothesized, that CckA is active as a phosphatase at the stalked pole but active as a kinase at the swarmer pole. This would result in a CtrA phosphorylation gradient inside the predivisional cell [192]. The resulting CtrA~P phosphorylation gradient across the predivisional would prepare the different poles for their future fate after cell division (Fig. 8). Since regulation of CckA activity is crucial for cell cycle progression, the protein has been studied extensively.

Recent work suggested that CckA interacts with the pseudo histidine kinase DivL [193]. The DivL structure shows a conserved histidine kinase-fold, but the critical phospho-accepting histidine residue is mutated to a tyrosine and therefore most likely no longer capable of accepting phosphoryl groups [194]. Furthermore, the histidine kinase domains are dispensable for cell viability although the full length protein is essential [195,196]. It has been hypothesized that DivL might be a localization factor for CckA but these data remain largely

inconclusive. One of the functions of DivL could be to change CckA activity in the presence of phosphorylated DivK [193]. DivK is a single domain response regulator which has been shown to interact with DivL primarily in its phosphorylated state. The authors convincingly describe that phosphorylated DivK switches CckA from kinase into phosphatase mode by interacting with DivL, but there seems to be no direct interaction between DivK and CckA [193] (Fig. 8).

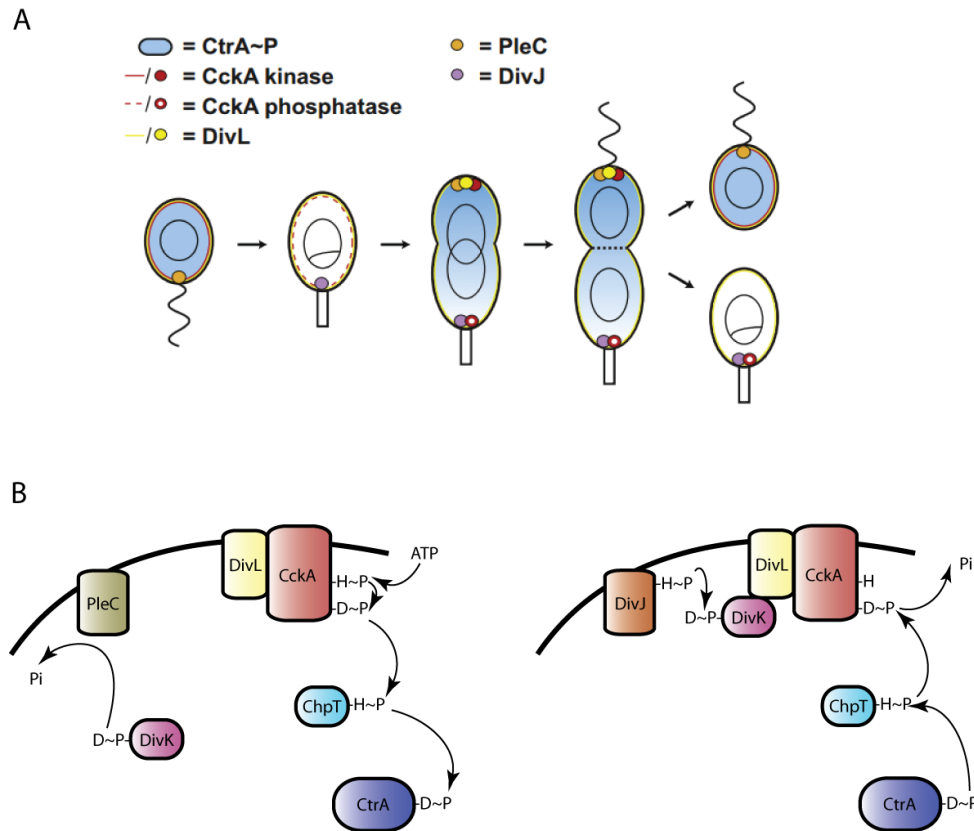


Figure 8: Cell cycle-specific regulation of CckA. (A) CtrA regulatory factors are shown. CckA activity switches from kinase to phosphatase at the swarmer to stalked cell transition. In the predivisive cell, CckA shows a bipolar localization which ultimately results in a CtrA phosphorylation gradient across the predivisive cell (light blue). Localization of DivL, PleC and DivJ is indicated. **(B)** Current model of the CckA regulation. DivK is phosphorylated by DivJ and dephosphorylated by PleC. Phosphorylation of DivK promotes interaction with DivL, which permanently interacts with CckA. If bound to DivK~P DivL switches CckA from kinase to phosphatase mode. Figures adapted from [192,193]

DivK itself is regulated by several histidine kinases, two of which are known [45]. In the swarmer cell, DivK is kept in the non-phosphorylated form by the histidine kinase PleC [45]. PleC is thought to be a bifunctional histidine kinase/phosphatase but in the swarmer cell, it is predominantly active as phosphatase [45,197] (Fig. 8). At the swarmer to stalked cell transition, PleC disappears from the stalked pole and is replaced by the histidine kinase DivJ [45,198]. At this stage, DivJ phosphorylates DivK which then switches CckA from kinase into phosphatase mode [193]. Later in the cell cycle DivJ adopts a bipolar localization while PleC reappears at the new flagellated pole. A current model suggests that in the predivisional cell, this configuration keeps DivK phosphorylated at the stalked pole while PleC keeps levels of phosphorylated DivK low in proximity of the flagellated pole [192,199]. The activities of PleC and DivJ would therefore provide an explanation for the underlying mechanisms required to form a CtrA phosphorylation gradient. DivK is not only controlled by PleC and DivJ, but it also acts as a positive regulator of these two kinases [45]. This forward feedback loop ensures a rapid increase of phosphorylated DivK at the swarmer to stalked cell transition. Interestingly, PleC and DivJ not only phosphorylate DivK but also the strong c-di-GMP cyclase PleD [7,12,200,201]. Phosphorylation of the receiver domain leads to localization of PleD to the stalked pole where it is presumably active at the swarmer to stalked cell transition providing the cell with high levels of c-di-GMP [200].

The general stress response

In the environment, bacteria encounter a multitude of stresses. Adaption to stress is therefore essential for bacterial survival. Response to stress requires expression of genes that prevent the cells from damage. Stress adaptation in α -proteobacteria involves the alternative sigma factor SigT required for the expression of stress related genes [202] (Fig. 9). In the cell, SigT activity is prevented by the anti-sigma factor NepR [203,204]. Upon stress perception, SigT is freed from NepR [205,206]. The mechanism of SigT activation depends on the activation of a two component system [202]. Releasing SigT requires a partner switch mechanism including PhyR [206,207]. PhyR is an anti-sigma factor antagonist consisting of a C-terminal receiver domain and an N-terminal sigma-like domain [208]. The sigma-like domain resembles the SigT transcription factor. Once PhyR is phosphorylated, it undergoes a conformational change resulting in sequestration of NepR and thereby releases SigT [203,204] (Fig. 9). Therefore, phosphorylation of PhyR is a crucial step for stress adaptation [209]. Numerous PhyR activating kinases (PAK) have been

shown to phosphorylate PhyR [202,210,211]. The input signals which activate these kinases are poorly understood. The only direct histidine kinase-activating signal described so far is blue light [211–213]. Other input signals are not known.

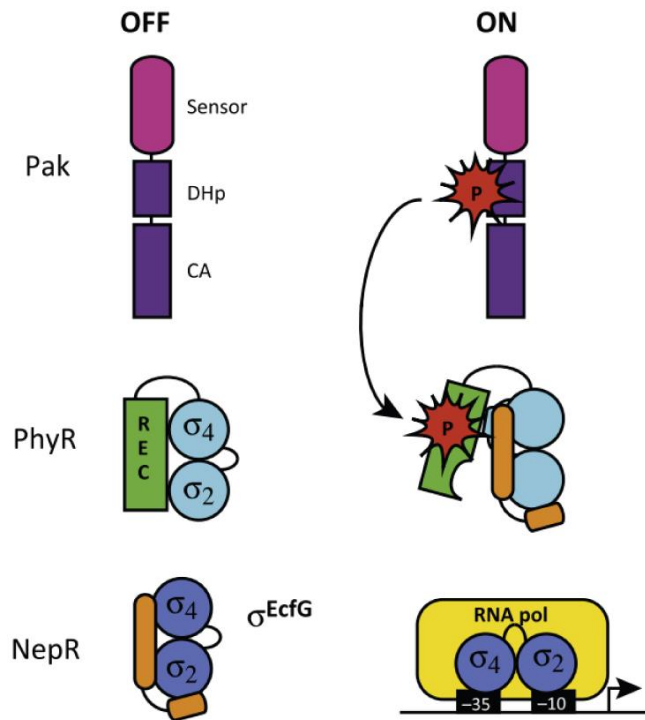


Figure 9: Activation of stress response in alphaproteobacteria. Schematic overview of activation of the general stress response in alphaproteobacteria. Phosphorylation of PhyR by dedicated PhyR-phosphorylating kinases (PAK) leads to release of Sig^{EcfG} (SigT in *C. crescentus*) from NepR by a partner switch mechanism [208]. This ultimately leads to transcription of stress related genes. Figure adapted from [208].

Aim of the thesis

The second messenger c-di-GMP is a central regulator of lifestyle decisions in bacteria. During the past ten years, a considerable amount of knowledge has been acquired on c-di-GMP signaling but its involvement in core cell cycle circuitry remains elusive. In this work, *Caulobacter crescentus* will be used to investigate the role of c-di-GMP on the cell cycle. Specifically, the G1-S transition will be followed in detail and the underlying mechanisms explored. The central components of this complex regulatory system will be assayed in an *in vitro* set up and the response to c-di-GMP will be tested. Moreover, the *in vivo* data will demonstrate the importance of c-di-GMP during the G1-S transition. Additionally, biochemical and structural analysis will give insights into the mechanisms which underlie kinase and phosphatase activities. Histidine kinases and response regulators also control various other functions in *C.crescentus*. Especially complex phosphorylation networks are required for stress adaptation. In the second part, the phosphorylation cascade leading to the activation of the general stress response will be analyzed in detail using biochemical approaches.

Results

Cyclic di-GMP acts as a cell cycle oscillator to drive chromosome replication

C. Lori*, S. Ozaki*, S. Steiner, R. Böhm, S. Abel, B. N. Dubey, T. Schirmer, S. Hiller & U. Jenal

* Both authors contributed equally to this work

Nature **523**, 236-239 (09 July 2015) [49]

Comments on article:

Linking cell differentiation and growth

Nature Reviews Microbiology **13**, 398-399 (2015) [214]

Cyclin-like function of bacterial c-di-GMP

Science Signalling **386**, 195 (2015) [215]

Statement of my work

The project was initiated after I made the observation that CckA is regulated by c-di-GMP. Subsequently, I performed all assays showing the *in vitro* activity and c-di-GMP binding of CckA. Plasmid construction and protein expression was done by me with the help of Samuel Steiner. Additionally, *in vivo* FROS and CckA overexpression experiments were also done by myself, as well as measurement of *in vivo* phosphorylation levels.

Cyclic di-GMP acts as a cell cycle oscillator to drive chromosome replication

Lori, C.*¹, Ozaki, S.*¹, Steiner, S.^{1,3}, Böhm, R.², Abel, S.^{1,4}, Dubey, B.N.², Schirmer, T.², Hiller, S.² & Jenal, U.^{1,5}

Affiliations:

¹Focal area of Infection Biology, Biozentrum, University of Basel

² Focal area of Structural Biology and Biophysics, Biozentrum, University of Basel

³Current address: Yale University School of Medicine, Boyer Center for Molecular Medicine, 295 Congress Avenue, New Haven, CT 06536, USA

⁴ Current address: UiT, The Arctic University of Norway, Department of Pharmacy, Faculty of Health Sciences, N-9037 Tromsø, Norway

⁵ For correspondence: urs.jenal@unibas.ch

* equal contribution

Key words: Two-component system; histidine kinase/phosphatase; phosphorylation cascade; c-di-GMP; cell cycle regulation; cell fate determination; replication initiation; cyclin; bacteria; *Caulobacter crescentus*.

Summary:

Fundamental to all living organisms is the capacity to coordinate cell division and cell differentiation to generate appropriate numbers of specialized cells. While eukaryotes use cyclins and cyclin-dependent kinases to balance division with cell fate decisions, equivalent regulatory systems have not been described in bacteria. Moreover, the mechanisms used by bacteria to tune division with developmental programs are poorly understood. Here we demonstrate that *Caulobacter crescentus*, a bacterium with an asymmetric division cycle, uses oscillating levels of the second messenger c-di-GMP to drive its cell cycle. We demonstrate that c-di-GMP directly binds to the essential cell cycle kinase CckA to inhibit kinase and stimulate phosphatase activity. An upshift of c-di-GMP during the G1-S transition switches CckA from the kinase into the phosphatase mode, thereby licensing replication initiation and cell cycle progression. Finally, we show that during division, c-di-GMP imposes spatial control on CckA to install replication asymmetry of future daughter cells. These studies expose c-di-GMP as a cyclin-like molecule in bacteria that coordinates chromosome replication with cell morphogenesis in *Caulobacter*. The observation that c-di-GMP mediated control is conserved in the plant pathogen *Agrobacterium tumefaciens* unfolds a general mechanism through which this global regulator of bacterial virulence and persistence coordinates behaviour and cell proliferation.

To enable tissue homeostasis, metazoans tightly regulate the balance between cell proliferation and differentiation [216]. Central players in cell proliferation, development and cell fate decisions are cyclin-dependent kinases (CDKs) [217,218]. To drive cell cycle progression, CDKs associate with oscillating, stage-specific regulatory subunits called cyclins [219]. While in higher organisms cells generally undergo terminal differentiation, bacteria often rely on rapid growth to exploit available nutrients and thus need to dynamically tune behavioural programs with cell proliferation. How exactly bacteria couple behavioural processes with cell cycle progression remains unclear.

A prime model to study the coupling of cell growth and behaviour in bacteria is the aquatic organism *Caulobacter crescentus*, which strictly separates cell motility from cell proliferation. *C. crescentus* divides asymmetrically to generate two specialized progeny, a sessile and replication competent stalked and a motile and replication inert swarmer cell. The swarmer cell (G1-phase) re-enters the replication cycle during differentiation into a stalked cell (S-phase) (Figure 1a). To control the motile-sessile transition, *C. crescentus* makes use of c-di-GMP, a second messenger controlling a wide range of behavioural processes in bacteria, including virulence, motility and biofilm formation [6]. C-di-GMP levels are low in swarmer cells, increase during differentiation to peak in stalked cells and later reach intermediate levels in the predivisional cell [38]. One of the main drivers of c-di-GMP fluctuations is the diguanylate cyclase PleD, which is active in stalked but turned off in swarmer cells [220] (Figure 1a). While a *pleD* mutant has reduced levels of c-di-GMP, a strain lacking all diguanylate cyclases (cdG0) is devoid of c-di-GMP [38]. The complete loss of motility and surface attachment in the cdG0 strain illustrates the importance of c-di-GMP oscillation for *Caulobacter* cell fate determination [38]. In contrast, the role of c-di-GMP in cell cycle progression is unclear.

Our studies originated from a genetic screen for synthetic lethal mutants in the cdG0 background. This strain, although viable, shows pronounced morphology and cell cycle defects [38]. We thus reasoned that c-di-GMP controls cell cycle progression together with a parallel pathway with partial functional redundancy. The screen revealed a strain with a transposon (Tn) insertion in the promoter region of the gene encoding the single-domain response regulator DivK (*PdivK::Tn*) (Extended Data Fig. 1a). Crossing back the Tn into the cdG0 mutant produced a strain with severe cell cycle defects

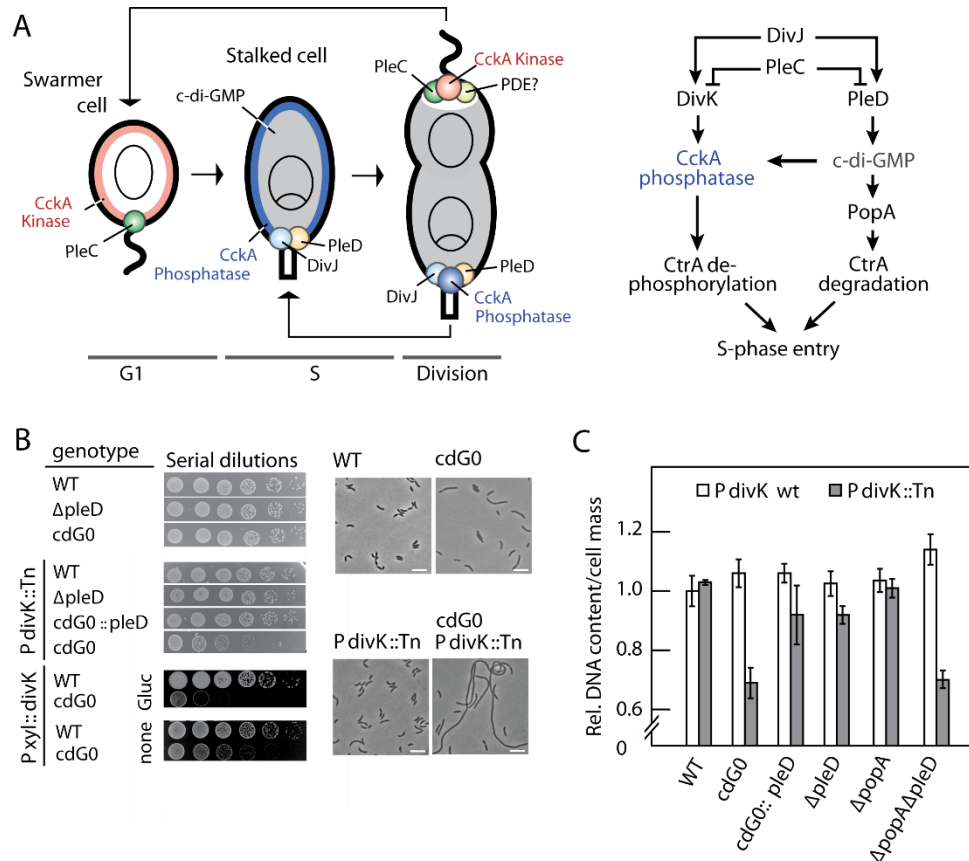


Figure 1: C-di-GMP regulates cell cycle progression via the CckA-CtrA phosphorelay.

(a) Left: Localization of CckA and factors regulating CckA activity throughout the *C. crescentus* cell cycle. CckA kinase (red) and phosphatase (blue) activities are indicated. High and low levels of c-di-GMP are shown as grey or white areas, respectively. PDE=phosphodiesterase. Right: Regulatory modules inactivating CtrA to control *Caulobacter* S-phase entry. **(b)** Growth (left) and cell morphology (right) of strains indicated. 5-fold serial dilutions are shown. P xyl::divK strains were grown on PYE (none) or PYE glucose (Gluc) plates. Representative of two biological replicates is shown. **(c)** Effect of P divK::Tn on DNA replication in different genetic backgrounds. DNA content and cell mass were determined by flow cytometry. Averages and standard deviations for DNA content/cell mass were obtained from 4 biological replicates.

(Figure 1b, Extended Data Fig. 1b). This, and the observation that the DNA content per cell mass unit was severely reduced (Figure 1c), indicated that cells are severely compromised for replication initiation. In contrast, growth, division and replication were not affected when the *PdivK::Tn* was crossed into a cdG^+ strain (Figure 1b, c). DivK levels were reduced about 10-fold in the $cdG0$ *PdivK::Tn* strain (Extended Data Fig. 1c), suggesting that DivK may be limiting for growth. This was confirmed by replacing the *divK* promoter upstream of the *divK* gene with the xylose-dependent promoter *P_{xyI}*. In the absence of the inducer or in the presence of glucose, which further represses *P_{xyI}* activity, DivK levels were strongly reduced compared to wild type (Extended Data Fig. 1d), resulting in severely reduced growth and replication in the $cdG0$ strain, but not in a cdG^+ background (Figure 1b, Extended Data Fig. 1e). Together, this indicated that c-di-GMP and DivK convergently regulate cell cycle progression.

DivK was recently shown to down-regulate the central cell cycle kinase CckA through a direct interaction with DivL, an unorthodox kinase that controls CckA via protein-protein interaction [46,194]. CckA initiates a phosphorelay controlling the activity of the response regulator CtrA [187,221] (Figure 1a). CtrA is phosphorylated and active in swarmer cells (G1) where it binds to the origin of replication (*Cori*) to inhibit replication initiation [178]. During differentiation into stalked cells CtrA is inactivated to license replication initiation [44]. CckA is bifunctional and can act both as kinase and as phosphatase to control CtrA via the phosphotransfer protein ChpT [170]. Accordingly, switching CckA from kinase to phosphatase activity during G1-S would rapidly reverse the phosphate flux to inactivate CtrA and authorize replication initiation. Hence, we reasoned that DivK and c-di-GMP could cooperate to inactivate CtrA. Because c-di-GMP controls CtrA degradation during G1-S transition through the effector protein PopA [34] (Figure 1a), the G1 arrest of the $cdG0$ *PdivK::Tn* strain could conceivably result from simultaneous over-activation and stabilization of CtrA. However, a mutant combining the *PdivK::Tn* allele with a *popA* deletion stabilizing CtrA was not affected in growth or DNA replication. In contrast, a *PdivK::Tn* $\Delta popA$ strain that also lacked PleD, produced a strong G1 arrest (Figure 1c, Extended Data Fig. 1f). From this we concluded that c-di-GMP regulates both stability and phosphorylation levels of CtrA during the cell cycle (Figure 1a).

To analyze how c-di-GMP regulates CtrA activity, individual components of the CckA-CtrA phosphorelay were purified and examined *in vitro*. In the absence of c-di-GMP CckA autophosphorylation and phosphotransfer via

ChpT to CtrA were readily observed. Strikingly, the addition of c-di-GMP completely abolished phosphorylation of all three components (Extended Data Fig. 2a). When CckA auto-phosphorylation was first carried out in the absence of c-di-GMP followed by the addition of c-di-GMP to the reaction mixture, rapid dephosphorylation of CckA was observed, arguing that c-di-GMP is a potent stimulator of CckA phosphatase activity (Figure 2a, Extended Data Fig. 2b). Stimulation of the CckA phosphatase was specific to c-di-GMP with GMP, GTP or cGMP having no observable effect (Figure 2a). Experiments with all three components of the phosphorelay demonstrated that c-di-GMP effectively reverses the phosphate flux of the phosphorelay leading to the inactivation of CtrA (Figure 2b). To test if c-di-GMP also regulates CckA kinase activity we compared phosphorylation of wild-type CckA with CckA(V366P), a mutant lacking phosphatase activity *in vitro* (Extended Data Fig. 2c) [170]. When c-di-GMP was added together with [³²P]ATP at reaction start, CckA(V366P) phosphorylation was strongly reduced as compared to a control lacking c-di-GMP (Extended Data Fig. 2c), indicating that c-di-GMP inhibits CckA kinase activity.

These experiments demonstrated that c-di-GMP is a potent trigger to switch CckA from its default kinase into the phosphatase state. Consistent with this, purified CckA specifically binds radiolabeled c-di-GMP (Figure 2c, Extended Data Fig. 2d). Further studies exposed the catalytic ATP-binding domain (CA) as minimal binding region for c-di-GMP (Extended Data Fig. 2e-g). To identify amino acid residues of the CA domain that are specifically involved in c-di-GMP binding, we concentrated on a candidate mutation that was recently isolated in the CckA homolog of the plant pathogen *Agrobacterium tumefaciens* (CckA_{At}). In this organism a spontaneous Y674D substitution in the CA domain of CckA_{At} was isolated as a motile suppressor of a mutant lacking PleC [222]. We hypothesized that CckA_{At} is also regulated by c-di-GMP and that in a *pleC* mutant with elevated levels of c-di-GMP (Figure 1a) the Y674D mutation restores its kinase/phosphatase balance by interfering with c-di-GMP binding. As shown in Extended Data Fig. 2h, autophosphorylation of purified wild-type CckA_{At} was specifically reversed when c-di-GMP was added, while the CckA_{At}(Y674D) mutant failed to respond to c-di-GMP. Moreover, c-di-GMP binding to CckA_{At}(Y674D) was strongly reduced as compared to the wild-type form of the protein (Extended Data Fig. 2h).

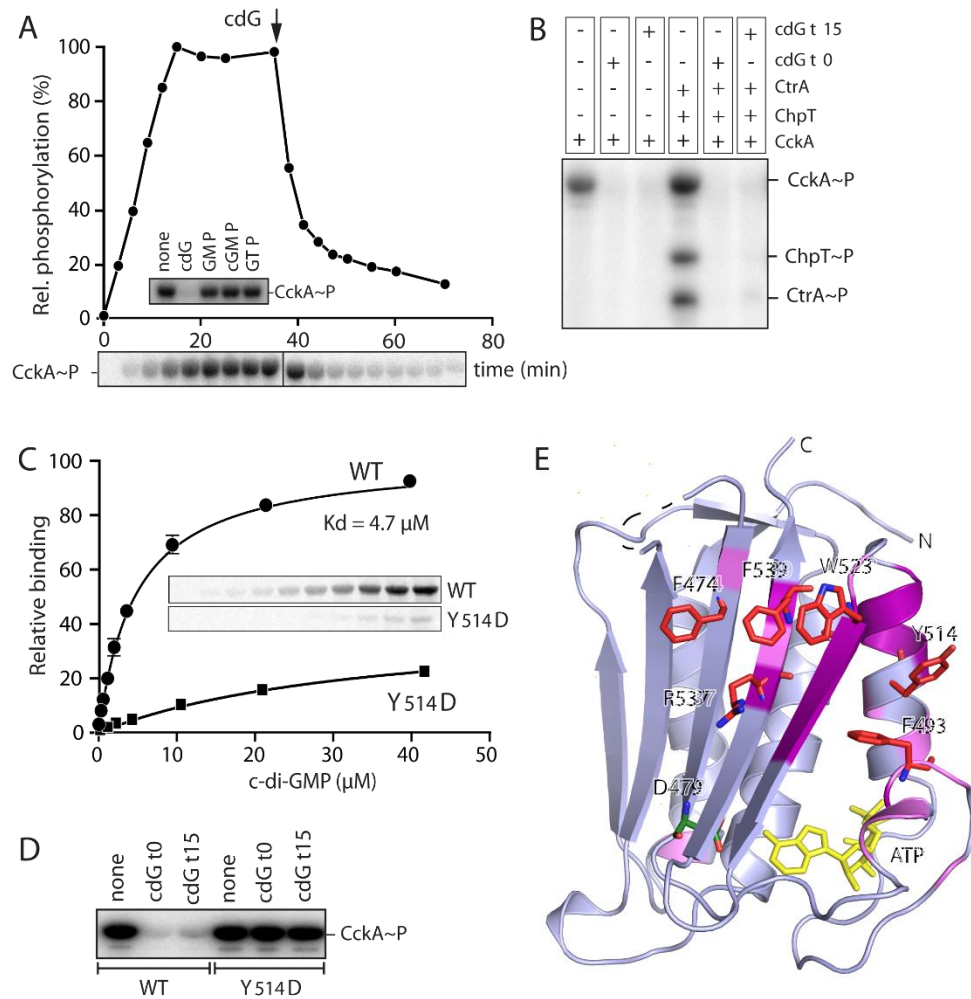


Figure 2: C-di-GMP binds to the catalytic domain to induce CckA phosphatase activity.

(a) C-di-GMP specifically stimulates CckA dephosphorylation. CckA phosphorylation reactions were started by adding [32 P]ATP (0 min) and supplemented with c-di-GMP (75 μ M) at the time indicated (arrow). The inset shows CckA phosphorylation reactions supplemented with c-di-GMP and other nucleotides (75 μ M). Representative of two technical replicates is shown. **(b)** C-di-GMP reverses the phosphate flux of the CckA-ChpT-CtrA phosphorelay. Reactions were run for 30 min and c-di-GMP was added together with [32 P]ATP at time 0 min (t0) or 15 min after reaction start (t15). Representative of three technical replicates is shown. **(c)** C-di-GMP binding affinity of CckA. Binding of wild-type CckA (WT) and CckA(Y514D) was determined by UV-crosslinking at increasing concentrations of [33 P]c-di-GMP(inset) and quantified as shown in the graph. Averages and standard deviations were obtained from three technical replicates. **(d)** C-di-GMP fails to

stimulate phosphatase activity of the CckA(Y514D) mutant. Phosphorylation reactions with wild-type CckA (WT) and Y514D mutant protein were analysed without (none) or with c-di-GMP added at time point 0 (t0) or after 15 min (t15). Representative of three technical replicates is shown. **(e)** Homology model of the CA domain of CckA based on a crystal structure of DivL (pdb 4q20). Residues that show large ($\Delta\delta(\text{HN}) > 2$ s.d.) and intermediate ($2 \text{ s.d.} > \Delta\delta(\text{HN}) > 1$ s.d.) amide chemical shift perturbations upon addition of c-di-GMP are shown in purple and pink, respectively. Side chains of residues that contribute to c-di-GMP binding and c-di-GMP mediated phosphatase activity are shown in stick representation and coloured in red. A single molecule of ATP (yellow) was modelled into its putative binding site based on homology to CpxA (PDB: 4bix). D479, which is involved in ATP binding, is shown green. For more information, see legend to Extended Data Fig. 3.

The equivalent substitution in *Caulobacter* CckA (Y514D) also resulted in strongly diminished c-di-GMP binding (Figure 2c). Importantly, the CckA(Y514D) mutant showed normal kinase activity but failed to dephosphorylate upon addition of c-di-GMP (Figure 2d). This was not due to a general lack of phosphatase activity, as the CckA(Y514D) mutant showed unaltered basal level phosphatase activity upon ATP depletion (Extended Data Fig 2i). Together this demonstrated that CckA(Y514D) is compromised for c-di-GMP binding and, as a consequence, cannot switch to the phosphatase mode upon addition of c-di-GMP, resulting in constitutive CckA kinase activity *in vitro*. To define the c-di-GMP binding pocket on the surface of the CA domain we used a combination of structural modelling, biochemical analysis and NMR spectroscopy (Figures 2e, Extended Data Figs. 2i and 3a, b). This approach identified a set of six amino acids, F474, F493, Y514, W523, R537, and F539, which show significant NMR chemical shift perturbations upon c-di-GMP titration experiments and are strictly required for c-di-GMP binding and phosphatase but not kinase activity (Figure 2e, Extended Data Figs. 2i and 3b). All of these residues locate in close proximity of Y514 in a homology model of CckA (Figure 2e). Interestingly, six of these amino acid residues feature aromatic side chains and are well conserved in CckA homologs (Extended Data Fig. 4). This argues that c-di-GMP is coordinated by the CA domain of CckA via hydrophobic interactions, akin to the binding mode described for the human STING receptor [192].

Next, we set out to test if c-di-GMP executes its important cell cycle role primarily by interfering with the CckA kinase/phosphatase balance *in vivo*. We reasoned that a combination of *PdivK::Tn* and *ckkA(Y514D)* should cause a

similar G1 arrest as observed for a strain lacking c-di-GMP altogether. Moreover, this combination should lead to a cell cycle arrest irrespective of the presence of c-di-GMP (Extended Data Fig. 5a). Indeed, cells carrying *PdivK::Tn* and *cckA(Y514D)* showed severe growth defects (Figure 3a), increased binding of CtrA to the Cori region (Extended Data Fig. 5b), and a strong G1 arrest (Figure 3b, Extended Data Fig. 5c). While this phenotype was independent of PleD, viability of the CckA phosphatase mutant (V366P) strictly depended on c-di-GMP (Figure 3a, b, Extended Data Fig. 5c). This indicated that down-regulation of CckA kinase activity by c-di-GMP is sufficient to balance the kinase/phosphatase activities of the V366P mutant. To corroborate these findings we tested the same *cckA* alleles in strains expressing *divK* from the xylose-dependent promoter *P_{xyI}*. When *P_{xyI}::divK* cells were grown in the absence of xylose, DivK dropped below 10% of wild type and, as a consequence, cells developed a mild G1 arrest (Extended Data Fig. 5d).

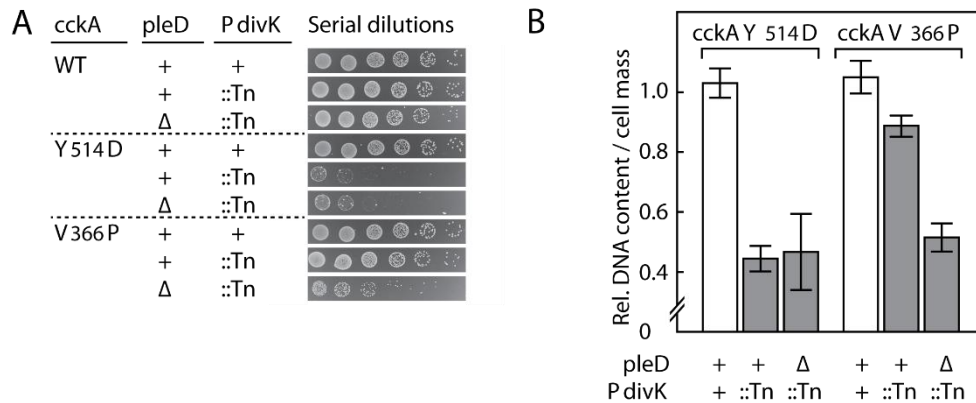


Figure 3: C-di-GMP controls CckA activity to initiate chromosome replication.

(a) The *cckA(Y514D)* allele shows synthetic lethality with *PdivK::Tn*. 5-fold serial dilutions of strains containing combinations of *cckA*, *PdivK*, and *pleD* alleles were incubated on PYE plates for 2 days. Representative of two biological replicates is shown. **(b)** Combining the *cckA(Y514D)* and *PdivK::Tn* alleles leads to a G1 arrest. Exponential cultures of mutants containing combinations of *cckA*, *PdivK*, and *pleD* alleles were analysed by flow cytometry. Values of DNA content per cell mass are shown relative to *C. crescentus* wild type and were obtained as described in the legend for Figure 1c. Averages and standard deviations were obtained from three replicates.

This effect was aggravated in strains expressing *ckA(Y514D)* resulting in a strong reduction of the DNA/cell mass ratio (Extended Data Fig. 5d), severely reduced growth (Extended Data Fig. 5e), increased CckA~P phosphorylation levels (Extended Data Fig. 5f) and an overall reduction of the number of chromosomal origins per cell mass (Extended Data Fig. 5g).

Taken together, these experiments lead us to propose a model where two convergent regulatory inputs, DivK and c-di-GMP, control the CckA kinase/phosphatase switch to authorize G1-S transition through the inactivation of the replication initiation inhibitor CtrA (Figure 1a). Intriguingly, cell type specific activity of both PleD and DivK is regulated by DivJ and PleC, two histidine kinase/phosphatase antagonists, which localize to opposite poles of the predivisional cell and during division asymmetrically partition into the daughter cells to determine their respective programs (Figure 1a) [223]. Thus, the two regulators show similar activation profiles during the cell cycle [45,220], thereby imposing tight coordination between the DivK branch and the c-di-GMP branch of the CckA switch. This connection is further strengthened by the role of DivK as allosteric activator of the DivJ kinase, a positive feedback mechanism through which both DivK and PleD activity can be rapidly upregulated during G1-S transition [45]. Hence, DivK and c-di-GMP act as molecular connectors between two hierarchical phosphorylation modules, explaining how the cellular dynamics of PleC and DivJ translate into differential activities of the central cell cycle kinase CckA (Figure 4). Because the parallel morphogenetic program critically depends on PleD activation and the concomitant rise in c-di-GMP concentration [38], c-di-GMP induced inactivation of CtrA directly couples development to cell cycle progression. This is reminiscent of redundant pathways regulating cell cycle progression in higher eukaryotes, where a multitude of signals converge to control the activity of CDKs [224,225].

In addition to its role in G1-S transition, CckA facilitates cell polarity during division. CckA localizes to both poles of dividing *Caulobacter* cells but adopts differential kinase/phosphatase activities at opposite poles [191,192] (Figure 1a). The resulting cellular gradient of CtrA~P was proposed to establish asymmetric replication activities, which propagate to future daughter cells [192]. To test if c-di-GMP contributes to replication asymmetry during division we made use of fluorescent repressor-operator systems (FROS) to spatially resolve replication initiation events (Extended Data Fig. 6a,b) [226]. While in a majority of wild-type cells chromosome replication originated at the old stalked pole, cells expressing *ckA(V366P)* or *ckA(Y514D)* lost replication

asymmetry almost entirely (Extended Data Fig. 6c). Cells lacking PleD also partially lost their replication preference for the stalked pole. Because active PleD, PleD~P, specifically localizes to the stalked pole [200,220], we analysed replicative asymmetry in a cdG0 strain expressing a heterologous diguanylate cyclase, DgcZ, from *E. coli*, which is uniformly distributed in the cell [14,38]. Although expression of *dgcZ* restored all developmental defects in this strain [38], it failed to establish the characteristic spatial replication bias (Extended Data Fig. 6c). From this we conclude that the spatial organization of c-di-GMP metabolism contributes to cell polarity by differentially regulating CckA at opposite cell poles. For example, a local environment with high levels of c-di-GMP might impose CckA phosphatase activity at the stalked pole. Alternatively, a local trough of c-di-GMP may exist at the swarmer pole with the rest of the cell body containing high levels of c-di-GMP. To distinguish between these possibilities, we made use of a CckA variant that is unable to localize to cell poles because it lacks its membrane anchor (*cckAΔTM*). Expression of this mutant causes massive over-replication and cell filamentation, arguing that delocalized CckA functions primarily as a phosphatase for CtrA [170]. In agreement with this, expression of *cckAΔTM(V366P)*, lacking phosphatase activity, did not show any adverse effects (Extended Data Fig. 6d). Strikingly, expression of *cckAΔTM(Y514D)* in a cdG⁺ strain (Extended Data Fig. 6d) or expression of *cckAΔTM* in a strain lacking c-di-GMP (Extended Data Fig. 6e) led to a strong G1 arrest, a hallmark of the CckA kinase mode. This indicated that the cellular pool of c-di-GMP strictly imposes phosphatase activity on delocalized CckA molecules.

Based on these results we propose that the bulk volume of dividing *C. crescentus* cells experiences high levels of c-di-GMP and that CckA adopts strong kinase activity at the swarmer pole as a consequence of a microenvironment with low levels of c-di-GMP. This view is consistent with the idea that sequestration of CckA to the swarmer pole creates a microenvironment within the cell where CckA can avoid down-regulation by its other inhibitor, DivK~P [46,192]. We propose that CckA sequestration to this subcellular site also shields the protein from the cellular pool of c-di-GMP. Ultimately, it is the PleC phosphatase that reduces PleD~P and DivK~P levels at this subcellular site and, possibly together with one or several swarmer pole specific phosphodiesterases, imposes this spatial regime (Figure 1a, 4). The input from c-di-GMP might also explain how the entire cellular pool of CckA can be tightly regulated. Throughout the cell cycle, CckA localization is often patchy and dynamic without being strictly limited to polar regions [191]. Since the degree of co-localization of DivK and CckA is unclear, c-di-GMP could effectively maintain

CckA in the phosphatase state in all cell types or subcellular regions harbouring high levels the second messenger.

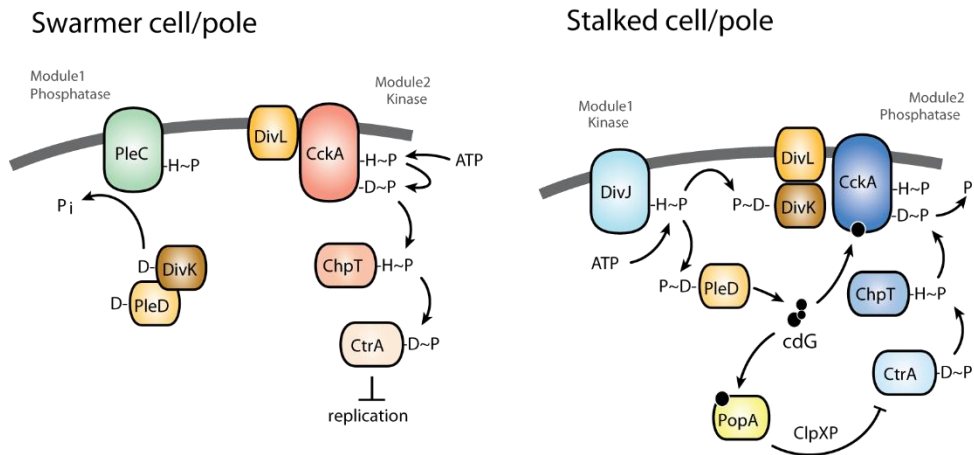


Figure 4: Model of the regulatory circuitry controlling cell cycle progression in *C. crescentus*.

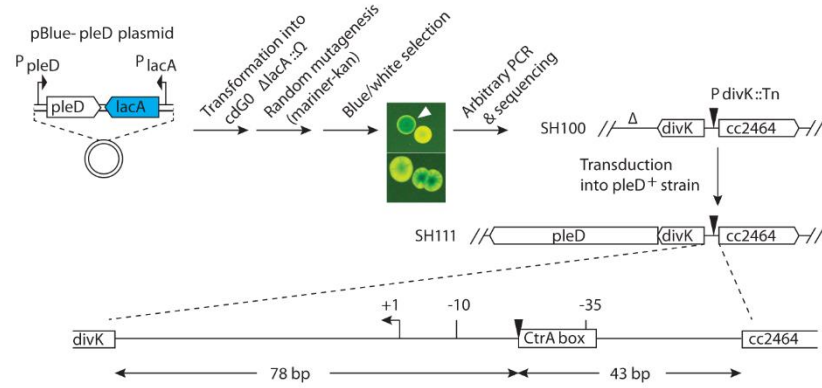
Two intercalated phosphorylation modules control replication initiation through the activity of the replication initiation inhibitor CtrA. When the PleC phosphatase is present at the swarmer pole, PleD and DivK are dephosphorylated. In this situation, phosphorylation modules 1 and 2 are uncoupled and CckA adopts DivL-imposed kinase mode to activate CtrA and block replication initiation. When the DivJ sensor kinase is present at the stalked pole, phosphorylation module 1 imposes control on module 2. PleD and DivK are phosphorylated, thereby switching CckA into the phosphatase mode and inactivating CtrA. In parallel, c-di-GMP facilitates CtrA degradation via PopA and the ClpXP protease.

C-di-GMP is only one of several novel nucleotide-based second messengers that were recently discovered in bacteria [106]. Their global impact on cell physiology raised the question how these signalling compounds mediate specific cellular responses and how they integrate with other general signalling systems, in particular with two-component phosphorylation networks [227]. Our finding that c-di-GMP acts as a cyclin-like molecule in *C. crescentus* to control the activity of the cell cycle kinase CckA, establishes the first direct connection between the two most widespread regulatory networks of bacterial cells. The CckA-ChpT-CtrA pathway is conserved among most known members of the α -proteobacteria, including important pathogens like *Bartonella* or *Brucella* [228]. This opens up the exciting possibility that c-di-GMP-imposed control of sensor histidine kinases might represent a general and widespread

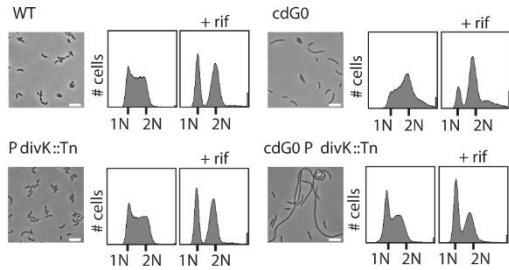
regulatory mechanism in bacteria. Considering that c-di-GMP plays a major role in regulating virulence and persistence, this provides important new entry points into better understanding the behaviour and propagation of bacterial pathogens.

Extended Data Figure 1

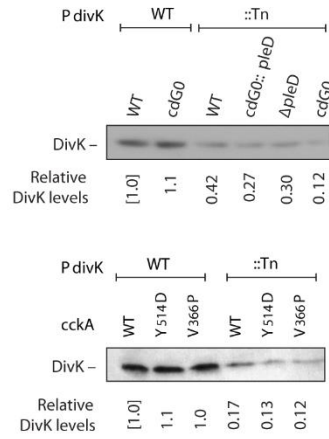
a



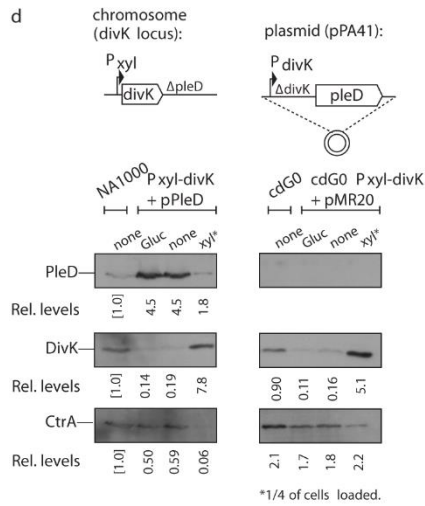
b



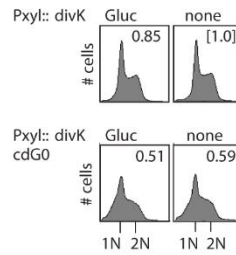
c



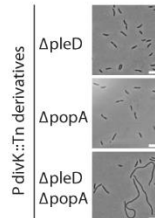
d



e



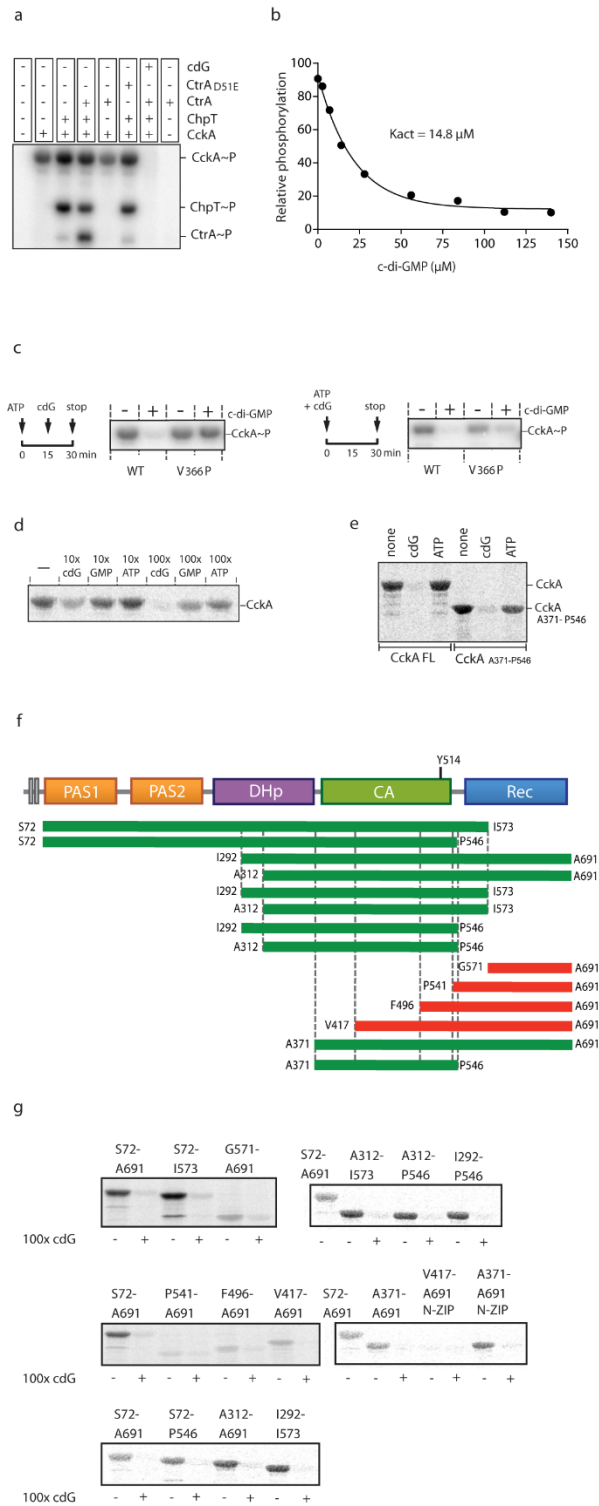
f

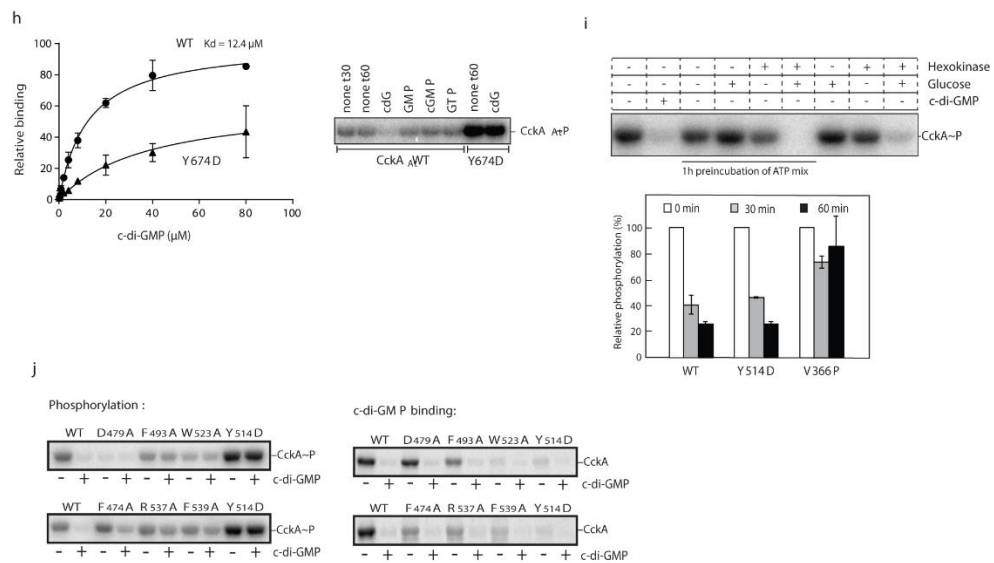


Extended Data Figure 1: Characterization of P*divK*::Tn and P*xyt*::*divK* derivatives

(a) Schematic of the synthetic lethality screen. pBlue-*pleD* is a low copy number plasmid carrying both *pleD* and *lacA* genes, each with its own promoter. The *lacA* gene encodes a subunit of the LacABC dehydrogenase responsible for the breakdown of β -galactosides in *C. crescentus* [229]. An open arrowhead in the top panel indicates a representative blue colony on an X-gal agar plate. Out of independent 142,000 transformants representative white colonies or colonies with blue sectors indicating segregation of the unstable pBlue-*pleD* plasmid are indicated in the upper and lower panel. Genomic organizations of the *divK* locus in strains SH100 and SH111 are shown schematically. The exact position of the transposon insertion (P*divK*::Tn) in the *divK* promoter region adjacent to the CtrA box is indicated by closed arrowheads. The transcription start site (+1) and the -10 and -35 elements are shown [230]. Mapping of the Tn to the CtrA binding site in the *divK* promoter region might imply that this lesion reduces *divK* expression by interfering with CtrA-mediated positive control. **(b)** Cell morphology and chromosome replication activity. Indicated strains were analysed microscopically and by flow cytometry to measure DNA content. Cells were grown with or without rifampicin as indicated. Chromosome equivalents (N) are indicated. Phase-contrast images are shown with scale bars of 5 μ m. Representative of two biological replicates is shown. **(c)** DivK levels deduced by immunoblot analysis. Cells grown in PYE were harvested at OD₆₆₀ of ~0.2 and subjected to SDS-13% PAGE, followed by immunoblot analysis using anti-DivK antibodies. The intensities of the DivK bands were quantified using Image J and are shown as relative values to NA1000 wild type levels. Representative of two biological replicates is shown. **(d)** Subcellular levels of PleD, DivK, and CtrA in the P*xyt*::*divK* derivatives. Cells of strains NA1000, UJ5065, UJ8012, and UJ8013 grown in PYE (none) or PYE supplemented with 0.2% glucose or 0.03% xylose were analysed by immunoblots as indicated. The intensities of the protein bands were quantified using ImageJ and are shown as relative values to NA1000 wild type. The vector control (pMR20) is indicated. Representative of two biological replicates is shown. **(e)** Chromosome replication activity of wild-type (UJ8012) and cdG0 (UJ8013) strains expressing *divK* from the P*xyt* promoter. Strains were grown exponentially in PYE (none) or PYE + glucose (Gluc), followed by flow cytometry analysis. Representative of two biological replicates is shown. **(f)** Effect of P*divK*::Tn on cell morphology in strains lacking *pleD*, *popA*, or both. Scale bar = 5 μ m. Representative of two biological replicates is shown.

Extended Data Figure 2.1





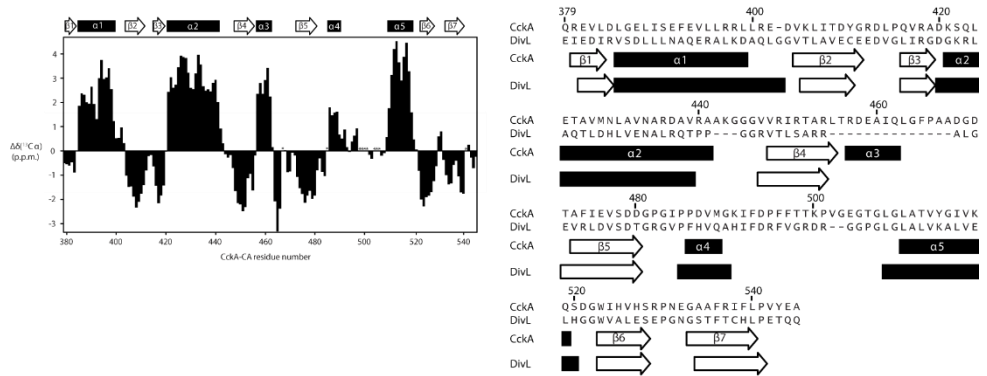
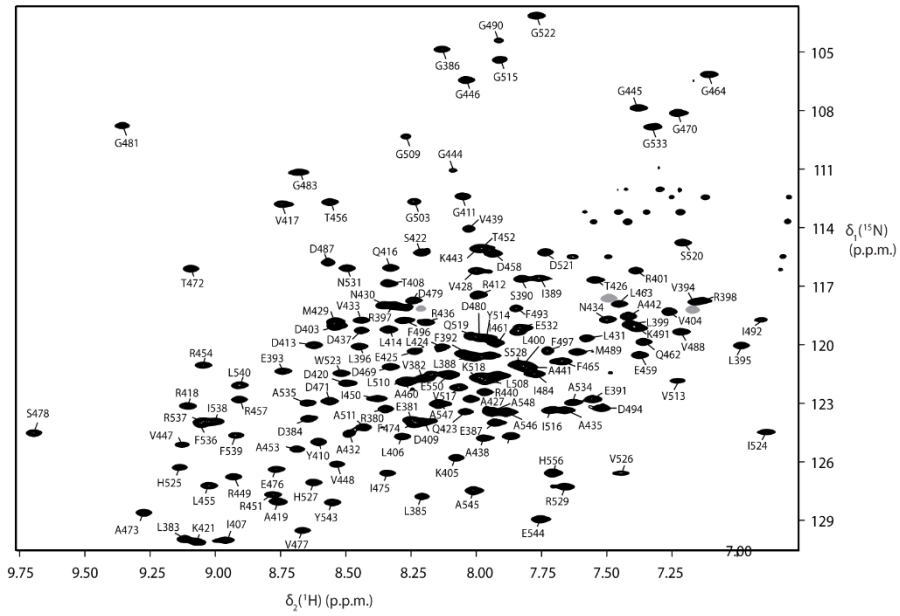
Extended Data Figure 2: C-di-GMP binds to CckA to induce phosphatase activity.

(a) C-di-GMP inhibits the CckA phosphorelay. *In vitro* phosphorylation reactions with purified proteins (+) in the presence or absence of c-di-GMP (75 μM). A CtrA mutant (D51E) lacking the phosphoryl-acceptor site is shown as a control. Phosphorylated proteins are marked. The weak band with a size similar to CtrA (lines 3 and 6) corresponds to a phosphorylated breakdown product of ChpT. Representative of three technical replicates is shown. **(b)** C-di-GMP stimulates CckA dephosphorylation. Phosphorylation reactions with purified CckA were carried out as outlined in Figure 2a. After reaching saturation, dephosphorylation was initiated by the addition of increasing concentrations of c-di-GMP. Reactions were run for 15 min and were analysed by autoradiography. Representative of two technical replicates is shown **(c)** C-di-GMP inhibits CckA auto-phosphorylation. Purified CckA wild-type and phosphatase mutant (V366P) were incubated with [^{32}P]ATP and with (+) or without (-) c-di-GMP (75 μM) as indicated. C-di-GMP was added at the time points indicated. Representative of three technical replicates is shown. **(d)** C-di-GMP specifically binds to CckA. Purified CckA protein was incubated with [^{33}P] labelled c-di-GMP and cross-linked with UV light in the presence or absence of a 10-fold or 100-fold excess of competing non-labelled nucleotides as indicated. Representative of three technical replicates is shown. **(e)** The CA

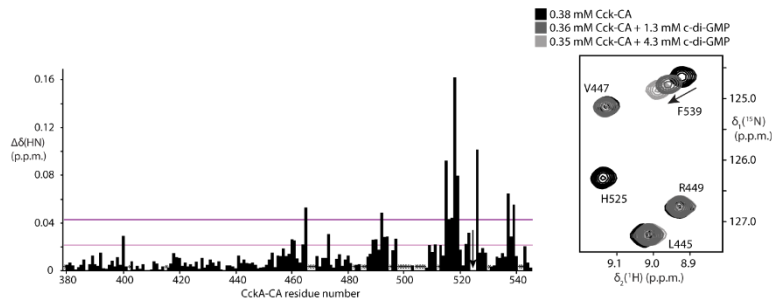
domain of CckA specifically binds c-di-GMP. Purified protein of full length CckA (FL, lacking N-terminal TM domains) and the minimal binding unit (see (f)) was incubated with [³³P] labelled c-di-GMP and cross-linked with UV light in the presence or absence of a 100-fold excess of non-labelled ATP or c-di-GMP as indicated. Representative of three technical replicates is shown. **(f)** Schematic of the domain architecture and truncated constructs of CckA. Amino acids marking the boundaries of each construct are indicated. Constructs marked by green and red bars showed c-di-GMP binding or failed to bind c-di-GMP, respectively. **(g)** Truncated versions of the CckA proteins indicated in (a) were expressed, purified, and analysed for c-di-GMP binding using UV-crosslinking of [³³P] labelled c-di-GMP³⁷ (10 μM) in the presence (+) or absence (–) of a 100-fold excess of non-labelled c-di-GMP (1 mM). Samples were analysed by SDS-PAGE and autoradiography as indicated. Representative of two technical replicates is shown **(h)** Left: CckA_{At}, the CckA homolog of *A. tumefaciens* binds c-di-GMP. The c-di-GMP binding affinities of wild-type CckA_{At} and the CckA_{At}(Y674D) mutant protein were determined by UV-crosslinking at increasing concentrations of [³³P]c-di-GMP. Relative binding units and affinities are shown. Error bars are standard deviations. Averages and standard deviations were obtained from three technical replicates. Right: CckA_{At} is regulated by c-di-GMP. Wild-type CckA_{At} and CckA_{At}(Y674D) mutant were incubated with [³²P]ATP (0 min) and supplemented with c-di-GMP and other nucleotides (75 μM) at 30 min. Fractions were removed after 30 min or 60 min as indicated and analysed by autoradiography. Representative of two technical replicates is shown. **(i)** Phosphatase activity of CckA alleles in the absence of ATP. Reactions were allowed to autophosphorylate for 15 min before hexokinase and D-glucose were added to rapidly deplete ATP. A representative gel image for wild-type CckA is shown (top). Kinetic analysis revealed that CckA(Y514D) retains wild type-like phosphatase activity (bottom). Error bars are standard deviations. Averages and standard deviations were obtained from three technical replicates. **(j)** Mutational analysis of amino acids contributing to c-di-GMP binding and phosphatase control. Purified CckA wild-type and mutant forms were analysed for phosphorylation activity and [³³P] c-di-GMP binding as indicated above. Note that the residue D479 is involved in ATP binding. Consequently, the D479A mutant lacks kinase activity, but is unaltered in its ability to bind c-di-GMP. Representative of two technical replicates is shown.

Extended Data Figure 3

a



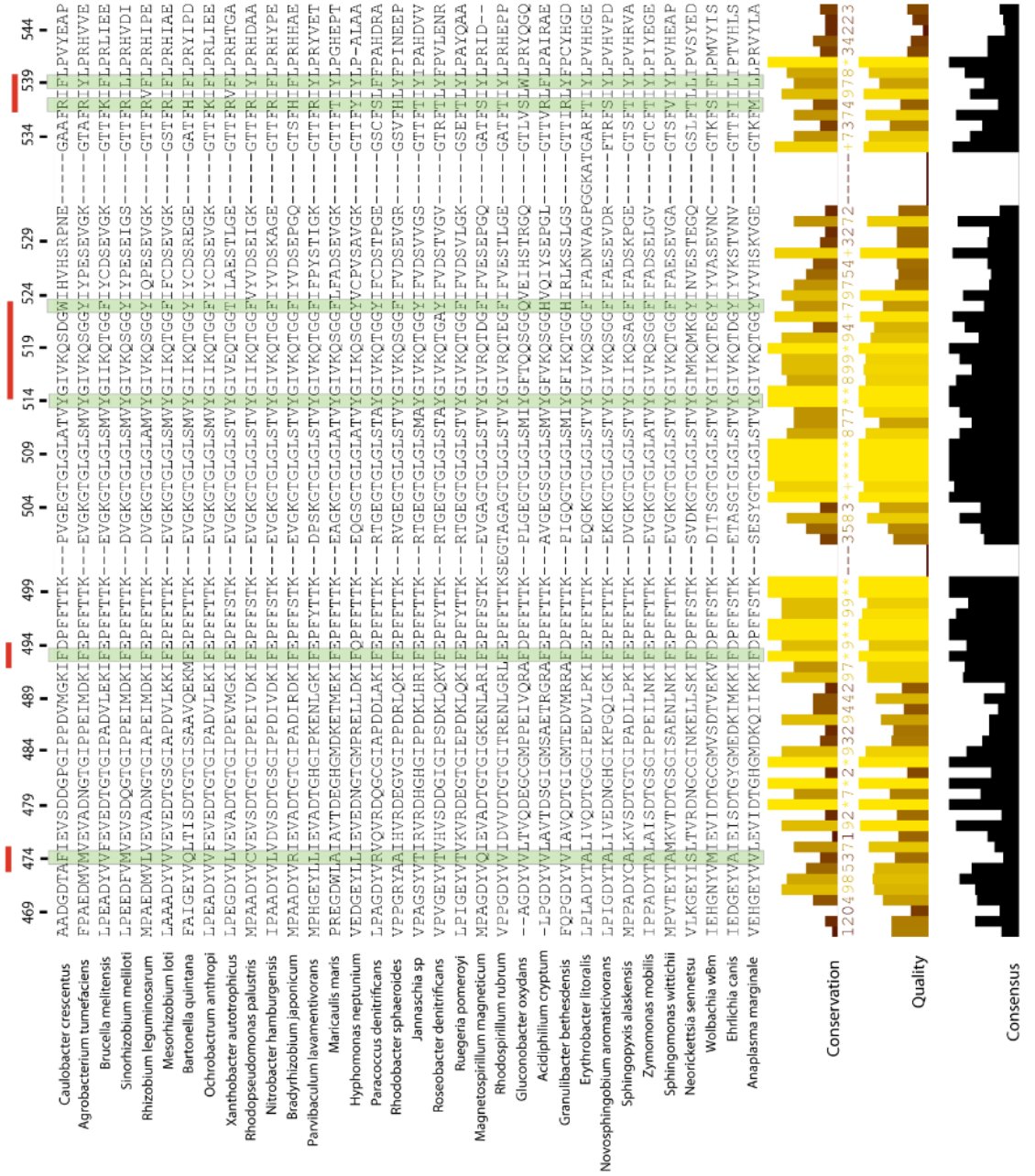
b



Extended Data Figure 3: Characterization of the c-di-GMP binding site by NMR spectroscopy.

(a) Top: 2D [¹⁵N,¹H]-TROSY spectrum of 0.38 mM CckA-CA recorded at 20°C. The sequence-specific resonance assignments are indicated. Bottom left: Sequence-specific secondary backbone ¹³C chemical shifts of CckA-CA relative to the random coil values of Kjaergaard *et al.* [231]. A 1–2–1 smoothing function was applied to the raw data. Consecutive stretches with positive and negative values indicate α-helical and β-strand secondary structure, respectively. The secondary structure elements inferred from these data are indicated above. Asterisks indicate unassigned residues. Bottom right: Profile-profile alignment of the CA domains of CckA and DivL carried out with HHpred [232] and formed the basis for the generation of the CckA homology model (shown in Fig. 2G) using the Modeller software [233]. The sequence identity is 25%. Secondary structure elements of CckA as determined by ¹³C^α secondary chemical shifts and of DivL, as derived from the crystal structure (pdb 4q20) are shown below the sequence alignment. The residue numbering of CckA is indicated. **(b)** Chemical shift perturbation of Cck-CA backbone amide moieties upon c-di-GMP binding. Left: Combined chemical shift changes of amide moieties, Δδ(HN), are plotted against the residue number. The magnitudes of one s.d. (0.021 p.p.m.) and two s.d. (0.042 p.p.m.) are indicated by a purple and pink line, respectively. The arrow points to residues I524 and H525 that experience intermediate chemical exchange upon c-di-GMP binding. Asterisks indicate unassigned residues. Right: Region of a 2D [¹⁵N,¹H]-TROSY spectrum of a titration of c-di-GMP to CckA-CA at 20°C. Sequence-specific resonance assignments are indicated.

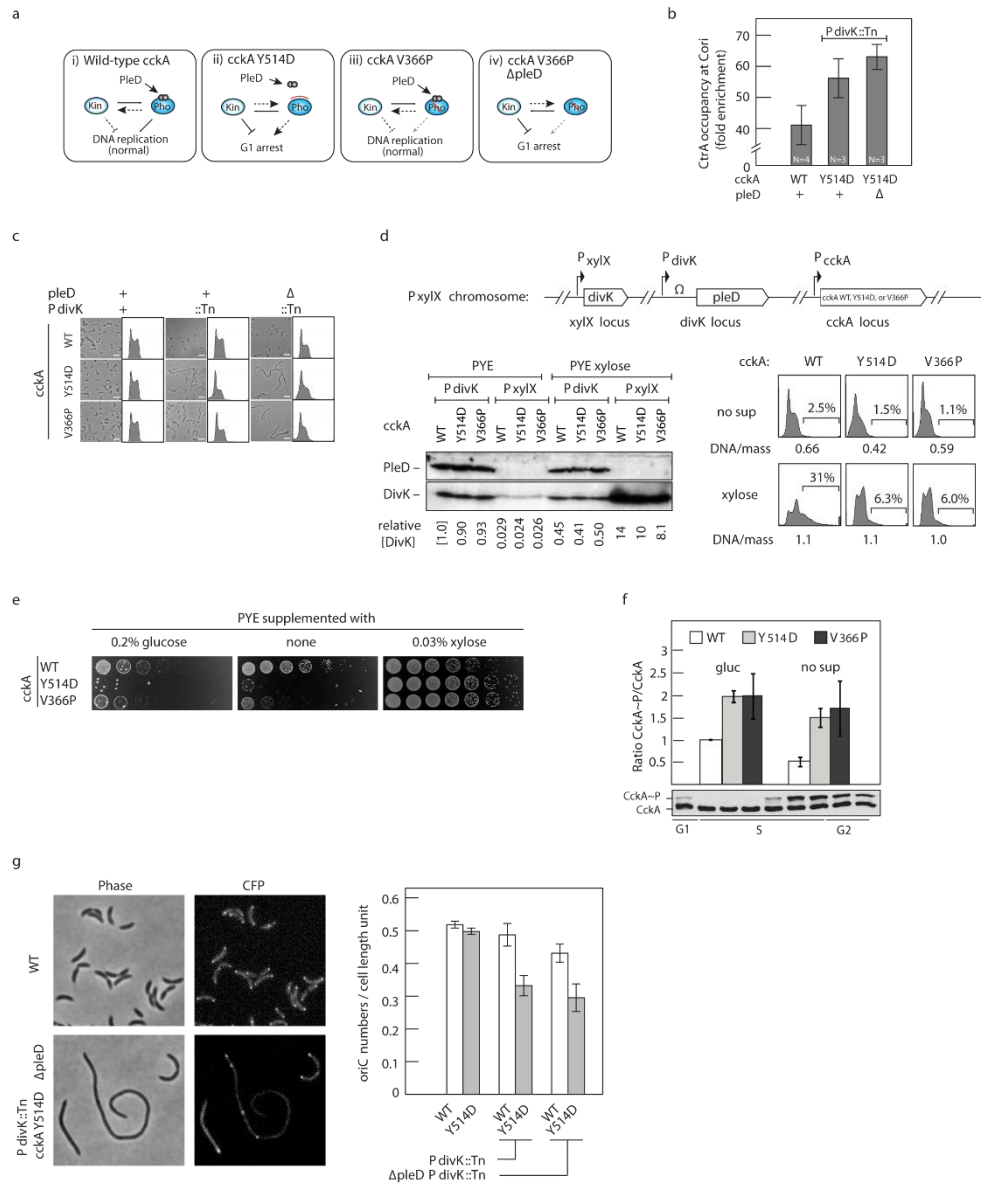
Extended Data Figure 4



Extended Data Figure 4: CLUSTALW alignment of the CA domain of CckA

A CLUSTALW program is used to align the CA domain of CckA from *C. crescentus* and from different α -proteobacteria. A fragment of the CA domain is shown that corresponds to amino acids 467-546 of *C. crescentus* CckA. Residues involved in c-di-GMP binding are boxed (green) and red bars above the sequence indicate regions with significant chemical shift in NMR spectroscopy upon c-di-GMP titration. CLUSTALW scores for conservation, quality and consensus are indicated.

Extended Data Figure 5

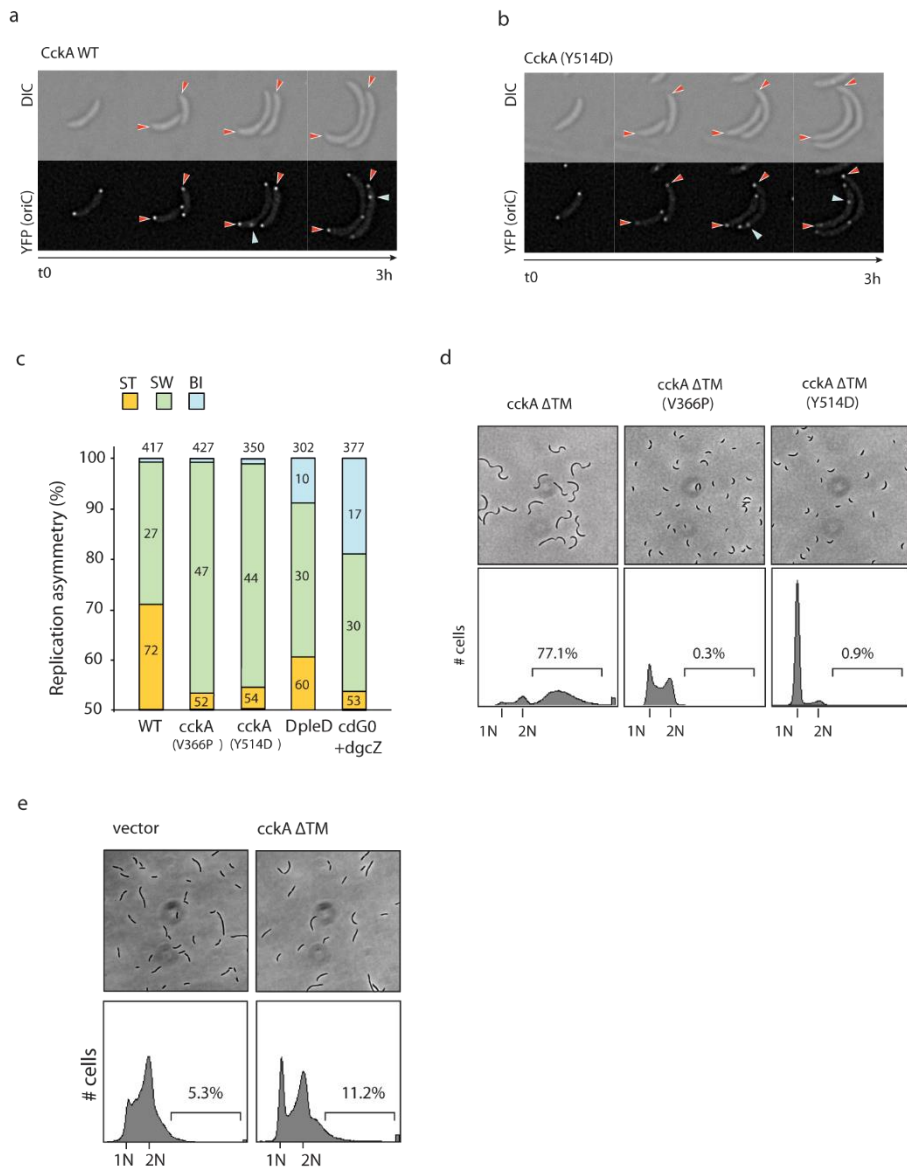


Extended Data Figure 5: DivK and c-di-GMP convergently control *C. crescentus* growth and replication.

(a) Model for the regulation of chromosome replication by the CckAkinase/phosphatase switch at reduced levels of DivK. Bold and dotted lines indicate strong and weak reactions, respectively. Dark circles indicate c-di-GMP. Kinase (Kin) and phosphatase mode (Pho) of CckA are indicated. i) C-di-GMP authorizes S-phase entry by inducing CckA phosphatase. ii) C-di-GMP is unable to bind to and induce phosphatase activity of CckA(Y514D) resulting in a G1 arrest. iii) C-di-GMP authorizes S-phase entry by reducing kinase activity of the phosphatase mutant CckA(V366P). iv) Cells lacking PleD fail to downregulate CckA(V366P) kinase activity. **(b)** CtrA binding to the Cori region is increased in cells harbouring *ckkA(Y514D)* and *PdivK::Tn*. CtrA occupancy at Cori was analysed using ChIP and qPCR as described in Experimental Procedures. Error bars are s.d. **(c)** Combining the *ckkA(Y514D)* and *PdivK::Tn* alleles leads to a G1 arrest. Exponential cultures of mutants containing different combinations of *ckkA*, *PdivK*, and *pleD* alleles were analysed by light microscopy and flow cytometry. Representative examples of two biological replicates for phase contrast images and profiles of DNA content are shown with scale bars of 5µm. **(d)** Reduced *divK* expression in *PxyIX::divK* strains containing the *ckkA(Y514D)* allele leads to G1 arrest. Top: Schematic of the chromosomal arrangement of cells expressing *divK* from the *PxyI* promoter (*PxyIX::divK*) and harbouring different *ckkA* alleles. The *divK* gene is fused to the *PxyIX* promoter in the *xyIX* locus. The chromosomal copy of *divK* at the original locus was replaced with a Ω -cassette. Different *ckkA* alleles were introduced at the *ckkA* locus by allelic exchange. Bottom left: Cellular levels of DivK and PleD as determined by immunoblot analysis in strains grown in the presence or absence of xylose. Cells expressing *divK* from its own promoter at the native locus (*PdivK*) were used as control. Note that for *PxyIX::divK* derivatives grown in PYE, twice as many cells were used. Band intensities were determined with ImageJ and the respective values shown as relative units compared to wild type. Bottom right: DNA content per cell mass (DNA/mass) was analyzed as described in Figure 1c and values are shown below the graphs. Fractions of cells containing more than two chromosomes are indicated by brackets. Representative of two biological replicates is shown. **(e)** Colony forming ability of *PxyIX::divK* strains carrying different *ckkA* alleles. Five-fold serial dilutions of the indicated strains were spotted and grown for 2d at 30°C on PYE plates with the supplements indicated. Representative of two biological replicates is shown. Note that these results are consistent with individual DNA replication profiles shown in Figure 3 and panel d. **(f)** Reduced *divK* expression

in *P_{xyIX}::divK* strains containing the *ckA(Y514D)* allele leads to increased CckA phosphorylation levels. The cellular fraction of phosphorylated CckA (CckA~P) was determined using Phos-tag gel electrophoresis. As a control CckA~P and CckA levels were determined in synchronized populations of wild-type cells proceeding through the cell cycle (bottom). *P_{xyIX}::divK* strains harbouring different *ckA* alleles were analysed during exponential growth at 30°C in the presence or absence of glucose (0.3%). The addition of glucose reduces leaky expression from the *P_{xyI}* promoter. Relative ratios of CckA~P to total CckA protein are shown. Error bars are s.d. Averages and standard deviations were obtained from three biological replicates. **(g)** Single cell analysis of the replication status of mutants with reduced DivK levels and abolished CckA control by c-di-GMP. Strains producing LacI-CFP and harbouring an array of *lac* operator (*lacO*) sites near the origin of replication were analysed [234]. FROS strains contained wild-type *ckA* or the *ckA(Y514D)* mutant allele, as well as *P_{divK}::Tn-tet* with wild-type *pleD* or $\Delta pleD$ as indicated. Representative phase contrast and fluorescence images of two biological replicates are shown. Numbers of origins per cell length units were analyzed statistically and the mean value and standard deviations obtained from two biological replicates are shown as a column graph. For each strain, a total of >900 cells were analysed using MicrobeTracker (<http://microbetracker.org>). Note that these results are consistent with the DNA replication profiles of equivalent strains without the FROS module shown in Figure 3 and panels c and d.

Extended Data Figure 6



Extended Data Figure 6: C-di-GMP mediated spatial control of CckA directs replication asymmetry in dividing cells.

Fluorescent repressor–operator system (FROS) analysis to visualize DNA replication in individual cells. Dividing cells of *C. crescentus* wild type (**a**) and *cckA(Y514D)* mutant (**b**) producing TetR-YFP and harbouring an array of tet operator (*tetO*) sites near the origin of replication were analysed by fluorescence microscopy. Frames from representative time-lapse movies used for panel c are

shown. Stalked/old poles of newly divided daughter cells are marked with red arrows; newly replicated origins are marked with blue arrows. **(c)** Spatial patterns of DNA replication were scored using a Tet-based FROS system and divided into three classes as indicated: Replication initiation at the Cori located at the stalked pole (ST, orange), swarmer pole (SW, green), or at both poles (BI, blue). The bar diagram shows the quantification of wild-type and mutant strains as indicated with numbers indicating percentage of cells falling into the three classes. Total number of cells analysed (n) is indicated above each bar. **(d)** Expression *ckAΔTM* leads to c-di-GMP dependent overreplication. *C. crescentus* wild-type strains expressing different *ckAΔTM* alleles were analysed by light microscopy and flow cytometry as indicated. The fraction of cells bearing more than two chromosomes is indicated and shown as percentage. Representative of two biological replicates is shown. **(e)** Expression *ckAΔTM* leads to c-di-GMP dependent overreplication. *C. crescentus* cdG0 strain expressing *ckAΔTM* was analysed by light microscopy and flow cytometry as indicated. The fraction of cells bearing more than two chromosomes is indicated and shown as percentage. Representatives of two biological replicates are shown.

Methods

Strains and plasmids

Strains used in this study are listed in Extended Data Table 1. *Caulobacter* strains are grown in Peptone Yeast extract medium (PYE) or minimal medium supplemented with glucose (M2G) at 30°C [235]. When necessary, medium was supplemented with glucose (0.2%), xylose (0.03% 0.3%), and antibiotics as described [236]. When synchronized *Caulobacter* cell cultures were used, newborn cells were harvested by LUDOX density-gradient centrifugation method [38]. Generalized CR30 phage transduction was performed as described [235].

Strain UJ6777 was constructed by sequential 2-step transduction using a CR30 phage lysate of MT15 [234]. Strains UJ8306, UJ8307, UJ8308 and UJ8314 were constructed by sequential 2-step transduction using a CR30 phage lysate of MT16 [234]. UJ8312 was constructed by sequential transduction using parental strain SoA1273 and CR30 phage lysates of MT16 and UJ6777. Strains UJ7212 and UJ7214 were constructed using a parental NA1000 strain and suicide vectors pNPTS-cckA(Y514D) and pNPTS-cckA(V366P), respectively. To construct strains UJ6861 and UJ7304, *lacA::Ω* was transduced into UJ5065 using a phage lysate of UJ6168. Subsequently, pBlue-*pleD* was transformed into the transductant, yielding UJ6861. *xyiX::tipNgfp* was transformed into UJ6861, yielding UJ7304. Strain UJ7525 was constructed by sequential 2-step transduction. First, *xyiX::pPA28* was transduced into NA1000 using a phage lysate of UJ286. Resulting kanamycin-resistant colonies were subsequently transduced with $\Delta divK::\Omega$ using a phage lysate of strain CJ403. Strains UJ7527, UJ7529, UJ7618, UJ7619, and UJ7620 were constructed similarly using UJ7212, UJ7214, UJ7417, UJ7418, and UJ7419, respectively, as a parental strain instead of NA1000. Strains UJ7417, UJ7418 and UJ7419 were constructed by double homologous recombination using pNPTS-cckA-3xF and parental strain NA1000, UJ7212 or UJ7214. Strains UJ7511 and UJ7512 were generated by integration of pMCS1-cckA into NA1000 and UJ7212. Strains UJ7873 and UJ7992 were constructed by double homologous recombination using pNPTS-XdivK and a parental strain NA1000 (for UJ7873) or UJ5065 (for UJ7992), respectively. Strains UJ7939 and UJ7940 were constructed by transformation of pMCS5-k2t into NA1000 *PdivK::Tn* and NA1000 $\Delta pleD$ *PdivK::Tn*, respectively.

Plasmids and Oligonucleotides used in this study are listed in Extended Data Tables 2 and 3, respectively. To construct pBlue-*pleD*, a 2.5 kb fragment containing the *pleD* gene under control of the *divK* promoter was amplified using pPA41 and primers 5156 and 104, followed by digestion with *ScaI* and ligation to the *ScaI* fragment of pJC389. The insert was verified by DNA sequencing. To construct pNPTS-XdivK, the upstream (694 bp) of *divK* was amplified using NA1000 genome and primers 6151 and 6152. The product was digested with *XhoI* and *SacII*, ligated to the *Sall-SacII* fragment of pXMCS-1, resulting in pXdivKr. In parallel, a 1kb fragment containing the *divK* gene and its downstream region was amplified using SH119 genome and primers 6153 and 6154, followed by digestion with *EcoRI* and *NdeI* and ligation to the *EcoRI-NdeI* fragment of pXdivKr, resulting in pXdivKrl. Finally, the *EcoRI-SphI* fragment of pXdivKrl was subcloned into pNPTS138, yielding pNPTS-XdivK. For pMCS5-k2t, a part (444 bp) of the *nptIII* gene was amplified by PCR using pAlmar1 and primers 6693 and 6694, followed by digestion with *KpnI* and *SacI* and ligation to the *KpnI-SacI* fragment of pMCS-5. For pXTCYC4-tipNgfp, the *tipNgfp* gene was amplified using pMR20-tipNgfp (UJ6350) and primers 5242 and 105, followed by ligation into pGEM vector. The resulting plasmid was digested with *NdeI* and *SacI*, followed by ligation to the *NdeI-SacI* fragment of pXTCYC-4. To construct pET28a-His-MBP, the His-MBP fragment was amplified using pHIS-MBP-DEST and *ckkA* and primers 5196 and 5278 followed by digestion with *BamHI* and *NcoI* and subsequent ligation into pET28a. To construct pET-cckA, *cckA* was amplified using primers 5276 and 5277 followed by digestion with *BamHI* and *Sall* and ligation into pET28a-His-MBP. To introduce point mutations into pET-cckA SOE-PCR was used. Generally, pET-cckA was used as template with 5276/5277 as outside primers and internal mutagenic primers to introduce mutations. The following internal primers were used to introduce point mutations: V366P (5134/5135), Y514D (5448/5449), F474A (7725/7726), D479A (7727/7728), F493A (7729/7730), W523A (7735/7736), R537A (5502/5503), F539A (7737/7738). After fusion PCR inserts were *BamHI* and *Sall* digested and ligated into pET28a-His-MBP.

To amplify truncated *ckkA* fragments the following primers were used. pET-cckA S72-I573 (5276/5454), pET-cckA G571-A691 (5455/5277), pET-cckA P541-A691 (5456/5277), pET-cckA F496-A691 (5457/5277), pET-cckA V417-A691 (5458/5277), pET-cckA S72-P546 (5276/5644), pET-cckA A312-A691 (5646/5277), pET-cckA I292-P546 (5280/5644), pET-cckA A371-A691 (5645/5277). Resulting PCR products were digested with *BamHI* and *Sall* and ligated into pET28a-His-MBP. To generate pET-cckA V417-A691 (N-ZIP) and pET-cckA A371-A691 (N-ZIP) N-ZIP was amplified using primers 5647

and 5648 using pUT18C-zip as template. The resulting PCR product was digested with *Bam*HI and ligated into pET-cckA V417-A691 and pET-cckA A371-A691. Correct orientation of insert verified by sequencing. pET21b-CckA Q379-A545 was generated using primers 7244 and 7249 and chromosomal DNA as template. Resulting PCR product was *Not*I and *Nde*I digested and ligated into pET21b.

To construct pET-Agroccka, *cckA* was amplified from chromosomal DNA of *Agrobacterium tumefaciens* C58 using primers 6430 and 6431. To introduce Y674D mutation SOE-PCR was used using mutagenic primers (6436/6437). Inserts were digested with *Bam*HI and *Sa*I and ligated into pET28a-His-MBP.

To construct pNPTS-cckA V366P the insert of pET-cckA V366P was cut out using *Bam*HI and *Hind*III and ligated into pNPTS138. To construct pNPTS-cckA Y514D a fragment was amplified using primers 5458 and 670 and pET-cckA Y514D as template. PCR product was *Bam*HI and *Hind*III digested and ligated into pNPTS138. To construct pNPTS-cckA-3xF a first fragment was amplified using primers 5456 and 5938 and *cckA* as template. A second PCR was run on the first PCR product to extend 3xFLAG using primers 5456 and 5939. Downstream fragment was amplified from chromosomal NA1000 DNA using primers 5940 and 5941. The downstream and 3xFLAG fragments were fused by SOE-PCR using primers 5456 and 5941. This PCR product was *Bam*HI and *Hind*III digested and ligated into pNPTS138.

To construct pSA241.1 *ctrA* was amplified from chromosomal DNA using primers 1505 and 3708. PCR product was digested with *Bam*HI and *Hind*III and ligated into pTRcHisA. pTRc-ctrA D51E was generated as pSA241.1 except that SOE-PCR was used to introduce D51E mutation using mutagenic primers 4818 and 4819 and outside primers 1505 and 3708. To construct pMCS-cckA a fragment from pET-cckA P541-A691 was cut out using *Sa*I and *Hind*III and subcloned into pMCS-1.

To construct pBXMCS-cckA, pBXMCS-cckA V366P and pBXMCS-cckA Y514D a fragment was amplified from plasmid DNA (pET-cckA, pET-cckA V366P or pET-cckA Y514D) using primers 7200 and 7369. The resulting PCR product was *Nde*I and *Eco*RI digested and ligated into pBXMCS-2.

Screen for synthetic lethality

Although a mutant unable to synthesize c-di-GMP (cdG0) shows pronounced abnormalities in cellular DNA content and cell morphology, its overall growth and viability were not affected. We reasoned that c-di-GMP, together with redundant pathways, maintains core bacterial cell cycle processes like cell division or chromosome replication. To probe for such interactions a genetic screen for synthetic lethality was adapted for the *C. crescentus* cdG0 strain [237]. The screen identifies transposon (Tn) mutants that stably retain the plasmid (pBlue-pleD) under non-selective conditions. pBlue-pleD expresses the diguanylate cyclase PleD as the sole source of c-di-GMP present in the screening strain. While this plasmid is unstable and easily lost in the absence of selection, a Tn insertion generating synthetic lethality in the cdG0 strain should render pBlue-pleD essential for growth, which in turn results in its stable maintenance without antibiotic selection. pBlue-pleD also carries *lacA*, a gene required for the metabolism of β -galactosides [229]. Because the *lacA* copy was deleted in the screening strain, its ability to metabolize β -galactosides relies on plasmid-borne *lacA*. Consequently, mutants that stably maintain the plasmid yield solid blue colonies on plates supplemented with X-gal, while mutants that lose the plasmid are easily recognized by their blue/white sector appearance.

Random transposon (Tn) mutagenesis was performed by transforming a transposon donor plasmid pAlmar1 into the screening strain (UJ7304 or UJ6861). Total 142,000 Tn mutants were grown at 30°C for 1 week on PYE plates supplemented with 20 μ g/mL kanamycin and 40 μ g/mL X-gal. Solid blue colonies were streaked and incubated on an X-gal supplemented PYE plate for 3 days at 30°C. Transposons were mapped by a 2-step arbitrary PCR as described [238]. Briefly, downstream of Tn was amplified by first PCR using primers 1228 and 1365. After purification, DNA fragments were further enriched by second PCR using primers 1365 and 1657. The products were sequenced using the primer 2614 (SO. and UJ, unpublished result).

Spot growth assay

The cell density of each culture was adjusted to OD₆₆₀ of 0.014, followed by preparation of serial 5-fold dilutions. 5 μ L of the culture were spotted onto PYE plate containing appropriate supplements and incubated for 2 days at 30°C.

Western blotting

Anti-PleD (1:2000), anti-DivK (1:5000), and anti-Flag (1:10000) antibodies were used as primary antibodies, which were detected by HRP-conjugated rabbit anti-mouse or swine anti-rabbit secondary antibodies (Dako), followed by development with ECL detection reagents.

Flow cytometry

This assay was performed essentially as described [34]. Briefly, exponentially growing cells (100 μ L) were fixed in ice-cold 70% ethanol. For rifampicin treatment, cells were incubated for 1h at 30°C in the presence of rifampicin (final 30 μ g/mL) before fixation. Cells were harvested by centrifugation, resuspended in 0.5 mL FACS buffer (10 mM Tris HCl pH 7.5, 1 mM EDTA, 50 mM sodium citrate, and 0.01 % TritonX-100) containing 0.1 mg/mL RNaseA, and incubated at RT for 30 min. After harvesting cells by centrifugation, DNA was stained in 1 mL FACS buffer including 1.5 μ M YO-PRO-1 iodide (Invitrogen) at RT for 2h. The fluorescent intensity and the light scattering were analyzed using FACS Canto II (BD Biosciences).

Protein purification

Expression plasmids were transformed into *E. coli* BL21 (DE3) cells. Cells were grown in LB at 30°C to an OD₅₇₈ of 0.5 and subsequently induced with 300 μ M IPTG for 4 hours. Cells were pelleted and frozen at -80°C. Proteins were purified on a Äkta purifier using 1 ml HisTrap HP columns (GE Healthcare) and if higher purity was desired proteins were run on a size exclusion column (HiLoad 16/60 Superdex 200). For the purification the following buffers were used: lysis buffer (wash Buffer supplemented with protease inhibitor), wash buffer (16 mM Na₂HPO₄, 3.6 mM KH₂PO₄, 5.4 mM KCl, 500 mM NaCl, 2 mM β -mercaptoethanol, 10 mM imidazole, pH 7.0), elution buffer (16 mM Na₂HPO₄, 3.6 mM KH₂PO₄, 5.4 mM KCl, 500 mM NaCl, 2 mM β -mercaptoethanol, 500 mM imidazole, pH 7.0), storage and activity Buffer (10 mM HEPES-KOH, 50 mM KCl, 10% glycerol, 0.1 mM EDTA, 5mM MgCl₂, 5 mM β -mercaptoethanol, pH 8.0). The *A. tumefaciens* CckA homolog was stored in an optimized buffer (10 mM HEPES, 125 mM KAc, 10% glycerol, 5 mM MgCl₂, 5 mM β -mercaptoethanol, pH 7.5).

Kinase and phosphatase assays

Generally, kinase and phosphatase assays were adapted from [170] and [239]. Reactions were run in activity buffer in presence of 500 μ M ATP and 5 μ Ci [γ^{32} P]-ATP (3000 Ci/mmol, Hartmann Analytic) at RT. Additional nucleotides were added at indicated time points. Reactions were stopped with SDS sample buffer and subsequently loaded (or stored on ice) on 10% SDS gels. Wet gels were exposed to phosphor screen (0.5-3h) before being scanned using a Typhoon FLA 7000 imaging system (GE Healthcare). When needed, ATP was depleted from the reaction mixtures by the addition of 1.5 U hexokinase (Roche) and 5 mM D-glucose after 15 min of phosphorylation.

UV crosslinking with [33 P] c-di-GMP

[33 P] labeled c-di-GMP was produced using [α^{33} P]-GTP (Perkin Elmer) and the *E. coli* diguanylate cyclase DgcZ. Purification of DgcZ and production of c-di-GMP is as described [14]. Purified proteins were incubated with labeled c-di-GMP for 30 min in activity buffer at RT. Proteins were cross-linked at 254 nm for 3 min at 4°C and then diluted into SDS sample Buffer as described [240]. After 5 min boiling the samples were separated by SDS-PAGE. Gels were dried and exposed to phosphor screen overnight and then scanned on an imaging system. Band intensities were quantified using imageJ and binding curves were fitted with Graphpad Prism.

Quantification of CckA~P levels *in vivo*

Colonies grown on PYE plates or PYE supplemented with 0.2% glucose were resuspended in PYE and adjusted to the same OD. Cells were pelleted and resuspended in 100 μ L lysis buffer (10 mM Tris-HCl, 4% SDS, one tablet phos-stop (Roche), pH 7.5). Lysates were diluted into SDS sample buffer and analyzed by SDS-PAGE gels (7.5%) supplemented with 50 mM phos-tag acrylamide (Wako) and 100 mM manganese chloride. Gels were run at 4°C at 100 V for 3 hours. Before immunoblotting the gels were incubated for 10 minutes in transfer buffer (1X TrisGlycine, 20% Ethanol) containing 1 mM EDTA and for another 10 minutes in transfer buffer without EDTA. Proteins were detected using anti-flag antibodies.

NMR experiments

NMR spectra were recorded at 20°C on Bruker Avance-700 and -900 spectrometers equipped with cryogenic triple-resonance probes. CckA-CA

protein samples were prepared in 30 mM Tris-HCl at pH 7.5 with 100 mM NaCl, 5 mM MgCl₂ and 2 mM DTT in 95%/5% H₂O/D₂O. For the sequence-specific backbone resonance assignment of [*U*-²H, ¹⁵N, ¹³C]-labeled Cck-CA, the following NMR experiments were recorded: 2D [¹⁵N,¹H]-TROSY-HSQC [241], 3D TROSY-HNCA [242] and 3D [¹H,¹H]-NOESY-¹⁵N-TROSY with a NOE mixing time of 100 ms [243]. For the c-di-GMP binding experiments a series of 2D [¹⁵N,¹H]-TROSY-HSQC spectra of 380 μM [*U*-¹⁵N]-CckA-CA were recorded with c-di-GMP concentrations of 0 mM, 0.04 mM, 0.24 mM, 0.6 mM, 1.32 mM, 2.54 mM and 4.27 mM. Chemical shift perturbations ($\Delta\delta(\text{HN})$) of amide moieties were calculated as:

$$\Delta\delta(\text{HN}) = [((\delta H_{\text{ref}} - \delta H)^2 + ((\delta N_{\text{ref}} - \delta N)/5)^2) / 2]^{0.5}.$$

Chromatin immunoprecipitation (ChIP) and quantitative PCR (qPCR)

ChIP was performed as described previously [244]. Cells were grown in 20 mL PYE until OD₆₆₀ reached ~0.2. To crosslink protein-DNA complexes, 0.2 mL of 1M Na-phosphate pH7.6 (final 10 mM) and 540 μL of 37% formaldehyde (final 1%) were added to the culture and incubated at RT for 10 min, followed by incubation on ice for 30 min. After harvesting cells by centrifugation (2600xg for 30 min), cells were washed twice in 20 mL of ice-cold PBS and resuspended in Buffer A (10 mM Tris HCl pH 8.1, 20% sucrose, 50 mM sodium chloride, 10 mM EDTA, and 20 mg/mL lysozyme) to adjust final OD₆₆₀ of 8. After incubation at 37°C for 30 min, the equal volume of Buffer IP' (100 mM Tris HCl pH 7.5, 300 mM sodium chloride, 2% Triton X-100, and 2x cOmplete protease inhibitor (Roche)) was added to the sample and incubation was continued for 15 min at 37°C. Subsequently genomic DNA was sheared by sonication and cell debris was removed by centrifugation, yielding a clear lysate. A portion (30 μL) of the lysate was mixed with 70 μL TE buffer including 1% SDS to use as an input DNA. Another portion (0.2 mL) was incubated with the anti-CtrA antibody (0.8 μL) in a cold room for >12h with gentle agitation. The incubation was continued for 4h in the presence of Protein-A agarose beads (100 μL slurry), followed by washing beads 7 times in 0.5 mL of ice-cold buffer IP (50 mM Tris HCl pH 7.5, 150 mM sodium chloride, and 1% Triton X-100) and two times in 0.5 mL of TE buffer. The beads were resuspended in 0.1 mL TE buffer containing 1% SDS and incubated at 65°C for >12h to reverse crosslinking. DNA samples were purified using a DNA purification kit (Macherey-Nagel). qPCR was performed as described [245]. Briefly, *oriC* DNA was amplified by quantitative PCR StepOne Plus (Applied Biosystems) using Power SYBR Green PCR Master

Mix (Applied Biosystems) and primers 6708 and 6709. To measure background signals, a part of the *ctrA* coding region was amplified similarly using primers 6710 and 6711.

Scoring replication initiation using an *oriC* specific fluorescent repressor-operator system (FROS)

To visualize DNA replication in individual cells we made use of a fluorescent repressor-operator system (FROS) that allows tracking of chromosomal origins during the cell cycle [229,234]. Cells used in these experiments produce TetR-YFP and harbour tet operator (*tetO*) sites near the origin of replication. Binding of TetR-YFP molecules to the operator arrays yields a fluorescent signal that stains the Cori. Upon initiation of chromosome replication, duplicated operator arrays produce two discrete fluorescent foci. This enables tracking of replication initiation events at opposite poles of the predivisional cell. A (*tetO*)_n cassette was integrated at the *α0006* locus by phage transduction using a phage lysate of MT16. TetR-YFP was expressed from the xylose promoter by induction with 0.3% xylose. *tetR-yfp* was introduced by transduction using a phage lysate of MT15.

Replication asymmetry in the predivisional cell was investigated as described [192]. Briefly, cells grown O/N in PYE were diluted into PYE and grown to OD of 0.3. One hour before microscopy cells were induced with 0.3% xylose and subsequently mounted on an agar-pad supplemented with PYE 0.3% xylose and cephalixin (10 µg/mL), followed by time-lapse microscopy with 10 min intervals for 5 hours.

Microscopy

Differential interference contrast (DIC), phase-contrast, and fluorescent microscopy analyses were performed using a DeltaVision system, Olympus IX71 microscope, and Photometrix CoolSnap HQ2 camera. Cells were mounted on 1.2% agar containing appropriate supplements. For statistics, cell length and the number of fluorescent foci were analyzed using MicrobeTracker (<http://microbetracker.org>).

Statistical analysis

For biochemistry we performed experiments as described earlier. All results documented are highly reproducible. Where indicated, mean values and standard deviations were obtained from at least three independent experiments

(biological replicates). For flow cytometry, we analysed more than two biological replicates. The results were highly reproducible with reasonable standard deviation. For replicative asymmetry measurements, we used Z-test to show that confidence levels for all measurement were above 99.9% (www.mccallum-layton.co.uk/tools/statistic-calculators).

Acknowledgments

We thank Timothy Sharp from the Biozentrum Biophysics Facility for help with protein analysis and Fabienne Hamburger for plasmid constructions. S.O. is a recipient of a Japan Society for the Promotion of Science (JSPS) Postdoctoral Fellowships for research abroad. This work was supported by Swiss National Science Foundation grant 310030B_147090 to U.J. and an ERC Advanced Research Grant to U.J.

Author contributions

C.L., S.O., S.A., S.S. and U.J. initiated the project. All authors designed experiments. S.O. carried out genetic experiments. C.L. and S.S. carried out biochemical experiments. C.L. and S.O. carried out microscopy experiments. R.B. and S.H. carried out NMR experiments. B.N.D. and T.S. contributed to structural analysis. U.J., S.O., and C.L. wrote the manuscript.

Strains used in this study

NAME	RELEVANT GENOTYPE	REF.
JOE2913	CB15 $\Delta lacA::\Omega$	[229]
MT15	NA1000 <i>xylX::pHPV472 Cori::(lacO)n</i>	[234]
MT16	NA1000 <i>ori::(tetO)n; xyl::pHPV472</i>	[234]
NA1000	<i>Caulobacter crescentus</i> wild type strain	[246]
SH100	UJ7304 <i>PdivK::Tn</i>	This study
SH111	UJ7214 <i>PdivK::Tn</i>	This study
UJ2827	NA1000 $\Delta popA$	[34]
UJ286	NA1000 $\Delta pleD$ <i>xylX::pPA28</i>	[247]
UJ2874	NA1000 $\Delta popA \Delta pleD$	A. Duerig
UJ4450	NA1000 $\Delta pleD$	[38]
CJ403	NA1000 $\Delta divK::\Omega$ <i>pdivK-egfp</i>	[199]
UJ5059	NA1000 <i>cdG0::pleD+</i>	[38]
UJ5065	NA1000 <i>cdG0</i>	[38]

UJ6122	NA1000 $\Delta cc1850, \Delta cc0740, \Delta cc0857, \Delta cc3285, \Delta cc3094, \Delta cc0896, \Delta cc0655 \Delta cc2462$ pRXMCS-2	This study
UJ6777	NA1000 $\Delta cc1850, \Delta cc0740, \Delta cc0857, \Delta cc3285, \Delta cc3094, \Delta cc0896, \Delta cc0655 \Delta cc2462$ $cc0006::(lacO)n$ $xyIX::pHPV472$	This study
UJ6861	UJ5065 $\Delta lacA::\Omega$ pBlue-pleD	This study
UJ7212	NA1000 <i>ckkA</i> Y514D	This study
UJ7214	NA1000 <i>ckkA</i> V366P	This study
UJ7304	UJ6861 $xyIX::tipNgfp$	This study
UJ7417	NA1000 <i>ckkA</i> -3xF	This study
UJ7418	NA1000 <i>ckkA</i> Y514D-3xF	This study
UJ7419	NA1000 <i>ckkA</i> V366P-3xF	This study
UJ7525	NA1000 $xyIX::pPA28(divK)$ $\Delta divK::\Omega$	This study
UJ7527	UJ7212 $xyIX::pPA28(divK)$ $\Delta divK::\Omega$	This study
UJ7529	UJ7214 $xyIX::pPA28(divK)$ $\Delta divK::\Omega$	This study
UJ7618	UJ7417 $xyIX::pPA28(divK)$ $\Delta divK::\Omega$	This study
UJ7619	UJ7418 $xyIX::pPA28(divK)$ $\Delta divK::\Omega$	This study
UJ7620	UJ7419 $xyIX::pPA28(divK)$ $\Delta divK::\Omega$	This study
UJ7873	NA1000 $\Delta pleD$ <i>divK::PxyL-divK</i>	This study
UJ7939	NA1000 <i>PdivK::Tn-tet</i>	This study
UJ7940	NA1000 $\Delta pleD$ <i>PdivK::Tn-tet</i>	This study
UJ7992	UJ5065 <i>divK::PxyL-divK</i>	This study
UJ8012	UJ7873 pPA41	This study
UJ8013	UJ7992 pMR20	This study
UJ8303	NA1000 pBXMCS-ckkA	This study
UJ8304	NA1000 pBXMCS-ckkA V366P	This study
UJ8305	NA1000 pBXMCS-ckkA Y514D	This study
UJ8306	NA1000 <i>ori::(tetO)n; xyL::pHPV472</i>	This study
UJ8307	UJ7212 <i>ori::(tetO)n; xyL::pHPV472</i>	This study
UJ8308	UJ7214 <i>ori::(tetO)n; xyL::pHPV472</i>	This study
UJ8312	NA1000:: <i>Plac-dgcZ-3xflag</i> $\Delta cc0655 \Delta cc0740 \Delta cc0857 \Delta cc0896 \Delta cc1850 \Delta cc2462 \Delta cc3094 \Delta cc3285$ <i>ori::(tetO)n; xyL::pHPV472</i>	This study
UJ8314	NA1000 $\Delta pleD$ <i>ori::(tetO)n; xyL::pHPV472</i>	This study
UJ8328	NA1000 $\Delta cc0091 \Delta cc0655 \Delta cc0740 \Delta cc0857 \Delta cc0896 \Delta cc1086 \Delta cc1850 \Delta cc2462 \Delta cc3094 \Delta cc3148 \Delta cc3285 \Delta cc3396$ pBXMCS-ckkA	This study
BL21 λ DE3	<i>E. coli</i> strain for protein purification: <i>F- ompT gal dcm lon hsdSB(rB- mB-) λ(DE3 [lacI lacUV5-T7 gene 1 ind1 sam7 nin5])</i>	New England Biolabs
BL21 Rosetta	<i>E. coli</i> strain for protein purification	Novagen

DH10 β	<i>E. coli</i> donor strain for plasmid conjugation: F-mcrA D(mrr-hsd RMS-mcrBC) f80dlacZDM15DlacX74 endA1 recA1 deoR D(ara, leu)7697 araD139 galU galK nupG rpsL	Life Technologies
DH5 α	A general <i>E. coli</i> cloning strain: F' endA1 hsdR17 (rK-mK plus) glnV44 thi1 recA1 gyr delta(Nahr) relA1 delta(lacIZYA-argF)U169 deoR(ϕ 80dlac delta(lacZ) M15)	[248]
S17	<i>E. coli</i> donor strain for plasmid conjugation	[249]
MT607	<i>E. coli</i> strain containing helper plasmid pRK600 for conjugation experiments	[250]
<i>A. tumefaciens</i> C58	<i>Agrobacterium tumefaciens</i> wild-type strain	[251]

Plasmids used in this study

NAME	DESCRIPTION	REF.
pNPTS138	a kan ⁺ suicide vector	[38]
pMR20	a tet ⁺ low copy vector	[252]
pJC389	a low copy vector carrying lacA	[229]
pBlue-pleD	a pJC389 derivative carrying PdivK-driven pleD	This study
pNPTS-XdivK	a pNPTS138 derivative to create Xylose-driven divK at the divK locus	This study
pAlmar1	a donor plasmid of the mariner-kan transposon	A. Levi
pPA28	a kan ⁺ integrating plasmid to create xylose-driven divK at the xylX locus	[247]
pMCS5	a tet ⁺ integrating plasmid	[236]
pMCS5-k2t	a pMCS5 derivative integrating at the mariner-kan locus	This study
pXTCYC-4	a gent ⁺ integrating plasmid carrying the xylose promoter	[236]
pXTCYC4-tipNgfp	a pXTCYC-4 derivative carrying tipNgfp	This study
pPA41	a pMR20 derivative carrying PdivK-driven pleD	[247]
pXMCS-1	a spec/strep ⁺ integrating plasmid carrying the xylose promoter	[236]
pMCS-1	a spec/strep ⁺ integrating plasmid	[236]
pMCS1-cckA	a pMCS-1 derivative, integrates spec/strep ⁺ downstream of cckA	This study
pMR20tipNgfp	a pMR20 derivative carrying tipNgfp	[199]
pGEM-T	a cloning vector	Promega
pRXMCS-2	a kan resistant low-copy plasmid carrying the xylose promoter	[236]
pBXMCS-2	a kan resistant high-copy plasmid carrying the xylose promoter	[236]
pBXMCS-cckA	a pBXMCS-2 derivative expressing cckA (S72-A691)	This study

pBXMCS-cckA V366P	a pBXMCS-2 derivative expressing cckA V366P (S72-A691)	This study
pBXMCS-cckA Y514D	a pBXMCS-2 derivative expressing cckA Y514D (S72-A691)	This study
pET28a	Expression vector	Novagen
pET28a-His-MBP	Expression vector to express N-terminal His-MBP fusion proteins	This study
pET32b	Expression vector to generate trx-fusions	Novagen
pNPTS-cckA-3xFLAG	a pNPTS138 derivative to introduce C-terminal cckA 3xFLAG tag	This study
pNPTS-cckA V366P	a pNPTS138 derivative to introduce V366P into chromosomal cckA	This study
pNPTS-cckA Y514D	a pNPTS138 derivative to introduce Y514D into chromosomal cckA	This study
pSA241.1	pTrcHisA derivative for overexpression of N-terminally His-tagged ctrA	This study
pTRC-ctrA D51E	Derivat of pSA241.1 overexpressing ctrA D51E	This study
pENTR:chpT	Entry clone of chpT lacking the first 28 codons of the annotated CC3470 gene	[170]
pENTR:cckA-HK-RD	Entry clone of cckA containing only the kinase and receiver domains	[170]
pTRX-HIS-DEST	For producing thioredoxin-His ₆ -tagged proteins	[170]
pHIS-MBP-DEST	For producing His ₆ -MBP-tagged proteins	[170]
pET-cckA	To express N-terminal His-MBP-cckA fusion, cckA from <i>C. crescentus</i> without TM (S72-A691)	This study
pET-cckA V366P	Derivat of pET-cckA carrying indicated mutation	This study
pET-cckA Y514D	Derivat of pET-cckA carrying indicated mutation	This study
pET-cckA F474A	Derivat of pET-cckA carrying indicated mutation	This study
pET-cckA D479A	Derivat of pET-cckA carrying indicated mutation	This study
pET-cckA F493A	Derivat of pET-cckA carrying indicated mutation	This study
pET-cckA W523A	Derivat of pET-cckA carrying indicated mutation	This study
pET-cckA R537A	Derivat of pET-cckA carrying indicated mutation	This study
pET-cckA F539A	Derivat of pET-cckA carrying indicated mutation	This study
pET-cckA S72-I573	To express N-terminal His-MBP fusions of truncated cckA alleles	This study
pET-cckA G571-A691	To express N-terminal His-MBP fusions of truncated cckA alleles	This study
pET-cckA P541-A691	To express N-terminal His-MBP fusions of truncated cckA alleles	This study
pET-cckA F496-A691	To express N-terminal His-MBP fusions of truncated cckA alleles	This study
pET-cckA V417-A691	To express N-terminal His-MBP fusions of truncated cckA alleles	This study
pET-cckA S72-P546	To express N-terminal His-MBP fusions of truncated cckA alleles	This study

pET-cckA A312-A691	To express N-terminal His-MBP fusions of truncated cckA alleles	This study
pET-cckA I292-I573	To express N-terminal His-MBP fusions of truncated cckA alleles	This study
pET-cckA A312-I573	To express N-terminal His-MBP fusions of truncated cckA alleles	This study
pET-cckA A312-546	To express N-terminal His-MBP fusions of truncated cckA alleles	This study
pET-cckA I292-P546	To express N-terminal His-MBP fusions of truncated cckA alleles	This study
pET-cckA A371-A691	To express N-terminal His-MBP fusions of truncated cckA alleles	This study
pET-cckA R189-A691	To express N-terminal His-MBP fusions of truncated cckA alleles	This study
pET-cckA I292-A691	To express N-terminal His-MBP fusions of truncated cckA alleles	This study
pET-cckA V417-A691(N- ZIP)	To express N-terminal His-MBP fusions of truncated cckA alleles, additional C-terminal N-zip	This study
pET-cckA A371-A691(N- ZIP)	To express N-terminal His-MBP fusions of truncated cckA alleles, additional C-terminal N-zip	This study
pET- AgrocckA	To express N-terminal His-MBP-cckA fusion, cckA from agrobacterium without TM (G74-E860)	This study
pET- Agroccka- Y674D	Derivat of pET-Agroccka carrying indicated mutation	This study
pET21b-CckA Q379-A545	To express CckA CA domain (379-545) with C-terminal His-tag	This study

Primers used in this study

NAME	SEQUENCE
104	TGTAACGACGGCCAGT
105	CAGGAAACAGCTATGAC
670	TGCTAGTTATTGCTCAGCGG
1033	GGAATTCATATGACGAAGAAGGTCCTCATCGT
1505	ATAAAGCTTTCAGGCGGCGTTAACCTGCTCGTT
3708	AAAAGGATCCC GCGTACTGTTGATCGAGGAT
4818	GATCTTATCCTGCTCGAGCTCAATCTTCCG
4819	CGGAAGATTGAGCTCGAGCAGGATAAGATC
5134	CGCCGCGACCTCCC GCGCAAGCTCTTG
5135	CAAGAGCTTGCGCGGGAGGTCGGCGGCG
5156	AACGAGCTCTGGGCGCCCGCTGCTC
5196	CATGCCATGGGCAAACATCACCATCACCATCACCCC
5242	GAACATATGAAGCCTAAGAAGCGCCAACC
5276	CGCGGATCCTCAGCGCTTTCGGCGGCGAC
5277	ACGCGTCGACCTACGCCGCTGCAGCTGCTG

5278 CGCGGATCCGGTGAAGGGGGCGGCCGCGGAGC
5279 CCGGGATCCCGCGCCGCCCCGCCACCCAGC
5280 CCGGGATCCATCGACGTGTCCGAGCAGAAG
5448 CGGGCCTAGGCCTAGCCACGGTCGATGGCATCGTTAAGCAGAG
CGAC
5449 GTCGCTCTGCTTAACGATGCCATCGACCGTGGCTAGGCCTAGG
CCCG
5454 ACGCGTCGACTTAGATGCGGCCGGCGCCCGAC
5455 CGCGGATCCGGCCGCATCCTGTTGTCGAGG
5456 CGCGGATCCCGGTCTATGAAGCGCCCGCC
5457 CGCGGATCCTTCTTCACCACCAAGCCGGTGGG
5458 CGCGGATCCGTGCGCGCCGACAAGAGCCAG
5502 CCGAACGAAGGCGCGGCCTTCGCCATCTTCCTGCCGGTCTATGA
AG
5503 CTTTCATAGACCGGCAGGAAGATGGCGAAGGCCGCGCCTTCGTT
CGG
5644 ACGCGTCGACTTAGGGCGCTTCATAGACCGGCAGG
5645 CGCGGATCCGCTTTCTCGCGCAAGCAGACCG
5646 CGCGGATCCGCCATCGGTCAGCTGGCCGG
5647 CGCGGATCCGTACCTATCCAGCGTATGAAACAGC
5648 CGCGGATCCACGTTACCCACCAGTTTTTTTC
5938 GTCGATATCATGATCTTTATAATCACCGTCATGGTCTTTGTAGT
CGAACGCCGCTGCAGCTGCTGCTTG
5939 AAGGACGCAAGGCTTTTATTTATCGTCGTCATCTTTGTAGTCGA
TATCATGATCTTTATAATCACCGTC
5940 TATCGACTACAAAGATGACGACGATAAATAAAAAGCCTTGCGTCC
TTCGAGGCCCG
5941 CCGAAGCTTCGGCTATCTGATCATGCTGATCGGGC
5942 CTAGCTAGCTTATGCAGGCTGCCTTTCCAGCAGG
5943 CAGACCTGATTCGATGGACATCGCGCTGCCCGAAATCTCGGG
TCTG
5944 CAGACCCGAGATTTCCGGCAGCGCGATGTCCATCAGAATCAGG
TCTG
6151 GAAGTCTCGAGCAGATCATGAAAGAGCTTCATG
6152 GAACCGCGGCATGCGGCAAAAAGGTCGTCGATGAAG
6153 GCCGAATTCAGCCAGTCGCCATAGGTCG
6154 CAACATATGACGAAGAAGGTCCTCATCGTGG
6430 CGCGGATCCGGCTTCATCGAGGTGATGCCGC
6431 ACGCGTCGACTTACTCCTTGTCGTCGAGCATTTCG
6436 GGTCTTGGCCTTTTCGATGGTCGACGGCATCGTCAAGCAGTCGG
GTGGT
6437 ACCACCCGACTGCTTGACGATGCCGTCGACCATCGAAAGGCCAA
GACC
6693 CGTGGTACCTGATTGAACAAGATGGATTGC
6694 TACGAGCTCGCTCGATGCGATGTTTCG
6708 GCCTTCCCACATGGGGTT
6709 CTGTCGTGTCTCAGGACGTT

6710 TACCCTTGCGCAGGGAGAGG
6711 TTCGAAGGGTCACGCCAGT
7200 GGAATTCCTACGCCCTGCAGCTGCTGC
7244 ATAATGCGGCCCGCCTTCATAGACCGGCAGGAA
7249 ATAATCATATGCAGCGGAGGTGCTGGATCTG
7369 GGATTTCCATATGTCAGCGCTTTCCGGCGGCGAC
7725 CCGCCGACGGCGACACGGCCGCCATTGAGGTCAGTGACGATG
7726 CATCGTCACTGACCTCAATGGCGGCCGTGTCGCCGTCGGCGG
7727 GGCCTTCATTGAGGTCAGTGCCGATGGTCCGGGCATTCCG
7728 CGGAATGCCCCGACCATCGGCACTGACCTCAATGAAGGCC
7729 CCCGACGTCATGGGCAAGATCGCCGACCCGTTCTTCACCACCAA
G
7730 CTTGGTGGTGAAGAACGGGTCGGCGATCTTGCCCATGACGTCG
GG
7735 CGTTAAGCAGAGCGACGGCGCCATTCACGTCCACAGCCGTC
7736 GACGGCTGTGGACGTGAATGGCGCCGTCGCTCTGCTTAACG
7737 CGAAGGCGCGGCCTTCCGCATCGCCCTGCCGGTCTATGAAGCG
CCC
7738 GGGCGCTTCATAGACCGGCAGGGCGATGCGGAAGGCCGCGCC
TTCG

Second messenger enforced bi-functionality of a central cell cycle switch

Badri N. Dubey^a, Christian Lori^b, Shogo Ozaki^b, Geoffrey Fucile^c, Ivan Plaza-Menacho^a, Urs Jenal^b, Tilman Schirmer^a

^a Focal Area of Structural Biology and Biophysics, Biozentrum, University of Basel, CH-4056 Basel, Switzerland

^b Focal Area of Infection Biology, Biozentrum, University of Basel, CH-4056 Basel, Switzerland

^c sciCore, Biozentrum, University of Basel, CH-4056 Basel, Switzerland

Manuscript in preparation for submission.

Keywords: c-di-GMP, histidine kinase, phosphatase, caulobacter, Cell cycle

Statement of my work: *In vitro* phosphorylation assays were done by myself.

Abstract

Regulatory kinases represent central cellular switches in all kingdoms of life. Accurate regulation of their activity is vital for the execution of specific cellular programs [150]. In bacteria, signal transduction is mainly mediated by histidine kinases (HKs) that in response to specific stimuli initiate phospho-transfer to down-stream targets. Many HKs are bifunctional and can change, upon regulatory input, from kinase to phosphatase mode, thereby reversing the flux within the phosphorelay [167]. The cell cycle kinase CckA from *Caulobacter crescentus* controls the master regulator CtrA [187] and changes to phosphatase mode during the G1-S transition [49] to initiate cell replication. The switch is triggered directly by the second messenger c-di-GMP [49], thereby linking two signalling pathways, but it is unclear how this works mechanistically and whether c-di-GMP control of HKs is a general trait in bacteria.

Here, we use a combination of structure determination, modeling and functional analysis to demonstrate that c-di-GMP allosterically up-regulates CckA phosphatase activity by noncovalently cross-linking the CA with the DHp domain. This domain constellation allows access of the phospho-Rec domain to the dimeric DHp stem [253], the pre-requisite for dephosphorylation. Furthermore, we show that also ADP promotes CckA phosphatase activity and infer that both ADP and c-di-GMP stabilize the same quarternary structure.

Bioinformatic analyses predict c-di-GMP mediated control for a large class of HKs where it would substitute, modulate or overwrite transmembrane signalling and, thus, constitute a crucial and ancient input to the signal cascade.

The action of HKs hinges on domain rearrangements. The core of HKs comprises the DHp dimerization domain with the phosphorylatable histidine and the CA domain with the substrate binding pocket [155]. Both domains can form a tight complex to catalyze the transfer of the γ -phosphate of the CA bound ATP substrate onto the histidine of the DHp domain. How auto-phosphorylation is controlled by external signals has been the subject of many studies [254,255] and re-arrangements in the dimeric DHp helix bundle in response to conformational changes in the periplasmic sensory domain appear to be central. Next, for phosphoryl transfer, the CA domain has to disengage to allow the Rec domain of the cognate response regulator to accept the phosphoryl group from the P~His [165,256].

Many HKs are bifunctional in that they also catalyze the reverse reaction, i.e. dephosphorylation of the phospho-Rec domain. Such bifunctionality has been shown theoretically and experimentally to confer “absolute concentration robustness” to the signal output [257–259]. Mechanistically, dephosphorylation is believed to require rebinding of the phosphorylated Rec domain to the DHp stem and subsequent phosphoryl transfer to a trapped water molecule [253]. Here, we investigate structure/function relationships in CckA that has been shown to be exquisitely sensitive to c-di-GMP control [49].

CckA_CA structure. CckA is a hybrid histidine kinase carrying a C-terminal Rec domain. The N-terminal part is predicted to consist of two transmembrane helices (with no intervening periplasmic domain) and two successive PAS domains (Fig. 1a). Various constructs were generated for structural and functional analysis. Figure 1b shows the high resolution crystal structure of the CA domain in complex with c-di-GMP and AMPPNP/Mg²⁺ (Tab. S1). The structure adopts the canonical CA fold with, however, a long insertion (between β 4 and β 5) that is folded as a helix/loop “tower” firmly attached to the outer face of the β -sheet by hydrophobic interactions. The c-di-GMP effector forms to H-bonds the main-chain of β 6 and the edge of the β -sheet. In addition, the base stacks with Trp523 and, at an angle, with Tyr514. In addition, guanine N7 is H-bonded to Lys518. The identified primary binding site is consistent with NMR and mutant data published previously [49]. The remainder of the ligand forms artefactual crystal contacts with the His-tail of an adjacent molecule. Summarizing, the crystal structure defines a specific c-di-GMP binding sub-site (primary binding site) on the CA domain and suggests that the distal part of the ligand may be available for binding to another domain in full-length CckA.

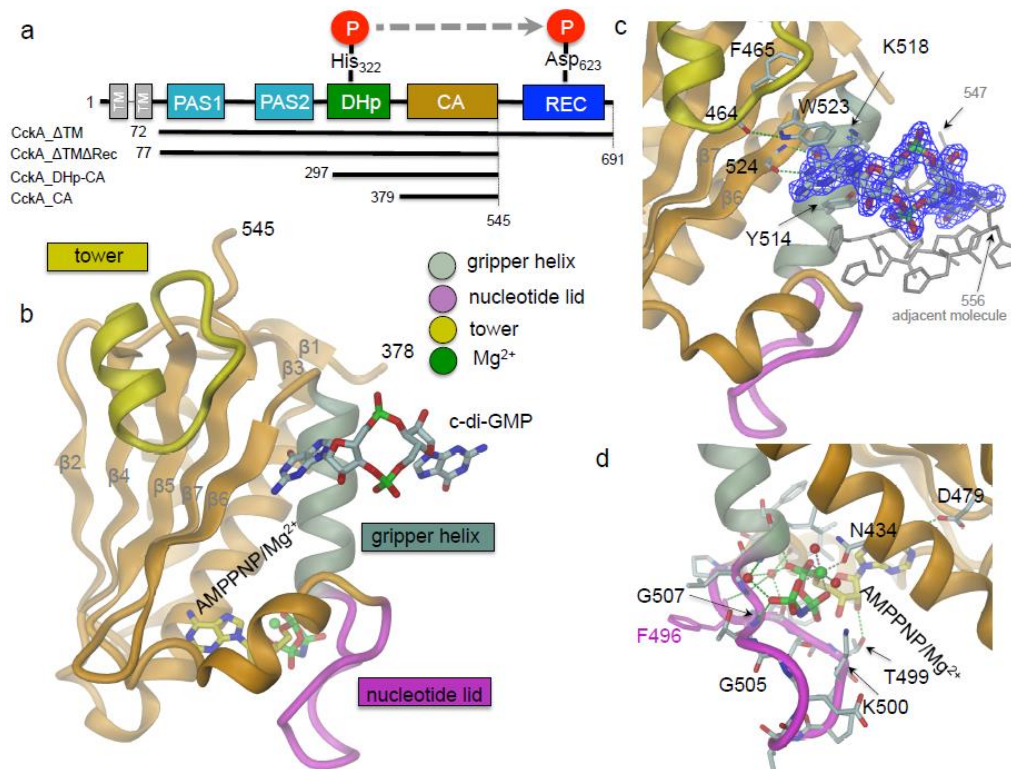


Figure 1: CckA domain arrangement and crystal structure of the CA domain in complex with c-di-GMP. (a) CckA domain arrangement and constructs used. **(b-d)** Crystal structure of CckA_CA with bound c-di-GMP and AMPPNP/Mg²⁺. The nucleotide lid partly covering the mononucleotide site (magenta), the gripper helix (grey), and the CckA specific insertion (tower, yellow) are distinguished by color. Detailed views of the c-di-GMP and the mononucleotide protein interactions are shown in **(c)** and **(d)** H-bonds are shown with green broken lines.

CckA_DHp-CA structure. The dimeric DHp-CA histidine kinase core structure (Figs. 2, S2a) shows a symmetric open domain constellation with the DHp helix bundle potentially accessible for Rec docking. Similar constellations have been found previously for HK853/RR468 [166] and CpxA/ADP [260]. In all cases and here, the CA domain is binding to the DHp stem via the "gripper" helix and the "thumb" (Phe496). Strikingly, the two CA domains of the CckA dimer are found to be swapped compared to the other kinases (compare e.g. with Fig. 4a). Possibly, this difference is due to distinct crystal contacts (Fig. S1). The ATP lid (with bound ADP) is ordered and shows a similar conformation as in the structure of the isolated CA domain in complex with AMPPNP (Fig. 1). Unfortunately, no crystals were obtained in presence of c-di-GMP.

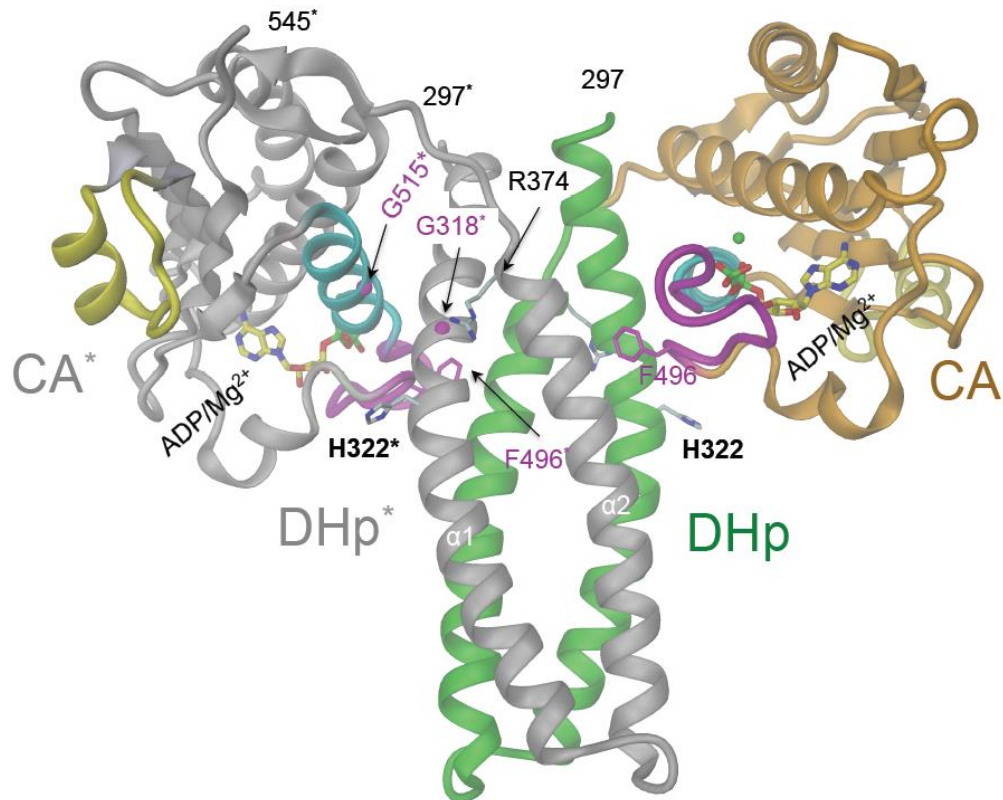


Figure 2: Crystal structure of CckA_DHp-CA dimer. Cartoon representation with one of the subunits is colored in green (DHp domain) and orange (CA domain), the other in grey (with asterisked labels); other colors as in Figure 1. Some important residues and ADP/Mg²⁺ are shown in full. The

C α atoms of Gly318 and Gly515 are shown as magenta spheres. The domain arrangement is similar as in CpxA/ADP/Mg²⁺ [260], but with domains swapped in the dimer (Fig. S4). The Phe496 "thumb" of CA is inserted between DHp helices, the "gripper" helix (cyan, residues 508 - 520) mediates most of the inter-domain contact. The connection of the DHp helices is right-handed.

CckA ligand affinity. Ligand binding has been measured by ITC (Figs. 3, S3, Tab S2). The ATP analog AMPPNP binds with high affinity ($K_d \sim 10 \mu\text{M}$) to the CA domain and to the full cytosolic CckA_ Δ TM construct, whereas the ADP affinity is considerably lower. C-di-GMP binds to the isolated CA domain, both in presence of ADP or AMPPNP (Fig. 3c) with a dissociation constant of about 20 μM , i.e. clearly above the physiological c-di-GMP concentration [49], but in line with the crystal structure that shows only half of the c-di-GMP ligand bound to the domain (Fig. 1).

Strikingly, the full cytosolic construct (CckA_ Δ TM), binds c-di-GMP only in presence of ADP, and not AMPPNP. The K_d (1.4 μM) is about an order of magnitude lower than that for CckA_CA (Fig. 3), suggesting that additional domain(s) contribute to binding and that ADP stabilizes a domain constellation that is competent for c-di-GMP binding. Indeed, distinct HK constellations have been observed in presence of ADP and AMPPNP [166,260,261] and, most relevantly, these have been correlated with phosphatase and kinase activity, respectively. Thus, c-di-GMP and ADP would synergistically stabilize the phosphatase state of the enzyme. The double domain construct (CckA_DH_p_CA) binds c-di-GMP less strongly than the full cytosolic construct (Fig. 3). Thus, either additional domains contribute to the interaction or the structure of the dimeric DH_p bundle is perturbed due to the absence of the N-terminal PAS2 domain, which is predicted to form a homotypic dimer (Fig. S9).

Modeling suggests CA - DH_p cross-linking by c-di-GMP. More insight into possible c-di-GMP binding modes was obtained upon superimposition of CckA_CA/c-di-GMP ligand on CckA_DH_p_CA (Fig. S2) or on a CckA model based on CpxA/ADP (Fig. 4a).

In both cases, the "distal" (not CA bound) half of c-di-GMP points towards Arg374 of the second DH_p helix. In fact, upon minor manual adjustment of the conformations, both moieties can be brought into close juxtaposition to form a canonical [262] O6, N7 - guanidinium interaction (Fig. S4). Crucially for the discussion later, this appears possible only when no side-chain is present in position 318 (Gly318 of DH_p helix α 1). In addition, Gln315 seems well poised

to interact with the ligand.

Through such a binding mode, c-di-GMP would act as a non-covalent cross-linker to stabilize the “open” domain constellation, the pre-requisite for access of the phospho-Rec domain to the DHp stem and phosphatase action. Such a mechanistic model would be fully consistent with the observed ligand binding characteristics (Fig. 3), in particular, the requirement of ADP for high-affinity c-di-GMP binding. Still, why c-di-GMP binding to the ATP bound conformation of CckA (Fig. 3c) is completely, and not only partially, abolished remains to be investigated. The elevated K_d for AMPPNP in presence of (non-saturating) c-di-GMP (Fig. 3b) is further evidence for negative cooperativity between these two ligands.

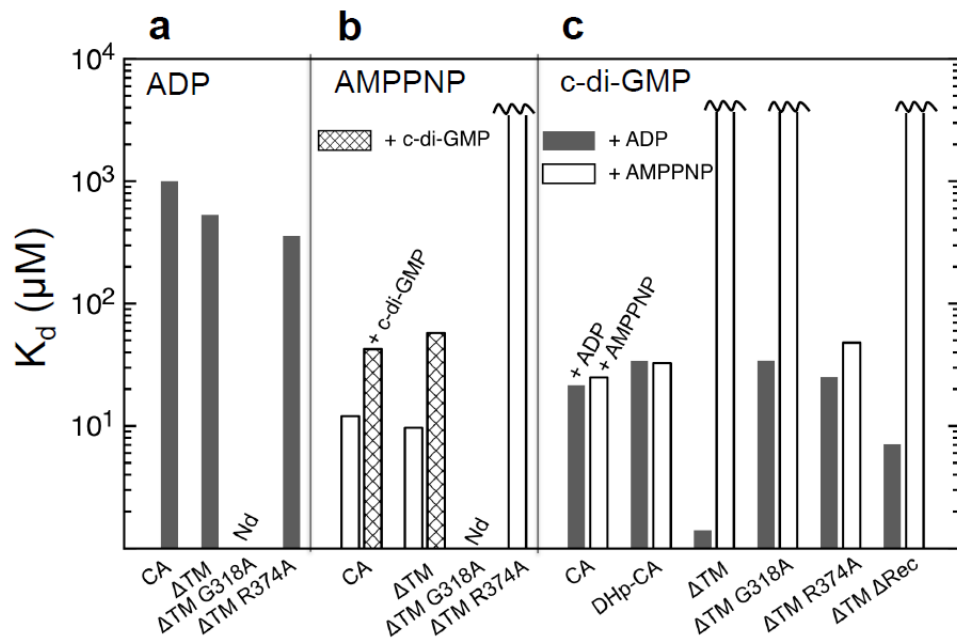


Figure 3: Ligand binding to CckA. Dissociation constants of various CckA constructs as measured by isothermal titration calorimetry (ITC). **(a)** ADP. **(b)** AMPPNP in absence or presence of 100 μM c-di-GMP. **(c)** c-di-GMP in presence of 5 mM ADP or AMPPNP. Further information is given in Table S2 and Fig. S5.

Functional analysis supports the mechanistic model. Functionally, CckA was assayed *in vitro* by auto-radiography upon incubation with [$\gamma^{32}\text{P}$]-ATP. The time course (Figs. 5a, b) shows non-linear accumulation of the phosphorylated species indicating both kinase and phosphatase activity. As observed before [49], the protein gets efficiently dephosphorylated upon addition of c-di-GMP and phosphorylation is impeded when present from the beginning (Fig. 4c). Since c-di-GMP binds to CckA only in presence of ADP (Fig.3) and thereby promotes CckA dephosphorylation, we reasoned that ADP on its own might have a similar effect. Indeed, ADP induced dephosphorylation was observed as shown in Figures 5a,b. Enhanced dephosphorylation by ADP has been seen before for EnvZ/OmpR [263] and PhoQ/PhoP [264] and is the cornerstone for a feed-back model [265] that explains the transient surge of phospho-PhoP upon activation .

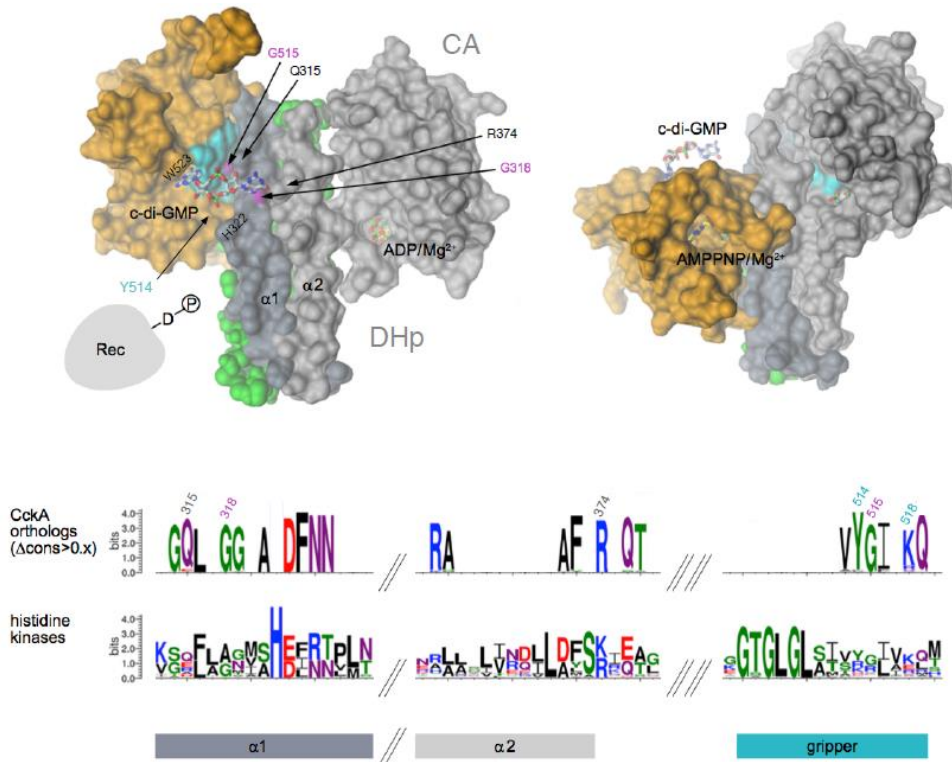


Figure 4: Modeled CckA_DHP_CA domain constellations. The crystal structures of the individual DHP helices and the CA domains of CckA are shown as obtained upon superposition on selected CpxA structures. **(a)** Phosphatase constellation as in CpxA/ADP complex (PDB code 4bix). C-di-GMP is cross-linking the primary site (CA domain; Y514, K518, W523) with

the secondary site (DHp domain; G318, R374 nitrogens in blue). Full model shown in Extended Data Fig. 4. This constellation is predicted to be competent for dephosphorylation of cognate P~Rec (represented symbolically). **(b)** Kinase constellation as in CpxA/AMPPNP complex (PDB code 4biw). Note, that relative to the constellation in **(a)**, the CA domain has turned around by about 70° to bring the AMPPNP substrate analog close to the phosphor-acceptor histidine 322 (not shown, buried within the interface). **(c)**, Excerpts of sequence logos for CckA orthologs (top) and histidine kinases in general (CckA orthologs plus paralogs; bottom). For the upper logo, only residues with a conservation contrast (Δ cons) score in the upper quartile are shown. Residues related to c-di-GMP binding are labeled by their CckA numbers.

Mechanistic model of CckA probed by mutagenesis. To test the mechanistic cross-linking model, we mutated Gly318 as well as Arg374 of the putative secondary binding site. Both mutants exhibited a decrease in c-di-GMP affinity (Fig. 3) consistent with a loss of binding to the secondary site. Functionally, the G318A mutant was fully competent for auto-phosphorylation and ADP induced dephosphorylation (Figs. 5c,d), but showed virtually no response to c-di-GMP (Fig. 5c). Both is consistent with a loss of c-di-GMP mediated domain cross-linking due to the presence of the C β atom that would prevent the distal guanine to reach Arg374 (Fig. S4). Mutation of this arginine (R374A) completely abolished AMPPNP binding (Fig. 3A) and the mutant was consequently not amenable to further *in vitro* investigations. That this residue is important for substrate binding has been seen for the homologous arginyl residue in CpxA [260]. In addition, the role of residue Gly515 was tested. This residue is part of the domain interface (Fig. 2) and interacts with Gln315, which in turn appears well poised to interact with c-di-GMP (Fig. S4). A side-chain at position 515 would disturb the domain arrangement and, thus, may interfere with c-di-GMP mediated domain cross-linking. Indeed, the phenotype of G515D was identical to that of G318A (Figs. 5b and c) further strengthening the cross-linking model.

Additional functional insight was obtained with a CckA construct that lacks the receiver domain (CckA_ Δ TM Δ Rec) and is therefore, by definition, phosphatase deficient. Fig. 5d shows that, under assay conditions, addition of c-di-GMP did not interfere with auto-phosphorylation. This is consistent with the mechanistic model that predicts lack of cross-linking for the ATP complex.

The mutants were also investigated *in vivo* (Figure S6) taking DNA content as measured by flow cytometry as read-out for chromosome replication activity [49]. As previously reported [49], overexpression of CckA_ Δ TM in a wild-type

cdG+ strain resulted in over-replication indicating dephosphorylated CtrA and hence dominant CckA phosphatase activity. The effect was found c-di-GMP dependent, since a distinct, more vector control like phenotype was observed upon expression in a cdG0 background [49]. The (kinase deficient) R374A mutant also caused over-replication, but in this case, the phenotype was virtually independent of expression strain and most likely due to basal (ADP activated) phosphatase activity superseding endogenous CckA kinase activity. Mutants Y514D and G515D showed severe replication deficiency indicating dominant kinase activity, which would be explained by the loss of c-di-GMP mediated auto-dephosphorylation. In the cdG0 background, expression of these variants was lethal, possibly due to aggravation of the mutant effect by the absence of c-di-GMP mediated CtrA proteolytic turn-over [47,266]. Finally, the G318A mutation was toxic consistent with full replication deficiency, whereas Q315A was indistinguishable with wild-type over-expression indicating a minor contribution (if any) of Gln315 to c-di-GMP binding. Summarizing, the *in vivo* data appear fully consistent with the proposed regulatory c-di-GMP mechanism.

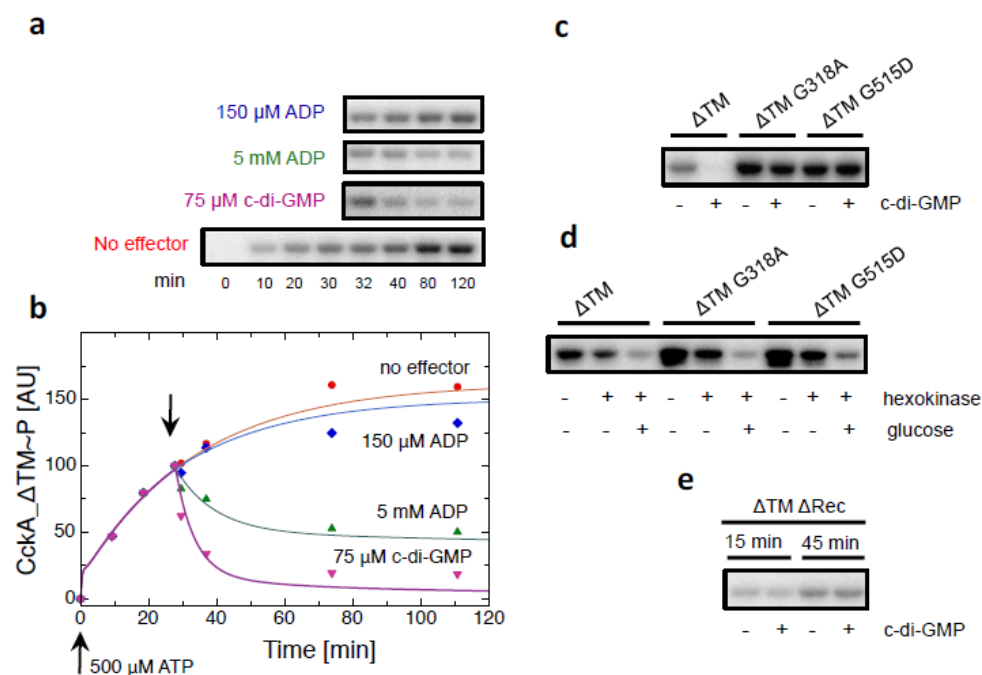


Figure 5: Net phosphorylation of CckA_ΔTM and other variants in response to c-di-GMP and ADP. (a) Time course of net CckA_ΔTM~P formation as measured by autoradiography upon addition of 500 μ M

radioactively spiked ATP (bottom row). ADP or c-di-GMP was added to aliquots after 30 mins (top three rows). **(b)** Quantification of the data of **(a)**. Continuous lines have been calculated based on the kinetic model shown in Fig. 6 obtained from the global fit to the data. **(c)** Net CckA phosphorylation for the indicated variants after 15 mins of ATP incubation, in absence and presence of c-di-GMP. **(d)** Net CckA phosphorylation for the same variants as in (c), but with addition (at $t = 15$ mins) of hexokinase/glucose for complete ATP to ADP conversion. The reaction was stopped after 65 mins. **(e)** Same as in (c), but for the mono-functional (kinase only) CckA_ΔTMΔRec construct with indicated incubation times.

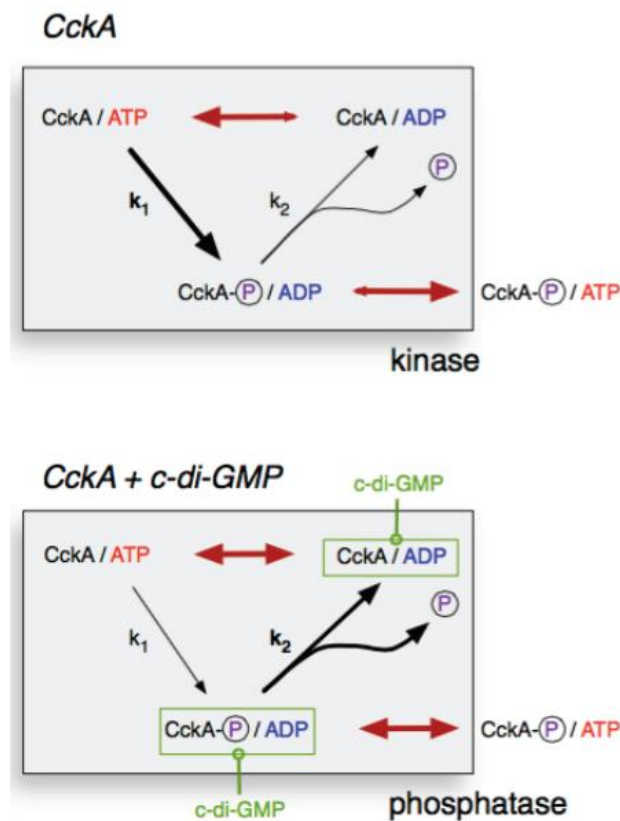
Bioinformatics. Having identified residues crucial for c-di-GMP mediated CckA control, we set out to study their conservation in other bacterial HKs. Two HK sequence families that broadly cover α -proteobacteria were generated based on the sequences of CckA from *C. crescentus* and a distant paralog, respectively (Fig. S10). While both groups carry the canonical residues that qualify them as histidine kinases, the orthologous group shows, in addition well defined, specificity determining positions (SPDs, [267]) as indicated in Fig. S8. Strikingly, all of the c-di-GMP related positions (labeled in Fig. 4) are SPDs, and moreover, highly or strictly conserved amongst the orthologs (with the only exception of Trp523 that often is replaced by Tyr or Phe).

Kinetic model of CckA regulation. The various structural and functional aspects of CckA regulation by c-di-GMP and ADP have been consolidated in the kinetic model shown in Figure 6. Under physiological conditions and in absence of the c-di-GMP effector, the enzyme will be predominantly complexed with ATP, considering its tighter affinity and larger cellular concentration compared to ADP. Not considering other input signals, the enzyme will auto-phosphorylate and come to a halt as ATP complex after nucleotide exchange. The effect of c-di-GMP is proposed to rest on the (thermodynamic and probably also kinetic) stabilization of the ADP complex, which would be the only state competent for dephosphorylation. At the same time kinase action would get ADP product inhibited.

This simple kinetic model fits well the progress curves of CckA phosphorylation acquired in absence and presence of the allosteric effectors (Fig. 4a), considering the small number of free parameters (Table S3). The fit gave a drastically enhanced ADP affinity in presence of saturating amount of c-di-GMP and this was modeled by a respective increase in the on-rate. Furthermore, the equivalent effects induced by c-di-GMP and ADP are

reproduced, although the ADP effect at low concentration is somewhat underestimated. Interestingly, simulations show that the ADP effect is very sensitive to the rate of debinding (k_r) and the data are only fittable with a rather slow rate (10^{-2} to 10^{-3} s $^{-1}$, similar to reaction rates k_1 and k_2 ; Table S3). A similar observation has been made for PhoQ/PhoP by Yeo et al. (2012) [265]. Further experiments are needed to obtain direct kinetic information.

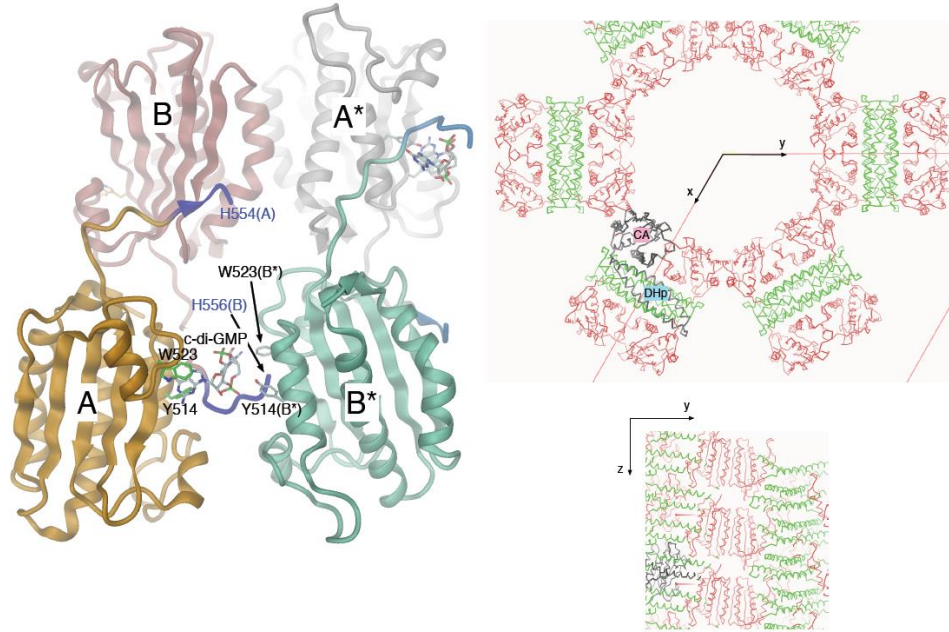
Figure 6: Kinetic model of CckA regulation. Kinetic regulatory model of



CckA. Auto-phosphorylation and auto-dephosphorylation proceed with first-order rates k_1 and k_2 , respectively. For simplicity, no distinction is made between phosphorylation of H322 (DHP), D623 (Rec), or both. Red double arrows indicate ADP ↔ ATP exchange. Top: After auto-phosphorylation the ADP product gets efficiently replaced by ATP. The dephosphorylation branch is not effective and the enzyme can catalyze phospho-transfer to the cognate down-stream partner (ChpT, not shown). Bottom: C-di-GMP allosterically stabilizes the ADP, the state that is competent for CckA autodephosphorylation. Note that re-phosphorylation is impeded due to ADP product inhibition. Phosphoryl groups will flow back along the phosphorelay.

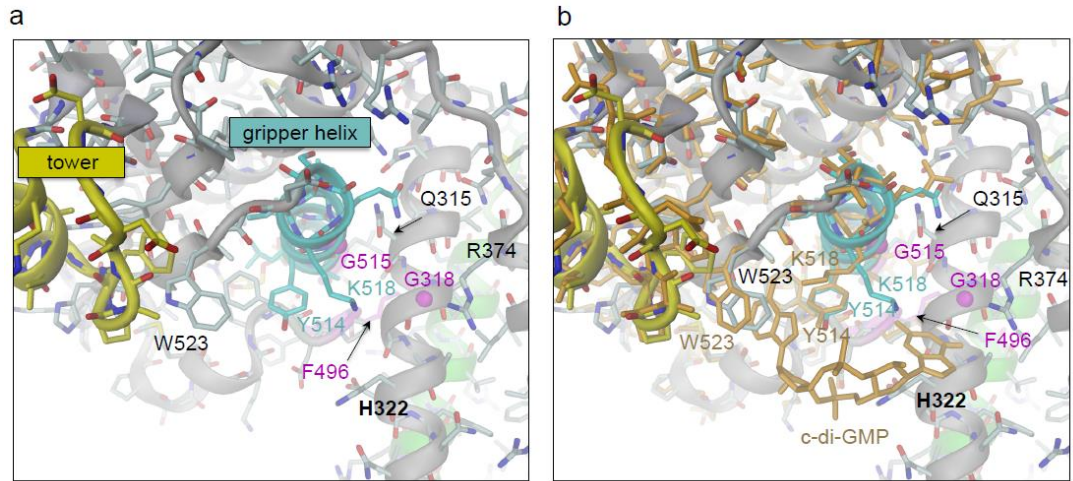
In summary, we have shown that c-di-GMP, in synergy with ADP, reciprocally regulates kinase/phosphatase activity of a HK by stabilizing the "open", phosphatase competent constellation. In this way, the enzyme is rapidly converted to a sink for the phosphorelay, with the corresponding effect on the down-stream targets. Interestingly, ultrasensitive effector response has been predicted theoretically for such bifunctional enzymes with antagonistic activities [268] and this will be investigated further.

Extended Data Figure 1



Extended Data Figure 1: CckA crystal packings. **(a)** Crystal packing of CckA_CA with two molecules in asymmetric unit (A, B). Also shown are two symmetry related molecules (A*, B*). The C-terminal His(6)-tails are shown blue. C-di-GMP is bound to the primary site of molecule A (orange). The primary binding site of B* (green) is blocked by the His-tail of a symmetry related molecule (B). The His-tail of A is mediating a crystal contact by interacting laterally with a β -sheet edge of B. **(b and c)** Crystal packing of CckA_DHp-CA. The crystal of space-group P6(3)22 is formed by β -sheet edge-to-edge association of CA domains across a crystallographic dyad. In combination with the crystallographic 6(3) screw axis, nano-tubes with a diameter of 45 Å are formed in z-direction. The nano-tubes are held together by DHp domains that form crystallographic dimers.

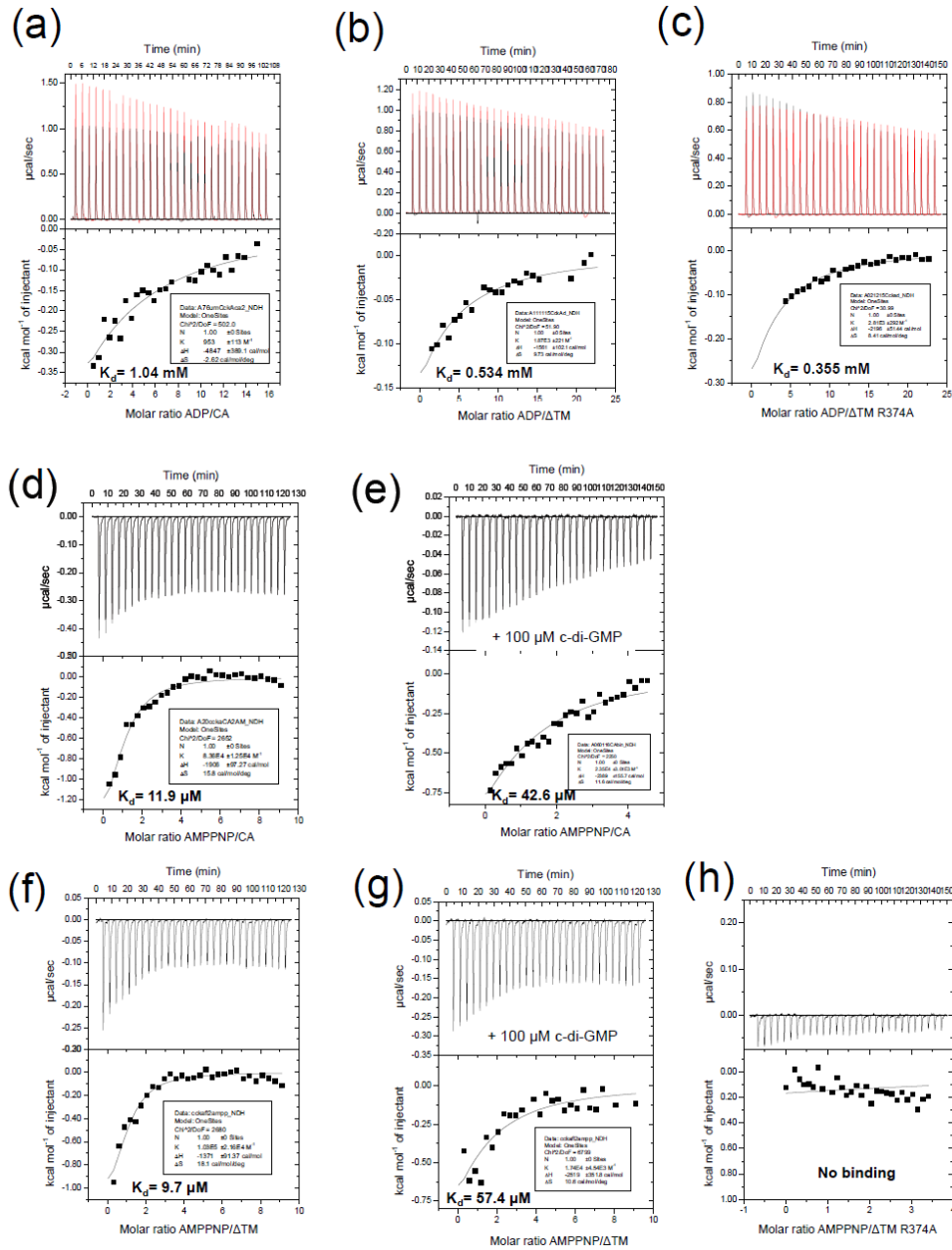
Extended Data Figure 2

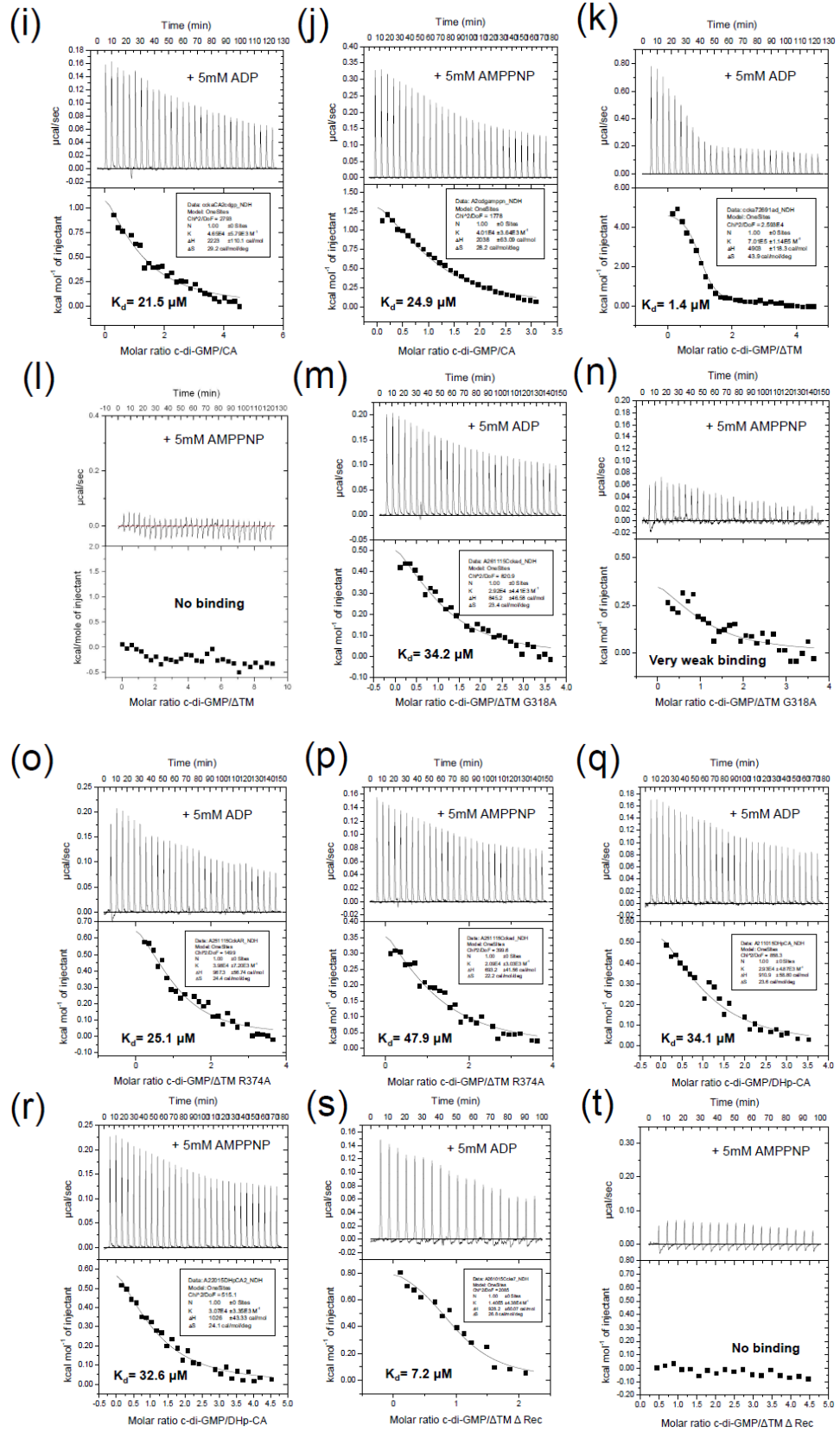


Extended Data Figure 2: Detailed views on CckA_DHp_CA and CckA_CA/c-di-GMP crystal structures. Viewing direction same as in Figure 2. **(a)** Close up of domain interface. The "gripper" helix (residues 509 - 520) and the tower (456 - 471) are shown in cyan and yellow, respectively. The α atoms of Gly318 and Gly515 are shown as magenta spheres. **(b)** Same as (a), but showing, in addition, crystal structure of CckA_CA with bound c-di-GMP (all atoms, orange) superimposed.

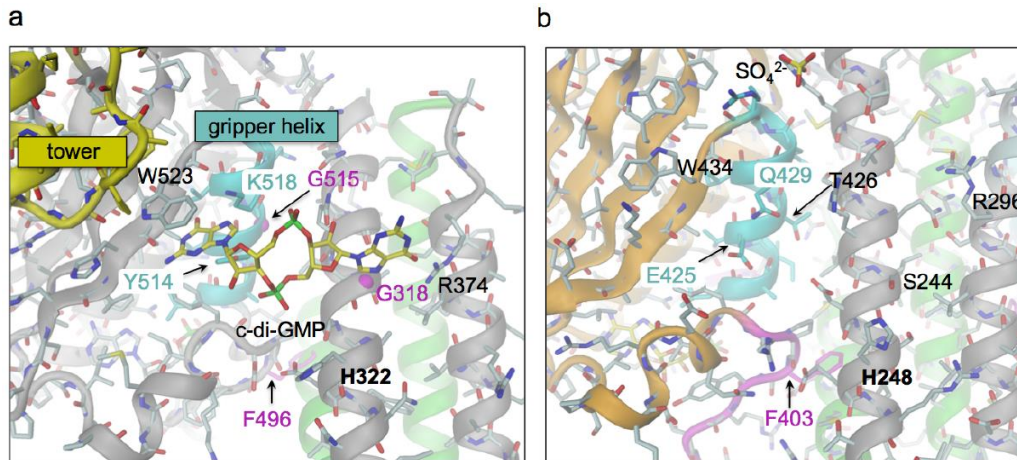
Extended Data Figure 3

Extended Data Figure 3: ITC binding profiles of several CckA constructs to ADP, AMPPNP and c-di-GMP.



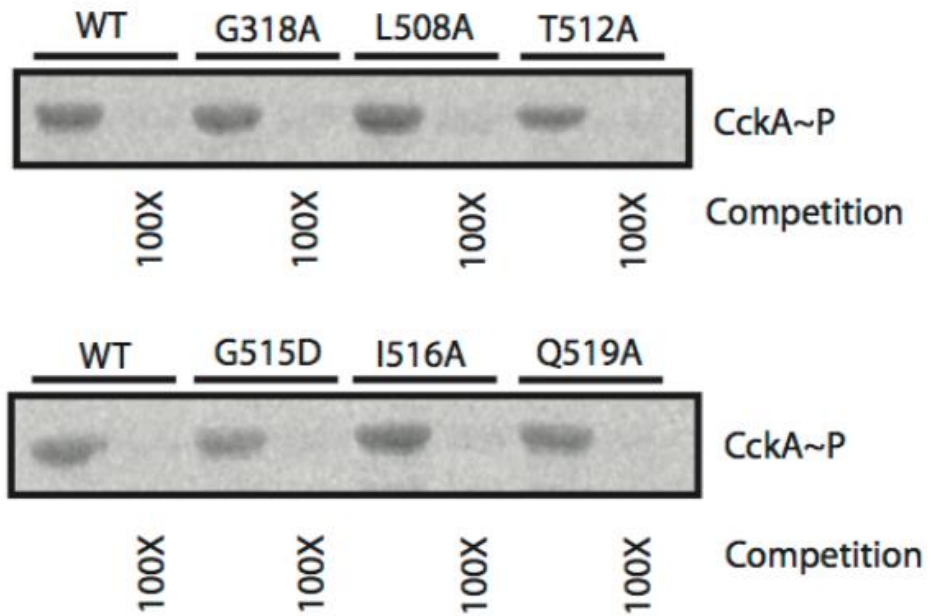


Extended Data Figure 4



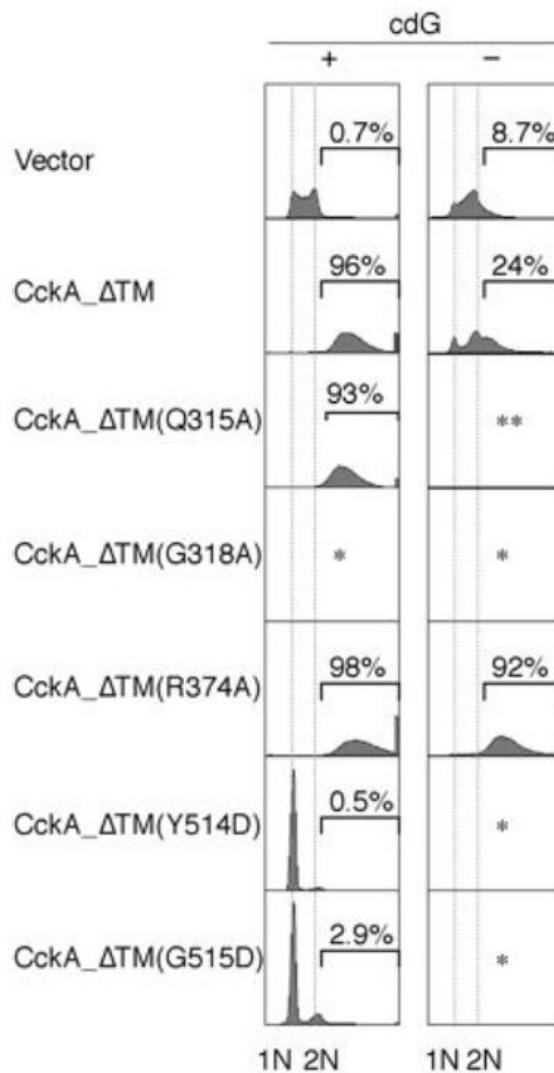
Extended Data Figure 4: Proposed model of full c-di-GMP binding to CckA_DHp_CA. The C α atoms of Gly318 and Gly515 are shown as magenta spheres. **(a)** CckA model obtained by superposition of CckA DHp helices and CA domain onto the CpxA/ADP structure. The distal part of the c-di-GMP ligand (right) has been remodeled in extended conformation as (e.g.) obtained when bound to EAL domain [17]. The side-chain conformation of Arg374 has been changed to allow interaction with the c-di-GMP ligand. **(b)** Same view of CpxA/ADP structure has been shown. Phe403 (shown in magenta) engaged in the CA–DHp interface but key residues involve in c-di-GMP is missing.

Extended Data Fig. 5



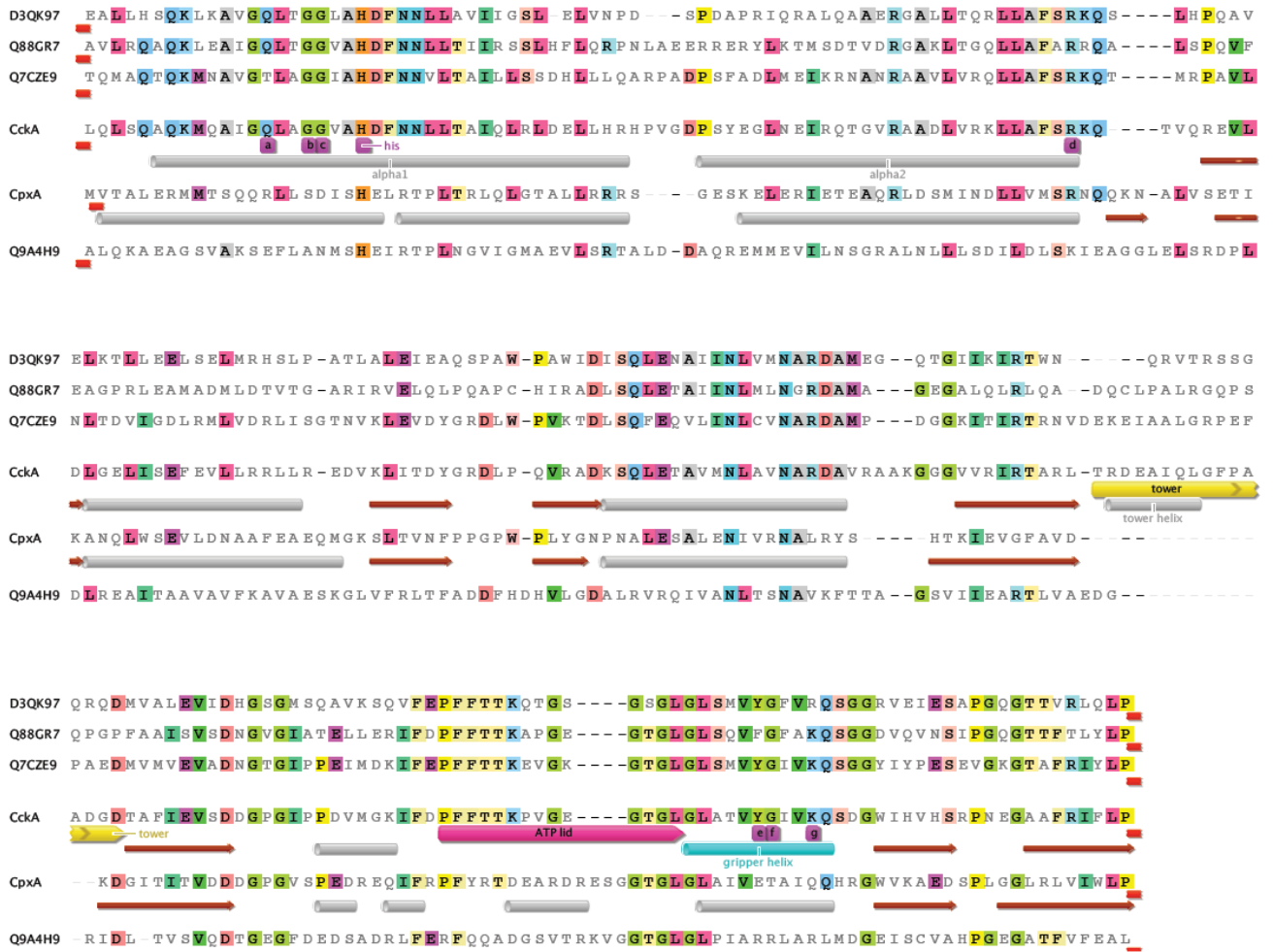
Extended data Figure 5: C-di-GMP specifically binds to CckA mutants. Purified CckA protein was incubated with [33 P] labelled c-di-GMP and cross-linked with UV light in the presence or absence of a 100-fold excess of competing non-labelled nucleotides as indicated.

Extended Data Figure 6



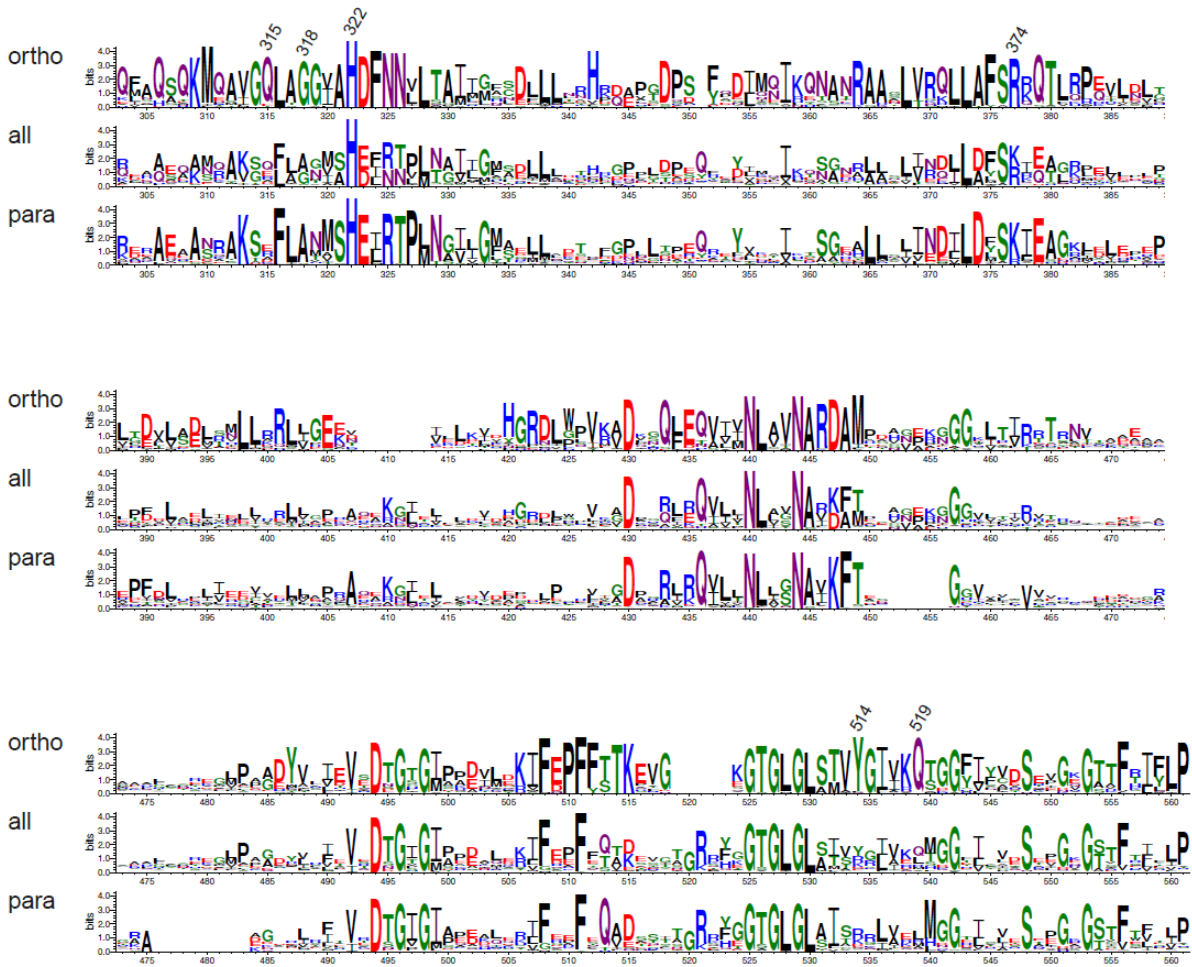
Extended Data Figure 6: DNA replication activity of cells expressing various CckA variants. The indicated *cckA*(Δ TM) variants were expressed in the wild-type (+) or cdG0 (-) strain, followed by analysis of DNA content using flow cytometry. Representative DNA profiles of the two biological replicates are shown. The fraction of cells bearing more than two chromosomes is indicated and shown as percentage. Note that the cdG0 strain harboring either Y514D or G515D did not grow under the current experimental conditions. Q315A allele was tested only in the wild-type strain. *, Transformants did not grow. **, not tested.

Extended Data Figure 7



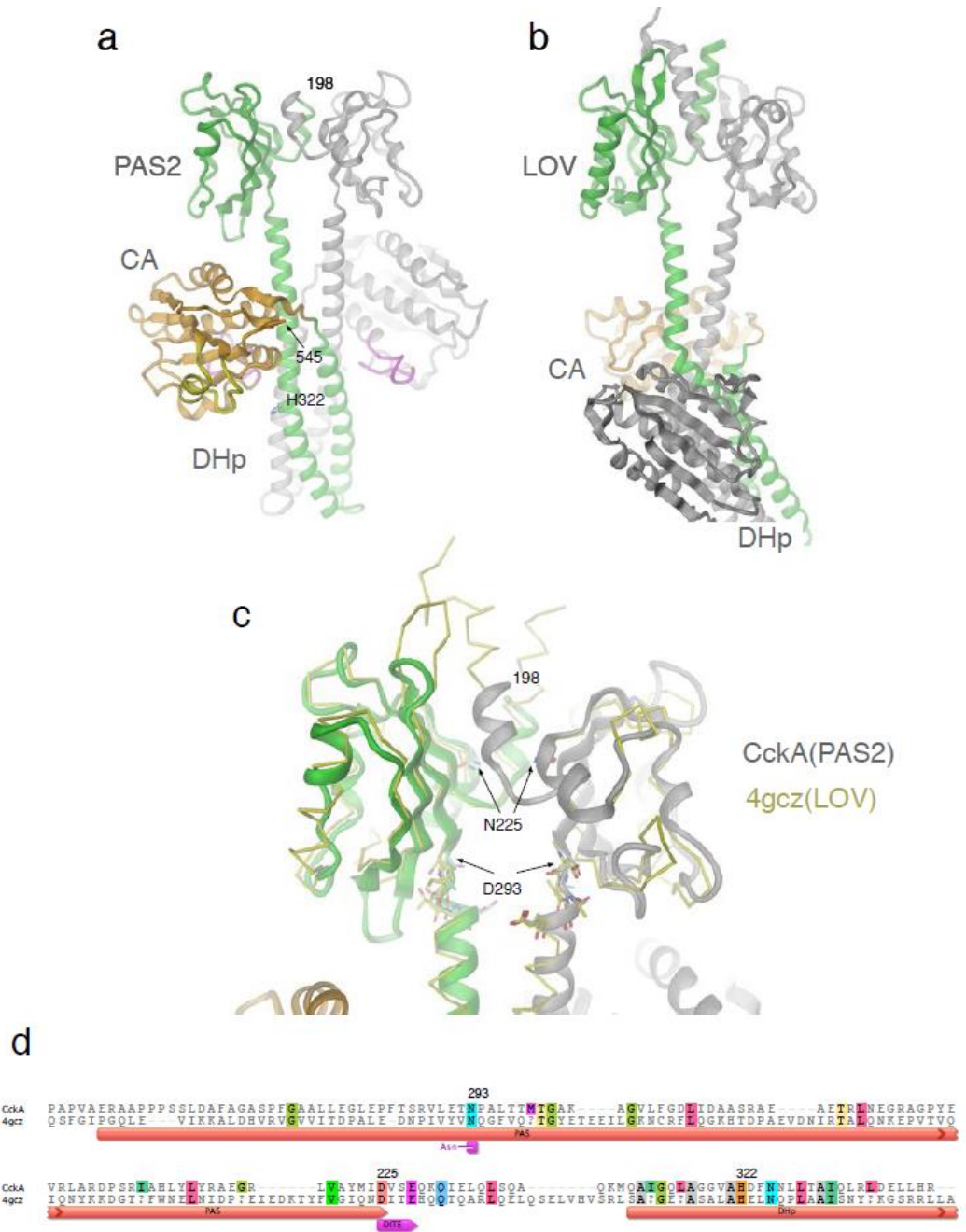
Extended Data Figure 7: Sequence alignment between CckA ortho- and paralogues. CckA orthologues from UPEC *E.coli* (UNIPROT D3QK97), *Pseudomonas putida* (Q88GR7), *Agrobacterium tumefaciens* (Q7CZE9), and CckA from *Caulobacter crescentus* (H7C7G9) are shown at the top. Paralogues CpxA from *E.coli* (P0AE82) and Q9A4H9 from *Caulobacter crescentus* are shown at the bottom. The sequence alignment between CckA and CpxA conforms to the alignment between the crystal structures and secondary structure elements are indicated. Important CckA residues are annotated: a, Q315; b-c, G318, G319; d, R374; e, Y514; f, G515; g, K318. All of these residues are specifically conserved in the orthologous group.

Extended Data Figure 8



Extended Data Figure 8: Specificity determining positions of CckA orthologs. Weblogos are shown for CckA orthologs, paralogs (bottom, yy sequences) and both groups together (middle). Latter graph highlights the residues that are essential for general histidine kinase function. Residues specifically conserved ($\Delta\text{cons} > x$) in the orthologous CckA group (top) are indicated with an asterisk (to be done) and labeled with their CckA number, otherwise global residue numbering.

Extended Data Figure 9



Extended Data Figure 9: Structure prediction for PAS2 domain of CckA.

(a) CckA_DHp-CA structure with joined homology model for the N-terminal PAS2 dimer. The PAS2 homology model was obtained based on PDB entry 4gcz (structure of an engineered LOV-DHp-CA construct based on the LOV domain of YtvA and the DHp-CA domains of FixL. **(b)** YtvA/FixL template structure (PDB ocde 4gcz). Orientation such that the N-terminal LOV dimer is in same orientation as the PAS2 dimer in (a). **(c)** Sequence alignment of CckA_PAS2-DHp with YtvA(LOV)-FixL(DHp) as obtained by HHpred and used for homology modeling. Note that the domain linker is shorter by 7 residues in CckA, which is compatible with a coiled-coil dimer shortend by two turns.

Extended Data Table 1: Data collection and refinement statistics

	CckA_CA/AMPPNP/ c-di-GMP/Mg ²⁺	CckA_DH-CA/ADP/Mg ²⁺
Data collection		
Synchrotron source	SLS, PXIII	SLS, PXI
Space group	P 2 ₁ 2 ₁ 2 ₁	P 6 ₃ 2 2
a, b, c (Å)	56.3, 62.1, 103.9	164.9, 164.9, 48.0
α, β, γ (°)	90, 90, 90	90, 90, 120
Resolution (Å)	30-1.9 (2.0-1.9)*	30-3.0 (3.1-3.0)
Unique reflections	29150 (4197)	7413 (575)
Completeness	99.2 (99.3)	91.4 (51.2)
I/σ(I)	13.8 (5.9)	15.0 (1.7)
Redundancy	6.4 (6.5)	11.3 (1.6)
R _{merge} (%)	8.8 (30.0)	10.3 (32.7)
R _{pim} (%)	3.8 (16.3)	3.1 (28.6)
CC (1/2) %	99.8 (91.9)	99.9 (77.4)
Refinement		
R _{work} /R _{free} (%)	19.3/22.9	21.1/27.8
rmsd		
Bond length (Å)	0.009	0.011
Bond angles (°)	1.62	1.65
Molecules/asymmetric unit	2	1
No. of atoms		
Protein	2735	1869
Ligand	110	28
Metals	2	1
Water	428	1
Average B-factor (Å ²)	17.4	90.0
Protein	16.7	90.3
Nucleotides	7.9	74.1
Metals	10.3	63.5
Water	24.6	61.3
Ramachandran statistics (%)		
Favoured regions	97.1	87.9
Allowed regions	2.6	9.2
Disallowed regions	0.3	2.9
PDB codes	5IDM	5IDJ

* The values recorded in parentheses are those for the highest resolution shell

Extended Data Table 2: ITC binding parameters for CckA with ligands

(a) ADP binding								
CckA construct	C _{cell} (μM)	C _{syringe} (μM)	- c-di-GMP			+ 100 μM c-di-GMP*		
			K _d (mM)	ΔH (kcal/mol)	-TΔS (kcal/mol)	K _d (μM)	ΔH (kcal/mol)	-TΔS (kcal/mol)
CA	76	5000	1.0	-4.8	0.8	Nd		
ΔTM	50	5000	0.53	-1.6	-2.9	†)	~ 0.3	
ΔTM G318A			Nd			Nd		
ΔTM R374A	50	5000	0.36	-2.2	-2.5	Nd		

(b) AMPPNP binding								
CckA construct	C _{cell} (μM)	C _{syringe} (μM)	- c-di-GMP			+ 100 μM c-di-GMP*		
			K _d (μM)	ΔH (kcal/mol)	-TΔS (kcal/mol)	K _d (μM)	ΔH (kcal/mol)	-TΔS (kcal/mol)
CA	20	800	12	-1.9	-4.5	43	-2.4	-3.3
ΔTM	20	800	9.7	-1.4	-5.2	57	-2.5	-3.0
ΔTM G318A			Nd			Nd		
ΔTM R374A	40	600	no significant binding			Nd		

(c) c-di-GMP binding								
CckA construct	C _{cell} (μM)	C _{syringe} (μM)	+ 5 mM ADP			+ 5 mM AMPPNP		
			K _d (μM)	ΔH (kcal/mol)	-TΔS (kcal/mol)	K _d (μM)	ΔH (kcal/mol)	-TΔS (kcal/mol)
CA	20/44	400/600	22	2.2	-8.3	25	2.0	-8.0
DHp-CH	45/40	700/800	34	0.9	-6.7	33	1.0	-6.9
ΔTM	20	400/800	1.4	4.9	-12.5	No significant binding		
ΔTM G318A	50	800	34	0.9	-6.7	Very weak binding		
ΔTM R374A	50	800	25	1.0	-7.0	48	0.7	-6.3

* Note that at the employed concentration, the protein is not saturated with c-di-GMP at the start of titration. Thus, upon titration, a contribution to the generated heat by c-di-GMP binding or unbinding should be considered. Furthermore, the problem is compounded by the distinct sign of the two ΔH contributions (endo- and exothermic binding of c-di-GMP and mononucleotide, respectively). Therefore, the given parameters are only effective values.

Materials and Methods

Plasmids

For structural work and binding studies, the coding sequences for various CckA constructs were cloned into pET21b vectors between NdeI and NotI restriction sites which yielded C-terminally His₆ tag variants. Plasmids and oligonucleotides are listed below.

For *in vitro* activity assays, the previously described CckA_ΔTM construct cloned into the pET28a-His-MBP vector between BamHI and SalI restriction sites [49] and the derived point mutants were used.

For *in vivo* studies pBXMCS-cckAQ315A, pBXMCS-cckAR374A, and pBXMCS-cckAG515D were generated by SOE-PCR using pBXMCS-2-cckAWT as a template DNA, 7200 and 7369 as outside primers, and internal mutagenic primers. The mutagenic primers were as follows: 8543 and 8544 for Q315A, 6483 and 6484 for R374A, and 7901 and 7902 for G515D. After fusion PCR, the products were digested with EcoRI and NdeI, followed by ligation to the EcoRI-NdeI fragment of pBXMCS-2. To construct pBXMCS-cckAG318A, PCR was performed using SH339 genomic DNA (Ozaki and Jenal, unpublished) and primers 7200 and 7369. The products were digested with EcoRI and NdeI, followed by ligation to the EcoRI-NdeI fragment of pBXMCS-2.

Expression and Purification

Proteins were expressed in *E. coli* Rosetta (DE3) cells. LB media were inoculated with 1% pre-culture at 37°C. Bacterial cultures were induced with 0.1 mM IPTG at OD₆₀₀ (0.6-0.8) and the incubation temperature was shifted to 22 °C. Cells were finally harvested overnight post induction by spinning the cultures at 5,000 rpm for 10 minutes (at 4°C using F8-6 rotor). For purification, the cell pellet was resuspended in buffer A (30 mM Tris HCl pH 7.5, 500 mM NaCl, 20 mM imidazole and 5mM MgCl₂) with protease inhibitor cocktail supplied by Roche. Cells were lysed using a microfluidizer and the lysate was centrifuged at 16,000 rpm for 30 minutes (at 4°C using Sorvall SS34 rotor) to remove cell debris and any suspended particles.

Clear supernatant was applied on a Ni-NTA column (5 ml pre pack column, GE healthcare) pre-equilibrated with buffer A. The column was pre-equilibrated with buffer A until the baseline was reached. Bound protein was eluted with a 0 to 100 % linear gradient of buffer B (30 mM Tris HCl, pH 7.5, 500 mM NaCl, 500 mM imidazole and 5 mM MgCl₂). Fractions containing the

desired protein were pooled and concentrated to a final volume of 2-4 ml. The concentrated protein was then loaded on a Superdex S200-26/60 gel filtration column pre-equilibrated with SEC buffer (30 mM Tris HCl pH 7.5, 100 mM NaCl and 5mM MgCl₂). Eluted protein peak was collected and the protein concentration was quantified by UV absorption (Nanodrop from Thermo scientific) and stored at -80°C.

For *in vitro* activity assays, CckA_ΔTM and the derived point mutants were purified as described [49].

Crystallization, data collection and structure solution.

Crystallization was performed using the sitting-drop vapour diffusion method. The CckA_CA construct was crystallized at a concentration of 15 mg/ml in presence of AMPPNP and c-di-GMP (1:5:3 molar ratio) in 30 mM Tris-HCl, pH 7.5, 200 mM NaCl, 5 mM MgCl₂. Initial plate-like crystals were appeared after 10 days in 0.15 M ammonium sulfate, 25% polyethylene glycol 4000 and 0.1 M MES pH 5.5 and were used for seed stock preparation. Upon seeding, well-diffracting plate-like crystals were obtained in 0.1 M ammonium sulfate, 28.4% polyethylene glycol 4000 and 0.1 M MES pH 5.5. Crystals were frozen with cryo-oil (Hampton) as a cryoprotectant.

After extensive crystallization trials the CckA_DHp-CA yielded a single hit obtained at a concentration of 15 mg/ml in presence of ADP (1:5 molar ratio) in 30 mM Tris-HCl, pH 7.5, 300 mM NaCl, 5 mM MgCl₂. The protein crystallized in 30% PEG 550 MME, 30% PEG 2000 MME, Morpheus (Hampton) buffer 1 pH 6.5 and Morpheus carboxylic acids after 3-4 weeks. The crystals were frozen without any cryoprotectent.

X-ray diffraction datasets were collected at the Swiss Light source, Villigen, Switzerland at 100 K. Datasets were processed either with MOSFLM [269] or XDS [270] and resulting intensities were scaled using SCALA from the CCP4 suite [271]. Both structures were solved by molecular replacement. For determination of the CckA_CA structure, the CA domain of DivL (PDB code 4q20 [194]) was used as search model.

For determination of the CckA_DHp-CA structure, the CckA_CA was used as search model and the DHp domain was obtained by iterative model building and refinement.

All structures were refined using REFMAC5 (CCP4). Model building was performed using COOT [272] and O. Ligand molecules and metal ions were modeled in Fo-Fc electron density maps. Finally, water molecules were added where the difference density in Fo-Fc map exceeded 3σ and potential hydrogen bonds could be formed. Data processing, structure refinement and validation

statistics are given in Extended Table 1.

Binding studies by isothermal titration calorimetry

Thermodynamic parameters for ligand binding to CckA variants were measured by isothermal titration calorimetry (ITC) using a Microcal VP-ITC microcalorimeter. All calorimetric titrations were carried out at 25 °C or 12 °C, a syringe stirring speed of 300 rpm, a preinjection delay of 200 s and a recording interval of 250 s. Equilibrium association constant, binding stoichiometry (N), entropy (ΔS) and enthalpy (ΔH) of the binding reaction were derived by fitting the data to a single binding site model using ORIGIN7 (OriginLab). Since all N values indicated (within 25%) 1:1 stoichiometry, the data were refitted with a fixed N=1 value.

Protein phosphorylation assay

CckA phosphorylation was assayed by auto-radiography following the protocol given in [49]. Reactions were run in presence of using 500 μM ATP and 5 μCi $\gamma\text{-}^{32}\text{P}$ ATP (3,000 Ci mmol^{-1} , Hartmann Analytic) at room temperature. Additional nucleotides were added at indicated time points. Reactions were stopped with SDS sample buffer and subsequently loaded (or stored on ice) on 10% SDS gels. Wet gels were exposed to phosphor screen (0.5–3 h) before being scanned using a Typhoon FLA 7000 imaging system (GE Healthcare). Where applicable, ATP was converted to ADP by the addition of 1.5 U hexokinase (Roche) and 5 mM D-glucose.

Flow cytometry

This assay was performed as described previously [49]. Briefly, pBXMCS-2 or its derivatives carrying a cckA(ΔTM) variant was transformed into NA1000 (wt) or UJ5065 (cdG0). After incubation on PYE agar supplemented with 20 $\mu\text{g}/\text{mL}$ kanamycin and 0.1% glucose at 30°C for 2 d, the transformants were grown overnight at 30°C in PYE medium supplemented with 5 $\mu\text{g}/\text{mL}$ kanamycin and 0.1% glucose. A portion (0.2 mL) was diluted in 4 mL of PYE medium supplemented with 5 $\mu\text{g}/\text{mL}$ kanamycin and 0.03% xylose and incubated for 4h, followed by cell fixation in 70% ethanol. After RNase treatment, DNA was stained with YO-PRO-1 iodide (Invitrogen) and the fluorescent intensity was analyzed using FACS Canto II (BD Biosciences).

Bioinformatics

Consensus scores were calculated from multiple sequence alignments using an entropic (21-type) and Karlin-Like transformation of the BLOSUM45 matrix as per [273]. Specificity Determining Position Conservation Contrast Scores (SDP- Δ cons) were calculated for each site of the *C. crescentus* CckA protein sequence by the difference in consensus score between an alignment of CckA orthologs and an alignment of CckA orthologs and paralogs multiplied by the consensus score of the CckA orthologs alignment.

Fitting of kinetic data and simulations

Enzymatic reactions were fitted to standard first-order and second-order reaction kinetics according to the model shown in Fig. 6. The system of coupled ordinary differential equations (ODEs) was set up using the Complex Pathway Simulator (COPASI) software [274]. Global fitting and simulations were performed using ProFit 6.2.14 (QuantumSoft).

Strains used in this study

ORGANISM	NAME	RELEVANT GENOTYPE	REFERENCE
<i>C. crescentus</i>	NA1000	<i>Caulobacter crescentus</i> wild-type strain	[246]
	UJ5065	NA1000 cdG0	[38]
	UJ 8195	NA1000 cckA_77-545	This study
	UJ 8198	NA1000 cckA_297-545	This study
	UJ 8200	NA1000 cckA_379-545	This study
<i>E. coli</i>	BL21 λ DE3	<i>E. coli</i> strain for protein purification: F ⁻ ompT gal dcm lon hsdSB(rB- mB-) λ(DE3 [lacI lacUV5-T7 gene 1 ind1 sam7 nin5])	New England Biolabs
	BL21 Rosetta	<i>E. coli</i> strain for protein purification	Novagen
	DH10β	<i>E. coli</i> donor strain for plasmid conjugation: F ⁻ mcrA D(mrr-bsd RMS-mcrBC) f80dlacZDM15DlacX74 endA1 recA1 deoR D(ara, leu)7697 araD139 galU galK nupG rpsL	Life Technologies
	DH5α	A general <i>E. coli</i> cloning strain: F ⁺ endA1 hsdR17 (rK-mK plus) glnV44 thi1 recA1 gyr delta(Nalr) relA1 delta(lacIZYA-argF)U169 deoR(ö80dlac delta(lacZ) M15)	[248]

Primers used in this study

NAME	SEQUENCE
5276	CGCGGATCCTCAGCGCTTTCGGCGGCGAC
5277	ACGCGTCGACCTACGCCCTGCAGCTGCTG
6483	GCGCAAGCTCTTGGCTTCTCGgcgAAGCAGACCGTGCAGCGCGAGG
6484	CCTCGCGCTGCACGGTCTGCTTcgCGAGAAAGCCAAGAGCTTGCCG
7200	GAATTCCTACGCCCTGCAGCTGCTGC
7243	ATAAT CATATG GGC GAC GCC GAC CAG GCT GAG
7244	ATAAT GCGGCCGC CGTTCATAGACCGGCAGGAA
7245	ATAAT CATATG TCG CCG TTC GGC GCG GCC CTG
7246	ATAAT CATATG GCCCTGCTGGAAGGCCTGGAG
7247	ATAAT CATATG CAGAAGCAGATCGAGCTGCAG
7248	ATAAT CATATG AAGATGCAGGCCATCGGCCAG
7248	ATAAT CATATG CAGCGCGAGGTGCTGGATCTG

Plasmids used in this study

NAME	DESCRIPTION	REFERENCE
pBXMCS-2	a kan resistant high-copy plasmid carrying the xylose promoter	[236]
pBXMCS-CckA	a pBXMCS-2 derivative expressing CckA (S72-A691)	[49]
pBXMCS-CckA Q315A	a pBXMCS-2 derivative expressing CckA Q315A (S72-A691)	This study
pBXMCS-CckA G318A	a pBXMCS-2 derivative expressing CckAG318A (S72-A691)	This study
pBXMCS-CckA R374A	a pBXMCS-2 derivative expressing CckAR374A (S72-A691)	This study
pBXMCS-CckA Y514D	a pBXMCS-2 derivative expressing CckAY514D (S72-A691)	[49]
pBXMCS-CckA G515D	a pBXMCS-2 derivative expressing CckAG515D (S72-A691)	This study
pET28a	Expression vector	Novagen
pET28a-His-MBP	Expression vector to express N-terminal His-MBP fusion proteins	[49]
pET-CckA	To express N-terminal His-MBP-cckA fusion, cckA from caulobacter without TM (S72-A691)	[49]
pET-CckA G318A	Derivat of pET-CckA_ΔTM carrying indicated mutation	This study
pET-CckA R374A	Derivat of pET-CckA_ΔTM carrying indicated mutation	This study
pET-CckA G515D	Derivat of pET-CckA_ΔTM carrying indicated mutation	This study
pET21b	Expression vector	Novagen
pET21b-CckA S72-A691	To express C-terminal His fusions of CckA_ΔTM (S72-A691)	This study
pET21b-CckA G77-A545	To express CckA_ΔTMΔRec (77-545) with C-terminal His-tag	This study
pET21b-CckA Q297-A545	To express CckA_DHp-CA domain (297-545) with C-terminal His-tag	This study
pET21b-CckA Q379-A545	To express CckA_CA domain (379-545) with C-terminal His-tag	This study
pET21b-CckA G318A	Derivat of pET-CckA carrying indicated mutation	This study
pET21b-CckA R374A	Derivat of pET-CckA carrying indicated mutation	This study

Multifunctional single domain response regulator
mediates SigT-dependent stress response in
Caulobacter crescentus

Lori C^{1*}, de Jong I^{1*}, Hamburger F¹, Schmidt A², Glatter T^{2,3}, Jenal U¹

¹ Focal area of Infection Biology, Biozentrum, University of Basel, 4056
Basel, Switzerland

² Proteomics core Facility, Biozentrum, University of Basel, 4056 Basel,
Switzerland

³ Current address: Mass Spectrometry and Proteomics, Max Plank Institute
for terrestrial Microbiology, 35043 Marburg, Germany

* Both authors contributed equally to this work

Manuscript in preparation for submission

Key words: Stress response, single domain response regulator, histidine
kinase, two-component system, SigT, *Caulobacter crescentus*, bacteria

Statement of my work

The *in vitro* activity assays were done by myself.

Abstract

Bacteria are exposed to constantly changing environments and to survive detrimental conditions they need to be able to rapidly respond to diverse stresses. In α -proteobacteria, the general stress response is coordinated by the alternative sigma factor SigT. SigT activation requires a partner switch mechanism initiated by the phosphorylation of the response regulator PhyR. In this work, we present evidence that the histidine kinase LovK contributes to PhyR phosphorylation and that the single domain response regulator MrrA, in its phosphorylated form, allosterically activates LovK. We have indentified at least two novel histidine kinases which activate MrrA through phosphorylation. Genetic data confirmed that MrrA plays a central role in the *Caulobacter crescentus* stress response and development and indicated the existence of additional upstream components and additional MrrA target kinases contributing to SigT activation in this organism. We conclude that MrrA acts as a connecting signalling hub that serves to integrate information input from a range of upstream stress responsive histidine kinases and passes this information on to the general stress response to activate SigT.

Introduction

The general stress response (GSR) is critical to adapt to changing environments. In α -proteobacteria, response to stress requires transcription mediated by the alternative sigma-factor SigT. In non-stressed cells, SigT is sequestered and kept in an inactive form by the anti-sigma factor NepR [206]. Release of SigT involves a partner switch mechanism with the anti-sigma antagonist PhyR [203]. PhyR consists of a phosphorylated receiver domain and a sigma-like output domain. Phosphorylation of PhyR leads to a partner switch whereby the C-terminal sigma-like domain of PhyR binds to NepR thereby releasing SigT to induce the general stress response [204]. Since the partner switch mechanism depends on activated PhyR~P, the cognate histidine kinases involved in PhyR phosphorylation have an important role in activating the cascade. Several PhyR activating histidine kinases (PAKs) have been described [205,210]. *In vivo* experiments in *Sphingomonas melonis* have shown that certain PAKs are required to respond to certain stimuli [205]. For example PakC and PakF are required for heat shock response and PakF is also involved in response to NaCl induced stress [205]. How these kinases are activated remains unclear. *C. crescentus* has 12 presumable PhyR phosphorylating kinases but not many activating signals are known. [207,275]. One of these kinases, LovK, harbors a LOV (light, oxygen and voltage) sensing domain and is believed to respond to and to be activated by blue light [211] but otherwise signals remain obscure. One class of proteins that are known to control histidine kinases are single domain response regulators (SDRR) [45]. Single domain response regulators are found in all three kingdoms of life. They represent the 2nd largest subgroup of response regulators (RR) that can account for up to 90% of all RR in specific organisms [149]. Response regulators are phosphorylated on a conserved aspartate residue in the receiver domain [144]. Phosphorylation often leads to a change in the activity of domains fused to the receiver domain [147]. However, in the case of SDRR the output function is difficult to determine. The paradigmatic SDRR is CheY, which when phosphorylated, interacts with the flagellar motor to direct its rotational bias and to mediate a chemotactic response [151,152]. Based on sequence similarities and clustering with other chemotaxis genes, *C. crescentus* harbors seven presumable CheY proteins (CC0432, CC0437, CC0588, CC0591, CC0596, CC3258, CC3471). The remaining SDRRs of *C. crescentus* are generally summarized as ‘other’ CheY-like proteins (CC0440, CC1364, CC2249, CC310, CC3155) and ‘non-CheY-like’ SDRRs (LovR, CC0630, CpdR, DivK, CC2576, CC3015, CC3286) [149,276]. The function of most of these proteins is unclear. So far only few examples have been functionally characterized, including CpdR, DivK and LovR. CpdR

is phosphorylated by the CckA ChpT phosphorelay. CpdR in its non-phosphorylated form recruits the ClpXP protease to the stalked pole at the G1-S transition [40,48,184,189]. DivK is an essential SDRR that controls cell cycle progression and development in *C. crescentus* [45,186,193,199,277,278]. DivK is phosphorylated by the two histidine kinases PleC and DivJ [45]. DivK~P interacts with its downstream target DivL to control the activity of the bifunctional histidine kinase CckA. Additionally DivK is part of a feedback loop that controls the activity of PleC and DivJ. Another SDRR is LovR that was implicated in regulating LovK mediated general stress response by acting as a phosphate sink to promote inactivation of PhyR [202,211].

Because of their small size, SDRRs are thought to freely diffuse within the cytoplasm [149]. This makes SDRRs ideal candidates for cross-talk between different phosphorylation cascades and qualifies them as mediators that enable quick cellular responses to extracellular conditions and intracellular changes [146]. SDRRs show the conserved ($\beta\alpha$)₅ fold that is typical for receiver domains [279,280]. Phosphorylation on the conserved aspartate residue leads to subtle conformational changes on the α 4- β 5- α 5 surface [279,280], through which SDRRs like CheY interact with their downstream targets [281]. Some SDRRs are phosphorylated by cognate kinases, while others solely function by protein-protein interaction without phosphotransfer reactions being involved [281]. Because SDRRs lack dedicated output domains it is challenging to determine their downstream targets solely based on structural cues. Moreover, despite of recent progress in decoding interactions of response regulators with their cognate HKs [161,164] it remains challenging to accurately predict kinase-RR interactions if the respective genes are not clustered on the chromosome [161]. As a consequence, the signaling connectivity of many SDRRs is unclear with upstream HK(s) and potential downstream target(s) remaining unknown. Here we identify and characterize MrrA, a novel SDRR involved in the general stress response in *C. crescentus*. By combining genetic, biochemical and proteome approaches we were able to determine both upstream and downstream components of MrrA. In particular, we demonstrate that MrrA, in its phosphorylated form, acts as an allosteric activator of the LovK HK to stimulate the general stress response through phosphorylation of the anti-sigma factor antagonist PhyR. Taken together we suggest a complex phosphoregulatory circuit resulting in the activation of the general stress response in *C. crescentus*.

Results

MrrA is involved in several cell cycle-regulated processes

The genome of *C. crescentus* encodes 19 single-domain response regulators (SDRRs), 7 of these are CheY-like SDRRs [276]. Three of the non-CheY SDRRs (LovR, DivK, CpdR) have previously been characterized [40,184,202,221]. We screened four non-CheY SDRRs mutants (CC0630, CC2576, CC3015, CC3286) for phenotypes and found CC3015 (MrrA) to be involved in several cellular processes. Remarkably, MrrA has a negative effect on attachment as well as on motility (Figure 1A). In the wild type, these cell cycle-regulated processes are inversely controlled: Dividing *Caulobacter* cells give rise to one motile cell and one cell which is able to attach to surfaces. The adhesive cell can directly initiate chromosome replication and subsequently undergo cytokinesis, whereas the motile cell first needs to develop into an adhesive cell before it replicates its chromosome. Therefore it ejects its flagellum and initiates holdfast production and stalk formation during G1-S phase transition (reviewed in [282]). $\Delta mrrA$ mutants not only show increased attachment after 24h in PYE medium and increased colony size on PYE supplemented with 0.3% agar after 3 days, but also exhibited decreased biomass levels in stationary phase compared to wild type (Figure 1A). Furthermore, MrrA deficient cells could not be synchronized using a ludox centrifugation gradient. Instead, stalked cells and rosettes were found all over the centrifugation gradient. The defect in synchronizability and the solid pellet during preparation of the cells appeared to be holdfast-dependent (data not shown) and were therefore not analyzed in more detail. The other phenotypes were observed in stationary phase. When testing a fully functional 3xFLAG-tagged version of MrrA, we found that MrrA is present throughout the cell cycle, and in exponential phase and in stationary phase at very low levels (data not shown). To check whether the function of MrrA is restricted to stationary phase, we took snapshots of wild type and $\Delta mrrA$ cultures in exponential phase ($OD_{660} = 0.3$) and compared the number and size of rosettes found in 20 randomly taken pictures. As shown in Figure 1B, $\Delta mrrA$ forms more and bigger rosettes compared to wild type, suggesting that MrrA functions in exponential as well as in stationary phase. Accordingly, attachment is increased in exponential phase as well (data not shown). We wondered whether the increased attachment found in $\Delta mrrA$ cultures resulted from more holdfast material. Therefore, microscopy was performed using green-fluorescent Oregon Green® 488 WGA which stains the holdfast. Neither the holdfast area

nor the signal intensity was significantly different in cells lacking MrrA compared to wild type cultures (Table S1).

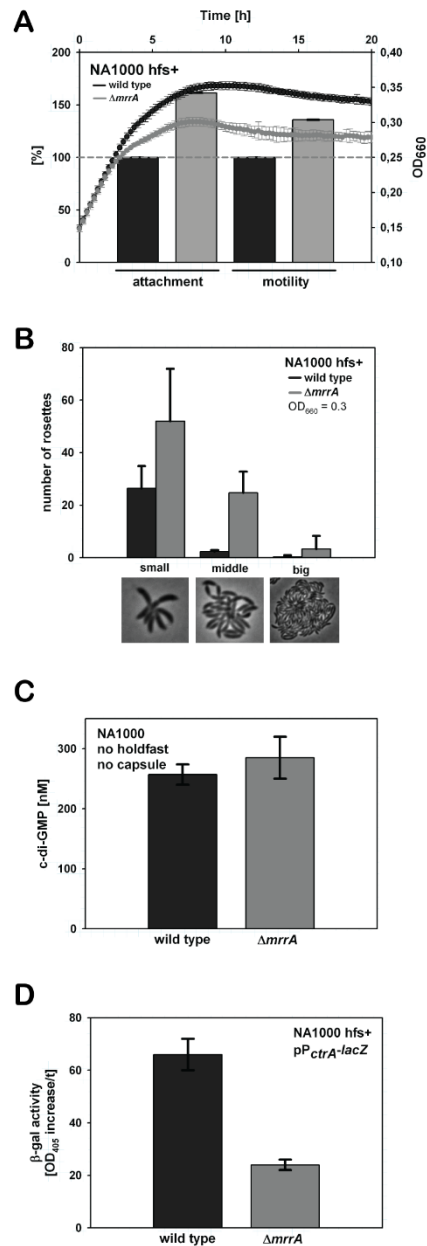


Figure 1: MrrA phenotypes. PYE medium was used for all experiments. **(A)** $\Delta mrrA$ shows increased attachment, increased motility on agar plates and decreased biomass in stationary phase compared to wild type. **(B)** $\Delta mrrA$ forms more and bigger rosettes compared to wild type. 20 random snapshots of exponential phase cultures were taken and the number of rosettes were counted. The pictograms below the graph are an indication for the respective rosette size. **(C)** The c-di-GMP levels of wild type and $\Delta mrrA$ are not significantly different. **(D)** $\Delta mrrA$ shows decreased pP_{drA}-lacZ levels compared

to wild type. Exponential phase cultures were used for a kinetic β -galactosidase assay. Western blot analysis did not reveal a difference in CtrA levels.

Since all processes found to be affected by MrrA are cell-cycle regulated, we checked whether the effect of MrrA depends on cyclic di-GMP (c-di-GMP). C-di-GMP is a secondary messenger responsible for the G1-S phase transition. Motility is only allowed in cells with low c-di-GMP levels, whereas attachment requires high c-di-GMP levels (reviewed in [283]). Indeed, all MrrA phenotypes depend on c-di-GMP (Figure S1). The lack of MrrA cannot restore the attachment defect of a strain which fails to produce c-di-GMP (cdG⁰ strain) (Figure S1A). Similarly, motility is not restored by $\Delta mrrA$ in a cdG⁰ strain (Figure S1B). Finally, in a cdG⁰ background, the lack of MrrA does not result in decreased biomass in stationary phase (Figure S1C). However, c-di-GMP levels of wild type and $\Delta mrrA$ cultures are not significantly different in mixed populations (Figure 1C). In summary, the SDRR CC3015 of *C. crescentus* was so far not analysed in literature. In this study, we show that attachment as well as motility are negatively regulated by CC3015 and that, in addition CC3015 plays a role in biomass production. Therefore, we renamed CC3015 MrrA for ‘multifunctional single domain response regulator A’.

The kinases CC2554 and CC2874 are potential interaction partners of MrrA

MrrA negatively regulates two inversely controlled processes, attachment and motility. Additionally, it is required in *C. crescentus* cultures to reach wild type biomass levels in stationary phase (Figure 1). In order to find interaction partners of MrrA which could explain the observed phenotypes, we followed two independent approaches. Co-immunoprecipitation (Co-IP) experiments were carried out using exponential phase cultures with 3xFLAG-tagged MrrA. As controls wild type cells were used as well as 3xFLAG-tagged CC3286 to minimize the number of false positives that were obtained by subsequent mass spectrometry. Wild type cells functioned as a control for unspecific interactions with FLAG and CC3286 was selected as a control to minimize potential unspecific hits for SDRRs. Table 1A shows the hits which were double-checked by bacterial two hybrid assays or *in vitro* phosphorylation experiments and Table S2 contains the complete data set obtained from Co-IP using mass spectrometry. DgcB, ChpT, ParE, CC2874 and CC1056 were selected for further analysis, either because they showed a high fold change (3xFLAG-MrrA/wild type) or because the potential interaction partner might be associated with one of the MrrA phenotypes. CC2874 and ParE were amongst the best hits in terms of fold change together with several proteins involved in

amino acid metabolism or fatty acid synthesis (Table S1). Bacterial two hybrid assays showed interaction of MrrA with itself, but did not reveal interaction between MrrA and DgcB, ChpT, ParE or CC1056 (data not shown).

In addition to Co-IP, we performed a yeast two hybrid screen in *S. cerevisiae* PJ69-4A [284]. MrrA was used as bait to fish potential interaction partners for the SDRR. Stringent selection on plates lacking adenine (SC-Trp-Leu-Ade) did not give rise to a single yeast colony that could be re-grown in liquid media. In a second approach 2.2×10^6 transformants were screened using less stringent selection on plates lacking histidine (SC-Trp-Leu-His +5 mM 3'AT). This screen resulted in 40 yeast colonies that were used for further analysis. Isolation of the prey library plasmids and subsequent sequencing showed that half of the transformants harboured plasmids that contained *C. crescentus* coding regions that were not in frame. The corresponding proteins are CC0648, CC0649, CC1107, CC2021, CC2407, CC2408, CC2952, CC3586, CC3587. We cannot exclude the possibility that despite the frame shift, true positive hits are among these proteins, since yeast is known to be able to compensate for translational frame shifts. Additionally, we found transformants with in frame coding regions on the prey library plasmids. Sequence analysis of the isolated plasmids revealed that (part of) the coding region of the following proteins was present on the plasmids: 1x CC1108 (methyltransferase FkbM), 1x CC2044 (transposase) and on the same plasmid in frame CC1627 (LacI-like transcriptional regulator), 2x CC2330 (Xre-like transcriptional regulator), 1x CC2554 (PAS histidine kinase), 5x CC2874 (PAS histidine kinase, was also fished with Co-IP), 2x CC3164 (HipB-like transcriptional regulator), 1x CC3654 (conserved hypothetical protein, DUF domain). Autoactivation controls were positive for CC1108, CC2330 (one of two transformants) and CC3164. Transformants with CC2044-CC1627 and CC3654 did not grow after restreaking on selective plates without histidine (SC-Trp-Leu-His +5 mM 3'AT). The remaining hits CC2554 and CC2874 as well as the second transformant with CC2330 on the plasmid (negative for autoactivation) were used for further analysis to investigate the potential interaction with MrrA. CC2330 did neither interact with MrrA in a bacterial two hybrid screen nor was phosphotransfer observable in *in vitro* phosphorylation experiments using purified proteins (data not shown). Since CC2330 also appeared several times in yeast two hybrid screens using other bait proteins (data not shown) it might be a false positive hit that appears with the yeast two hybrid library used in the laboratory.

In summary, at least CC2554 (Y2H) and CC2874 (Y2H and Co-IP) seem to be potential interaction partners for MrrA.

CC2554 and CC2874 phosphorylate and dephosphorylate MrrA *in vitro*

In search for potential interaction partners of MrrA we applied Y2H and Co-IP experiments and found the kinases CC2554 and CC2874 to possibly interact with the SDRRs (Table S1). In addition, we selected the kinases CC2324 and CC2501 for our studies (Figure 2A). They were found by Capra *et al.* to weakly interact with MrrA in *in vitro* phosphorylation experiments [227]. Notably, Capra and co-workers purified truncated versions of the kinases and indicated that removal of the receiver domain might eventually result in unspecific phosphate transfer. In order to test whether CC2324, CC2501, CC2554 and/or CC2874 are real interaction partners of MrrA we constructed plasmids from which His₆-MBP-kinase protein could be expressed (pIDJ079-081). The membrane spanning regions of CC2324, CC2501 and CC2874 are not encoded on the plasmids.

First, we tested whether the purified kinases are active and able to phosphorylate MrrA. Therefore, 5 μ M kinase and 10 μ M MrrA were incubated with 500 μ C labelled ATP for 10 min. Figure 2B shows that all kinases autophosphorylate independent of the presence of MrrA. CC2324 is the weakest kinase. The brightness and contrast of the radiogram had to be optimized in order to visualize CC2324 and the phosphotransfer to MrrA (Figure 2B, lane 1 and 2). The transfer therefore is likely to be unspecific. CC2501 reveals a strong autophosphorylation signal, but does not phosphorylate MrrA (Figure 2B, lane 3 and 4). CC2554 does not seem to be a strong kinase (compared to CC2501 and CC2874), but clearly autophosphorylates (Figure 2B, lane 5). Interestingly, as soon as MrrA is added to the reaction, MrrA becomes visible in the radiogram and the band of CC2554 disappears (Figure 2B, lane 6). CC2874 is the strongest of all four kinases and the phosphotransfer to MrrA is clearly apparent (Figure 2B, lane 7 and 8). Accordingly, we continued working with CC2554 and CC2874 since they show clear autophosphorylation signals and in addition seem to interact with MrrA. The weak phosphotransfer shown by Capra *et al.* between the kinases CC2324 and CC2501 and the SDRR MrrA might, as they suggested, indeed result from unspecific phosphotransfer due to the truncation of the protein (missing the REC domain) [227]. These kinases were thus excluded from further *in vitro* phosphorylation analysis.

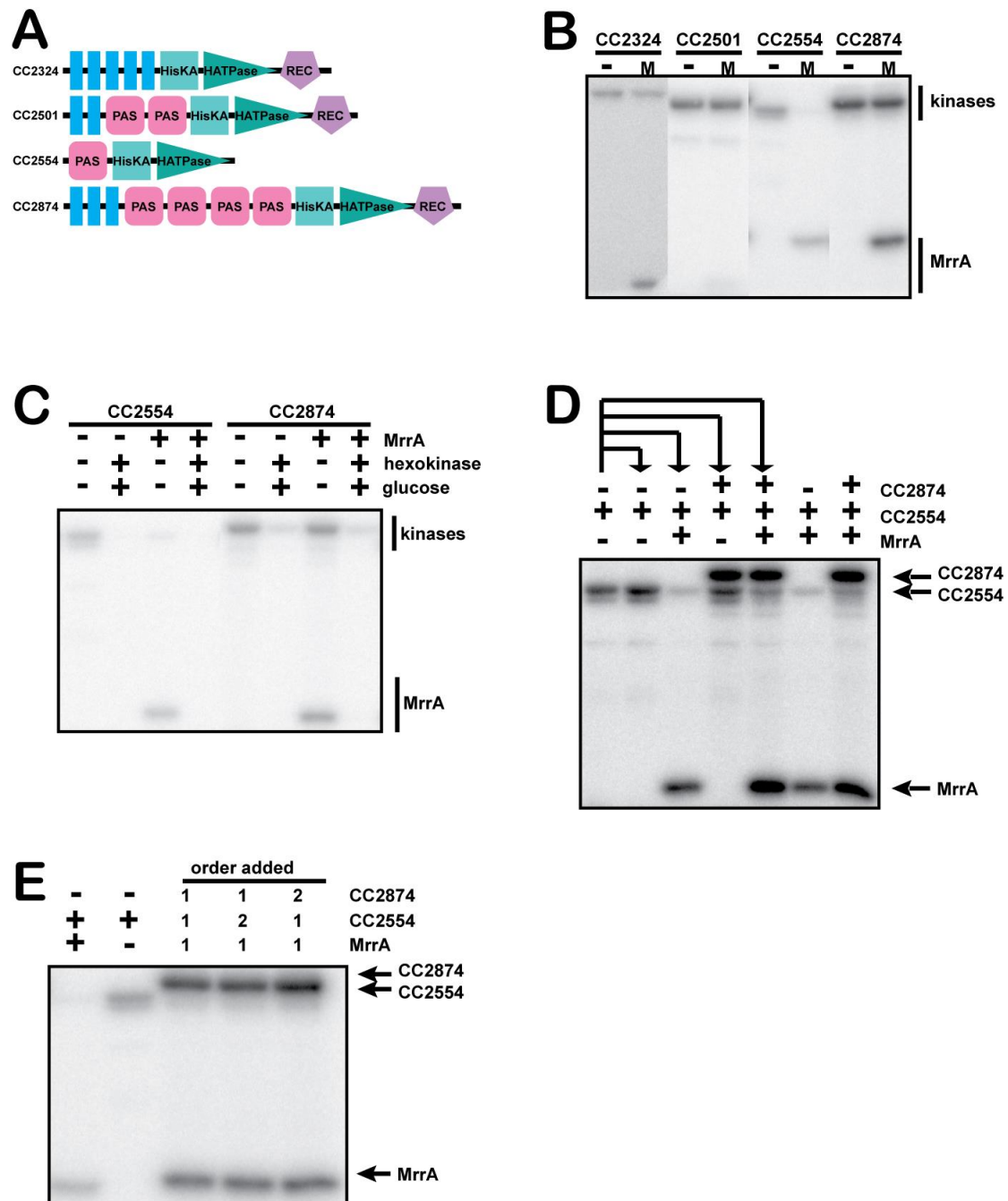


Figure 2: *In vitro* analysis of potential MrrA kinases. Proteins were used in the following concentrations: 10 μ M MrrA, 5 μ M of potential MrrA kinases (CC2324, CC2501, CC2554, CC2874), 1.5 units hexokinase, 5 mM D-glucose. 500 μ M ATP and 2.5 μ Ci [γ ³²P]ATP (3,000 Ci mmol⁻¹) were used and the reactions were carried out for 15 minutes (unless indicated otherwise) at room temperature. **(A)** Domain architecture of the potential MrrA kinases CC2324,

CC2501, CC2554 and CC2874. **(B)** None of the kinases tested depends on MrrA for autophosphorylation. CC2324 is the weakest kinase tested. Autophosphorylation and the phosphotransfer to MrrA is only detectable when brightness and contrast of the radiogram are adjusted. CC2501 shows clear autophosphorylation but does not seem to be a kinase for MrrA. CC2554 autophosphorylates and phosphotransfers to MrrA. MrrA inhibits the CC2554 autophosphorylation signal. CC2874 is the strongest kinase and results in the highest MrrA signal. **(C)** CC2554 and CC2874 both have phosphatase activity and are able to dephosphorylate MrrA. **(D-E)** CC2554 was prephosphorylated before added to other reactions as indicated by arrows or number. MrrA also inhibits CC2554 activity if CC2554 or MrrA are prephosphorylated.

To check whether the phosphotransfer between the kinases CC2554 and CC2874 and MrrA is specific, we tested different incubation times (2 min – 30 min) and different kinase concentrations. CC2554 autophosphorylates instantly (2 min) (Figure S2A, lane 1) and shows full activation between 10 min and 30 min (Figure S2A, lane 3-5). The phosphotransfer to MrrA is also instant, after 2 min the signal for CC2554 is gone and MrrA is clearly visible (Figure S2A, lane 6). MrrA phosphorylation increases with increasing concentration of CC2554 (Figure S2A, lane 7-10), whereas the band for CC2554 remains absent in the presence of the SDRR (Figure S2A, lane 7-10). Similarly, CC2874 is instantly autophosphorylated (no signal difference between 2 min up to 30 min incubation) and directly transfers phosphate to MrrA (Figure S2B, left panel, lane 1). The more MrrA is titrated into the mix, the more MrrA becomes phosphorylated by CC2874 (Figure S4B, right panel). Together these results suggest specific phosphotransfer between the kinases (CC2554 and CC2874) and MrrA.

Next, we tested whether CC2554 and CC2874 can also act as phosphatases and if so, whether they are able to dephosphorylate MrrA. Therefore, each kinase was mixed with hexokinase and glucose +/- MrrA. As controls, hexokinase and glucose were not added to the *in vitro* phosphorylation reactions. As can be seen in Figure 2C, the signals for CC2554 (Figure 2C, lane 2) and CC2874 (Figure 2C, lane 6) disappear in the presence of hexokinase and its substrate, indicating that both kinases have phosphatase activity. When MrrA is present in the mix as well, the signal for MrrA vanishes (Figure 2C, lane 4 and 8), suggesting that CC2554 as well as CC2874 can act as phosphatases for MrrA. The hypothesis that CC2554 is a phosphatase rather than a kinase for MrrA is supported by the finding that 20-fold excess of MrrA results not only in a loss of the CC2554 signal, but also in loss of the MrrA signal (Figure S4C, lane 9)

which was observed for two-fold excess of MrrA (Figure 2B, lane 6). Additionally, MrrA^{D53E} mutant protein is not able to inhibit CC2554 kinase activity (data not shown).

In order to analyse CC2554 and CC2874 in more detail, we expressed truncated versions of the proteins in which the PAS domains are missing (pIDJ088 = CC2554 Δ PAS, pIDJ089 = CC2874 Δ TM Δ PAS). Furthermore, pIDJ090 was created for production of CC2874 without transmembrane domains and without REC domain (CC2874 Δ TM Δ REC), and pIDJ094 to express only the REC domain of CC2874 (REC^{CC2874}). Figure S2C shows that the PAS domain of CC2554 is required for its function, CC2554 Δ PAS does not autophosphorylate (Figure S2C, lane 4). We did not succeed in expressing CC2874 without its PAS domains from pIDJ090, the purified protein was very unstable and could not be used for the experiments. We wondered whether the observed signal of CC2874 was due to the phosphorylation of the histidine residue in the kinase domain, or due to the D782 in its REC domain and whether the REC domain of CC2874 competes for phosphorylation with MrrA. As can be seen in Figure S2D, the REC domain of CC2874 is neither required for the autophosphorylation activity of the kinase (Figure S2D, lane 2) nor for the phosphotransfer to MrrA (Figure S2D, lane 4). This observation also indicates that the histidine of CC2874 is stable. Next, we mixed CC2874 with different concentrations of MrrA and/or REC²⁸⁷⁴. Like MrrA, the REC²⁸⁷⁴ shows no signal without CC2874 being present (Figure S2E, lane 1 and lane 3) and REC²⁸⁷⁴ becomes readily phosphorylated by CC2874 (Figure S2E, lane 5) even if MrrA is present (Figure S2E, lane 6). In a competition experiment, either 5-fold excess of REC²⁸⁷⁴ or of MrrA was used to investigate whether one REC domain is preferred by CC2874. CC2874 is active enough to phosphorylate both REC domains even if one is present in excess (Figure S4E, lane 7 and 8). Considering the high activity of CC2874 and the fact that MrrA is always present at very low levels in *C. crescentus*, it is unlikely, that the potential competition between the REC domain of CC2874 and MrrA has physiological relevance *in vivo*. Interestingly, CC2554 is also inhibited if prephosphorylated before addition of other components suggesting that MrrA indeed activates CC2554 phosphatase activity (Figure 2D and Figure 2E). If MrrA is prephosphorylated by CC2874 and mixed with prephosphorylated CC2554, the signal from CC2554 disappears indicating that removal of phosphate from CC2554 is not due to a phosphate transfer reaction to MrrA (Figure 2D and Figure 2E).

Functional characterization of CC2554 and CC2874 *in vivo*

We have validated, that at least CC2554 and CC2874 can act as kinases as well as phosphatases for MrrA *in vitro*. CC2324 and CC2501, which were suggested by Capra *et al.* to phosphorylate MrrA could not be identified as true MrrA kinases in our *in vitro* phosphorylation analyses [227]. However, since we cannot exclude CC2324 and CC2501 to be involved in MrrA-mediated signalling, we investigated the *in vivo* function of all four kinases. We constructed single deletion mutants for each kinase in wild type and $\Delta mrrA$ backgrounds as well as a strain in which all four kinases are lacking and IPTG-inducible overproduction constructs for each kinases in wild type and $\Delta mrrA$ backgrounds and tested them for the phenotypes identified for MrrA. Attachment, motility and biomass production were monitored. The only kinase that showed MrrA related phenotypes is CC2324. In a $\Delta CC2324$ strain, attachment is downregulated to 50% (Figure 3A), whereas motility colonies size is upregulated to 140% (Figure 3B) and the corresponding cultures also produce more biomass in stationary phase (Figure S3A, upper left panel) compared to wild type. However, these phenotypes tested are still sensitive to the loss of MrrA, indicating that the effect of CC2324 on attachment, motility and biomass production in stationary phase is independent on MrrA. $\Delta CC2501$, $\Delta CC2554$ and $\Delta CC2874$ did not reveal a phenotype and are still sensitive to loss of MrrA (Figure 3A, Figure 3B and Figure S3A). Since it might be a possibility, that loss of one kinase is compensated by other MrrA kinases, we constructed a strain in which all four kinases are missing. The strains behaved like a $\Delta 2324$ single mutant and was also still sensitive to loss of MrrA (Figure 3A, Figure 3B and Figure 3C). Our findings suggests that other MrrA kinases must exist which contribute to wild type levels for attachment, motility and biomass production in an MrrA-dependent manner.

Nevertheless, while testing the overproduction strains, we could confirm that at least CC2554 and CC2874 are linked to MrrA *in vivo*. Figure S5B shows the attachment analysis of the kinase overproduction strains in the wild type and $\Delta mrrA$ background. As expected, the empty vector control shows an increase in attachment when MrrA is absent and induction with 200 μ M IPTG does not significantly change the percentage of attachment in the empty vector controls (Figure S5B). The overproduction strains for CC2324 and CC2501 resemble the empty vector controls (Figure S3B). Overproduction of CC2554 in a wild type background, however, results in an increase of attachment, mimicking a $\Delta mrrA$ mutant. This observation is in line with our *in vitro* data, which indicate that CC2554 is a phosphatase rather than a kinase for MrrA. In this model,

overproduction of CC2554 would result in MrrA dephosphorylation *in vivo*, which would be equal to a loss of MrrA if phosphorylated MrrA is the active species. Indeed, an MrrA^{D53N} mutant that cannot phosphorylate MrrA phenocopies a $\Delta mrrA$ strain (data not shown). In addition, purified MrrA^{D53N} is not able to extinguish the CC2554 signal in *in vitro* phosphorylation assays (Figure S4C, lane 6), indicating that MrrA functions by phosphotransfer and not by protein-protein interaction. Notably, CC2554 overproduction not only has an effect on attachment in an MrrA-dependent manner (Figure S3B), but also on biomass production in stationary phase (Figure S3D). As expected, in the empty vector controls $\Delta mrrA$ shows decreased biomass in stationary phase compared to wild type. When CC2554 is overexpressed in the $\Delta mrrA$ background, more biomass is produced than in *Caulobacter* cultures that produce MrrA (Figure S3D).

In summary our data show, that CC2554 likely acts as a phosphatase for MrrA to regulate attachment and biomass production in stationary phase cultures, but that CC2554 does not seem to be involved in the regulation of motility (Figure S3C). CC2874 overproduction results in wild type attachment and motility levels not only in the wild type, but also in cells lacking MrrA (Figure S3B and Figure S3C). This observation suggests that CC2874 might cross signal to another target that can compensate for the loss of MrrA as long as CC2874 is present at high levels.

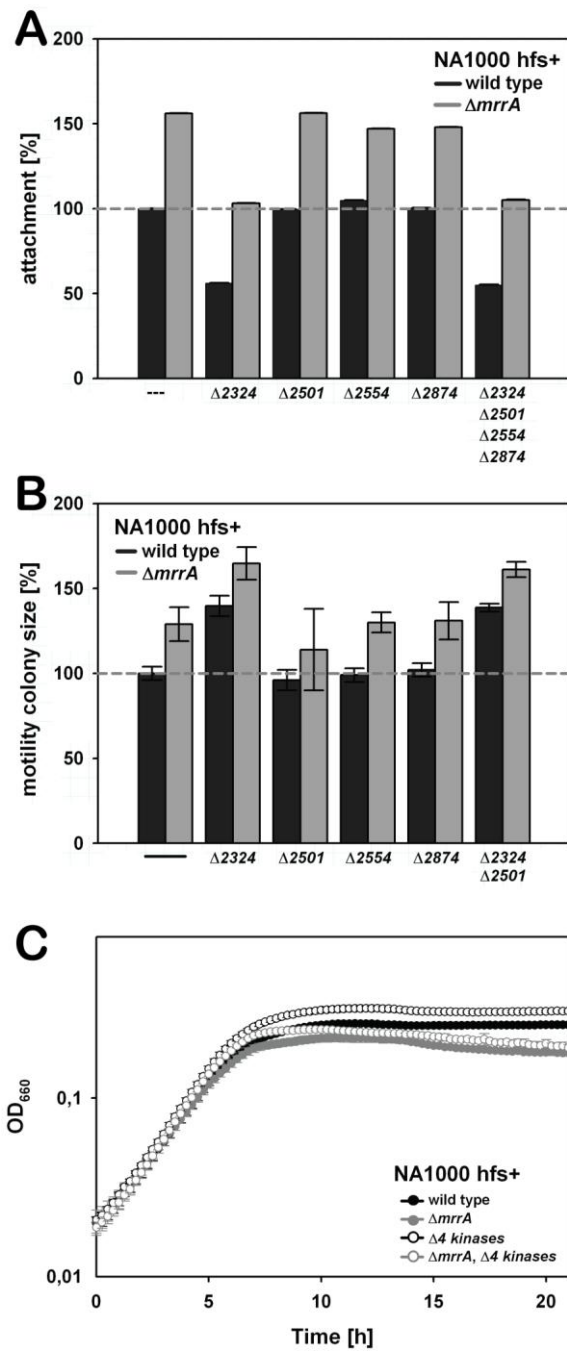


Figure 3: *In vivo* characterization of CC2324, CC2501, CC2554 and CC2874. PYE medium was used for all experiments. CC2324 is the only kinase that shows a phenotype for attachment and motility, but it is still sensitive to a loss of *mrrA*. Deletion of all four kinases results in phenotypes similar to $\Delta CC2324$, indicating that more kinases must exist to explain the $\Delta mrrA$ phenotypes. None of the kinases mutants showed a phenotype for biomass

production. **(A)** A 96-well plate attachment assay was analysed 24h after inoculation. Two biological and six technical replicates were used per experiment. At least three experiments have been performed per strain. **(B)** PYE plates supplemented with 0.3% agar were inoculated and colony sizes were measured 3 days after inoculation. 5 independent plates were analysed per experiment. At least 3 experiments have been performed per strain. **(C)** Biomass production was followed in a 96-well plate. Two biological and six technical replicates were used per experiment. At least three experiments have been performed per strain. Error bars indicate the standard deviation for each graph.

In search for additional MrrA network components

Our data suggest that CC2554 primarily acts as a phosphatase for MrrA, whereas CC2874 is a strong kinase for MrrA. Nevertheless, other kinases must exist to explain the phenotypes found for $\Delta mrrA$. Since Co-IP and Y2H screening did not reveal additional true positive hits for phosphotransfer, and since so far we lacked downstream targets of MrrA, we compared the proteome between $\Delta mrrA$ and wild type cells. Table 1C shows all hits, that were at least four times up- or downregulated and Table S3 contains the whole data set. Amongst the best scores were three components of the SigT stress pathway of *C. crescentus*: the sigma factor SigT itself, which is required to control genes required for adaptation to stress; NepR, the anti-sigma factor; and PhyR, the anti-anti-sigma factor. Under growth-promoting conditions, NepR is bound to SigT to prevent the activation of the stress regulon. Upon stress, PhyR becomes phosphorylated by its cognate kinase PhyK upon which it undergoes a conformational change which allows the anti-anti-sigma factor to bind to NepR and to titrate it away from SigT. This sequence of events ultimately allows free SigT molecules to bind to the *sigT* motif present in promoters of genes under its regulation [203,206,207,275]. Indirect evidence led to the proposition, that LovK, a kinase which results in superattachment when overexpressed with its cognate response regulator LovR [211], might regulate the phosphorylation status of PhyR and thus, the response to stress in *C. crescentus* [202]. Nevertheless, direct evidence was not found so far. Notably, not only SigT, NepR and PhyR were dramatically downregulated in $\Delta mrrA$ cultures, but also LovK was downregulated to a ratio of 0.4 in $\Delta mrrA$ compared to wild type cultures (Table S3).

The proteome comparison seems to place MrrA in the context of stress regulation, especially when considering that all MrrA phenotypes (attachment, motility, biomass production) were originally scored in stationary phase when

cells are known to be stressed by factors like high cell density and nutrient limitation. We first set out to investigate the link between MrrA and SigT in more detail, before testing whether LovK might be a phospho-regulator for MrrA, since it was not identified in Co-IP or Y2H and the potential link to PhyR had not been validated so far.

MrrA functions within the SigT stress pathway of *C. crescentus*

In order to investigate whether MrrA is involved in the SigT stress pathway of *C. crescentus*, we used the pP_{sigU}-lacZ reporter (pRKlac290-SigU, [202]). SigT is the master regulator of the general stress response in *C. crescentus* and regulates more than 40 transcriptional units, amongst others *sigU*. In literature, SigU is generally used as a reporter for SigT activity since so far SigT is the only protein identified to regulate *sigU* transcription by binding to its promoter region [207,275,285]. However, we cannot exclude that other factors contribute to regulate P_{sigU}. To monitor whether MrrA feeds into the SigT pathway, we first compared exponential phase cultures with stationary phase cultures in the wild type, $\Delta mrrA$, $\Delta sigT$ and the double mutant background $\Delta mrrA\Delta sigT$. P_{sigU} activity is detectable in exponential phase and, as expected, increases in stationary phase in wild type cells (Figure 4A). β -galactosidase activity was nearly not measurable in $\Delta mrrA$, $\Delta sigT$ and the double mutant background $\Delta mrrA\Delta sigT$, indicating that not only *sigT* is required for adaptation to stresses, but that the SDRR MrrA is also needed to activate the *sigT* pathway. To minimize the chance of artifacts due to heterogeneity and difficulties with cell lysis of stationary phase cells, we used exponential phase cultures for further experiments. Figure 5B shows that P_{sigU}-reporter activity increases in response to osmotic stress (150 mM sucrose or 75 mM NaCl, applied for 10 min) in the wild type, but not in $\Delta mrrA$, $\Delta sigT$ and the double mutant background $\Delta mrrA\Delta sigT$, again highlighting the importance for MrrA to regulate stress adaptation. None of the exponential phase cultures responded to a temperature shift from 30 to 37°C during 20 min of stress exposure (Figure 4B). To define whether MrrA acts upstream or downstream of SigT, we performed western blot analysis and used P-*egfp* fusions in batch cultures. Neither overproduction of SigT, nor the addition of 150 mM sucrose to exponential phase cultures resulted in a detectable increase of MrrA-3xFLAG on western blots (data not shown). Similarly, P_{sigT}-*egfp* levels were not increased in cultures overproducing or lacking MrrA (data not shown).

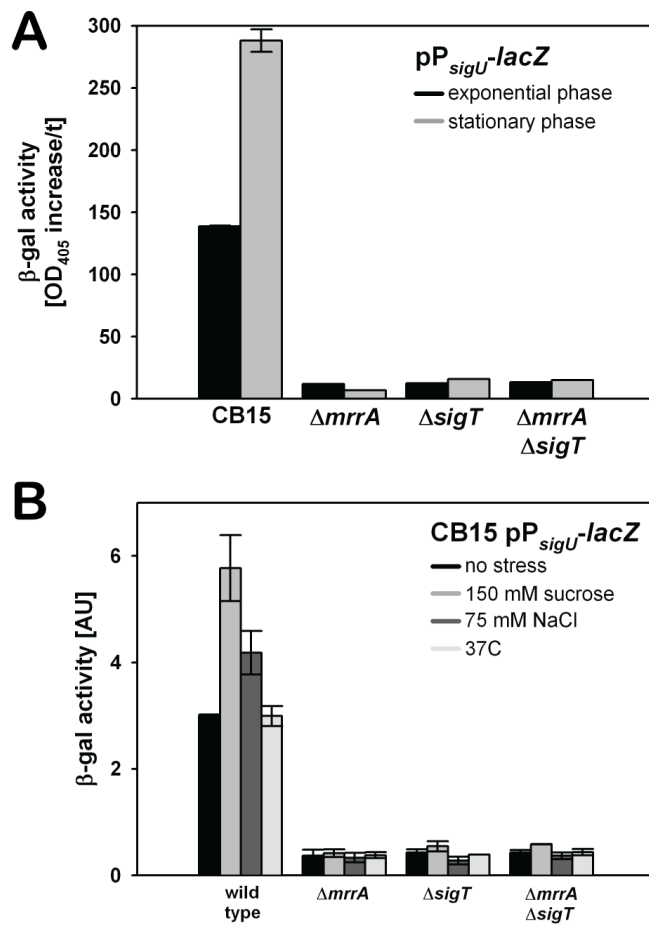


Figure 4: MrrA is involved in the SigT-stress pathway. PYE medium was used for all experiments. Two biological replicates were used per experiment and at least two experiments were performed per strain and condition. All strains shown harbour a plasmid on which *lacZ* is under control of the *sigU* promoter (pP_{sigU}-*lacZ* = pRKlacZ290-sigU). Error bars indicate the standard deviation. **(A)** Kinetic β -galactosidase experiments were carried out using exponential as well as stationary phase cultures. 20 time points have been measured and the β -galactosidase activity is plotted as the slope (OD₄₀₅) over time. **(B)** Overnight cultures were diluted to an OD₆₆₀ of 0.05 and grown until OD₆₆₀ of 0.3 before being exposed to the indicated stresses. 150 mM sucrose and 75 mM NaCl were applied for 10 min, the temperature shift to 37°C for 20 min.

LovK directly connects MrrA with the SigT pathway of *C. crescentus*

Our *in vivo* data show, that MrrA is required to activate the SigT stress pathway (Figure 4). A proteome comparison revealed that not only the stress pathway components SigT, PhyR and NepR are downregulated in $\Delta mrrA$ cultures compared to wild type, but that also the LovK kinase showed great reduction in its protein levels (Table S3). Since LovK has been proposed to feed into the SigT stress pathway [202], we purified all components and tested their connectivity by *in vitro* phosphorylation. Figure 5A shows, that LovK was not active by itself (also see Figure 5C lane 3), *i.e.* autophosphorylation as well as phosphotransfer to LovR (its cognate response regulator) and MrrA was not detectable (Figure 5A, lane 3-4). However, when we mixed all four proteins (CC2874, MrrA, LovK and LovR), a faint band for LovR became visible (lane 7). Since CC2874 was not able to phosphorylate LovR (lane 5), the signal seen for LovR in lane 7 was likely to result from active LovK, which seemed to require either CC2874 or MrrA or both for activation. To get more insight, we performed another experiment in which CC2874, MrrA and LovK were mixed without LovR. Figure 5B shows that LovK was not active in the presence of CC2874 alone (Figure 5B, lane 2), but clearly autophosphorylated in the presence of CC2874 and MrrA (lane 3). As observed before, the LovK signal was lost in the presence of LovR (lane 5). Together, these data indicate that LovK requires phosphorylated MrrA for its activity. Although no LovR phosphorylation was detectable when the SDRR is solely incubated with CC2874, a faint signal became visible when MrrA was added to the mix (lane 4), indicating that eventually, CC2874 might be able to cross-phosphorylate LovR. Equivalent results are obtained when CC2874 and MrrA are pre-incubated with hot ATP before LovR, LovK or both LovR and LovK are added to the mix (lane 6-8).

Next, we tested the connectivity between MrrA-LovK and the SigT stress pathway (Figure 5C). Surprisingly, when CC2874, MrrA, LovK and PhyR were incubated with radioactively labelled ATP, almost no signal was visible for PhyR (Figure 5C, lane 6). A recent study by Herrou *et al.* showed, that PhyR phosphorylation becomes stable in the presence of NepR in *in vitro* phosphorylation assays [204]. They kindly provided us with the plasmid for NepR purification with which we managed to show for the first time with *in vitro* studies, that LovK indeed might transfer phosphate to PhyR (Figure 5C, lane 7). Since this experiment did not exclude that one of the other components in the mix required to activate LovK results in PhyR phosphorylation, we performed a control experiment in which first only CC2874, LovK, PhyR and

NepR were mixed with hot ATP. Figure 5D shows, that LovK is not active and that PhyR is also not detectable in the radiogram (Figure 5D, left radiogram, lane 1). Next, MrrA was added to the mix and time-course samples were taken ranging from 0.5 to 30 min (left radiogram, lane 2-7). As can be seen, LovK directly autophosphorylated and PhyR became visible after 2 min. The PhyR signal increased with incubation time. Interestingly, upon addition of LovR, the signal for MrrA was almost and the LovK signal totally lost after 0.5 min (Figure 5D, right radiogram, lane 2), whereas the PhyR signal remained stable within the 30 min tested (right radiogram, lane 2-7). This finding suggests that LovR switches LovK into phosphatase mode, and that LovK can dephosphorylate MrrA (the activator for LovK kinase) but not PhyR. To test whether LovK can function as phosphatase in our experimental set-up, we performed a phosphatase assay in which CC2874 and MrrA were incubated with LovK to activate LovK kinase activity (Figure 5E, lane 1). When hexokinase and glucose were added, the LovK signal was lost (lane 2), indicating that LovK can act as kinase and phosphatase in our buffer.

Together, our findings show that LovK requires MrrA for kinase activity, and that LovR might function as the MrrA counterpart which switches LovK into its phosphatase mode. We show for the first time that indeed PhyR becomes phosphorylated by LovK in *C. crescentus*, and that this phosphorylation (at least *in vitro*) depends on active MrrA.

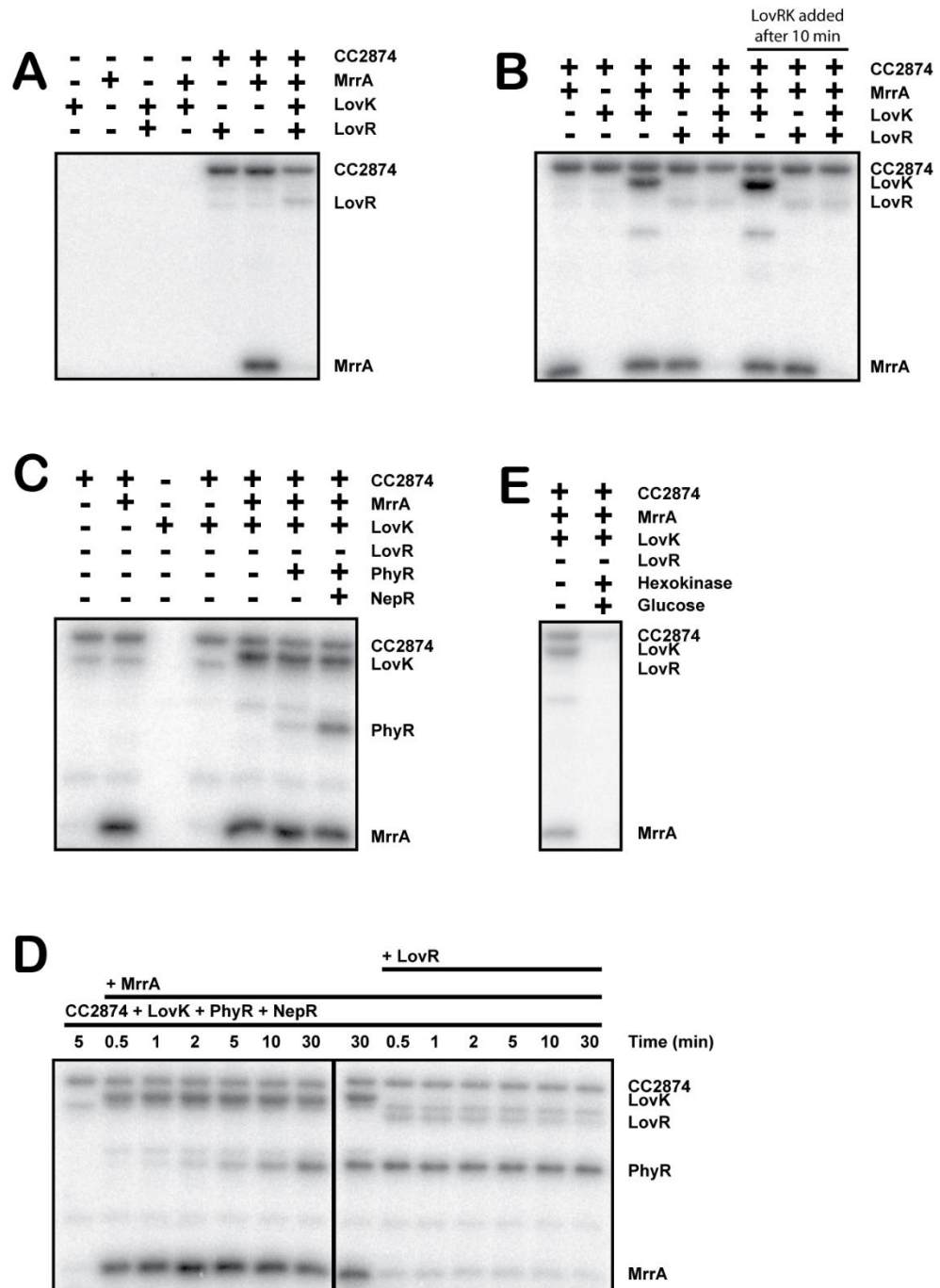


Figure 5: LovK connects MrrA with the SigT-stress pathway by phosphorylating PhyR. Proteins were used in the following concentrations: 10 μM MrrA, 5 μM of CC2874, 5 μM of LovR, 5 μM of LovK, 5 μM of PhyR, 5 μM of NepR, 1.5 units hexokinase, 5 mM glucose. 500 μM ATP and 2.5 μCi [$\gamma^{32}\text{P}$]ATP (3,000 Ci mmol^{-1}) were used and the reactions were carried out for

15 minutes (unless indicated otherwise) at room temperature. **(A)** LovK by itself does not autophosphorylate (lane 1) and cannot phosphotransfer to LovR (lane 3) or MrrA (lane 4). CC2874 is not able to phosphorylate LovR (lane 5). When all four proteins are mixed, MrrA phosphorylation by CC2874 is not visible and a weak signal for LovR becomes apparent, whereas LovK is not detectable in the radiogram (lane 7). **(B)** CC2874 cannot activate LovK autophosphorylation (lane 2), but when MrrA is added to the mix, LovK becomes visible in the radiogram (lane 3), indicating that phosphorylated MrrA is required for LovK kinase activity. The combination of CC2874 and MrrA is not potent to phosphorylate LovR (lane 4), but LovR addition to a mix containing CC2874, MrrA and LovK results in signal loss for MrrA and LovK (lane 5). As controls, CC2874 and MrrA were pre-incubated and LovR, LovK or both LovRK were added 10 minutes later (lane 6-8). The results are comparable to the corresponding lanes in which all proteins were mixed directly. **(C)** Activated LovK seems to transfer phosphate to PhyR, but the signal of PhyR is very weak (lane 6). Addition of NepR to the mix results in a strong PhyR signal (lane 7). **(D)** CC2874, LovK, PhyR and NepR were pre-incubated with hot ATP resulting in a specific bands for CC2874 and some bands from degraded His₆-MBP-CC2874 (left radiogram, lane 1). MrrA was added to the mix and time-course samples were taken between 0.5 min and 30 min. Next to CC2874, MrrA and LovK become directly visible (left radiogram, lane 2), whereas PhyR phosphorylation by LovK increases with time (left radiogram, lane 2-7). LovR was added to the mix and time-course samples were taken from 0.5 to 30 min (right radiogram, lane 2-7). The signal for LovK vanishes completely, the signal for MrrA becomes very weak and the signal for PhyR remains visible on the radiogram (right radiogram, lane 2-7), supporting the idea that LovR switches LovK from kinase to phosphatase mode and that LovK dephosphorylates itself and also MrrA, whereas it cannot dephosphorylate PhyR. A signal for LovR is visible as well. **(E)** LovK has phosphatase activity (lane 1). Whether LovK can dephosphorylate MrrA cannot be tested, since CC2874 (which can function as a phosphatase for MrrA) is required in the mix to phosphorylate MrrA.

Discussion

In this study we characterised the single domain response regulator CC3015 of *C. crescentus* and renamed it MrrA (multifunctional single domain response regulator A). Cells lacking MrrA show increased surface attachment, increased motility on semi-solid agar plates and reduced biomass in stationary phase (Figure 1). Moreover, a $\Delta mrrA$ mutant is not synchronizable using standard centrifugation procedure with ludox. Instead of two separate bands for swarmer and stalked/predivisinal cells, a culture lacking MrrA shows stalked cells all over the gradient (data not shown). However, this phenotype is holdfast-dependent and was therefore not analyzed in more detail. MrrA is evenly distributed in the cytosol and present at low levels in all cell types. In line with the observation that the $\Delta mrrA$ phenotypes analysed in this study are most pronounced in stationary, phase its concentration is slightly increased in non-growing cultures (data not shown).

In contrast to other bacteria, stress adaptation of *C. crescentus* is regulated by only one sigma factor. *C. crescentus* only encodes two sigma factors, SigT and SigU [286]. The sigU-promoter is generally used as a control for SigT activity. In wild type *C. crescentus* cells, SigT is usually bound by the anti-sigma factor NepR to prevent the activation of genes required for stress adaptation in growth promoting conditions. When cells encounter stress, the anti-anti-sigma factor PhyR becomes phosphorylated. This reaction goes along with a conformational change of the protein allowing PhyR~P to bind NepR and consequently to titrate NepR away from SigT. Accordingly, free SigT molecules can bind the SigT-recognition sequence (GGAAC-N₁₆₋₁₇-CGTT) in SigT-regulated promoters [207,275,285]. A proteomics analysis revealed that the stress pathway consisting of the sigma factor SigT, the anti-sigma factor NepR and the response regulator PhyR are significantly downregulated in a mutant lacking *mrrA* (Table S1). This could explain the observed stress sensitivity of the *mrrA* mutant, *i.e.* reduced biomass in stationary phase when cells encounter high cell density and lack of nutrients and oxygen (Figure 1A). In line with this, we found that MrrA is required for transcriptional activation of a SigT-specific reporter (P_{sigU}) (Figure 4). However, western blot analysis with a specific antibody raised against MrrA and microscopy analysis using P_{mrrA} -*egfp* fusions showed that MrrA levels are not upregulated by osmotic stress and do not seem to be under control of SigT (data not shown). Together, these observations suggest, that MrrA functions upstream of SigT to regulate stress adaptation and that MrrA activity rather than MrrA expression is increased during harsh conditions. In line with this, we found that the conserved phosphoryl-acceptor

aspartic acid D53 is required for MrrA functionality, arguing that the protein elicits its functions through phosphorylation. Both an MrrA^{D53N} and an MrrA^{D53E} mutant both phenocopy a $\Delta mrrA$ strain (data not shown).

Since MrrA seems to be involved in different signal transduction cascades and developmental pathways, we expected MrrA to interact with multiple proteins. We used co-immunoprecipitation (Co-IP) as well as yeast two hybrid screening (Y2H) to identify interaction partners of MrrA and unravel the MrrA network (Table 1). Ideally, we expected to find at least one kinase to regulate MrrA activity and different target proteins downstream of MrrA to regulate cell development and stress response. Since SDRR are known to kiss-and-fly during protein-protein interaction, we used formaldehyde in the Co-IP experiments to cross-link MrrA to its potential interaction partners. Interesting hits were double checked with bacterial two hybrid (B2H). In contrast to Co-IP, Y2H experiments are more likely to reveal direct interaction partners without revealing hits that are based on complex formation. As true positive hits the combination of assays revealed only two PAS histidine kinases, CC2874 and CC2554 (Figure 2). Both kinases were subsequently subjected to *in vitro* phosphorylation analysis using purified protein.

Our data show that CC2554 is a weak kinase and can dephosphorylate MrrA in the presence of hexokinase and glucose. The PAS domain of CC2554 is required for autophosphorylation. Interestingly, we found that MrrA inhibits CC2554. When MrrA is incubated with autophosphorylated CC2554, a signal for MrrA becomes visible (CC2554 phosphorylates MrrA), but the autophosphorylation signal for CC2554 vanishes. This implies that either CC2554 cannot autophosphorylate in the presence of MrrA or that MrrA turns CC2554 in its phosphatase mode. Considering that CC2554 can act as a phosphatase for MrrA, the sole inhibition of autophosphorylation seems to be the more likely explanation. Inhibition of CC2554 is observed even in 3-fold excess of CC2554, but is not monitored with MrrA^{D53N} mutant protein. The latter again suggests that phosphorylated MrrA is the active species. (Figure 2 and Figure S2).

The second kinase, CC2874, is the strongest kinase seen so far in our lab. Mutant CC2874 protein without PAS domains is unstable and could thus not be analyzed in our study. The REC domain of the kinase is not required for its function and CC2874 readily phosphorylates its REC domain as well as MrrA even if one of the proteins is present in 5-10 fold excess. Our results show that not only the phosphorylated Asp of the REC domain, but also the

phosphorylated His of the kinase domain of CC2874 are stable enough to be detected (Figure 2 and Figure S2).

Using a phosphoproteomic screening method Capra *et al.* found two kinases, CC2324 and CC2501, that both showed weak phosphotransfer to MrrA when expressed without their REC domain (Figure 2A) [227]. Notably, they showed for another protein that removal of the REC domain results in unspecificity [150]. We therefore purified the kinases CC2324 and CC2501 with their REC domains (only the membrane spanning regions were excluded in our constructs) and investigated possible phosphotransfer to MrrA. CC2324 is the weakest kinases of this study. The brightness and contrast of the radiograms had to be optimized in order to see a signal. In the adapted images, CC2324 autophosphorylation as well as a signal for MrrA is slightly visible. CC2501 shows clear autophosphorylation signals, but phosphotransfer to MrrA was not detectable (Figure 2). Taken together, our *in vitro* phosphorylation assays suggest that CC2874 functions as a kinase for MrrA, whereas CC2554 might primarily be active as a phosphatase for the SDRR, which in turn deactivates CC2554 kinase activity. Although we cannot exclude that CC2324 and CC2501 are interacting with MrrA *in vivo*, our *in vitro* data suggest that MrrA is not a specific target for either of the two kinases.

To investigate whether the kinases CC2324, CC2501, CC2554 and CC2874 can explain the phenotypes observed for $\Delta mrrA$, we constructed overproduction and deletion mutants for each kinase. Overexpression of CC2874 resulted in loss of sensitivity to *mrrA* deletion when scored for attachment and motility (Figure S3). Overproduction of CC2554 showed increased attachment levels in wild type background and compared to that decreased surface adherence in a $\Delta mrrA$ background. Additionally, the cells were not sensitive to a loss of *mrrA* in motility assays on semi solid agar plates (Figure S3). These data imply, that CC2874 and CC2554 are indeed involved in regulating attachment and motility in an MrrA-dependent way. However, single deletions of CC2501, CC2554 and CC2874 are not impaired in attachment, motility or stress adaptation. In combination with $\Delta mrrA$, the double mutants phenocopy a $\Delta mrrA$ single mutant. Even a quadruple deletion mutant ($\Delta CC2324 \Delta CC2501 \Delta CC2554 \Delta CC2874$) is still sensitive to loss of *mrrA* (Figure 3), arguing that other kinases exist that feed into the MrrA signaling cascade. Deletion of CC2324 shows phenotypes when scored for attachment, motility and biomass production, but the mutant is still sensitive to a loss of $\Delta mrrA$, indicating that regulation of the phenotypes is MrrA-independent. In summary, our data imply that CC2554 and CC2874 are connected to MrrA *in vivo* (overproduction data) but that other

kinases must exist that feed into the MrrA signaling cascade (quadruple kinase knock-out mutants). Recent work on the MrrA homolog SdrG of *S. melonis* supports this notion. SdrG is phosphorylated by seven kinases (PakA – PakG) and these kinases also mediate phosphotransfer to the anti-anti sigma factor PhyR. Furthermore, phosphorylation of other SDRR (PkrB, PkrC, PkrD, PkrF) also depends on the Pak proteins and PhyR is additionally regulated by the phosphatase PhyP [205,210]. These findings mirror the complexity found in our *C. crescentus* system and might explain why phenotypes for the kinase knock-out mutants could not be found. Interestingly, SdrG has been shown to positively affect stress adaptation and to function upstream of PhyR, like MrrA [205,210].

Next we decided to focus on the connectivity between MrrA, LovK and the SigT stress pathway. In addition to dramatic downregulation of PhyR, NepR and SigT, we also found decreased LovK levels in $\Delta mrrA$ compared to wild type cells (Table S3). So far, the link between MrrA and LovK has not been shown and the potential connection between LovK and PhyR in *C. crescentus* is missing essential *in vitro* data [202]. LovK was originally identified to be involved in surface attachment [211] and it has been suggested, that LovK only functions as a phosphatase for PhyR (reviewed in [275]) whereas PhyR phosphorylation depends on PhyK [207]. Notably, no study is published in which purified *C. crescentus* PhyK was used *in vitro*. Although essential *in vitro* data were missing another study proposed, that LovK of *C. crescentus* might phosphorylate PhyR, at least in the absence of LovR [202]. In line with these studies it has been shown for *B. abortus* that LovK (Bab2_0652) interacts with PhyR (Bab1_1671) [287]. Our *in vitro* phosphorylation assays provide the missing information in the signaling cascade. We show that phosphorylated MrrA is required to activate LovK autophosphorylation. Furthermore, we provide *in vitro* data showing that activated LovK can phosphotransfer to PhyR of *C. crescentus*. The PhyR~P signal is increased in the presence of NepR (Figure 5). As described in the literature, the addition of NepR stabilizes phosphorylated PhyR by a yet unknown mechanism [204]. Interestingly, LovK can dephosphorylate MrrA, but is unable to act as a phosphatase for PhyR. Instead, LovK functions solely as a PhyR kinase in our assays (Figure 5). In order to switch off the activated SigT-stress adaptation pathway, PhyR would either have to be deactivated by dephosphorylation, or be degraded. At least in *B. abortus*, PhyR is degraded by ClpXP in the absence of stress [209]. Whether the same holds for true *C. crescentus* remains to be elucidated. Alternatively, other phosphatases, e.g. PhyK might function as deactivators for PhyR~P. Previous studies suggest that LovR functions as a phosphate sink for LovK,

resulting in LovK dephosphorylation [202,210,287]. Importantly, our data now show that LovR rather switches LovK into its phosphatase mode resulting in loss of the LovK and MrrA signal (Figure 5). Interestingly, *E. litoralis* harbours three LovK homologs (ELI02980 = EL368, ELI04860 = EL346 and ELI07650 = EL362). All three homologs can phosphotransfer to LovR. EL346 and EL368 were also tested positive for phosphorylation of PhyR and the MrrA homolog ELI09195, and EL368 in addition showed phosphotransfer to ELI14085 (DivK) and ELI07690 (CpdR) [288]. Whether LovK of *C. crescentus* can also regulate the activity of DivK and CpdR still remains to be elucidated. Notably, $\Delta mrrA$ is phenocopied by cells overproducing LovRK. LovK and its cognate response regulator LovR were originally identified to lead to a superattachment phenotype when overproduced simultaneously [202]. In addition, cells overexpressing *lovR* and *lovK* are less stress resistant and accordingly, a *lovRK* double mutant was found to show increased cell survival under osmotic stress [202]. And we found that LovRK overproduction results in elevated motility (data not shown, Figure XI). So far, LovRK regulation of motility was not published. Together with the literature data we conclude that a *lovRK* overexpression strain phenocopies $\Delta mrrA$.

Taken together, we propose a model in which phosphorylated MrrA is required for the activation of the SigT pathway *via* LovK and at least one other kinase that phosphotransfers to PhyR, likely PhyK. MrrA itself becomes activated by CC2874 and CC2554 as well as other kinases. Both, CC2874 and CC2554 have phosphatase activity and are able to dephosphorylate MrrA. MrrA in turn inhibits CC2554 resulting in a feedback loop. Phosphorylated MrrA activates kinase activity of LovK and is counteracted by LovR, a SDRR that switches LovK into phosphatase mode resulting in dephosphorylation of LovK and MrrA. LovK connects MrrA to the SigT pathway by acting as a kinase for PhyR (Figure 6). Furthermore, MrrA indirectly has a negative effect on attachment and motility, whereas LovK (when overproduced together with LovR) does not only positively affect surface adherence as described before [211], but also leads to increased motility levels. Whether the regulation of attachment and motility is also wired by the SigT pathway remains to be elucidated. At least for LovK it has been proposed that its effect on attachment is independent of PhyR (reviewed in [275]). Due to the abundance of components upstream of PhyR genetic approaches are inconclusive at this point (data not shown). Furthermore, *nepR* deletion as well as SigT overproduction results in a lethal phenotype (reviewed in [275]).

In summary, our research shows that the SDRR MrrA functions as a signaling bottleneck for stress adaptation and is also involved in the regulation of attachment and motility. Strikingly, MrrA has a negative effect on both, surface attachment and motility, although the corresponding cells types are inversely regulated in *C. crescentus*. How this is accomplished remains to be elucidated. Multiple kinases can activate MrrA by phosphorylation and in turn, MrrA affects downstream proteins in the signaling cascade. Importantly, the downstream proteins as well as upstream interaction partners of MrrA are redundant to ensure proper response when cells encounter stress. This redundancy increases the complexity of the MrrA network and explains the difficulty to interpret our phenotypes found for deletion mutants upstream of PhyR. Notably, we showed for the first time, that LovK functions as a connector between MrrA and the SigT-pathway *via* PhyR.

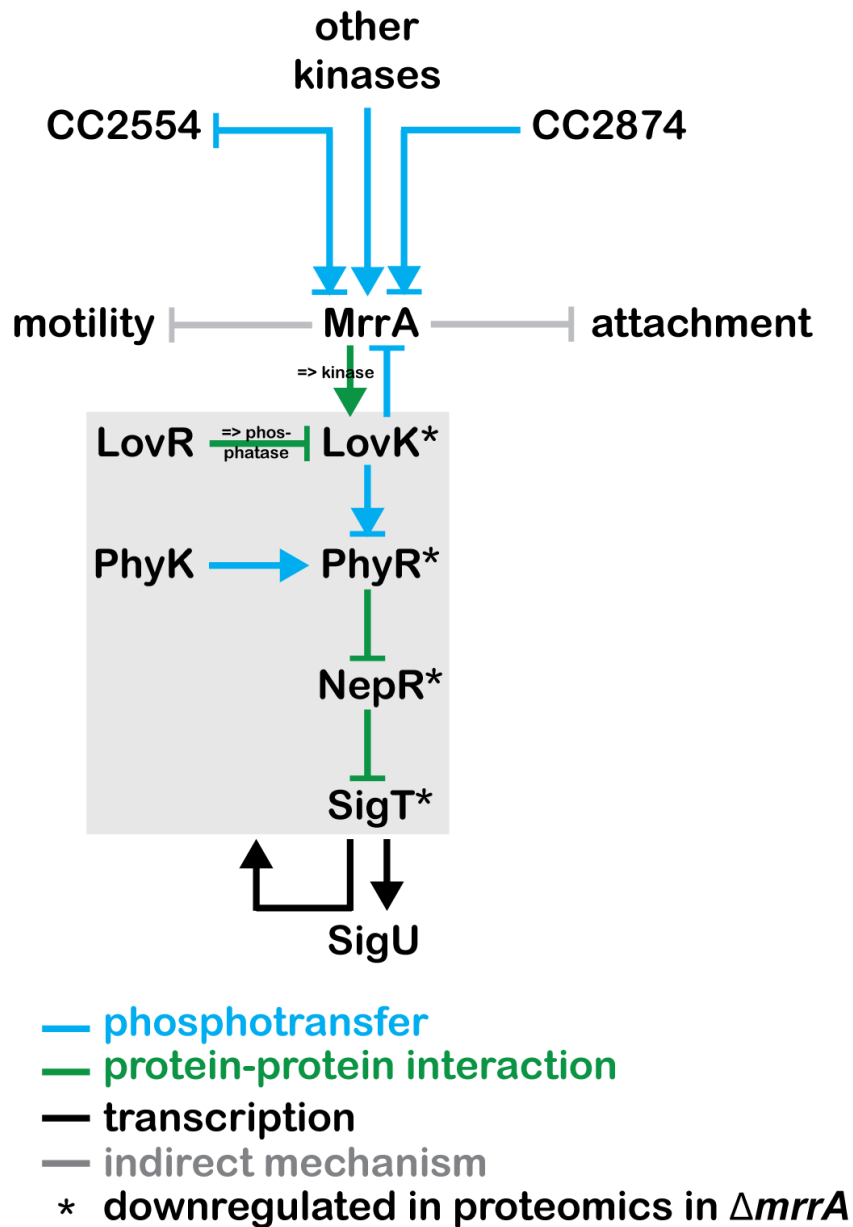
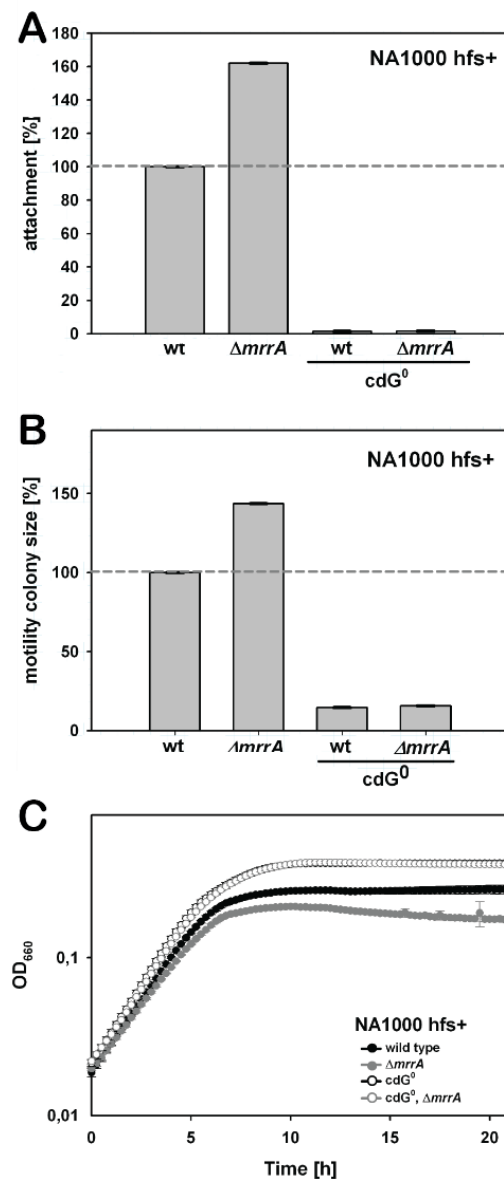


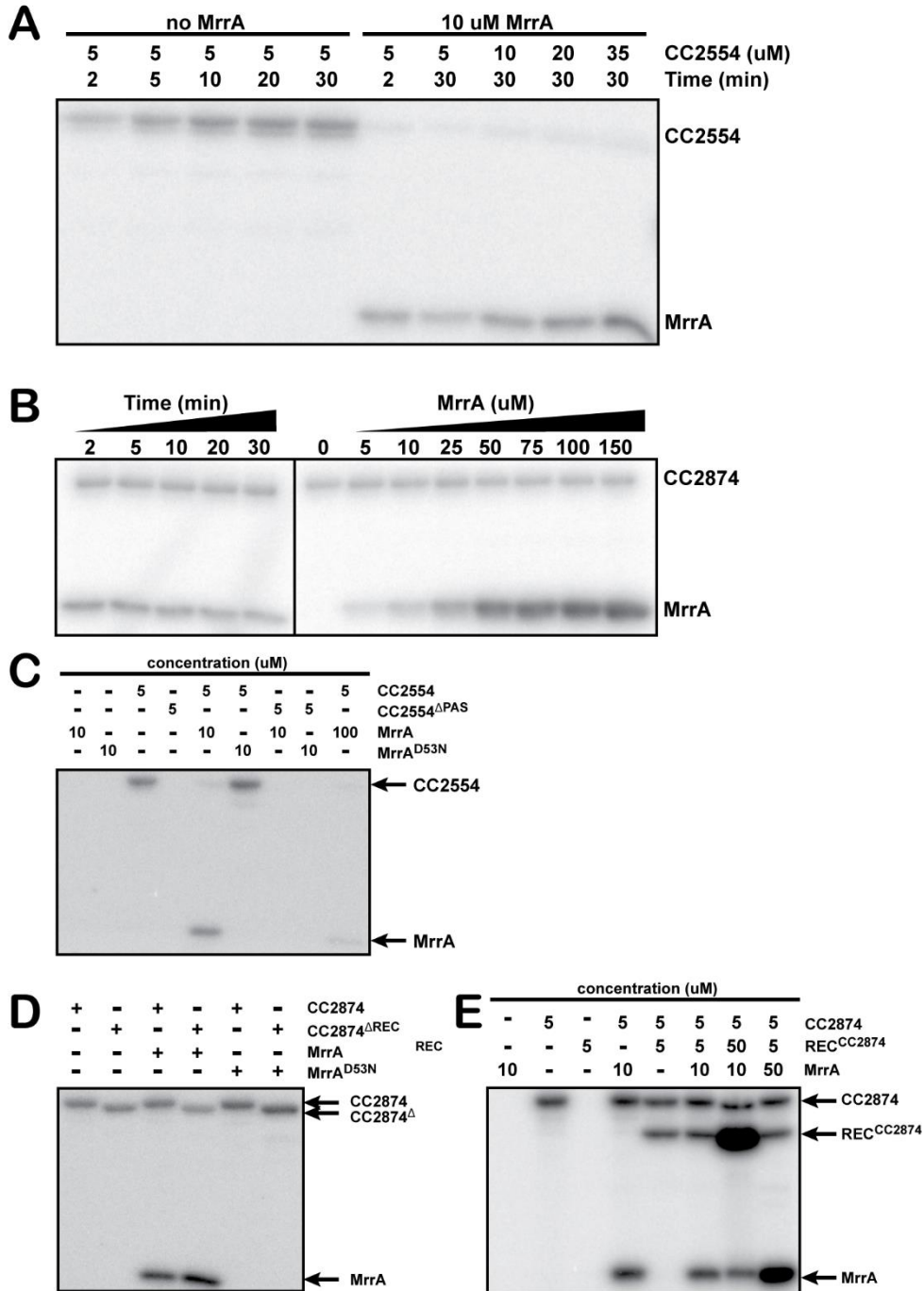
Figure 6: MrrA network configuration. Schematic overview of the SigT-activating cascade in *C. crescentus*.

Extended Data Figure 1



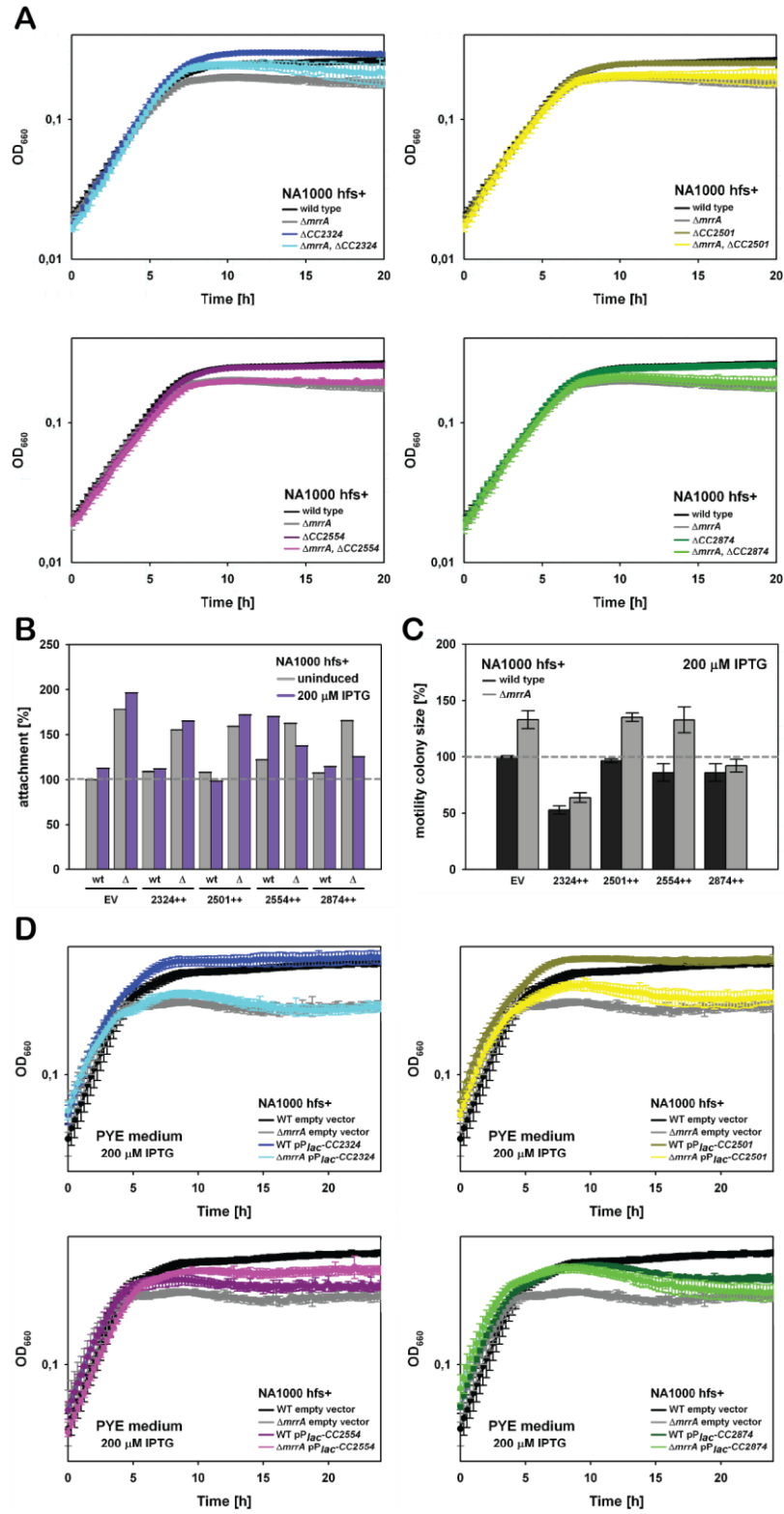
Extended Data Figure 1: MrrA phenotypes depend on cdG. PYE medium was used for all experiments. Error bars indicate the standard deviation for each graph. **(A)** A 96-well plate attachment assay was analysed 24h after inoculation. Two biological and six technical replicates were used per experiment. At least three experiments have been performed per strain. Attachment is fully abolished in a strain that cannot produce cdG. An *mrrA* deletion cannot restore attachment. **(B)** PYE plates supplemented with 0.3% agar were inoculated and colony sizes were measured 3 days after inoculation. 5 independent plates were analysed per experiment. At least 3 experiments have been performed per strain. Motility on 0.3% agar plates is fully abolished in a strain that cannot produce cdG. An *mrrA* deletion cannot restore motility under these conditions. **(C)** Biomass production was followed in a 96-well plate. Two biological and six technical replicates were used per experiment. Strains lacking cdG show increased biomass in stationary phase compared to wild type and $\Delta mrrA$ cultures, and deletion of *mrrA* does not result in decreased biomass in stationary phase in a cdG⁰ background.

Extended Data Figure 2



Extended Data Figure 2: Additional *in vitro* characterization of CC2554 and CC2874. Proteins were used in the following concentrations unless indicated otherwise: 10 μM MrrA, 5 μM of potential CC2554 and CC2874. 500 μM ATP and 2.5 μCi [$\gamma^{32}\text{P}$]ATP (3,000 Ci mmol^{-1}) were used and the reactions were carried out for 15 minutes (unless indicated otherwise) at room temperature. **(A)** Autophosphorylation of CC2554 is visible after two minutes (lane 1) and saturated after 10 minutes (lane 3). If CC2554 is titrated into the mix, more MrrA becomes phosphorylated (lane 7-10). In the presence of MrrA, the CC2554 autophosphorylation signal is not visible, indicating that MrrA inhibits the activity of CC2554. **(B)** Autophosphorylation of CC2874 and phosphotransfer to MrrA is instant (lane 1). If MrrA is titrated into the mix, its phosphorylation signal becomes more intense with increasing concentration, indicating that CC2874 is active for several rounds. **(C)** MrrA alone is not phosphorylated (lane 1). The same applies for MrrA^{D53N} (lane 2), which also does not become phosphorylated in the presence of CC2554 and cannot inhibit CC2554 (lane 6), supporting the idea that phosphorylated MrrA is the active species. The PAS domain of CC2554 is required for its function, as CC2554 Δ PAS does not show autoactivation (lane 4). A 20x excess of MrrA (100 μM) compared to CC2554 results not only in loss of the CC2554 autoactivation signal, but also in the loss of the MrrA signal (lane 9), supporting the idea that CC2554 is primarily a phosphatase for MrrA. **(D)** The REC domain of CC2874 is neither required for its autophosphorylation (lane 2), nor for phosphate transfer to MrrA (lane 4). Lane 4 also shows, that the phosphorylated His441 of CC2874 is stable, and that both, the His441 and the Asp728 in the REC domain can be made visible. **(E)** Like in the case of MrrA (lane 1), the REC domain of CC2874 cannot be phosphorylated without a kinase being present (lane 3). CC2874 can phosphotransfer to MrrA (lane 4) and to its own REC domain (lane 5). If both, MrrA and REC^{CC2874} are present in the mix, both become phosphorylated by CC2874 (lane 6). If one of the REC domains is present in 5-10x excess, still both signals are visible, indicating that CC2874 is active enough to phosphotransfer both REC domains efficiently (lane 7-8).

Extended Data Figure 3



Extended data Figure 3: Additional *in vivo* characterization of CC2324, CC2501, CC2554 and CC2874. PYE medium was used for all experiments. Error bars indicate the standard deviation for each graph. **(A)** Biomass production was followed in a 96-well plate. Two biological and six technical replicates were used per experiment. At least 3 experiments have been performed per strain. Deletion of *CC2324*, *CC2501*, *CC2554* and *CC2874* alone or in combination with $\Delta mrrA$ resemble wild type or $\Delta mrrA$ biomass production, respectively. **(B)** Overnight cultures were diluted to $OD_{660} = 0.05$, grown until $OD_{660} = 0.3$ before 200 μ M IPTG were added to induce kinase overexpression. Cells were directly transferred to a 96-well plate and attachment was scored 24h after inoculation. Two biological and six technical replicates were used per experiment. At least 3 experiments have been performed per strain. Only CC2554 and CC2874 overproduction have an effect on attachment. Overproduction of CC2554 in wild type results in increased attachment, supporting the idea that CC2554 is a phosphatase rather than a kinase for MrrA. Overproduction of CC2874 results in decreased attachment in the $\Delta mrrA$ background. **(C)** PYE plates supplemented with 0.3% agar and 200 μ M IPTG were inoculated and colony sizes were measured 3 days after inoculation. 5 independent plates were analysed per experiment. At least 3 experiments have been performed per strain. *CC2324* and *CC2874* are the only kinases that result in a phenotype when overexpressed. In both cases the strains are not susceptible to a loss of *mrrA* anymore. **(D)** Overnight cultures were diluted to $OD_{660} = 0.05$, grown until $OD_{660} = 0.3$ before 200 μ M IPTG were added to induce kinase overexpression. Cells were directly transferred to a 96-well plate and biomass was followed for 24h. Two biological and six technical replicates were used per experiment. Overexpression of *CC2324* and *CC2501* does not show phenotypes. Overexpression of *CC2554* or *CC2874* however results in insusceptibility for a loss of *mrrA*. In both cases, the deletion of *mrrA* does not result in less biomass in stationary phase compared to overexpression of the kinases in the wild type background.

Extended Data Table 1

A	Protein	Essential	Function	Total counts WT	Total counts MrrA	Fold change (MrrA/wt)	T-test
	DgcB	no	signaling	1	11	11	0.03
	ChpT	yes	signaling	0	9	9	0.00
	ParE	yes	DNA replication	0	22	22	0.01
	CC2874	no	signaling	0	24	24	0.04
	CC1056	no	DUF	1	15	15	0.05
B	Protein	Essential	Function	Transformants			
	CC2330	no	transcription factor	2			
	CC2554	no	kinase	1			
	CC2874	no	hybrid kinase	5			
C	Protein	Essential	Function	Ratio (<i>mrrA</i> / wt)			
	CC2576	no	SDRR	0.25			
	CC3147	no	TonB-dep receptor	4.34			
	MucRIII	no	transcription factor	0.02			
	NepR	yes	anti-sigma factor	0.10			
	PhyR	no	anti-anti-sigma factor	0.22			
	SigT	no	sigma factor	0.08			

Extended data Table 1: In search for potential MrrA interaction partners.

(A) Selected hits obtained by Co-IP using MrrA-3xFLAG to pull down potential interaction partners. All hits shown were double-checked by bacterial two hybrid either because of high fold change and/or because of possible association with one of the MrrA phenotypes. The full data set can be found in Table S2. **(B)** All in frame hits from the Y2H screen that did not show autoactivation and grew after restreaking on selective plates. **(C)** All hits from proteome comparison between wild type and $\Delta mrrA$ cultures that were minimally 4x down- or 4x upregulated. The full data set can be found in Table S3.

Tables S2 and S3 showing pulldown and mass spec data are not included in this thesis.

Materials and Methods

Protein purification

E. coli BL21 containing the plasmid of interest were grown at 30°C in LB medium and induced with 1 mM isopropyl β -D-1-thiogalactopyranoside (IPTG) for protein overproduction at $OD_{600} = 0.6$. Cells were harvested 2 h after induction (5.000 rpm, 15 min, 4°C) and the cell pellets were stored at -80°C. After resuspension of the pellet in lysis buffer (1x PBS, 10 μ g/ml DNase, 1 complete mini protease inhibitor tablet (Roche)), the cells were disrupted using french pressing (2 bar) and the supernatant containing the protein of interest was separated from the cell lysate by centrifugation (11.000 rcf, 1 h, 4°C). The supernatant was incubated with 1 ml Protino® Ni-NTA Agarose (Macherey-Nagel) (11 rpm, 1 h, 4°C) before being loaded to the column. The column was washed with wash buffer (2x PBS, 500 mM NaCl, 10 mM imidazole (pH 8.0), 1 mM DTT) and the protein was eluted in 1 ml elution buffer (1 x PBS, 500 mM NaCl, 250 mM imidazole (pH 8.0), 1 mM DTT). Protein was dialysed in Spectra/POR® membranes with a cutoff of 3.5 kDa (for MrrA-His₆ form plasmid pIDJ053) or 12-14 kDa (for all other proteins) (Spectrum Laboratories) using 500 ml dialysis buffer (10 mM HEPES-KOH, pH 8.0, 50 mM KCl, 10% glycerol, 0.1 mM EDTA, pH 8.0, 5 mM β -mercaptoethanol, 5 mM MgCl₂) per 1 ml protein. Soluble protein was separated from precipitated protein using ultracentrifugation (Optima™ Max-XP centrifuge and TLA-55 rotor from Beckmann Coulter) (100.000 rcf, 1h, 4°C). Protein concentrations (μ M) were determined with the following formula (A_{280} / extinction coefficient * 1000000 * dilution factor). The extinction coefficient was calculated on <http://web.expasy.org/protparam/>.

Attachment Assays

5 μ l of *C. crescentus* overnight cultures were used to inoculate 160 μ l PYE medium in standard 96-well plates. Unless stated otherwise, growth and attachment was allowed for 24h (200 rpm, 30°C). OD_{600} was measured in an EL800 plate reader using the corresponding KJ Junior software (both Bio-Tek Instruments) and the wells were gently washed four times with demineralized water. Attached cells were stained with 180 μ l 0.1% crystal violet (200 rpm, 20 min, 30°C) and cells were washed three times with water before dissolving the crystal violet with 200 μ l 20% acetic acid (200 rpm, 20 min, 30°C). A_{600} was measured in an EL800 plate reader using the corresponding KJ Junior software

(both Bio-Tek Instruments) and used to calculate the attachment corrected for the cell density.

Bacterial Two Hybrid

Bacterial two hybrid (B2H) assays were performed as described in [289]. Proteins of interest were fused N- or C-terminally to the T18 or T25 fragment of the *B. pertussis* adenylate cyclase. The test strain SöA1080 was freshly transformed with the pUT18 and pKT25 derivative plasmids in all possible combinations. Transformants were screened on LB plates supplemented with ampicillin, kanamycin and 40 µg/ml X-gal (ON, 37°C). Four single colonies of each transformation were grown in 100 µl LB supplemented with ampicillin and kanamycin in standard 96-well plates (200 rpm, 5 h, 37°C). 2 µl of each logarithmically growing culture was spotted on Mc-Conkey agar plates (0.4% Mac Conkey Agar Base, Difco) supplemented with ampicillin, kanamycin and 1% maltose. The plates were incubated at 30°C for two days. Interaction was seen for positive controls (red colony) and not observed for negative controls (white colonies).

β-galactosidase Assays

Two independent *C. crescentus* cultures were grown per strain in 5 ml PYE (ON, 150 rpm, 30°C). The next morning, the cultures were diluted to an OD₆₆₀ of 0.05 in 5 ml PYE and grown until OD₆₆₀ = 0.3 (unless for stationary phase cultures, which were taken directly from the ON culture). 2 ml culture were taken and the pellet resuspended in 2 ml fresh Z-buffer (0.06 M Na₂HPO₄, 0.04 M NaH₂PO₄, 0.01 M KCl, 0.001 M MgSO₄, 0.3% β-mercaptoethanol). 1 ml was used to measure the density of the suspension at A₆₆₀. To the remaining 1 ml 100 µl of 0.1 % SDS and 20 µl chloroform were added. The samples were vortexed for 10 sec and incubated for 15-30 min. Three technical replicates of 200 µl each were transferred to a 96-well plate. 25 µl fresh ONPG (β-D-galactopyranosid, 4 mg/ml stock) were added per well directly before measuring the kinetic β-galactosidase activity in an EL800 plate reader using the corresponding KJ Junior software (both Bio-Tek Instruments). 20 time points were taken for each measurement and the maximum slope was plotted as increase of OD₄₀₅ per time point corrected for OD₆₆₀ and volume.

Cyclic di-GMP Level Measurements

Four independent *C. crescentus* cultures were grown per strain in 5 ml PYE (ON, 150 rpm, 30°C). The next morning, the cultures were diluted to an OD₆₆₀ of 0.05 in 15 ml PYE and grown until OD₆₆₀ = 0.3. 10 ml of each culture was used for the cdG extraction. The cell pellets were resuspended in 100 µl H₂O and transferred into a 1.5 ml screwcap reaction tube (5 min, 5000 rcf, 4°C). H₂O was added up to 1 ml and the cells were pelleted after vortexing (1 min, full speed, 4°C). A 300 µl acetonitrile/methanol/water mixture (40/40/20 v/v) were used to lyse the cells using a three-step incubation (15 min at 4°C followed by 10 min at 95°C (shaking) and 1 min on ice). Cells and cell debris were collected (1 min, full speed, 4°C) and the supernatant (extraction 1) was transferred to a fresh 2 ml reaction tube. Extraction of cdG from the pellet was repeated using 200 µl acetonitrile/methanol/water mixture (40/40/20 v/v) for 15 min at 4°C followed by centrifugation (1 min, full speed, 4°C). The supernatant of extraction 2 was added to extraction 1 and a third extraction was performed on the pellet as described for extraction 2. In total 700 µl extraction volume were collected and stored overnight at -20°C. The supernatant was centrifuged twice (20 min, full speed, 4°C) and transferred to a fresh 1.5 ml reaction tube after each centrifugation step before being sent for mass spectrometry. Mass spectrometry was performed by Annette Garbe at Hannover University according to a facility-based standard protocol for cyclic di-GMP measurements.

Co-Immunoprecipitation

Four independent overnight *C. crescentus* cultures of UJ5511 and UJ6643 were diluted to an OD₆₆₀ of 0.05 in 500 ml fresh PYE. The diluted cultures were grown (30°C, 180 rpm) to an OD₆₆₀ of 0.3 and harvested (10.000 xg, 10 min, 4°C). The pellets were washed twice in 50 ml washing buffer (20 mM Tris pH 8.0, 100 mM NaCl) (10.000 xg, 20 min, 4°C) before being resuspended in 10 ml Bug Buster (Novagen) supplemented with 1 pil complete mini protease inhibitor (Roche), 200 µg/ml lysozyme and benzonase (0.5 µl/ml). After an incubation step at room temperature (20 min, gentle shaking), undisrupted cells, cell debris and precipitated proteins were removed by centrifugation (10.000 xg, 15 min, 4°C). The procedure was repeated with the precleaned supernatant. 150 µl Protino® Ni-NTA Agarose (Macherey-Nagel) was washed 3x in 500 µl Bug Buster (1.000 xg, 1 min, 4°C), and incubated with the cleared lysate (ON, 4°C, 10 rpm on a rotary wheel). The beads were transferred to a

Biospin column (Bio-Rad) and washed 4x with 700 μ l HNN-lysis buffer (50 mM HEPES pH 7.5, 150 mM NaCl, 50 mM NaF, 5 mM EDTA) with 0.5% IGEPAL CA-630 (Sigma-Aldrich), before being washed 4x with HNN-lysis buffer without detergent. The protein extract was eluted using 3x 150 μ l 0.2 M glycine (in HPLC water, pH 2.5). The eluate was neutralized with 150 μ l ABC-buffer (ammonium bicarbonate, 1M stock in HPLC grade water). Urea (8 M stock in 100 mM ABC-buffer) was added to a final concentration of 1.6 M and the sample was vortexed before reducing and alkylating disulfide bonds as follows. 1 μ l TCEP (tris(2-carboxyethyl)phosphine, 0.2 M in 100 mM ABC-buffer) was added per 40 μ l protein extract (37°C, 30 min, 1.000 xg). After cooling down, 1 μ l fresh iodacetamide (0.4 M stock in HPLC water) was added per 40 μ l protein extract and incubated in the dark (25°C, 30 min, 500 rpm). Finally, 1 μ l N-acetyl-cystein solution (0.5 M in 0.1 M ABC-buffer) was added per 40 μ l sample, vortexed and incubated (25°C, 10 min, 500 rpm). For proteolysis, 1 μ g porcine trypsin (0.4 μ g/ μ l stock, Promega) was added (ON, 37°C, 500 rpm). For peptide purification, 150 μ l TFA (trifluoroacetic acid, 5 % stock in HPLC water) was added to decrease the pH below 3. C18-microspin columns (Thermo Scientific) were conditioned twice with 150 μ l acetonitrile (1.600 rpm, 30 sec) and equilibrated 3x with 150 μ l 0.1 % TFA (2.400 rpm, 30 sec). The samples were loaded and the flow-through was collected in a fresh tube (1.800 rpm, 2 min). The flow-through was re-loaded and centrifuged again (1.800 rpm, 2 min). A mixture of 5 % acetonitrile, 95 % HPLC water (v/v) and 0.1 % TFA was used to wash the columns 3x with 150 μ l volume (2.400 rpm, 30 sec). Bonded peptides were eluted into a new tube using 3x 100 μ l elution buffer (50 % acetonitrile, 50 % HPLC water (v/v) and 0.1 % TFA) (1600 rpm, 30 sec). A speed vac (Eppendorf) was used to concentrate the eluted peptide mixture to dryness. The peptides were dissolved in 50 μ l LC-buffer A (0.15 % formic acid, 2 % acetonitrile) using 20 pulses ultrasonication (Vial Tweeter, Hielscher) (amplitude 100, cycle 0.5) and shaking (25°C, 5 min, 1.400 rpm).

Growth Experiments

Two independent overnight *C. crescentus* cultures of each strain were diluted to an OD₆₆₀ of 0.05 in PYE medium. Three technical replicates (165 μ l) of each culture were loaded in a 96-well plate and growth was monitored at 660 nm every 15 min in a Synergy H4 hybrid reader (BioTek) using Gen5 2.00 software (BioTek) at 30°C under shaking conditions (medium speed, continuous shaking).

***In vitro* Phosphorylation**

Kinase and phosphatase assays were adapted from [49]. Reactions were incubated in dialysis buffer in presence of 500 μ M ATP and 2.5 μ Ci [γ ³²P]ATP (3,000 Ci mmol⁻¹, Hartmann Analytic) at room temperature. Additional proteins were added and samples taken at indicated time points. Reactions were stopped by the addition of SDS sample buffer and subsequently loaded (or stored on ice) on 12% SDS gels. Wet gels were exposed to phosphor screens (0.5-1.5 h) before being scanned using a Typhoon FLA7000 imaging system (GE Healthcare). In experiments assessing phosphatase activity in the absence of ATP, ATP was depleted by the addition of 1.5 u hexokinase (Roche) and 5 mM D-glucose 15 minutes after phosphorylation.

Microscopy

Two independent overnight cultures of *C. crescentus* were either taken directly for microscopy, or first diluted to an OD₆₆₀ of 0.05 and grown until OD₆₆₀ 0.3. 500 μ l culture was pelleted (1 min, 16000 rpm) and the cells were resuspended in 50 μ l (exponential phase culture) or 500 μ l (stationary phase culture) fresh PYE medium. 0.4 μ l culture was spotted on a PYE patch containing 0.1 % agarose. For holdfast staining, 2.5 μ l green-fluorescent Oregon Green® 488 WGA (ThermoFisher Scientific) was added per 750 μ l PYE-agarose. Cells were monitored using a Deltavision set up from Applied Precision: IX-71 microscope (Olympus), CoolSnap HQ2 camera (Photometrix), Softworx 5.5 software. The following set up was used to acquire snapshots: 100x phase contrast objective (NA 1.3), GFP filterset (Ex 475/28, Em 525/50) for holdfast visualization, xenon-lamp.

Motility Assays

To compare motility colony size, fresh single colonies were picked and patched into a PYE motility agar plate (PYE medium supplemented with 0.3 % agar). Colony growth was allowed in a humid chamber (30°C, 3 days). The plates were scanned and the diameter of five independent colonies per strain was calculated using Image J software (freeware on <http://imagej.nih.gov/ij/>).

Proteome Comparison

Four independent cultures of *C. crescentus* were diluted in 15 ml PYE to an OD₆₆₀ of 0.05 and grown until OD₆₆₀ 0.3. 10 ml of the cultures was pelleted (4000 xg, 40 min, 4°C) and the pellets were dissolved in 200 µl cold lysis buffer (8 M Urea, 0.1 M ammonium bicarbonate, 0.1 % RapiGest) by vortexing (10 sec), ultrasonication (Vial Tweeter, Hielscher) (2x 10 sec, amplitude 100, cycle 0.5) and shaking in a Thermomixer C (Eppendorf, 5 min, 1400 rpm, RT). After centrifugation (30 min, 4°C, max speed), the supernatant containing the solubilized proteins was transferred to a fresh tube and the protein concentration was first measured using a standard Bradford assay (Bio-Rad) and then adjusted to a final concentration of 1 mg/ml. To reduce and alkylate disulfide bonds, 50 µg protein extract were taken and 1 µl TCEP (tris(2-carboxyethyl)phosphine, 0.2 M stock in 0.1 M Tris pH 8.5) was added per 40 µl protein extract (37°C, 1h, 1000 rpm). After the samples were cooled down, 1 µl fresh iodacetamide solution (0.4 M stock in HPLC water) was added per 40 µl sample and incubated in the dark (25°C, 30 min, 500 rpm). Finally, 1 µl N-acetyl-cysteine solution (0.5 M stock in 0.1 M Tris pH 8.5) was added per 40 µl sample, vortexed and incubated (RT, 500 rpm, 10 min). For the proteolysis Lys-C (0.2 µg/µl stock, Wako) was added to a final enzyme/protein ratio of 1:100 (37°C, 4 h, 550 rpm). The sample was diluted 1:5 (v/v) to a final urea concentration below 2 M using fresh 0.1 M ABC buffer (ammonium bicarbonate in HPLC water). Porcine trypsin (0.4 µg/µl stock, Promega) was added to a final trypsin/protein ratio of 1:50 (37°C, ON, 550 rpm). Post digestion, TFA (trifluoroacetic acid, 5 % stock in HPLC water) was used to decrease the pH below 2. For the solid phase extraction C18-microspin columns (Harvard Apparatus) were conditioned with 150 µl acetonitrile (2400 rpm, 30 sec) and equilibrated twice with 150 µl TFA (0.1 % stock in HPLC water, 2400 rpm, 30 sec). The sample was transferred twice through the column (2000 rpm, 2 min) before the column was washed 5x with 150 µl wash buffer (5 % acetonitrile, 95 % HPLC water and 0.1 % TFA) (2400 rpm, 30 sec). The peptides were eluted twice with 150 µl elution buffer (50 % acetonitrile, 50 % HPLC water and 0.1 % TFA) and concentrated under vacuum to dryness using a table top concentrator (Eppendorf). The peptides were dissolved to a final concentration of 0.5 µg/µl in LS-MS/MS buffer (0.15 % formic acid, 2 % acetonitrile, HPLC water) using 20 pulses ultrasonication (Vial Tweeter, Hielscher) (amplitude 100, cycle 0.5) and shaking in a Thermocycler (37°C, 5 min, 1.400 rpm) (Eppendorf).

Yeast Two Hybrid Screening

E. coli DH5 α pIDJ041 (UJ6743) was used to isolate high quantities of bait plasmid DNA to screen for MrrA interaction partners. *S. cerevisiae* PJ69-4A (UJ5292) [284] was transformed with pIDJ041 according to standard small-scale transformation procedure (Clontech Manual, Protocol No. PT1172-1, Version No. PR8Y2629). Single colonies of *S. cerevisiae* PJ69-4A containing the bait-plasmid pIDJ041 were used for library-scale transformation with a *C. crescentus* library made inhouse as described by Clontech (Clontech Manual, Protocol No. PT1172-1, Version No. PR8Y2629). Stringent selection on plates lacking adenine (SC-Trp-Leu-Ade) did not give rise to a single yeast colony that could be re-grown in liquid media. In a second approach 2.2×10^6 transformants were screened using less stringent selection on plates lacking histidine (SC-Trp-Leu-His + 5 mM 3'AT). To isolate prey plasmids for sequencing, cells of 8 ml overnight yeast culture (grown at 30°C, 180 rpm) were collected (5 min, 1000 xg) and resuspended in 500 μ l sorbitol buffer (1 M sorbitol, 1 mM EDTA pH 8.0, 14.5 mM β -mercaptoethanol, 300 u lyticase). The reaction was incubated for 30 min at 30°C and mixed every 10 min. The spheroblasts were collected (5 min, 1600 xg) and the plasmids were isolated using a standard plasmid isolation kit (Sigma).

Oligonucleotides, plasmids, strains and media

Oligonucleotides, plasmids and bacterial strains are listed in Table 1, 2 and 3, respectively. *Caulobacter crescentus* was grown in PYE or M2G medium at 30°C [235]. *E. coli* DH5 α was used as host for cloning and grown in LB at 37°C. When required, the growth media were supplemented with antibiotics at the following concentrations (liquid / solid medium): 5/50 μ g ml⁻¹ of ampicillin, 5/20 μ g ml⁻¹ of kanamycin, 2.5/5 μ g ml⁻¹ of tetracycline, 1/2 μ g ml⁻¹ of chloramphenicol, 15/20 μ g ml⁻¹ of nalidixic acid (*C. crescentus*) and 50/100 μ g ml⁻¹ of ampicillin, 30/50 μ g ml⁻¹ of kanamycin, 12.5/12.5 μ g ml⁻¹ of tetracycline, 20/30 μ g ml⁻¹ of chloramphenicol, 15/30 μ g ml⁻¹ of nalidixic acid (*E. coli*).

Table 1: Oligonucleotides used in this study

NAME	SEQUENCE (5'→3')	PURPOSE
prIDJ025_check_KOcc3015-F	CTGAAGGACCAGCTGAACG	check integration pIDJ005
prIDJ026_check_KOcc3015-R	CTTGACCGGTCGACACGAC	check integration pIDJ005
prIDJ033_cPCR_pNPTS138-F	CATGATTACGCCAAGCTACG	colony pcr pNPTS138
prIDJ034_cc0284up-F+HindIII	GGCCGGAAGCTTGACCGCGTTGC TTCACGAG	pIDJ002
prIDJ035_cc0284up-R+NheI	GGCCGCGCTAGCGATCAAAAGCG TCCTTGGCTATTG	pIDJ002
prIDJ036_cc0284down-F+TGA+NheI	GGCCGGGCTAGCTGATACGCCAG CTGGGGGGC	pIDJ002
prIDJ037_cc0284down-R+EcoRI	GGCCGGGAATTCCACCTTCTCGG CGGTGATCAGAC	pIDJ002
prIDJ043_cPCR_pNPTS138-R	CGACGGCCAGTCCGTAATAC	colony pcr pNPTS138
prIDJ044_cc0284-F+SLICpSRK	CAATTTTCACACAGGAAACAGCATA TGAGCCGGCCAGCGCTCGATGTT C	pIDJ007
prIDJ045_cc0284-R+SLICpSRK	CCGGGTGCAATTTGCTTTCGAATT GCTAGCTCAGGTCAGGGTGTCAA CCAC	pIDJ007, pIDJ050
prIDJ046_cPCR_pSRK-F	GCTCACTCATTAGGCACC	colony pcr pSRK
prIDJ047_cPCR_pSRK-R	GCGGCTATTTAACGACCC	colony pcr pSRK
prIDJ052_cc3015-F+SLICpSRK	CAATTTTCACACAGGAAACAGCATA TGAAGACACTCTCGTCCCTG	pIDJ010
prIDJ053_cc3015-R+SLICpSRK	CCGGGTGCAATTTGCTTTCGAATT GCTAGCTCAGGCGATCTGCGCGA CCAGC	pIDJ010
prIDJ056_cc3015up-F+HindIII	GGCCGGAAGCTTCTCAAGCGCA AGAACCAC	pIDJ005
prIDJ057_cc3015up-R+NheI	GGCCGGGCTAGCGGATCAGAGC TCCAAGGC	pIDJ005
prIDJ058_cc3015down-F+TGA+NheI	GGCCGGGCTAGCTGACGAGCCG GTCTCTGCATC	pIDJ005
prIDJ059_cc3015down-R+EcoRI	GGCCGGGAATTCCCACGACTTCC TCAACGGTGC	pIDJ005
prIDJ069_ccna3110up-R+ATG+2cod+EcoRI	GGCCCGGAATTCTGTCTTCATGG ATCAGAGCTCC	pIDJ015
prIDJ070_ccna3110-F_noATG+EcoRI+3xFLAG+KpnI	GGCCGGGAATTTCGACTACAAAGA CCATGACGGTGATTATAAAGATC ATGATATCGATTACAAGGATGAC GATGACAAAGggtaccAAGACTCTC GTCCCTG	pIDJ015
prIDJ071_ccna3110down-R+NheI	GGCCGGGCTAGCCCGATCCTGAC CCAGGTG	pIDJ015
prIDJ075_egfp-F+EcoRI	GGCCCGGAATTCAGCAAGGGCGA GGAGCTG	pIDJ020

prIDJ076_egfp-R+KpnI	GGCCGGggtaccCTTGTACAGCTCG TCCATGCC	pIDJ020
prIDJ077_check_KOccna028 6-F	CAGCTTGTCTACTTCTTCGG	
prIDJ078_check_KOccna028 6-R	GATCAACCTTGGTGGGTTCG	
prIDJ081_seq_pIDJ005-F	GCAAAAAGGGTCGAAACG	
prIDJ082_seq_pIDJ005-R	GTCCTCAAAAAGTACGCGC	
prIDJ083_3xFLAG_inner-F	CAAGGATGACGATGACAAG	
prIDJ084_3xFLAG_inner-R	CTTGTTCATCGTCATCCTTG	
prIDJ105_cPCR_pMR10-R	CTCTTCGCTATTACGCCAGC	pMR10
prIDJ106_ccna3110up- F+HindIII	GGCCGGAAGCTTCCAGACCTTCA TCTTCTACC	pIDJ028
prIDJ107_ccna3110-R+XbaI	GGCCGGTCTAGATCAGGCGATCT GCGCGACCAGC	pIDJ028
prIDJ110_ccna3110up+Hind III-F	GGCCGGAAGCTTCCTTTGGAAAG AGGACTTGC	pIDJ029
prIDJ111_ccna3110+EcoRI- R	GGCCCGGAATTCGGCGATCTGCG CGACCAGCCCTTC	pIDJ029
prIDJ112_EcoRI-3xFLAG- KpnI-ccna3110down-F	GGCCGGGAATTCGACTACAAAGA CCATGACGGTGATTATAAAGATC ATGATATCGATTACAAGGATGAC GATGACAAAGTGAGGTACCCGAGC CGGTCTCTGCATC	pIDJ029
prIDJ113_ccna3110down- R+NheI	GGCCGGGCTAGCCCTTGGTTTTTC AACGCCATG	pIDJ029
prIDJ114_egfp- F+EcoRI+3gly	GGCCCGGAATTCGGCGGCGGCG TGACCAAGGGCGAGGAGctg	pIDJ030
prIDJ115_egfp- R+KpnI+TAA	GGCCGGGGTACCTTACTTGTACA GCTCGTCCATGC	pIDJ030
prIDJ116_pIDJ030-seq-R	CATTGCCCAACAGGTTAG	
prIDJ117_egfp- R+link+KpnI	GGCCGGGGTACCGCCGCCGCCCT TGTACAGCTCGTCCATGC	pIDJ033
prIDJ118_egfp-F+EcoRI	GGCCCGGAATTCGTGAGCAAGG GCGAGGAGCTG	pIDJ033
prIDJ119_check-ccna3110- D53D-F	GATCGACGCAGCCCTGCTGG	pIDJ034
prIDJ120_ccna3110-D53N-R	CCAGGTTACGTTACAGCAGGGCT GC	pIDJ034
prIDJ121_ccna3110-D53N-F	GCAGCCCTGCTGAACGTGAACCT GG	pIDJ034
prIDJ122_ccna3110- downD53N-R+EcoRI	GGCCGGGAATTCGCCTTTCGGCC GCGTAGAAG	pIDJ034
prIDJ123_check-ccna3110- D53N-F	GATCGACGCAGCCCTGCTGA	pIDJ034
prIDJ129_lovK-up- F+HindIII	GGCCGGAAGCTTGCCTTCCTCGC GCAGGAGGAG	pIDJ040
prIDJ130_lovK-up-R+NheI	GGCCGGGCTAGCGGCTAAGCTCC CACCTCCC	pIDJ040
prIDJ131_lovK-down- F+NheI	GGCCGGGCTAGCCAAGGACGCTT TTGATCATG	pIDJ040
prIDJ132_lovK-down- R+EcoRI	GGCCGGGAATTCAGGTCAGGG TGTCACCAC	pIDJ040
prIDJ133_check-KOlovK-F	GGGCTTGGGCCCTTGAAGCAG	pIDJ040
prIDJ134_check-KOlovK-R	GACGCTTCAACATGAGGATG	pIDJ040
prIDJ135_ccna3110- F+EcoRI	GGCCGGGAATTCATGAAGACT CTCGTCCCTG	pIDJ041

prIDJ136_ccna3110-R+BamHI	GGCCCGGGATCCTCAGGCGATCT GCGCGACCAG	pIDJ041
prIDJ139_pGBD-C1-F-col	GCTAGAAAGACTGGAACAGC	
prIDJ140_pGBD-C1-R-col	GATCAGAGGTTACATGGCC	
prIDJ141_ccna3111-F+NdeI	GCCCGGCATATGTTGAAAGAGG ACTTGCGG	pIDJ043
prIDJ142_ccna3111-R+TGA	GGCCGGGCTAGCTCAGAGCTCCA AGGCGCGCAAAG	pIDJ043
prIDJ143_ccna3111up-F+HindIII	GGCCGGAAGCTTCTGGTTCGTCG ACGAGTACGG	pIDJ044
prIDJ144_ccna3111up-R+NheI	CGGCGGCTAGCAGGCCGCGG CGGATAGACC	pIDJ044
prIDJ145_ccna3111down-F+NheI+TGA	GGCCGGGCTAGCTGATCCATGAA GACACTCTC	pIDJ044
prIDJ146_ccna3111down-R+EcoRI	GGCCCGGAATTCATTGCCCAACA GGTTAGC	pIDJ044
prIDJ163_ccna0287-F+TTG+NdeI	GCCCGGCATATGTTGAAAGACTA TTCGGAATCG	pIDJ050
prIDJ168_pET28a-seq-F	CATACCACGCCGAAACAAGC	pET28a sequencing
prIDJ169_ccna3110noTGA-R+XhoI	GGCCGGCTCGAGGGCGATCTGC GCGACCAG	pIDJ053
prIDJ170_ccna3111-TGA-R+XbaI	GGCCGGTCTAGATCAGAGCTCCA AGGCGCGCAAAG	pIDJ054
prIDJ173_cPCRseq-egfp-R	GACTTGAAGAAGTCGTGCTGCTT C	pGFPC-2
prIDJ174_cPCRseq-pGFPC-2-F	GAAAGGCTCAGTCGAAAGAC	pGFPC-2
prIDJ183_ccna3110-D53E-R	CCAGGTTACCTCCAGCAGGGCT GC	
prIDJ184_ccna3110-D53E-F	GCAGCCCTGCTGGAGGTGAACCT GG	
prIDJ187_plac290_cPCR-F	GAGCTGCGCAAGGACATAATC	
prIDJ188_plac290_cPCR-R	GGCCTCAGGAAGATCGCAC	
prIDJ201_cPCR-seq_pGFPC2-R	GTGGATAACCGTATTACCGCC	
prIDJ202_cPCR-seq_pIDJ067-F	GCTGACCTATGATGTTTCCG	
prIDJ203_ccna2967up-F+NheI	GGCCGGGCTAGCCGCGAACATTC CAGTGATAGCC	pIDJ068
prIDJ204_ccna2967front-R+EcoRI	GGCCCGGAATTCCTTATCAGGCAT AGAGCGTCACCAGC	pIDJ068
prIDJ205_ccna2967back-F+EcoRI	GGCCCGGAATTCGATCATGCCTG GCGGCAAGAG	pIDJ068
prIDJ206_ccna2967down-R+HindIII	GGCCGGAAGCTTGGCAGTTCAAC CTCGACTTC	pIDJ068
prIDJ207_check-KOccna2967-F	CATTCCTCCTGGTACTGCCCTTC	pIDJ068
prIDJ208_check-KOccna2967-R	CCTCGTCCCCGATCTTCTTCG	pIDJ068
prIDJ213_ccna2409up-F+NheI	GGCCGGGCTAGCCCTCACAAGC ATGCGAATG	pIDJ070
prIDJ214_ccna2409front-R+EcoRI	GGCCCGGAATTCCTAGCAAAGCA CCTGAACACGG	pIDJ070
prIDJ215_ccna2409back-F+EcoRI	GGCCCGGAATTCGAGTTCGACCT CCTGATGCTG	pIDJ070

prIDJ216_ccna2409down-R+HindIII	GGCCGGAAGCTTGACTCGACCTT AATCACGTC	pIDJ070
prIDJ217_check-KOccna2409-F	GATCGATGCTCCGACAAAGC	pIDJ070
prIDJ218_check-KOccna2409-R	GATGGTGTCTGAAGAACCGCC	pIDJ070
prIDJ219_ccna2587up-F+NheI	CCGGCCGCTAGCCAAGCACGATG TCCTCTTCG	pIDJ071
prIDJ220_ccna2587up-R+EcoRI	GGCCCGGAATTCGATCGTGGCCG AAAACAGCTAAAATC	pIDJ071
prIDJ221_ccna2587down-F+EcoRI	GGCCCGGAATTCGAAACAGGCCG CGCGCTCAGGGTAAAC	pIDJ071
prIDJ222_ccna2587down-R+HindIII	GGCCGCAAGCTTCTGCGCACGGG CTTTGGCAATGTGG	pIDJ071
prIDJ223_check-KOccna2587-F	CAACGGCGAGATCTACAACG	pIDJ071
prIDJ224_check-KOccna2587-R	GTCGCTCTACAACGAGACCAAC	pIDJ071
prIDJ241_ccna2967-F+NdeI	GCCCCGCATATGGTGTTCGCGCT CTTAGGTAAG	pIDJ076
prIDJ242_ccna2967-R+TGA	GGCCGGGCTAGCCTGAACCGTCA GTGCGGTC	pIDJ076
prIDJ243_cc2501-F+NdeI	GCCCCGCATATGTTGGCCGCGAC GGATGTCTC	pIDJ077
prIDJ244_cc2501-R+TGA	GGGCCCCGCTAGCTCAGGCCGCGT GCGACCTTCC	pIDJ077
prIDJ245_cc2324-F+NdeI	GCCCCGCATATGTTGCTCGCCGA GCGCCGCCAGCAGTG	pIDJ078
prIDJ246_cc2324-R+TGA	GGCCGGGCTAGCCTAGGCGGCG ACCTTGGCGGGATCGGTCCG	pIDJ078
prIDJ247_cc2874noTM-F+BamHI	CCGGCCGATCCGTCGCAGCGGT CGCCGAAG	pIDJ079
prIDJ248_cc2874-R+EcoRI	GGCGGCGAATTCGAAACCGTCAG TGCGGTC	pIDJ079
prIDJ249_cc2501noTM-F+EcoRI	GGCGGCGAATTCCTCGAAACCAT GCACGCAGAG	pIDJ080
prIDJ250_cc2501-R+HindIII	GGCCGCAAGCTTTCAGGCCGCGT GCGACCTTCC	pIDJ080
prIDJ251_cc2324noTM-F+EcoRI	CCGGCCGAATTCCTGCTGATCAT TGCGCCGCTG	pIDJ081
prIDJ252_cc2324-R+HindIII	GGGCCCAAGCTTCTAGGCCGCGA CCTTGGCGGGATC	pIDJ081
prIDJ253_cPCR-seq_H-MBP-F	CGTCAGACTGTCGATGAAG	
prIDJ254_cPCR-seq_H-MBP-R	CTAGTTATGCTCAGCGGTG	
prIDJ255_cc2554-F+EcoRI	GGGCCCCGAATTCGTGGCCGAAGA AACATCGG	pIDJ082
prIDJ256_cc2554-R+HindIII	GGGCCCAAGCTTTCACCCCAGCG GCATGAATG	pIDJ082
prIDJ257_cc2554-F+NdeI	GCCCCGCATATGGTGGCCGAAGA AACATCGG	pIDJ083
prIDJ258_cc2554-R+TGA	GGGCCCAAGCTTTCACCCCAGCG GCATGAATG	pIDJ083
prIDJ259_lovK-R+TAA	GGCCGGGCTAGCTTACTATTGCG TCCCATTGATG	pIDJ084

prIDJ260_cc2554up-F+NheI	GGCCGGGCTAGCGCCATGGCCTC CTCCGAC	pIDJ085
prIDJ261_cc2554up- R+EcoRI	GGCCCCGAATTTCGCCACGTCCCT GCCCGAGAG	pIDJ085
prIDJ262_cc2554down- F+EcoRI	GGCGGGGAATTCTGAGCCTCACC CCGTATCCC	pIDJ085
prIDJ263_cc2554down- R+HindIII	GGCCGGAAGCTTCGCGAGACCTT CGGCTATTC	pIDJ085
prIDJ264_check-KOcc2554- F	CTGGCTGAACTCTTCGACTG	pIDJ085
prIDJ265_check-KOcc2554- R	GTTCCTGGTGCTGGAGGTTAC	pIDJ085
prIDJ266_seq_2874-F	CTACGAGGTCGAGTATCGTC	pIDJ076
prIDJ267_seq_2501-F	GCGATATCACCGAGCGTAAG	pIDJ077
prIDJ268_seq_2324-F	GACGCTGAGCCATGAAATTC	
prIDJ269_seq_2324-R	CAGCAACAGCAGTGTCTCGC	
prIDJ270_seq_2501-F	CATCATCCGCAGCCTTGAAC	
prIDJ277_MrrAnoATG- F+EcoRI	CCGGCCGAATTCAAGACTCTC GTCCCTGAAGG	pIDJ086
prIDJ278_MrrA-TGA- R+HindIII	GGGCCAAGCTTTCAGGCGATCT GCGCGAC	
prIDJ279_CC2554noPAS- F+EcoRI	CGGCCgGAATTCCTGGCGGAGAG CCATCGGC	
prIDJ280_CC2874noPAS- F+EcoRI	CGCGCCGAATTCCTCGAGGCCAAG CTGACCGGC	pIDJ087
prIDJ281_CC2874+TGA- R+HindIII	GGCCGGAAGCTTTCAGTGGGTC GCGCCTGGG	pIDJ087
prIDJ282_CC2874noTMD- F+EcoRI	GGCCGGGAATTCGGGCTGCGCG GCGCCATGCG	pIDJ088
prIDJ285_ccna3110-D53N-F	CGGCCGAGATCAACGCAGCCCTG C	pIDJ090
prIDJ286_ccna3110-D53E-R	GCAGGGCTGCCTCGATCTCGGCC G	pIDJ090
prIDJ287_ccna3110-D53E-F	CGGCCGAGATCGAGGCAGCCCTG C	
prIDJ295_RECofCC2874no ATG-F+BamHI	CGCGCCGGATCCCATATCCGCGC CCAGACGCC	pIDJ089
prIDJ298_cc2330-R+XbaI	GGCCGGTCTAGATCAGGGGGCG TCGTCGTCC	pIDJ094
prIDJ299_MrrA-F+XbaI	GGCCGGTCTAGACAAGACTCT CGTCCCTGAAGG	pIDJ094
prIDJ302_CC2330-F+XbaI	GGCCGCTCTAGACAACGATCGAC CCGCAGCCG	pIDJ097, 99, 101, 103
prIDJ303_CC2330-R+KpnI	GCGGCCGGTACCAAGGGGGCGT CGTCGTCCACCATG	pIDJ097, 103
prIDJ304_CC2330- R+TGA+KpnI	GCGGCCGGTACCAATCAGGGGG CGTCGTCTGTC	pIDJ099, 101
prIDJ305_CC1974-F+XbaI	GGCCGGTCTAGACTCCTCCTCCG ATAAGATCCC	pIDJ098, 100, 102, 104
prIDJ306_CC1974-R+KpnI	GGCCGCGGTACCAACAAATCCAG ATCCGCCGACG	pIDJ098, 104
prIDJ307_1974- R+TGA+KpnI	GGCCGCGGTACCAACTACAAATC CAGATCCGCCGACG	pIDJ0100, 102
prIDJ308_DgcB-F+XbaI	GGCCGGTCTAGACTCGGACGTCG AAACCACGCTG	pIDJ105, 106, 107, 108
prIDJ309_DgcB-R+KpnI	GGGCGCGGTACCAAGTTGGCGG CGCCGGGCATGGACTC	pIDJ105, pIDJ108

prIDJ310_DgcB-R+TGA+KpnI	GGGCGCGGTACCAATCAGTTGGC GGCGCCGGGCATGGACTC	pIDJ106, pIDJ107
prIDJ311_CC1056-F+XbaI	GGCCGGTCTAGACACTCAGCATC GCACTTGGCG	pIDJ109, 110, 111, 112
prIDJ312_CC1056-R+KpnI	GGGCGCGGTACCAACGTCGCGG GCTTGGCCAGCTC	pIDJ109, pIDJ112
prIDJ313_CC1056-R+TGA+KpnI	GGGCGCGGTACCAATCACGTCGC GGGCTTGGCCAGCTC	pIDJ110, pIDJ111
prIDJ314_CC1974-seq-F	GAGCACCTCCAGGTGTTCTC	pIDJ113, 114, 115, 116
prIDJ315_ParE-seq-F	CAGCTGAAGGAGACCACCATG	pIDJ113, pIDJ116
prIDJ316_DgcB-seq-F	GAGGAGTTCGCGATGATCTTC	pIDJ114, pIDJ115
prIDJ317_CC1056-seq-F	CCTCTATTTACCGCCTTCG	
prIDJ318_CC1056-seq-R	GTTGGCGATATTGGCGGCGTAC	
prIDJ319_CC1056-seq-R2	CITGGCGATCTCGCTGGACTTC	
prIDJ320_ChpT-F+XbaI	GGCGCCTCTAGACACCGAGACCG TCACCGAGACCACC	
prIDJ321_ChpT-R+KpnI	GGGCGCGGTACCAACGCCGGGA CCCAGGCGGCGATC	
prIDJ322_PhyR-F+XbaI	GGCGCCTCTAGACAGTCTTCTTGC TCGCTTGGC	
prIDJ323_PhyR-R+KpnI	GGGCGCGGTACCAAGGCCGCCTT AGCGGTGCGGC	pIDJ117-118- 119-120
prIDJ324_PhyR-F+NdeI	GCCCGGCATATGATGAGTCTTCT TGCTCGCTTGGC	pIDJ117-118- 119-120
prIDJ325_PhyR+TGA-R+NheI	GGCCGGGCTAGCTCAGGCCGCCT TAGCGGTG	pIDJ121-122- 123-124
prIDJ326_PhyRnoATG-F+BamHI	CGCGCCGGATCCAGTCTTCTTGCT CGCTTGGC	pIDJ121-122- 123-124
prIDJ327_PhyR+TGA-R+HindIII	GGGCCCAAGCTTCAGGCCGCCTT AGCGGTG	pIDJ125
prIDJ328_pUC18C-seq-F	GTCTTCTACGAGAACCGTGC	pIDJ125
prIDJ329_LovKnoTTG-F+BamHI	CGCGCCGGATCCGAAGACTATTC GGAATCGCG	pIDJ126
prIDJ330_LovK+TGA-R+HindIII	GGGCCCAAGCTTCTATTGCGTCC CATTGATGG	pIDJ126
prIDJ331_LovRnoATG-F+BamHI	CGGCCCGGATCCAGCCGGCCAGC GCTCGATGTTT	
prIDJ332_LovR+TGA-R+HindIII	GGGCCCAAGCTTTCAGGTCAGGG TGTCAACCAC	pIDJ127
prIDJ333_PhyKnoATG-F+EcoRI	CGCGCCGAATTCACCGTCTTTACC GGCCGC	pIDJ127
prIDJ334_PhyK+TGA-R+HindIII	GGGCCCAAGCTTTCAGCCAGCGG CGCTCAGCGC	pIDJ128
prIDJ335_PhyK-template-R	CGCCTTCGACCGTGTTCAG	pIDJ128
prIDJ336_PhyK-template-F	GAAATCTGTAATTGCGCCGTC	
prIDJ337_PhyKup-F+NheI	GGCCGGGCTAGCCCCGACCTTCG CGCTTTTGC	pIDJ130
prIDJ338_PhyKup-R+EcoRI	GGCCCGGAATTCGGTCACCGCAA GGCGCTCAATC	pIDJ130
prIDJ339_PhyKdown-F+EcoRI	GGCCGGGAATTCATCCGGAAC CGCGCTTCG	pIDJ130
prIDJ340_PhyKdown-R+HindIII	GGCCGGGAAGCTTCATTCGTCAGA TGGTGCCTG	pIDJ130

prIDJ341_check-KOphyK-F	GACGAGGTCGTCAACGAGCC	pIDJ130
prIDJ342_check-KOphyK-R	GATCCGCATGCTGATCAAG	pIDJ130
prIDJ343_seq_lacZ-plasmids-R	GCACCACAGATGAAACGCC	
prIDJ344_seq_lacZ-plasmids-F	GCCTTCCGGTTCATTCCTG	
prIDJ345_int-lacZ-R-atClaI	CACGCTCATCGATAATTTCCACCGC	
prIDJ346_NepRnoATG-F+EcoRI	CCGCGGGAATTCAACTTCGGCGT CGAGGACATG	pIDJ132
prIDJ347_NepR-TGA-R+HindIII	GGGCCCAAGCTTCTACTCGCCCCC CGCCGGAC	pIDJ132

Table 2: Plasmids used in this study

NAME	VECTOR	RELEVANT INFORMATION	REFERENCE
pNPTS138	pNPTS129	Suicide vector containing <i>sacB</i> and <i>nptII</i> , <i>kan^r</i>	[38][290]
pSRK-kan	pBBR1MCS-2	broad-host-range expression vector containing <i>lac</i> promoter and <i>lacI^q</i> , <i>lacZα⁺</i> , and <i>kan^r</i>	[291]
pRKlac290	pK2	for transcriptional fusions to <i>lacZ</i>	[292]
pRKlac290-P _{<i>sigU</i>}	pRKlac290	pP _{<i>sigU</i>} - <i>lacZ</i> , <i>tet^r</i>	[202]
pSGL1		pP _{<i>drA</i>} - <i>lacZ</i> , <i>tet^r</i>	[178]
pMR10		Low copy vector, <i>kan^r</i>	[252]
pBBR		Broad-host-range vector, <i>kan^r</i>	[293]
pGBD-C1		For yeast two-hybrid screening, GAL4BD, <i>trp1</i> , <i>amp^r</i>	[284]
pGBD-C1-kan	pGBD-C1	For yeast two-hybrid screening, GAL4BD, <i>trp1</i> , <i>kan^r</i>	
pGAD-C1		For yeast two-hybrid screening, GAL4AD, <i>leu2</i> , <i>amp^r</i>	[284]
pET28a		Expression vector	Novagen
pET-His ₆ -MBP	pET28a	Expression vector to express N-terminal His ₆ -MBP fusion proteins	[49]
pUT18	pUC19	For bacterial two-hybrid, <i>amp^r</i>	[289]
pUT18C	pUC19	For bacterial two-hybrid, <i>amp^r</i>	[289]
pKT25	pSU40	For bacterial two-hybrid, <i>kan^r</i>	[289]
pKNT25	pSU40	For bacterial two-hybrid, <i>amp^r</i>	[289]
pT18- <i>zip</i>	pT18	Positive control for bacterial two-hybrid, <i>amp^r</i>	[289]
pT25- <i>zip</i>	pT25	Positive control for bacterial two-hybrid, <i>amp^r</i>	[289]
pIDJ002	pNPTS138	clean knock-out of <i>lovR</i> , <i>kan^r</i>	This study
pIDJ005	pNPTS138	clean knock-out of <i>mrrA</i> , <i>kan^r</i>	This study
pIDJ007	pSRK-kan	pP _{<i>lac</i>} - <i>lovR</i> , <i>kan^r</i>	This study
pIDJ010	pSRK-kan	pP _{<i>lac</i>} - <i>mrrA</i> , <i>kan^r</i>	This study
pIDJ015	pNPTS138	3xFLAG- <i>mrrA</i> , <i>kan^r</i>	This study
pIDJ020	pNPTS138	<i>egfp</i> - <i>mrrA</i> , <i>kan^r</i>	This study
pIDJ028	pMR10	pP _{<i>mrrA</i>} - <i>mrrA</i>	This study
pIDJ029	pNPTS138	<i>mrrA</i> -3xFLAG, <i>kan^r</i>	This study
pIDJ030	pNPTS138	<i>mrrA</i> -linker-3xFLAG, <i>kan^r</i>	This study
pIDJ033	pNPTS138	3xFLAG-linker- <i>mrrA</i> , <i>kan^r</i>	This study
pIDJ034	pNPTS138	<i>mrrA</i> ^{D53N} , <i>kan^r</i>	This study

pIDJ038	pSRK-kan	pP _{lac-mrrA} ^{D53N} , kan ^r	This study
pIDJ040	pNPTS138	clean knock-out of <i>lovK</i> , kan ^r	This study
pIDJ041	pGBD-C1	Gal4DB- <i>mrrA</i>	This study
pIDJ043	pSRK-kan	pP _{lac-CCNA03111} , kan ^r	This study
pIDJ044	pSRK-kan	pP _{lac-CCNA03111-mrrA} , kan ^r	This study
pIDJ045	pNPTS138	clean knock-out of CCNA03111, kan ^r	This study
pIDJ046	pNPTS138	clean double knock-out of CCNA03111- <i>mrrA</i> , kan ^r	This study
pIDJ050	pSRK-kan	pP _{lac-lovRK} , kan ^r	This study
pIDJ053	pET28a	Production of <i>mrrA</i> -His ₆	This study
pIDJ054	pMR10	pP _{CCNA03111-CCNA03111} , kan ^r	This study
pIDJ060	pNPTS138	<i>mrrA</i> ^{D53E} , kan ^r	This study
pIDJ061	pSRK-kan	pP _{lac-mrrA} ^{D53E} , kan ^r	This study
pIDJ068	pNPTS138	knock-out of <i>CC2874</i> , kan ^r	This study
pIDJ070	pNPTS138	knock-out of <i>CC2324</i> , kan ^r	This study
pIDJ071	pNPTS138	clean knock-out of <i>CC2501</i> , kan ^r	This study
pIDJ076	pSRK-kan	pP _{lac-CC2874} , kan ^r	This study
pIDJ077	pSRK-kan	pP _{lac-CC2501} , kan ^r	This study
pIDJ078	pSRK-kan	pP _{lac-CC2324} , kan ^r	This study
pIDJ079	pET-His6-MBP	Production of His ₆ -MBP-CC2874 ^{noTM} , kan ^r	This study
pIDJ080	pET-His6-MBP	Production of His ₆ -MBP-CC2501 ^{noTM} , kan ^r	This study
pIDJ081	pET-His6-MBP	Production of His ₆ -MBP-CC2324 ^{noTM} , kan ^r	This study
pIDJ082	pET-His6-MBP	Production of His ₆ -MBP-CC2554, kan ^r	This study
pIDJ083	pSRK-kan	pP _{lac-CC2554} , kan ^r	This study
pIDJ084	pSRK-kan	pP _{lac-lovK} , kan ^r	This study
pIDJ085	pNPTS138	knock-out of <i>CC2554</i> , kan ^r	This study
pIDJ087	pET-His6-MBP	Production of His ₆ -MBP-MrrA ^{D53N} , kan ^r	This study
pIDJ088	pET-His6-MBP	Production of His ₆ -MBP-CC2554 ^{noPAS} , kan ^r	This study
pIDJ090	pET-His6-MBP	Production of His ₆ -MBP-CC2874 ^{noTMnoREC} , kan ^r	This study
pIDJ094	pET-His6-MBP	Production of His ₆ -MBP-CC2874 ^{onlyREC} , kan ^r	This study
pIDJ095	pET-His6-MBP	Production of His ₆ -MBP-MrrA ^{D53E} , kan ^r	This study
pIDJ097	pUT18	T18_MrrA-CyaA, amp ^r	This study
pIDJ098	pUT18	T18_CC2330-CyaA, amp ^r	This study
pIDJ099	pUT18C	T18_CyaA-MrrA, amp ^r	This study
pIDJ100	pUT18C	T18_CyaA-CC2330, amp ^r	This study
pIDJ101	pKT25	T25_CyaA-MrrA, kan ^r	This study
pIDJ102	pKT25	T25_CyaA-CC2330, kan ^r	This study
pIDJ103	pKNT25	T25_MrrA-CyaA, kan ^r	This study
pIDJ104	pKNT25	T25_CC2330-CyaA, kan ^r	This study
pIDJ105	pUT18	T18_ParE-CyaA, amp ^r	This study
pIDJ106	pUT18C	T18_CyaA-ParE, amp ^r	This study
pIDJ107	pKT25	T25_CyaA-ParE, kan ^r	This study
pIDJ108	pKNT25	T25_ParE-CyaA, kan ^r	This study
pIDJ109	pUT18	T18_DgcB-CyaA, amp ^r	This study
pIDJ110	pUT18C	T18_CyaA-DgcB, amp ^r	This study
pIDJ111	pKT25	T25_CyaA-DgcB, kan ^r	This study
pIDJ112	pKNT25	T25_DgcB-CyaA, kan ^r	This study
pIDJ113	pUT18	T18_CC1056-CyaA, amp ^r	This study

pIDJ114	pUT18C	T18_CyaA-CC1056, amp ^r	This study
pIDJ115	pKT25	T25_CyaA-CC1056, kan ^r	This study
pIDJ116	pKNT25	T25_CC1056-CyaA, kan ^r	This study
pIDJ117	pUT18	T18_ChpT-CyaA, amp ^r	This study
pIDJ118	pUT18C	T18_CyaA-ChpT, amp ^r	This study
pIDJ119	pKT25	T25_CyaA-ChpT, kan ^r	This study
pIDJ120	pKNT25	T25_ChpT-CyaA, kan ^r	This study
pIDJ121	pUT18	T18_PhyR-CyaA, amp ^r	This study
pIDJ122	pUT18C	T18_CyaA-PhyR, amp ^r	This study
pIDJ123	pKT25	T25_CyaA-PhyR, kan ^r	This study
pIDJ124	pKNT25	T25_PhyR-CyaA, kan ^r	This study
pIDJ125	pSRK-kan	pP _{lac} -phyR, kan ^r	This study
pIDJ126	pET-His6-MBP	Production of His ₆ -MBP-PhyR, kan ^r	This study
pIDJ127	pET-His6-MBP	Production of His ₆ -MBP-LovK, kan ^r	This study
pIDJ128	pET-His6-MBP	Production of His ₆ -MBP-LovR, kan ^r	This study
pIDJ129	pET-His6-MBP	Production of His ₆ -MBP-PhyK, kan ^r	This study
pIDJ130	pNPTS138	Knock-out of <i>phyK</i> , kan ^r	This study
pIDJ131	pET28a	Production of His ₆ -PhyR, kan ^r	This study
pIDJ132		NepR	This study

Table 3: Strains used in this study

NAME	RELEVANT GENETIC CONTENT	REFERENCE
<i>S. cerevisiae</i>		
UJ5292	PJ69-4A, MATa <i>trp1-901 leu2-3,112 ura3-52 his3-200 gal4Δ gal80Δ LYS2::GAL1-HIS3 GAL2-ADE2 met2::GAL7-lacZ</i>	[284]
<i>E. coli</i>		
UJ2710	DH5α, Δ(<i>lacZYA-argF</i>) U169 <i>deoR recA1 endA1 hsdR17 phoA sup144 thi-1 gyrA96 relA1 (ϕ80 lacZDM15)</i>	[248]
UJ257	S17-1, F ⁻ <i>lambda(-)</i> <i>thi pro recA hsdR-hsdM⁺</i> RP4 derivative	[249]
UJ6697	BL21 DE3, <i>fbuA2 [lon] ompT gal (λ DE3) [dcm] ΔhsdS λ DE3 = λ sBamHI ΔEcoRI-B int::(lacI::PlacUV5::T7 gene1) i21 Δnin5</i> , for protein expression	NEB
AB1768	MG1655 <i>cyaA::frrt</i> , for bacterial two-hybrid analysis	[73]
<i>C. crescentus</i>		
UJ5511	NA1000 <i>hfs+</i> (<i>hfsA</i> restored)	Elvira Friedrich
UJ6390	NA1000 <i>hfs+</i> Δ <i>mrrA</i>	This study
UJ6308	NA1000 <i>hfs+</i> Δ <i>lovR</i>	This study
UJ8020	NA1000 <i>hfs+</i> Δ <i>lovR</i> , Δ <i>mrrA</i>	This study
UJ6758	NA1000 <i>hfs+</i> Δ <i>lovK</i>	This study
UJ6890	NA1000 <i>hfs+</i> Δ <i>lovK</i> , Δ <i>mrrA</i>	This study
UJ7911	NA1000 <i>hfs+</i> Δ <i>CC2324</i>	This study

UJ7912	NA1000 hfs+ Δ CC2324, Δ mrrA	This study
UJ7913	NA1000 hfs+ Δ CC2501	This study
UJ7914	NA1000 hfs+ Δ CC2501, Δ mrrA	This study
UJ8078	NA1000 hfs+ Δ CC2554	This study
UJ8079	NA1000 hfs+ Δ CC2554, Δ mrrA	This study
UJ8102	NA1000 hfs+ Δ CC2874	This study
UJ8102	NA1000 hfs+ Δ CC2874, Δ mrrA	This study
UJ8548	NA1000 hfs+ Δ CC2324, Δ CC2501, Δ CC2554, Δ CC2874	This study
UJ8549	NA1000 hfs+ Δ CC2324, Δ CC2501, Δ CC2554, Δ CC2874, Δ mrrA	This study
UJ5934	NA1000 hfs+ Δ CC0091, Δ CC0655, Δ CC0740, Δ CC0857, Δ CC0896, Δ CC1086, Δ CC1850, Δ CC2462, Δ CC3094, Δ CC3148, Δ CC3285, Δ CC3396	Elvira Friedrich
UJ6630	NA1000 hfs+ Δ CC0091, Δ CC0655, Δ CC0740, Δ CC0857, Δ CC0896, Δ CC1086, Δ CC1850, Δ CC2462, Δ CC3094, Δ CC3148, Δ CC3285, Δ CC3396, Δ mrrA	This study
UJ7218	NA1000 hfs+ pSRK-kan, kan ^r	This study
UJ6728	NA1000 hfs+ Δ mrrA pSRK-kan, kan ^r	This study
UJ8097	NA1000 hfs+ pIDJ076, kan ^r	This study
UJ8098	NA1000 hfs+ Δ mrrA pIDJ076, kan ^r	This study
UJ8099	NA1000 hfs+ pIDJ077, kan ^r	This study
UJ8100	NA1000 hfs+ Δ mrrA pIDJ077, kan ^r	This study
UJ8182	NA1000 hfs+ pIDJ078, kan ^r	This study
UJ8193	NA1000 hfs+ Δ mrrA pIDJ078, kan ^r	This study
UJ8191	NA1000 hfs+ pIDJ083, kan ^r	This study
UJ8192	NA1000 hfs+ Δ mrrA pIDJ083, kan ^r	This study
UJ7127	NA1000 hfs+ pP _{sigU-lacZ} , tet ^r	This study
UJ7126	NA1000 hfs+ Δ mrrA, pP _{sigU-lacZ} , tet ^r	This study
UJ8957	NA1000 hfs+ Δ lovR, pP _{sigU-lacZ} , tet ^r	This study
UJ8958	NA1000 hfs+ Δ lovR, Δ mrrA, pP _{sigU-lacZ} , tet ^r	This study
UJ8816	NA1000 hfs+ Δ lovK, pP _{sigU-lacZ} , tet ^r	This study
UJ8817	NA1000 hfs+ Δ lovK, Δ mrrA, pP _{sigU-lacZ} , tet ^r	This study
UJ8688	NA1000 hfs+ pP _{ctrA-lacZ} , tet ^r	This study
UJ8689	NA1000 hfs+ Δ mrrA, pP _{ctrA-lacZ} , tet ^r	This study
NA1000	Holdfast mutant derivative of wild type CB15	[246]
UJ5760	NA1000 Δ CC0164	This study
UJ8172	NA1000 Δ mrrA, Δ CC0164	This study
SoA05	CB15 wild type	[35]
UJ7096	CB15 Δ mrrA	This study
UJ7014	CB15 Δ sigT	[203]
UJ7081	CB15 Δ sigT, Δ mrrA	This study
UJ8722	CB15 Δ lovK	This study
UJ8723	CB15 Δ lovK, Δ mrrA	This study
UJ8724	CB15 Δ lovK, Δ sigT	This study
UJ8725	CB15 Δ sigT, Δ lovK, Δ mrrA	This study
FC375	CB15 xyl::pMT585-lovR, kan ^r	[211]
FC437	CB15 van::pMT528-lovK, spec ^r ,strep ^r	[211]
FC438	CB15 xyl::pMT585-lovR van::pMT528-lovK, kan ^r spec ^r ,strep ^r	[211]
FC423	CB15 xyl::pMT585 van::pMT528, kan ^r , spec ^r ,strep ^r	[211]
UJ7285	CB15 pP _{sigU-lacZ} , tet ^r	This study
UJ7288	CB15 Δ mrrA, pP _{sigU-lacZ} , tet ^r	This study
UJ7124	CB15 Δ sigT, pP _{sigU-lacZ} , tet ^r	This study

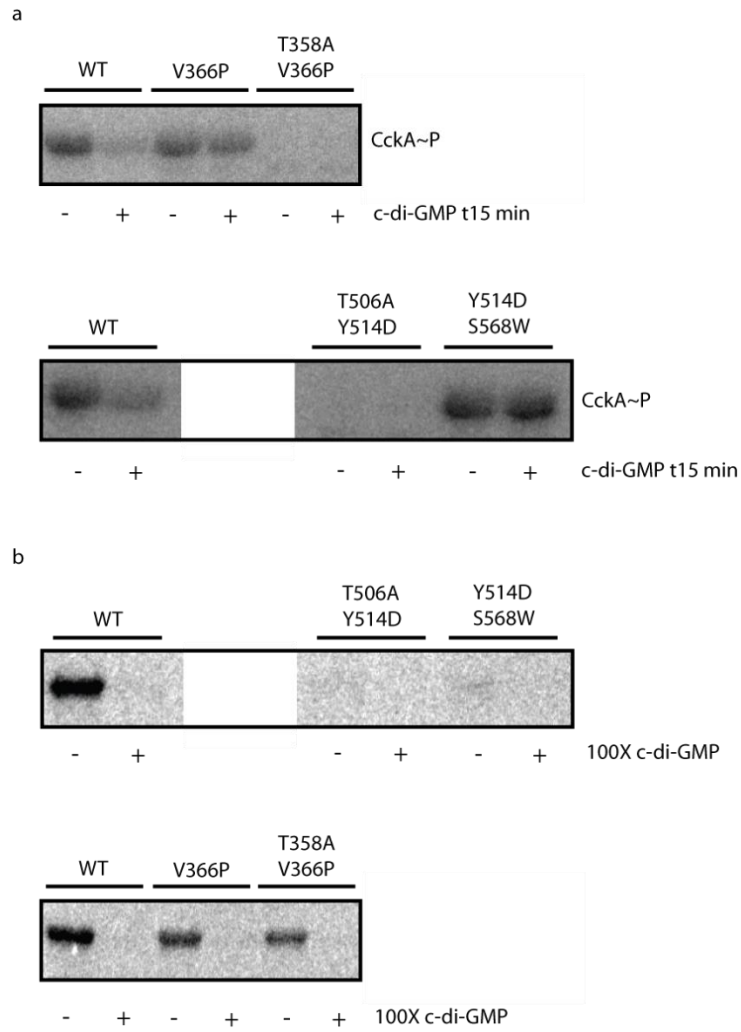
UJ7125	CB15 $\Delta sigT$, $\Delta mrrA$, pP _{sigU} -lacZ, tet ^r	This study
UJ8726	CB15 pP _{drA} -lacZ, tet ^r	This study
UJ8727	CB15 $\Delta mrrA$, pP _{drA} -lacZ, tet ^r	This study
UJ8696	CB15 $\Delta sigT$, pP _{drA} -lacZ, tet ^r	This study
UJ8697	CB15 $\Delta sigT$, $\Delta mrrA$, pP _{drA} -lacZ, tet ^r	This study

Recombinant DNA techniques and oligonucleotide procedures for DNA purification, restriction, ligation, agarose gel electrophoresis and transformation of *E. coli* were carried out as described before in [294]. Restriction enzymes were obtained from New England Biolabs (NEB) and all PCR were performed with Phusion (NEB). Oligonucleotides were purchased from Sigma-Aldrich Chemie. All constructs were sequence verified. *C. crescentus* and *E. coli* S17-1 were used for bi-parental conjugation as described before [235].

Additional results

CckA suppressor screen

In order to gain further insight into the CckA regulation mechanisms, a CckA suppressor screen was set up (done by Shogo Ozaki). The screening strain contained low levels of DivK and a single chromosomal copy of CckA V366P or CckA Y514D. Additionally, CpdR was deleted to prevent CtrA from degradation and therefore the strain completely relies on CtrA phosphorylation to be viable. This strain presumably has very high CtrA phosphorylation levels and therefore grows poorly. Suppressors easily arise and can be selected for when cells are grown in liquid culture. The DNA of the suppressors was isolated and the most likely targets to acquire a mutation were sequenced, namely, CckA, CtrA and DivL. Mutations were observed in all of the mentioned proteins, and the CckA suppressors were subsequently tested *in vitro* (Additional Data Figure 1). Interestingly, the suppressor mutations isolated for CckA V366P and Y514D were found within the same domain. CckA T358A/V366P shows no detectable autophosphorylation *in vitro* although this suppressor restores the growth defect. Similarly, CckA T506A/Y514D showed no autophosphorylation. Therefore, it seems that as long as CckA activity is not counterbalanced by its phosphatase activity the cells only require very little kinase activity. This is in contrast to the CckA Y514D/S568W suppressor. This allele showed autophosphorylation levels comparable to wildtype CckA. It is not clear how this suppressor restores the growth defect. The suppressor mutation is close to the receiver domain. Thus, it is conceivable that the phosphotransfer between the histidine in the DHP and the aspartate in the receiver domain is compromised and therefore results in lower levels of phosphorylated CtrA. Further investigations could aim at looking at the phosphotransfer between CckA and ChpT. In addition, the screen was certainly not saturated and presumably more suppressor mutations could be identified in a saturated screen and tested regarding their kinase activity.

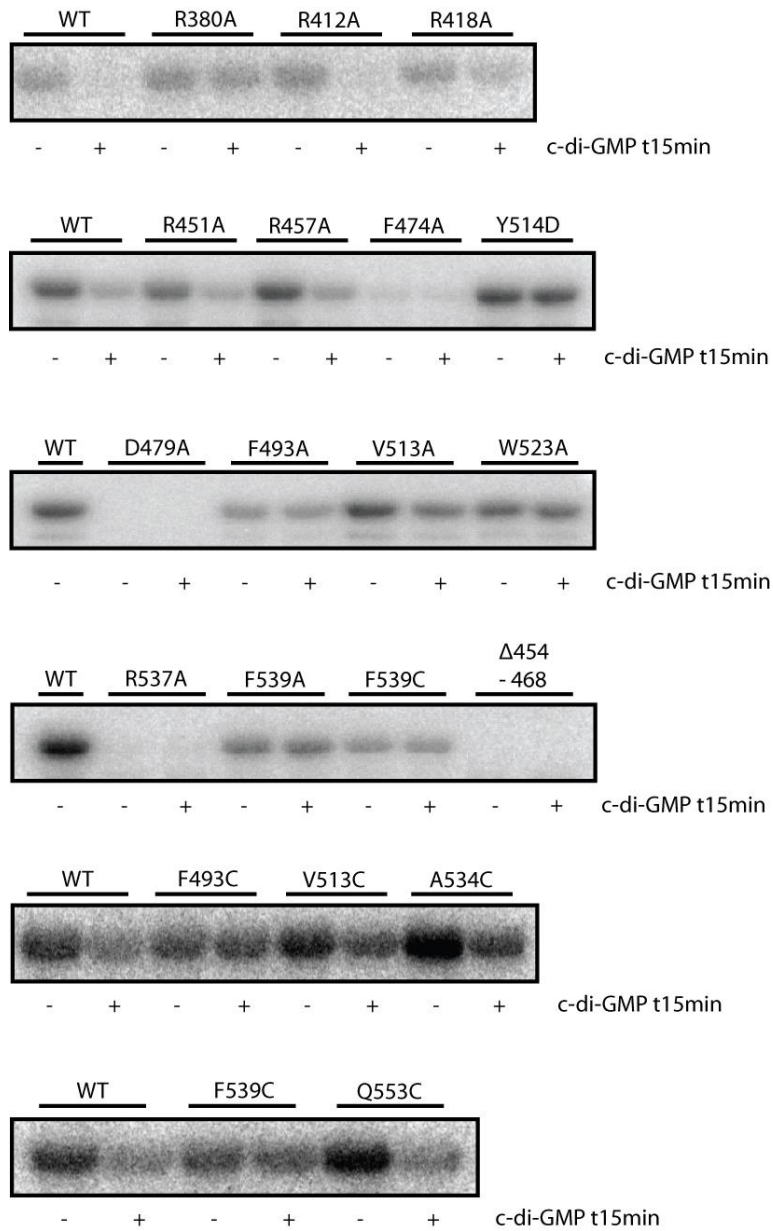


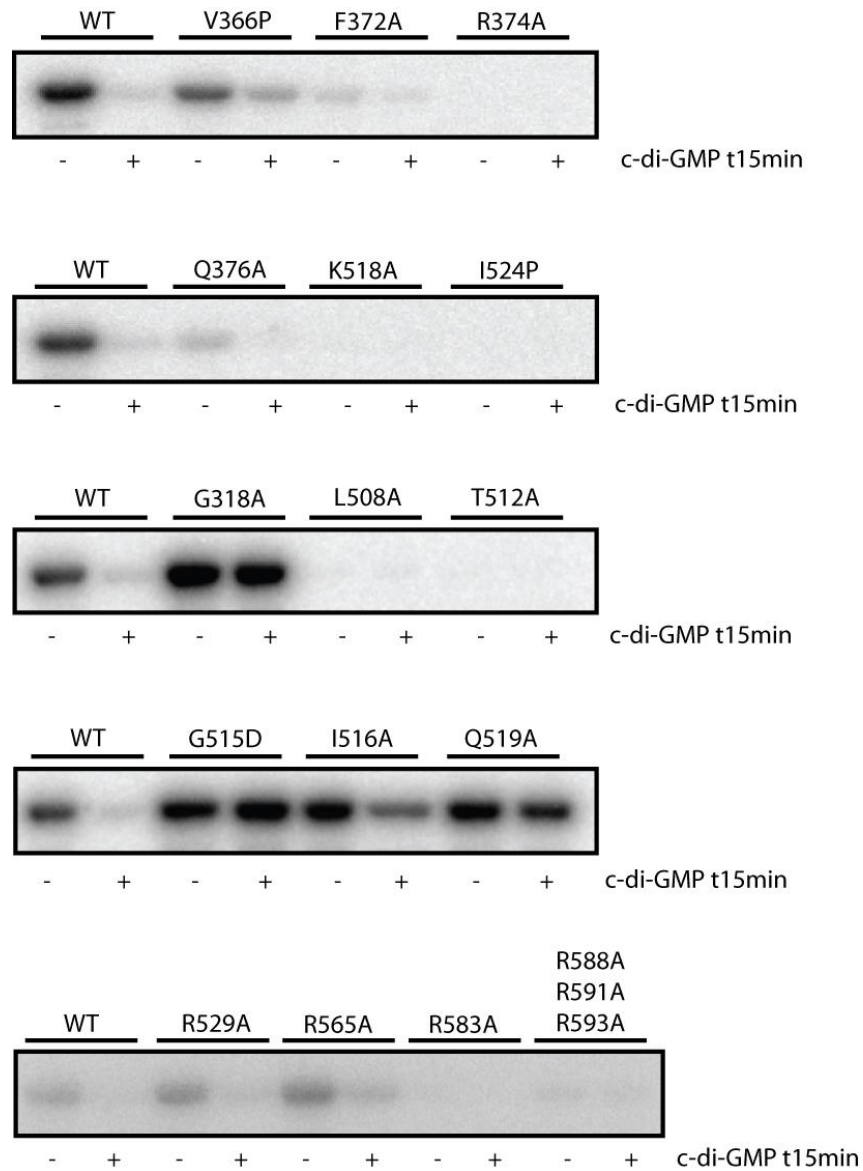
Additional Data Figure 1: Characterization of CckA suppressors.

(a) *In vitro* phosphorylation of CckA and derivatives. When indicated, c-di-GMP was added after 15 minutes of auto-phosphorylation and reactions were incubated for another 15 minutes. **(b)** Purified CckA protein was incubated with [³³P]c-di-GMP and cross-linked with UV light in the presence or absence of a 100-fold excess of competing non-labelled c-di-GMP as indicated.

Additional CckA mutants

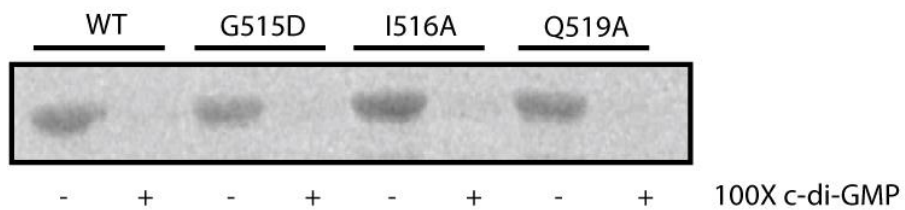
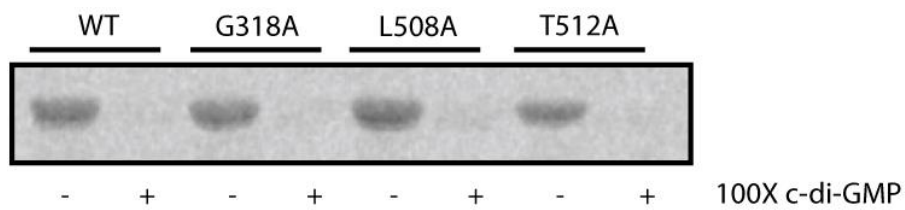
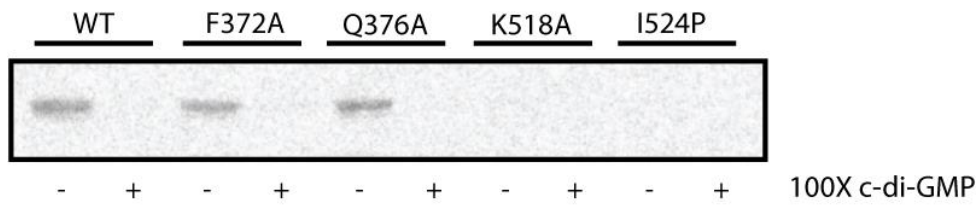
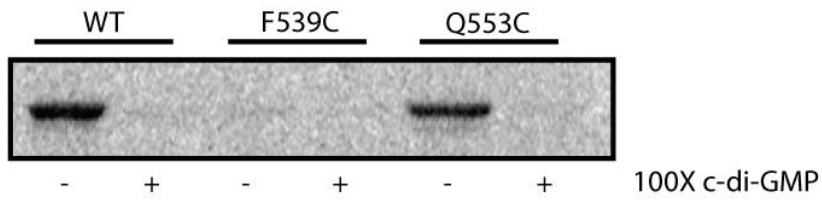
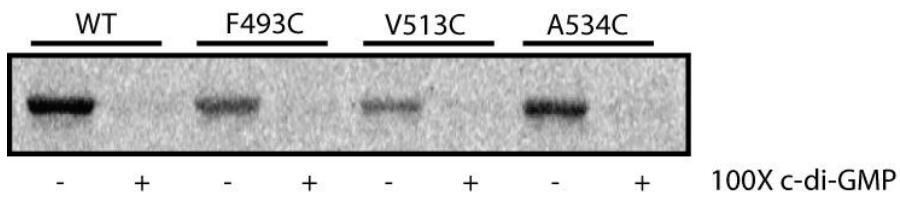
In the course of this thesis many CckA alleles were cloned, purified and tested for *in vitro* phosphorylation activity and c-di-GMP binding. These data were only partially used for publications. Therefore, in this section, the remaining data are presented.

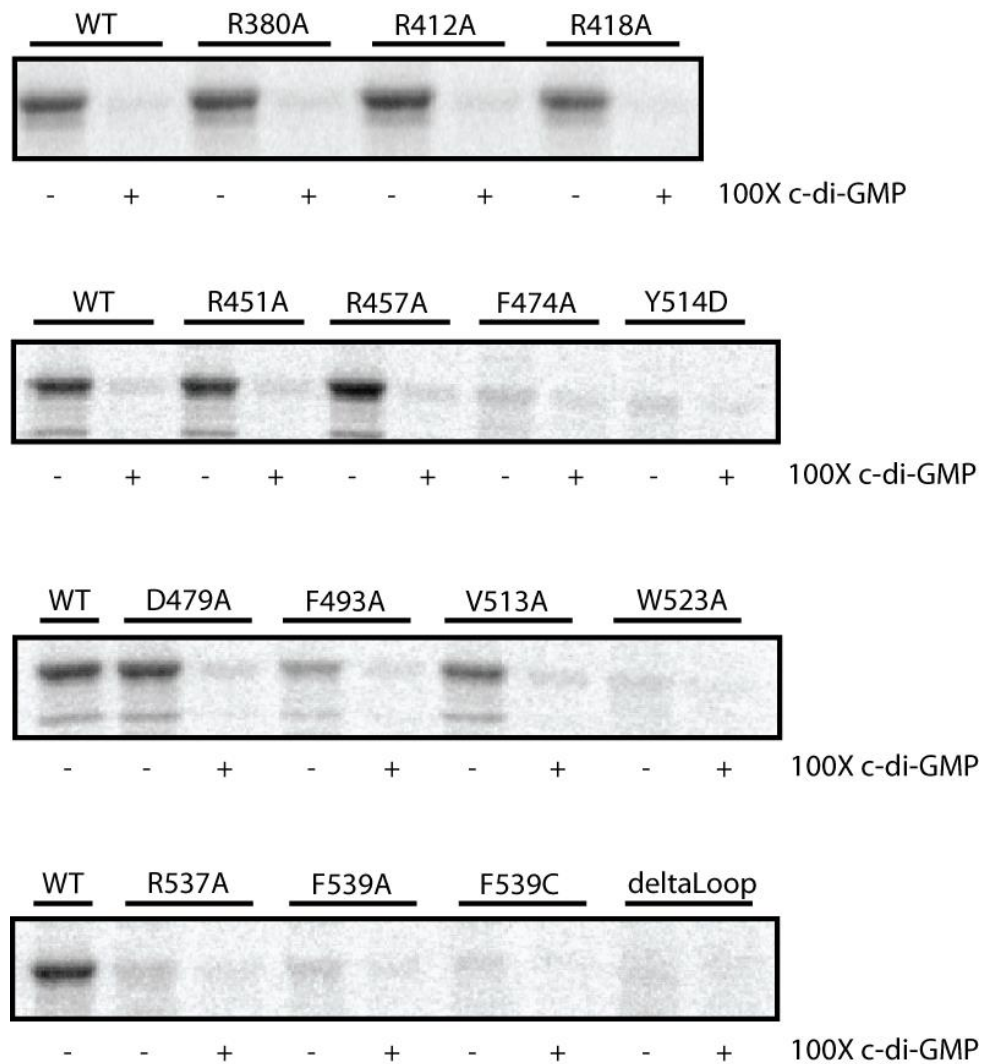




Additional Data Figure 2: *In vitro* activity of CckA mutants.

In vitro phosphorylation of CckA and derivatives. When indicated, c-di-GMP was added after 15 minutes of auto-phosphorylation and reactions were incubated for another 15 minutes.





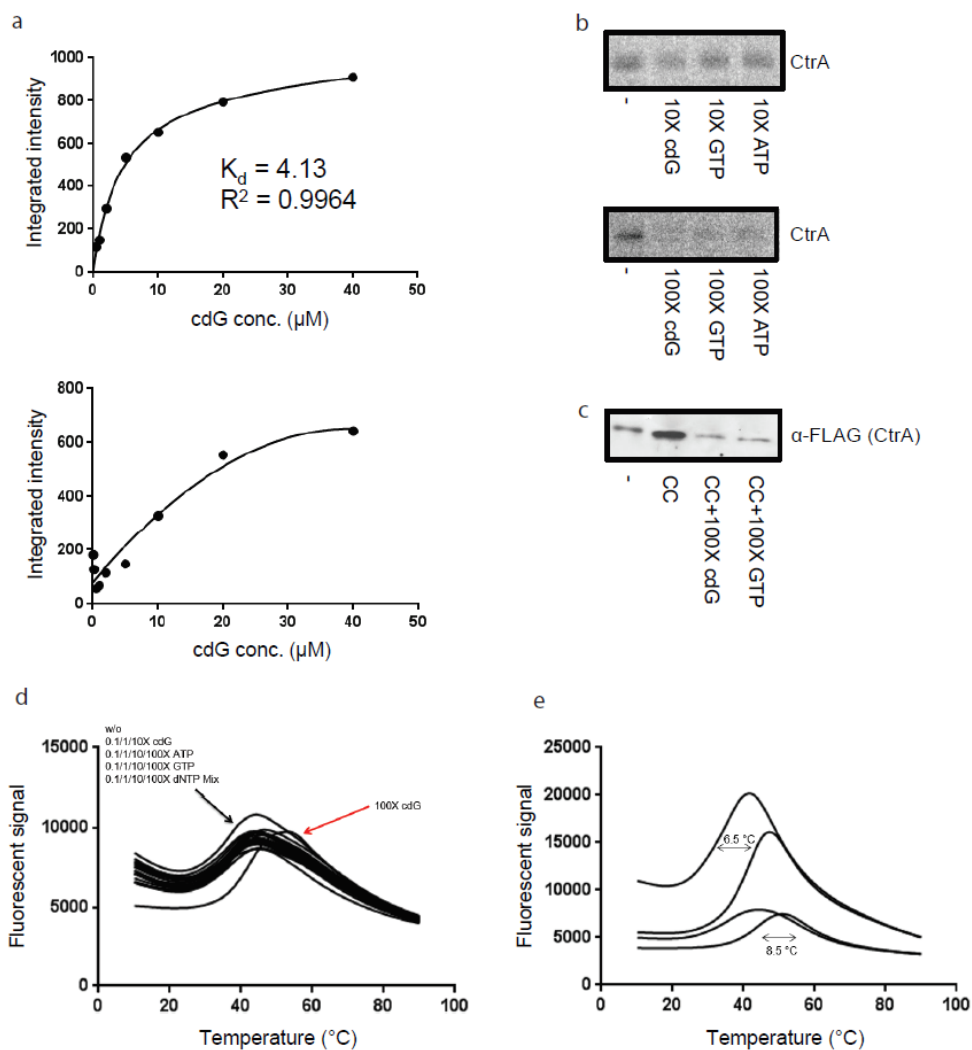
Additional Data Figure 4: C-di-GMP binding of CckA mutants.

Purified CckA protein was incubated with [³³P]c-di-GMP and cross-linked with UV light in the presence or absence of a 100-fold excess of competing non-labelled c-di-GMP as indicated.

CtrA-c-di-GMP interaction

In the previous chapters, it was described how c-di-GMP controls *C. crescentus* cell cycle by interfering with CtrA degradation and phosphorylation. In addition, it was suggested that CtrA might directly bind c-di-GMP. This observation was initiated by a screen which was performed in a c-di-GMP free strain. This strain has several phenotypes [38]. Lack of c-di-GMP causes an attachment defect, a motility defect and potentially also affects replication and cell division. The screen aimed to find spontaneous mutations that restore motility on swarm agar plates in a c-di-GMP free strain. Surprisingly, all isolated mutations are within the Helix-turn-Helix domain of CtrA (Sören Abel, unpublished). One mutation is known as SokA (suppressor of cold sensitive DivK). This mutation was isolated as a suppressor of an over-activated CtrA phosphorylation pathway indicating that a c-di-GMP free strain also suffers from over-activated CtrA. Before we discovered the c-di-GMP-dependent CckA regulation, we focused on the binding of c-di-GMP to CtrA. Sören Abel initiated this project and I continued the trials to prove a direct CtrA-c-di-GMP interaction.

C-di-GMP-binding of CtrA was assessed by several different methods. First, UV crosslink of ³³P-labelled c-di-GMP was tested (Additional Data Figure 4a). Unfortunately, it was not possible to reproduce a saturating binding curve to determine K_d values for c-di-GMP. To determine if the residual binding is specific, competition with non-labelled nucleotides was tested. Ten-fold excess of c-di-GMP, GTP or ATP over [³³P]c-di-GMP only mildly reduced binding. In contrast, 100X excess resulted in strong reduction of binding independent of the competing nucleotide (Additional Data Figure 4b). These experiments did not allow a satisfying conclusion and therefore, further assays were applied. CtrA could be pulled down using the capture compound but the competition control confirms the non-specific nature of the c-di-GMP interaction (Additional Data Figure 4c). Another assay used to test c-di-GMP-binding was differential scanning fluorimetry (DSF). This assay is used to determine the denaturation point of a protein. Often, interaction with a ligand increases protein stability and therefore, the melting point shifts to higher temperatures. Interestingly, from all tested nucleotides, only c-di-GMP induced a temperature shift. The shift varies between 6.5°C and 8.5°C depending on the protein concentration. To observe the shift, c-di-GMP concentrations need to reach 100X excess over the protein concentration, with lower c-di-GMP concentrations no shift was detectable (Additional Data Figure 4d, e).



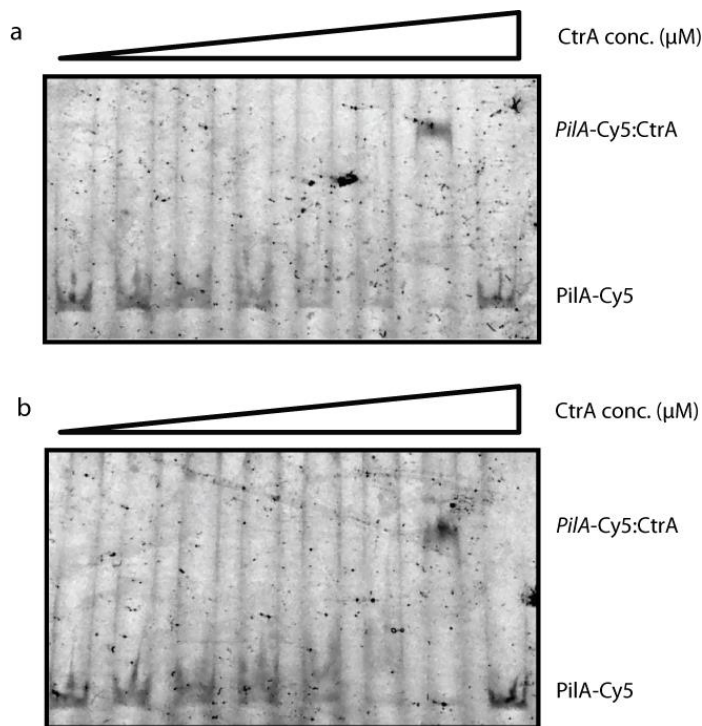
Additional Data Figure 4: Characterization of the CtrA-c-di-GMP interaction.

(a) C-di-GMP binding affinity for CtrA. Binding was determined by UV-crosslinking at increasing concentrations of [³³P]c-di-GMP. Quantified band intensity is shown. **(b)** Purified CtrA protein was incubated with [³³P]c-di-GMP and cross-linked with UV light in the presence or absence of a 10-fold or 100-fold excess of competing non-labelled nucleotides as indicated. **(c)** C-di-GMP binding determined by capture compound pulldown experiments. Amount of protein determined by western blot stained with α-FLAG antibody. Competition with non-labelled nucleotides as indicated. **(d)** C-di-GMP increases denaturation temperature of CtrA. Denaturation temperature determined by differential scanning fluorimetry (DSF). The red arrow indicates

the shifted curve for 100X c-di-GMP. **(e)** Temperature shift induced by c-di-GMP depends on protein concentration. Temperature shift increases from 6.5°C to 8.5°C if protein concentration is reduced from 20 μM to 5 μM .

CtrA DNA binding - Electrophoretic mobility shift assay

Considering that the output function of CtrA is DNA-binding, we tested if c-di-GMP alters the DNA-binding capacity of CtrA. The rationale behind the experiment is that at the G1-S transition, when CtrA has to be removed from the DNA, the c-di-GMP levels are high. Binding of c-di-GMP to CtrA could weaken the interaction with DNA and therefore clear the DNA from CtrA. The target promoter used for the experiments is *PilA*, a well-described CtrA target. The results show that CtrA binds the *PilA* promoter at high concentrations (Additional Data Figure 5). However, addition of c-di-GMP does not result in reduction of DNA binding activity.



Additional Data Figure 5: C-di-GMP does not interfere with CtrA binding to DNA. (a) Binding of CtrA to the *pilA* promoter was determined by electrophoretic mobility shift assay. CtrA concentrations used were 0, 0.02, 0.08, 0.2, 0.8, 3 and 12 μM . **(b)** An experiment identical to that described in (a) was performed, with the exception that 75 μM c-di-GMP was added.

Considering these experiments, we stopped further experiments investigating the effects of c-di-GMP on CtrA. However, it should be noted that when intracellular c-di-GMP levels raise, CtrA exists mostly in its phosphorylated state. Therefore, it could be possible that only phosphorylated CtrA is capable of binding c-di-GMP. To test this CtrA could be phosphorylated prior to measuring c-di-GMP and DNA-binding affinities.

Additional Data Materials and Methods

Unless not otherwise stated below, procedures required for the additional data are as described in [49].

Electrophoretic mobility shift assay (EMSA)

The assay was essentially done as described in [295]. CtrA-His₆ was diluted in binding buffer (25 mM Tris, 100 mM KCl, 5mM MgCl₂, 5% glycerol and 0.05% dodecyl maltoside, pH 7.5). Protein was mixed with BSA (0.5 mg ml⁻¹), sonicated salmon sperm DNA (0.05 mg ml⁻¹) and Cy3 labelled fragments of the *pilA* promoter region (25 nM). Samples were incubated for 10 min before loaded on 4% TBE polyacrylamide gels. Gels were scanned with a Typhon FLA 7000 imager (GE Healthcare)

Differential scanning fluorimetry (DSF)

Concentration of purified protein was adjusted to 20 μM. Reaction buffer contained 1X PBS (pH 7) supplemented with 2 mM β-mercaptoethanol. Nucleotides were added to the reaction as indicated. SYPRO orange dye was diluted to 5X final concentration. Reaction plate was incubated for 15 minutes before start of the experiment. Temperature gradient and fluorescence read-out was done using a Biorad thermocycler. Gradient was run from 10°C to 90°C at 0.5°C increments. BioRad CFX Manager 2.1 was used to analyze the data.

Capture compound pulldown experiments

Protein concentration was adjusted to 0.5 μM. Reaction was incubated in 1X PBS, 2 mM β-mercaptoethanol. Capture compound was used at a final concentration of 10 μM. Crosslink was done at 280 nm and 4 minutes at 4°C. Competition with unmodified nucleotides was done as indicated. Reactions were incubated with 30 μl magnetic streptavidin beads (Invitrogen). Reaction was washed six times with 1X wash buffer (50 mM Tris-HCl pH 7.5, 1mM

EDTA, 1M NaCl, 8.5 μ M n-octyl- β -D-glucopyranoside). Proteins were detected by western blot using α -CtrA antibody (rabbit) as described in [49].

Plasmid construction

Plasmids and Oligonucleotides used in this section are listed in Additional Data Tables 1 and 2.

To construct mutated CckA alleles, the following procedure was applied: Generally, pET-*ckkA* was used as template with 5276/5277 as outside primers and internal mutagenic primers to introduce mutations. The following internal primers were used to introduce point mutations: R374A (6483/6484), R380A (6485/6486), R412A (6489/6490), R418A (6491/6492), R451A (7721/7722), R457A (7723/7724), F474A (7725/7726), D479A (7727/7728), F493C (7729/7730), F493A (7729/7730), V513C (5542/5543), V513A (7731/7732), R529A (5500/5501), A534C (5544/5545), R537A (5502/5503), F539A (7737/7738), F539C (5546/5547), Q553C (5548/5549), R565A (5506/5507), R583A (5510/5511), R588A/R591A/R593A (5516/5517). To create CckA Δ 454-468 fragments were PCR amplified using primer combinations 5276/7742 and 5277/7741. After fusion PCR, inserts were *Bam*HI and *Sal*II digested and ligated into pET28a-His-MBP. The following mutants were amplified from a pBXMCS2 plasmid already containing the *ckkA* allele with the appropriate mutation. PCR products were amplified using 5276/5277. Plasmid templates were: pBXMCS2-*ckkA* F372A, pBXMCS2-*ckkA* Q376A, pBXMCS2-*ckkA* L508A, pBXMCS2-*ckkA* T512A, pBXMCS2-*ckkA* G515D, pBXMCS2-*ckkA* I516A, pBXMCS2-*ckkA* K518A, pBXMCS2-*ckkA* Q519A, pBXMCS2-*ckkA* I524P. Resulting PCR products were *Bam*HI and *Sal*II digested and ligated into pET28a-His-MBP. pET-*ckkA* T358A/V366P, pET-*ckkA* T506A/Y514D, pET-*ckkA* Y514D/S568W and pET-*ckkA* G318A were PCR amplified using chromosomal DNA containing the indicated mutations using Primers 5276/5277 and subsequent ligation into pET28a-His-MBP.

Additional Data Plasmids

NAME	DESCRIPTION	REF.
pET- <i>ackA</i> G318A	Overexpression of CckA alleles	This study
pET- <i>ackA</i> F372A	Overexpression of CckA alleles	This study
pET- <i>ackA</i> R374A	Overexpression of CckA alleles	This study
pET- <i>ackA</i> Q376A	Overexpression of CckA alleles	This study
pET- <i>ackA</i> R380A	Overexpression of CckA alleles	This study
pET- <i>ackA</i> R412A	Overexpression of CckA alleles	This study
pET- <i>ackA</i> R418A	Overexpression of CckA alleles	This study
pET- <i>ackA</i> R451A	Overexpression of CckA alleles	This study
pET- <i>ackA</i> R457A	Overexpression of CckA alleles	This study
pET- <i>ackA</i> F474A	Overexpression of CckA alleles	This study
pET- <i>ackA</i> D479A	Overexpression of CckA alleles	This study
pET- <i>ackA</i> F493A	Overexpression of CckA alleles	This study
pET- <i>ackA</i> F493C	Overexpression of CckA alleles	This study
pET- <i>ackA</i> L508A	Overexpression of CckA alleles	This study
pET- <i>ackA</i> T512A	Overexpression of CckA alleles	This study
pET- <i>ackA</i> V513A	Overexpression of CckA alleles	This study
pET- <i>ackA</i> V513C	Overexpression of CckA alleles	This study
pET- <i>ackA</i> G515D	Overexpression of CckA alleles	This study
pET- <i>ackA</i> I516A	Overexpression of CckA alleles	This study
pET- <i>ackA</i> K518A	Overexpression of CckA alleles	This study
pET- <i>ackA</i> Q519A	Overexpression of CckA alleles	This study
pET- <i>ackA</i> I524A	Overexpression of CckA alleles	This study
pET- <i>ackA</i> R529A	Overexpression of CckA alleles	This study
pET- <i>ackA</i> A534C	Overexpression of CckA alleles	This study
pET- <i>ackA</i> R537A	Overexpression of CckA alleles	This study
pET- <i>ackA</i> F539A	Overexpression of CckA alleles	This study
pET- <i>ackA</i> F539C	Overexpression of CckA alleles	This study
pET- <i>ackA</i> Q553C	Overexpression of CckA alleles	This study
pET- <i>ackA</i> R565A	Overexpression of CckA alleles	This study
pET- <i>ackA</i> R583A	Overexpression of CckA alleles	This study
pET- <i>ackA</i> R588A/R591A/R593A	Overexpression of CckA alleles	This study
pET- <i>ackA</i> deltaLooP	Overexpression of CckA alleles	This study
pET- <i>ackA</i> T358A/V366P	Overexpression of CckA alleles	This study

pET- <i>ckA</i> T506A/Y514D	Overexpression of CckA alleles	This study
pET- <i>ckA</i> Y514D/S568W	Overexpression of CckA alleles	This study
pBXMCS2- <i>ckA</i> F372A	To overexpress CckA Δ TM	Shogo Ozaki
pBXMCS2- <i>ckA</i> Q376A	To overexpress CckA Δ TM	Shogo Ozaki
pBXMCS2- <i>ckA</i> L508A	To overexpress CckA Δ TM	Shogo Ozaki
pBXMCS2- <i>ckA</i> T512A	To overexpress CckA Δ TM	Shogo Ozaki
pBXMCS2- <i>ckA</i> G515D	To overexpress CckA Δ TM	Shogo Ozaki
pBXMCS2- <i>ckA</i> I516A	To overexpress CckA Δ TM	Shogo Ozaki
pBXMCS2- <i>ckA</i> K518A	To overexpress CckA Δ TM	Shogo Ozaki
pBXMCS2- <i>ckA</i> Q519A	To overexpress CckA Δ TM	Shogo Ozaki
pBXMCS2- <i>ckA</i> I524P	To overexpress CckA Δ TM	Shogo Ozaki

Additional Data Primers

NAME	SEQUENCE
5276	CGCGGATCCTCAGCGCTTTCCGGCGGCGAC
5277	ACGCGTCGACCTACGCCGCTGCAGCTGCTG
5500	GGCTGGATTACAGTCCACAGCgcgCCGAACGAAGGCGCGGCCCTTC
5501	GAAGGCCGCGCCTTCGTTCGGgcgGCTGTGGACGTGAATCCAGCC
5502	CCGAACGAAGGCGCGGCCCTTCgccATCTTCCTGCCGGTCTATGAAG
5503	CTTCATAGACCGGCAGGAAGATggcGAAGGCCGCGCCTTCGTTCGG
5506	CCCGCCAAGCCGCGCGCCGCTgccGACCTGTCGGGCGCCGGCCGC
5507	GCGGCCGCGCCCCGACAGGTcggcAGCGGCGCGCGGCTTGGCGG
5510	GTCGAGGACGAGGACGCCGTGgccAGCGTCGCCGCCCGCCTGCTG
5511	CAGCAGGCGGGCGGCGACGCTggcCACGGCGTCTCGTCTCGAC
5516	GCCGTGCGCAGCGTCGCCGCCgccCTGCTGgccGCCgcgGGCTACGAG
5517	CGCCTCAAGCACCTCGTAGCCcgcGGCggcCAGCAGggcGGCGGCGAC
5540	CCCGACGTCATGGGCAAGATCtgcGACCCGTCTTCACCACCAAG
5541	CTTGGTGGTGAAGAACGGGTCgcaGATCTTGCCCATGACGTCCGGG
5542	CGGGCCTAGGCCTAGCCACGtgcTATGGCATCGTTAAGCAGAGCGA
5543	GTCGCTCTGCTTAACGATGCCATAgcaCGTGGCTAGGCCTAGGCC
5544	CACAGCCGTCCGAACGAAGGCtgcGCCTTCCGCATCTTCCTGCCG
5545	CGGCAGGAAGATGCGGAAGGCgcaGCCTTCGTTCGGACGGCTGTG
5546	CGAAGGCGCGGCCCTTCCGCATCtgcCTGCCGGTCTATGAAGCGCCC
5547	GGGCGCTTCATAGACCGGCAGgcaGATGCGGAAGGCCGCGCCTTC

5548 CCCGCCGGCGCGGTGCGCCGTctgcGCCGTCGCCGAGCCCGCCAAG
 5549 CTTGGCGGGCTCGGGCAGCGGcgaGACGGCGACCGCGCCGGCGG
 6483 GCGCAAGCTCTTGGCTTTCTCGgcgAAGCAGACCGTGCAGCGCGAG
 6485 CCTCGCGCTGCACGGTCTGCTTcgCGAGAAAGCCAAGAGCTTGCG
 6485 CTCGCGCAAGCAGACCGTGCAGgCGAGGTGCTGGATCTGGGCGA
 6486 GCTCGCCCAGATCCAGCACCTCcgCTGCACGGTCTGCTTGCGCGA
 6489 CAAGCTGATCACCGACTATGGCgCGGACCTGCCGCAGGTGCGCGCC
 6490 CGGCGCGCACCTGCGGCAGGTcCGGCCATAGTCGGTGATCAGCTT
 6491 GGCCGCGACCTGCCGCAGGTGgCGGCCGACAAGAGCCAGCTCGAG
 6492 GTCTCGAGCTGGCTCTTGTGCGGcCGCACCTGCGGCAGGTGCGGGC
 7721 GCGTCGTGCGCATCGCCACCGCGCGCCTGACCCG
 7722 CGGGTCAGGCGCGCGGTGGCGATGCGCACGACGC
 7723 CCGCACCGCGCGCCTGACCGCCGACGAGGCGATCCAGC
 7724 GCTGGATCGCCTCGTCGGCGGTGAGGCGCGCGGTGCGG
 7725 CCGCCGACGGCGACACGGCCGCCATTGAGGTCAGTGACGATG
 7726 CATCGTCACTGACCTCAATGGCGGCCGTGTCGCCGTGCGGCGG
 7727 GGCCTTTCATTGAGGTCAGTGCCGATGGTCCGGGCATTCGG
 7728 CGGAATGCCCGGACCATCGGCACTGACCTCAATGAAGGCC
 7729 CCCGACGTCATGGGCAAGATCGCCGACCCGTTCTTCACCACCAAG
 7730 CTTGGTGGTGAAGAACGGGTCGGCGATCTTGCCCATGACGTCGG
 7731 CGGGCCTAGGCCTAGCCACGGCCTATGGCATCGTTAAGCAGAGCG
 7732 GTCGCTCTGCTTAACGATGCCATAGGCCGTGGCTAGGCCTAGGCC
 7737 CGAAGGCGCGGCCTTCCGCATCGCCCTGCCGGTCTATGAAGCGCC
 7738 GGGCGCTTCATAGACCGGCAGGGCGATGCGGAAGGCCGCGCCTT
 7741 CGGCGTCGTGCGCATCCGCACCGCGGACGGCGACACGGCCTTCAT
 7742 CAATGAAGGCCGTGTCGCCGTCCGCGGTGCGGATGCGCACGACG

Discussion & Outlook

C-di-GMP has become a widely studied molecule in the past few years. During this time, it has become evident that c-di-GMP regulation goes beyond the motile-sessile transition and that this molecule controls a plethora of additional cellular processes in bacteria. Although our studies have added cell cycle progression and replication control to this growing list, the details of how c-di-GMP influences the bacterial cell cycle remain incomplete.

We have characterized a mechanism by which c-di-GMP controls the central cell cycle circuitry in *Caulobacter crescentus*. We have identified a novel c-di-GMP effector protein, CckA, which shares no common binding motif with known c-di-GMP binding proteins. CckA was isolated as a histidine kinase controlling the central cell cycle transcription factor CtrA [186]. CtrA itself controls the activity of more than 100 genes and, in addition, blocks DNA replication in the G1-phase swarmer cell [178]. Our data indicated that c-di-GMP binding to CckA changes its activity from the default kinase to phosphatase activity [49]. This ultimately results in dephosphorylation of CtrA upon entry into S-phase and licensing of replication initiation. It was shown previously that c-di-GMP levels fluctuate during the cell cycle with peak levels at the swarmer to stalked cell (G1-S) transition [38]. The strong upshift of c-di-GMP thus nicely coincides with the activation of CckA phosphatase activity.

However c-di-GMP is not the only determinant of CckA activity [186]. DivK is also involved in switching CckA into the phosphatase conformation, although it is neither entirely clear how DivK contributes to CckA regulation nor is the physiological reason for this redundancy evident from these studies [193]. Concluding from our data, we suggest a model where DivK and c-di-GMP together control G1-S transition. In contrast, it appears that in the predivisional cell, c-di-GMP is the only determinant of CckA activity and responsible for the differential activation at the poles. A c-di-GMP-blind mutant is no longer able to maintain replicative asymmetry during this stage of the cell cycle. Further research should thus aim at understanding how DivK and c-di-GMP synergistically control CckA at the G1-S transition. Furthermore, the role of DivL in CckA control is unclear. DivL is a histidine kinase-like protein lacking the conserved acceptor histidine [193,195]. Interestingly, DivL interacts with CckA and DivK but neither the consequences of this interaction nor the temporal and spatial pattern of this

interaction are known [193]. Hence, understanding the role of DivL could help understanding how CckA is controlled and why this additional pathway was introduced during evolution.

In the polarized predivisional cell, CckA localizes to both poles but is active as a phosphatase at the stalked pole and as a kinase at the swarmer pole [192]. It has been proposed that bipolar localization results in a gradient of activated CtrA~P across the predivisional cell [192]. We have shown that c-di-GMP is responsible for these opposing activities in the predivisional cell resulting in replicative asymmetry due to establishment of a CtrA phosphorylation gradient across the cell [49]. To explain our experimental observations, we proposed a model where c-di-GMP levels are lower at the swarmer cell pole as compared to the rest of the cytoplasm. This implies specific spatial control of c-di-GMP producing and degrading enzymes. We favour a model in which one or several PDEs colocalize with CckA at the flagellated pole, thereby installing a local trough of c-di-GMP which locally forces CckA into the kinase mode. However, we were not able to determine if a specific phosphodiesterase or a subset of phosphodiesterases at the swarmer cell pole is the cause of this gradient. Further research should investigate the key components involved in asymmetric c-di-GMP distribution and differential CckA activation.

Apart from highlighting the molecular and cellular details of *Caulobacter* cell cycle control, our results are especially interesting for the histidine kinase field in general. Many histidine kinases are bifunctional and also catalyze phosphatase reactions [167,263]. In most cases, the molecular and structural details to this switch are unclear and there are no structures available which show a histidine kinase in its phosphatase conformation. One reason for this lack of knowledge is that often signals responsible for kinase or phosphatase activation are unknown. Even if such signals have been identified, membrane integral HKs with the input domain separated from the catalytic kinase core by a lipid bilayer are difficult to dissect biochemically or structurally. To the best of our knowledge, CckA is the first example of a His kinase/phosphatase controlled by a small ligand. This has opened up a promising opportunity to gain deeper understanding of how histidine kinases are regulated. Our findings that c-di-GMP regulation is confined to the cytoplasmic kinase core domains, makes CckA an attractive and tractable protein to understand the important and widely conserved kinase/phosphatase switch.

Together with our collaborators in Structural Biology, we recently succeeded to solve the crystal structure of the CA domain of CckA bound to c-di-GMP. Not only did the structure confirm the region of c-di-GMP binding which we

have previously determined by a mutagenesis and NMR approach, but it also uncovered a completely new c-di-GMP binding site. Unfortunately, it was so far not possible to solve the structure of the full-length protein with and without c-di-GMP. Future work should thus focus on structure/function aspects of the full-length CckA and its regulation by c-di-GMP. This will allow to draw general conclusions about the conformational changes which histidine kinases undergo to switch to a phosphatase mode. In addition to c-di-GMP, ADP binding was described as potential activator of phosphatase activity [263]. However, how ADP induces phosphatase activity remains obscure. We could show that for CckA binding affinity of ADP was very low in the absence of c-di-GMP, but strongly increased upon addition of c-di-GMP. Based on this, we speculate that c-di-GMP stabilizes the ADP molecule which remains bound to the protein after ATP hydrolysis, thereby triggering phosphatase activation. Consequently, future work will aim at determining the off rates of ADP in the presence and absence of c-di-GMP.

We have shown that the c-di-GMP dependent kinase-phosphatase switch is conserved in the CckA homolog of *Agrobacterium tumefaciens* [49]. Since CckA is a conserved protein in α -proteobacteria it is conceivable that many CckA homologs are controlled by c-di-GMP [228,296]. At the same time it is tempting to speculate that c-di-GMP regulation of histidine kinases predates the evolutionary separation of different proteobacterial branches and that a subclass of this large signaling family has adopted c-di-GMP control in a wide range of different bacteria. *In silico* analyses have recently indicated that this is indeed the case and that a subgroup of histidine kinases shares key determinants for c-di-GMP binding with the CckA subgroup found in α -proteobacteria. This includes a set of HKs in gamma-proteobacteria like *Escherichia* or *Pseudomonas*. It will be most rewarding to investigate activity; c-di-GMP dependence; and cellular role of selected members of this newly identified subfamily of HKs.

The second major part of this thesis investigated the general stress response in *C. crescentus*. Similar to the core cell cycle events described above, the stress response is controlled by phosphorylation cascades [210,275]. In order to respond to various stresses, *C. crescentus* upregulates the alternative sigma factor SigT [285]. Activity and induction of SigT depend on a partner switch mechanism [206]. SigT is bound by NepR and kept in an inactive form [203]. Upon phosphorylation, the response regulator PhyR interacts with and sequesters NepR, thereby freeing SigT [202,207]. Hence, activation of this cascade by different sources of cellular stress critically depends PhyR phosphorylation. Several upstream kinases of PhyR have been described, one

of them being LovK [202,210]. Although LovK harbors a light sensing LOV domain, its mode of activation and its specific role in SigT control has remained elusive. In this work, we demonstrate that MrrA, a small single domain response regulator, controls the activity of LovK. We identified two cognate upstream kinases of MrrA capable of transferring phosphate onto MrrA. Phosphorylated MrrA was then shown to strongly induce autokinase activity of LovK, thereby activating the general stress response. Although our studies uncovered MrrA as a molecular connector between different layers of PhyR phosphorylation control, several questions remained unsolved. Mutational inactivation of MrrA completely prevented activation of SigT-dependent transcription *in vivo*, arguing that MrrA is indeed a central player of the stress response in *C. crescentus*. However, loss of its downstream target LovK had no significant effect. Based on this, we postulate the existence of additional downstream targets of MrrA, which contribute to signaling into the general stress response. A very attractive candidate is PhyK, since the mutational inactivation of this protein resulted in an abolished general stress response. Future work will thus focus on the *in vitro* activity of PhyK and its dependence on the presence of activated MrrA, MrrA~P. Moreover, it appears that additional components of this important stress pathway are missing upstream of MrrA. Although we have identified two cognate histidine kinases that specifically phosphorylate MrrA *in vitro*, mutational inactivation of these kinases was not sufficient to block activation of the general stress response. Therefore, additional histidine kinases must exist which are able to phosphorylate MrrA. Future work should aim at identifying such missing kinases to get a better insight into the activation of the general stress response in *C. crescentus*. Likewise, specific cellular stressors will have to be investigated in order to dissect the role of each of the upstream components and to appreciate the central role of MrrA in this general cellular homeostasis system.

Acknowledgments

The work presented in this thesis was carried out at the Biozentrum of the University of Basel, Switzerland in the group of Prof. Urs Jenal.

First of all, I thank Prof. Urs Jenal for hosting me for the last four years (and the year before during my Master studies). I also thank him for the continuous support, discussions and inputs.

I also thank my PhD committee members Prof. Christoph Dehio and Prof. Dirk Bumann. Prof. Christoph Dehio is especially acknowledged for suggesting NMR analysis to identify the c-di-GMP binding site.

Next I would like to thank Samuel Steiner who was my supervisor during my Master thesis. Our very good teamwork then continued throughout the course of my PhD studies, even after he left to the USA. His help in the beginning of the CckA project is highly appreciated and without him the project would not have given the result it did

I thank everyone involved in the CckA project, namely Shogo Ozaki for his extremely valuable contributions to the *in vivo* side of the project, Raphael Böhm and Prof. Sebastian Hiller for carrying out the NMR experiments for the revisions in almost no time. Further, I thank Badri Nath Dubey and Prof. Tilman Schirmer for structural analysis and ongoing collaborations and finally, Sören Abel for occasional help on *Caulobacter* cell cycle issues.

All the past and present lab members are acknowledged for help and making the lab a nice place to spend time. Especially the residents of 484 provided a good atmosphere: Jutta, Alberto, Kerstin, Imke, Victoriya and lately also Andreas. Of course also Beni needs to be mentioned for “experiments” involving unmanned aircraft and substances rapidly changing state of matter.

I also thank the people from the core facilities whose instruments I was allowed to use.

Katrin Treffon is especially acknowledged for the correction of this Thesis.

Lastly, I would like to thank my family and friends for sustaining me during the last years.

References

1. Pratt LA, Kolter R (1999) Genetic analyses of bacterial biofilm formation. *Curr Opin Microbiol* **2**: 598–603.
2. Southey-Pillig CJ, Davies DG, Sauer K (2005) Characterization of temporal protein production in *Pseudomonas aeruginosa* biofilms. *J Bacteriol* **187**: 8114–8126.
3. Waite RD, Papakonstantinou A, Littler E, Curtis MA (2005) Transcriptome analysis of *Pseudomonas aeruginosa* growth: Comparison of gene expression in planktonic cultures and developing and mature biofilms. *J Bacteriol* **187**: 6571–6576.
4. Lowe RMS, Baines D, Selinger LB, Thomas JE, McAllister TA, Sharma R (2009) *Escherichia coli* O157:H7 strain origin, lineage, and Shiga toxin 2 expression affect colonization of cattle. *Appl Environ Microbiol* **75**: 5074–5081.
5. Patell S, Gu M, Davenport P, Givskov M, Waite RD, Welch M (2010) Comparative microarray analysis reveals that the core biofilm-associated transcriptome of *Pseudomonas aeruginosa* comprises relatively few genes. *Environ Microbiol Rep* **2**: 440–448.
6. Römling U, Galperin MY, Gomelsky M (2013) Cyclic di-GMP: the first 25 years of a universal bacterial second messenger. *Microbiol Mol Biol Rev* **77**: 1–52.
7. Aldridge P, Paul R, Goymer P, Rainey P, Jenal U (2003) Role of the GGDEF regulator PleD in polar development of *Caulobacter crescentus*. *Mol Microbiol* **47**: 1695–1708.
8. Hinnen D (2014) Phosphodiesterase activity of YahA-EAL is regulated by changes in tertiary and quaternary structure. *Master Thesis*.
9. Barends TR, Hartmann E, Griese JJ, Beitlich T, Kirienko N V, Ryjenkov DA, Reinstein J, Shoeman RL, Gomelsky M, Schlichting I (2009) Structure and mechanism of a bacterial light-regulated cyclic nucleotide phosphodiesterase. *Nature* **459**: 1015–1018.
10. Schmidt AJ, Ryjenkov DA, Gomelsky M (2005) The Ubiquitous Protein Domain EAL Is a Cyclic Diguanylate-Specific Phosphodiesterase : Enzymatically Active and Inactive EAL Domains The Ubiquitous Protein Domain EAL Is a Cyclic Diguanylate-Specific Phosphodiesterase : Enzymatically Active and Inactive E.

11. Bellini D, Caly DL, Mccarthy Y, Bumann M, An SQ, Dow JM, Ryan RP, Walsh MA (2014) Crystal structure of an HD-GYP domain cyclic-di-GMP phosphodiesterase reveals an enzyme with a novel trinuclear catalytic iron centre. *Mol Microbiol* **91**: 26–38.
12. Wassmann P, Chan C, Paul R, Beck A, Heerklotz H, Jenal U, Schirmer T (2007) Structure of BeF₃⁻-modified response regulator PleD: implications for diguanylate cyclase activation, catalysis, and feedback inhibition. *Structure* **15**: 915–927.
13. Christen B, Christen M, Paul R, Schmid F, Folcher M, Jenoe P, Meuwly M, Jenal U (2006) Allosteric Control of Cyclic di-GMP Signaling. *J Biol Chem* **281**: 32015–32024.
14. Zähringer F, Lacanna E, Jenal U, Schirmer T, Boehm A (2013) Structure and signaling mechanism of a zinc-sensory diguanylate cyclase. *Structure* **21**: 1149–1157.
15. Rao F, Yang Y, Qi Y, Liang ZX (2008) Catalytic mechanism of cyclic di-GMP-specific phosphodiesterase: A study of the EAL domain-containing RocR from *Pseudomonas aeruginosa*. *J Bacteriol* **190**: 3622–3631.
16. Rao F, Qi Y, Chong HS, Kotaka M, Li B, Li J, Lescar J, Tang K, Liang ZX (2009) The functional role of a conserved loop in EAL domain-based cyclic di-GMP-specific phosphodiesterase. *J Bacteriol* **191**: 4722–4731.
17. Sundriyal A, Massa C, Samoray D, Zehender F, Sharpe T, Jenal U, Schirmer T (2014) Inherent regulation of EAL domain-catalyzed hydrolysis of second messenger c-di-GMP. *J Biol Chem* **289**: 0–27.
18. Hengge R, Galperin MY, Ghigo J-M, Gomelsky M, Green J, Hughes KT, Jenal U, Landini P (2016) Systematic nomenclature for GGDEF and EAL domain-containing c-di-GMP turnover proteins of *Escherichia coli*. *J Bacteriol* **198**: 7–11.
19. McKee RW, Kariisa A, Mudrak B, Whitaker C, Tamayo R (2014) A systematic analysis of the in vitro and in vivo functions of the HD-GYP domain proteins of *Vibrio cholerae*. *BMC Microbiol* **14**: 272.
20. Orr MW, Donaldson GP, Severin GB, Wang J, Sintim HO, Waters CM, Lee VT (2015) Oligoribonuclease is the primary degradative enzyme for pGpG in *Pseudomonas aeruginosa* that is required for cyclic-di-GMP turnover. *Proc Natl Acad Sci U S A* **112**: E5048–E5057.
21. Cohen D, Mechold U, Nevenzal H, Yarmiyhu Y, Randall TE, Bay DC, Rich JD, Parsek MR, Kaeffer V, Harrison JJ, et al. (2015)

Oligoribonuclease is a central feature of cyclic diguanylate signaling in *Pseudomonas aeruginosa*. *Proc Natl Acad Sci U S A* 1421450112 – .

22. Tuckerman JR, Gonzalez G, Sousa EHS, Wan X, Saito JA, Alam M, Gilles-Gonzalez MA (2009) An oxygen-sensing diguanylate cyclase and phosphodiesterase couple for c-di-GMP control. *Biochemistry* **48**: 9764–9774.
23. Schmidt A, Hammerbacher AS, Bastian M, Nieken KJ, Klockgether J, Merighi M, Lapouge K, Poschgan C, Kölle J, Acharya KR, et al. (2016) Oxygen-dependent regulation of c-di-GMP synthesis by SadC controls alginate production in *Pseudomonas aeruginosa*. *Environ Microbiol.*
24. Gomelsky M (2013) A zinc lock on GGDEF domain dimerization inhibits *E. coli* biofilms. *Structure* **21**: 1067–1068.
25. Mills E, Petersen E, Kulasekara BR, Miller SI (2015) A direct screen for c-di-GMP modulators reveals a *Salmonella Typhimurium* periplasmic L-arginine-sensing pathway. *Sci Signal* **8**: ra57.
26. Feirer N, Xu J, Allen KD, Koestler BJ, Bruger EL, Waters CM, White RH, Fuqua C (2015) A pterin-dependent signaling pathway regulates a dual-function diguanylate cyclase-phosphodiesterase controlling surface attachment in *Agrobacterium tumefaciens*. *MBio* **6**.
27. Chua SL, Sivakumar K, Rybtke M, Yuan M, Andersen JB, Nielsen TE, Givskov M, Tolker-Nielsen T, Cao B, Kjelleberg S, et al. (2015) C-di-GMP regulates *Pseudomonas aeruginosa* stress response to tellurite during both planktonic and biofilm modes of growth. *Sci Rep* **5**: 10052.
28. Enomoto G, Ni-Ni-Win, Narikawa R, Ikeuchi M (2015) Three cyanobacteriochromes work together to form a light color-sensitive input system for c-di-GMP signaling of cell aggregation. *Proc Natl Acad Sci* **112**: 201504228.
29. Reinders A, Hee C-S, Ozaki S, Mazur A, Boehm A, Schirmer T, Jenal U (2015) Expression and Genetic Activation of c-di-GMP specific Phosphodiesterases in *Escherichia coli*. *J Bacteriol* **198**: 448–462.
30. Lindenberg S, Klauck G, Pesavento C, Klauck E, Hengge R (2013) The EAL domain protein YciR acts as a trigger enzyme in a c-di-GMP signalling cascade in *E. coli* biofilm control. *EMBO J* **32**: 2001–2014.
31. Newell PD, Monds RD, O'Toole GA (2009) LapD is a bis-(3',5')-cyclic dimeric GMP-binding protein that regulates surface attachment by *Pseudomonas fluorescens* Pf0-1. *Proc Natl Acad Sci U S A* **106**: 3461–3466.

32. Newell PD, Boyd CD, Sondermann H, Toole GA (2011) A c-di-GMP effector system controls cell adhesion by inside-out signaling and surface protein cleavage. *PLoS Biol* **9**: 1–17.
33. Chatterjee D, Cooley RB, Boyd CD, Mehl R a, O’Toole G a, Sondermann H (2014) Mechanistic insight into the conserved allosteric regulation of periplasmic proteolysis by the signaling molecule cyclic-di-GMP. *Elife* **3**: e03650.
34. Duerig A, Abel S, Folcher M, Nicollier M, Schwede T, Amiot N, Giese B, Jenal U (2009) Second messenger-mediated spatiotemporal control of protein degradation regulates bacterial cell cycle progression. *Genes Dev* **23**: 93–104.
35. Poindexter JS (1964) Biological properties and classification of the caulobacter group. *Bacteriol Rev* **28**: 231–295.
36. Davis NJ, Cohen Y, Sanselicio S, Fumeaux C, Ozaki S, Luciano J, Guerrero-Ferreira RC, Wright ER, Jenal U, Viollier PH (2013) De- and repolarization mechanism of flagellar morphogenesis during a bacterial cell cycle. *Genes Dev* **27**: 2049–2062.
37. Kim C, Quon, Marczynski GT, Shapiro L (1996) Cell Cycle Control by an Essential Bacterial Two-Component Signal Transduction Protein. *Cell* **84**: 83–93.
38. Abel S, Bucher T, Nicollier M, Hug I, Kaefer V, Abel zur Wiesch P, Jenal U (2013) Bi-modal Distribution of the Second Messenger c-di-GMP Controls Cell Fate and Asymmetry during the Caulobacter Cell Cycle. *PLoS Genet* **9**: 1–17.
39. Paul R, Abel S, Wassmann P, Beck A, Heerklotz H, Jenal U (2007) Activation of the diguanylate cyclase PleD by phosphorylation-mediated dimerization. *J Biol Chem* **282**: 29170–29177.
40. Abel S, Chien P, Wassmann P, Schirmer T, Kaefer V, Laub MT, Baker TA, Jenal U (2011) Regulatory cohesion of cell cycle and cell differentiation through interlinked phosphorylation and second messenger networks. *Mol Cell* **43**: 550–560.
41. Siam R, Brassinga AKC, Marczynski GT (2003) A dual binding site for integration host factor and the response regulator CtrA inside the Caulobacter crescentus replication origin. *J Bacteriol* **185**: 5563–5572.
42. Reisenauer A, Quon K, Shapiro L (1999) The CtrA response regulator mediates temporal control of gene expression during the Caulobacter cell cycle. *J Bacteriol* **181**: 2430–2439.

43. Jenal U, Fuchs T (1998) An essential protease involved in bacterial cell-cycle control. *EMBO J* **17**: 5658–5669.
44. Domian IJ, Quon KC, Shapiro L (1997) Cell type-specific phosphorylation and proteolysis of a transcriptional regulator controls the G1-to-S transition in a bacterial cell cycle. *Cell* **90**: 415–424.
45. Paul R, Jaeger T, Abel S, Wiederkehr I, Folcher M, Biondi EG, Laub MT, Jenal U (2008) Allosteric regulation of histidine kinases by their cognate response regulator determines cell fate. *Cell* **133**: 452–461.
46. Tsokos CG, Perchuk BS, Laub MT (2011) A Dynamic Complex of Signaling Proteins Uses Polar Localization to Regulate Cell-Fate Asymmetry in *Caulobacter crescentus*. *Dev Cell* **20**: 329–341.
47. Ozaki S, Schalch-Moser A, Zumthor L, Manfredi P, Ebbensgaard A, Schirmer T, Jenal U (2014) Activation and polar sequestration of PopA, a c-di-GMP effector protein involved in *Caulobacter crescentus* cell cycle control. *Mol Microbiol* **94**: 580–594.
48. Joshi KK, Bergé M, Radhakrishnan SK, Viollier PH, Chien P (2015) An Adaptor Hierarchy Regulates Proteolysis during a Bacterial Cell Cycle. *Cell* **163**: 419–431.
49. Lori C, Ozaki S, Steiner S, Böhm R, Abel S, Dubey BN, Schirmer T, Hiller S, Jenal U (2015) Cyclic di-GMP acts as a cell cycle oscillator to drive chromosome replication. *Nature* **523**: 236–239.
50. Christen M, Kulasekara HD, Christen B, Kulasekara BR, Hoffman LR, Miller SI (2010) Asymmetrical distribution of the second messenger c-di-GMP upon bacterial cell division. *Science* **328**: 1295–1297.
51. Kulasekara BR, Kamischke C, Kulasekara HD, Christen M, Wiggins PA, Miller SI (2013) c-di-GMP heterogeneity is generated by the chemotaxis machinery to regulate flagellar motility. *Elife* **2**: 1–19.
52. Tuckerman JR, Gonzalez G, Gilles-Gonzalez M-A (2011) Cyclic di-GMP activation of polynucleotide phosphorylase signal-dependent RNA processing. *J Mol Biol* **407**: 633–639.
53. Dahlstrom KM, Giglio KM, Collins AJ, Sondermann H, Toole AO (2015) Contribution of Physical Interactions to Signaling Specificity between a Diguanylate Cyclase and Its Effector. *MBio* **6**: 1–11.
54. Den Hengst CD, Tran NT, Bibb MJ, Chandra G, Leskiw BK, Buttner MJ (2010) Genes essential for morphological development and antibiotic production in *Streptomyces coelicolor* are targets of BldD during vegetative growth. *Mol Microbiol* **78**: 361–379.

55. Tschowri N, Schumacher MA, Schlimpert S, Chinnam N babu, Findlay KC, Brennan RG, Buttner MJ (2014) Tetrameric c-di-GMP Mediates Effective Transcription Factor Dimerization to Control Streptomyces Development. *Cell* **158**: 1136–1147.
56. Bush MJ, Tschowri N, Schlimpert S, Flärdh K, Buttner MJ (2015) c-di-GMP signalling and the regulation of developmental transitions in streptomycetes. *Nat Rev Microbiol* **13**: 749–760.
57. Alvarez-Curto E, Saran S, Meima M, Zobel J, Scott C, Schaap P (2007) cAMP production by adenylyl cyclase G induces prespore differentiation in Dictyostelium slugs. *Development* **134**: 959–966.
58. Chen Z, Schaap P (2012) The prokaryote messenger c-di-GMP triggers stalk cell differentiation in Dictyostelium. *Nature* **488**: 680–683.
59. Boehm A, Kaiser M, Li H, Spangler C, Kasper CA, Ackermann M, Kaever V, Sourjik V, Roth V, Jenal U (2010) Second messenger-mediated adjustment of bacterial swimming velocity. *Cell* **141**: 107–116.
60. Ko M, Park C (2000) Two novel flagellar components and H-NS are involved in the motor function of Escherichia coli. *J Mol Biol* **303**: 371–382.
61. Paul K, Nieto V, Carlquist WC, Blair DF, Harshey RM (2010) The c-di-GMP Binding Protein YcgR Controls Flagellar Motor Direction and Speed to Affect Chemotaxis by a ‘Backstop Brake’ Mechanism. *Mol Cell* **38**: 128–139.
62. Chen Y, Chai Y, Guo J hua, Losick R (2012) Evidence for cyclic Di-GMP-mediated signaling in Bacillus subtilis. *J Bacteriol* **194**: 5080–5090.
63. Gao X, Mukherjee S, Matthews PM, Hammad LA, Kearns DB, Dann CE (2013) Functional characterization of core components of the bacillus: Subtilis cyclic-Di-GMP signaling pathway. *J Bacteriol* **195**: 4782–4792.
64. Baraquet C, Murakami K, Parsek MR, Harwood CS (2012) The FleQ protein from Pseudomonas aeruginosa functions as both a repressor and an activator to control gene expression from the Pel operon promoter in response to c-di-GMP. *Nucleic Acids Res* **40**: 7207–7218.
65. Baraquet C, Harwood CS (2013) Cyclic diguanosine monophosphate represses bacterial flagella synthesis by interacting with the Walker A motif of the enhancer-binding protein FleQ. *Proc Natl Acad Sci U S A* **110**: 18478–18483.
66. Su T, Liu S, Wang K, Chi K, Zhu D, Wei T, Huang Y, Guo L, Hu W,

- Xu S, et al. (2015) The REC domain mediated dimerization is critical for FleQ from *Pseudomonas aeruginosa* to function as a c-di-GMP receptor and flagella gene regulator. *J Struct Biol* **192**: 1–13.
67. Trampari E, Stevenson CEM, Little RH, Wilhelm T, Lawson DM, Malone JG (2015) Bacterial Rotary Export ATPases Are Allosterically Regulated by the Nucleotide Second Messenger Cyclic-di-GMP. *J Biol Chem* **290**: 24470–24483.
 68. Skotnicka D, Petters T, Heering J, Hoppert M, Kaefer V, Sogaard-Andersen L (2015) c-di-GMP regulates type IV pili-dependent-motility in *Myxococcus xanthus*. *J Bacteriol* **198**: 77–90.
 69. Jones CJ, Utada A, Davis KR, Thongsomboon W, Zamorano Sanchez D, Banakar V, Cegelski L, Wong GCL, Yildiz FH (2015) C-di-GMP Regulates Motile to Sessile Transition by Modulating MshA Pili Biogenesis and Near-Surface Motility Behavior in *Vibrio cholerae*. *PLOS Pathog* **11**: 1–27.
 70. Srivastava D, Hsieh ML, Khataokar A, Neiditch MB, Waters CM (2013) Cyclic di-GMP inhibits *Vibrio cholerae* motility by repressing induction of transcription and inducing extracellular polysaccharide production. *Mol Microbiol* **90**: 1262–1276.
 71. Ayala JC, Wang H, Silva AJ, Benitez JA (2015) Repression by H-NS of genes required for the biosynthesis of the *Vibrio cholerae* biofilm matrix is modulated by the second messenger cyclic diguanylic acid. *Mol Microbiol* **97**: 630–645.
 72. Park JH, Jo Y, Jang SY, Kwon H, Irie Y, Parsek MR, Kim MH, Choi SH (2015) The cabABC Operon Essential for Biofilm and Rugose Colony Development in *Vibrio vulnificus*. *PLOS Pathog* **11**: e1005192.
 73. Steiner S, Lori C, Boehm A, Jenal U (2013) Allosteric activation of exopolysaccharide synthesis through cyclic di-GMP-stimulated protein-protein interaction. *EMBO J* **32**: 354–368.
 74. Serra DO, Richter AM, Hengge R (2013) Cellulose as an architectural element in spatially structured *Escherichia coli* biofilms. *J Bacteriol* **195**: 5540–5554.
 75. Morgan JLW, McNamara JT, Zimmer J (2014) Mechanism of activation of bacterial cellulose synthase by cyclic di-GMP. *Nat Struct Mol Biol* **21**: 489–496.
 76. Pérez-Mendoza D, Rodríguez-Carvajal MÁ, Romero-Jiménez L, Fariás G de A, Lloret J, Gallegos MT, Sanjuán J (2015) Novel mixed-linkage β -glucan activated by c-di-GMP in *Sinorhizobium meliloti*. *Proc Natl*

Acad Sci U S A **112**: 757–765.

77. Bordeleau E, Purcell EB, Lafontaine DA, Fortier L-C, Tamayo R, Burrus V (2015) Cyclic Di-GMP Riboswitch-Regulated Type IV Pili Contribute to Aggregation of *Clostridium difficile*. *J Bacteriol* **197**: 819–832.
78. Peltier J, Shaw HA, Couchman EC, Dawson LF, Yu L, Choudhary JS, Kaefer V, Wren BW, Fairweather NF (2015) Cyclic diGMP Regulates Production of Sortase Substrates of *Clostridium difficile* and Their Surface Exposure through ZmpI Protease-mediated Cleavage. *J Biol Chem* **290**: 24453–24469.
79. Kariisa AT, Weeks K, Tamayo R (2016) The RNA Domain Vc1 Regulates Downstream Gene Expression in Response to Cyclic Diguanylate in *Vibrio cholerae*. *PLoS One* **11**: 1–17.
80. Krasteva P, Fong J, Beyhan S, Shikuma N, Navarro MVA, Yildiz FH, Sondermann H (2010) *Vibrio cholerae* VpsT Regulates by Directly Sensing Cyclic di-GMP. *Science (80-)* **327**: 866–868.
81. Weber H, Pesavento C, Possling A, Tischendorf G, Hengge R (2006) Cyclic-di-GMP-mediated signalling within the sigma network of *Escherichia coli*. *Mol Microbiol* **62**: 1014–1034.
82. Pesavento C, Becker G, Sommerfeldt N, Possling A, Tschowri N, Mehliis A, Hengge R (2008) Inverse regulatory coordination of motility and curli-mediated adhesion in *Escherichia coli*. *Genes Dev* **22**: 2434–2446.
83. Sommerfeldt N, Possling A, Becker G, Pesavento C, Tschowri N, Hengge R (2009) Gene expression patterns and differential input into curli fimbriae regulation of all GGDEF/EAL domain proteins in *Escherichia coli*. *Microbiology* **155**: 1318–1331.
84. Ross P, Weinhouse H, Aloni Y, Michaeli D, Weinberger-Ohana P, Mayer R, Braun S, de Vroom E, van der Marel GA, van Boom JH, et al. (1987) Regulation of cellulose synthesis in *Acetobacter xylinum* by cyclic diguanylic acid. *Nature* **325**: 279–281.
85. Morgan JLW, Strumillo J, Zimmer J (2012) Crystallographic snapshot of cellulose synthesis and membrane translocation. *Nature* **493**: 181–186.
86. Whitney JC, Whitfield GB, Marmont LS, Yip P, Neculai AM, Lobsanov YD, Robinson H, Ohman DE, Howell PL (2015) Dimeric c-di-GMP is required for post-translational regulation of alginate production in *Pseudomonas aeruginosa*. *J Biol Chem* **290**: 12451–12462.

87. Navarro M, Newell PD, Krasteva P V, Chatterjee D, Madden DR, O'Toole G a, Sondermann H (2011) Structural basis for c-di-GMP-mediated inside-out signaling controlling periplasmic proteolysis. *PLoS Biol* **9**: e1000588.
88. Kong W, Zhao J, Kang H, Zhu M, Zhou T, Deng X, Liang H (2015) ChIP-seq reveals the global regulator AlgR mediating cyclic di-GMP synthesis in *Pseudomonas aeruginosa*. *Nucleic Acids Res* **43**: 8268–8282.
89. Malone JG, Jaeger T, Manfredi P, Doetsch A, Blanka A, Bos R, Cornelis GR, Häussler S, Jenal U (2012) The YfiB/NR signal transduction mechanism reveals novel targets for the evolution of persistent *Pseudomonas aeruginosa* in cystic fibrosis airways. *PLoS Pathog* **8**: 1–19.
90. Blanka A, Düvel J, Dötsch A, Klinkert B, Abraham W-R, Kaefer V, Ritter C, Narberhaus F, Häussler S (2015) Constitutive production of c-di-GMP is associated with mutations in a variant of *Pseudomonas aeruginosa* with altered membrane composition. *Sci Signal* **8**: ra36.
91. Buchholz U, Bernard H, Werber D, Kühne M (2011) German Outbreak of *Escherichia coli* O104:H4 Associated with Sprouts. *N Engl J Med* **365**: 683–693.
92. Brzuszkiewicz E, Thürmer A, Schuldes J, Leimbach A, Liesegang H, Meyer FD, Boelter J, Petersen H, Gottschalk G, Daniel R (2011) Genome sequence analyses of two isolates from the recent *Escherichia coli* outbreak in Germany reveal the emergence of a new pathotype: Enteric-Aggregative-Haemorrhagic *Escherichia coli* (EAHEC). *Arch Microbiol* **193**: 883–891.
93. Richter AM, Povolotsky TL, Wieler LH, Hengge R (2014) Cyclic-di-GMP signalling and biofilm-related properties of the Shiga toxin-producing 2011 German outbreak *Escherichia coli* O104:H4. *EMBO Mol Med* **6**: 1622–1637.
94. Itoh Y, Rice JD, Goller C, Pannuri A, Taylor J, Meisner J, Beveridge TJ, Preston JF, Romeo T (2008) Roles of pgaABCD genes in synthesis, modification, and export of the *Escherichia coli* biofilm adhesin poly-beta-1,6-N-acetyl-D-glucosamine. *J Bacteriol* **190**: 3670–3680.
95. Wang X, Dubey AK, Suzuki K, Baker CS, Babitzke P, Romeo T (2005) CsrA post-transcriptionally represses pgaABCD, responsible for synthesis of a biofilm polysaccharide adhesin of *Escherichia coli*. *Mol Microbiol* **56**: 1648–1663.
96. Itoh Y, Wang X, Hinnebusch BJ, Iii JFP, Romeo T (2005) Depolymerization of β -1,6-N-Acetyl-D-Glucosamine Disrupts the Integrity of Diverse Bacterial Biofilms †. *J Bacteriol* **187**: 382–387.

97. Janoir C (2015) Virulence factors of *Clostridium difficile* and their role during infection. *Anaerobe* **37**: 13–24.
98. McKee RW, Mangalea MR, Purcell EB, Borchardt EK, Tamayo R (2013) The second messenger cyclic Di-GMP regulates *Clostridium difficile* toxin production by controlling expression of sigD. *J Bacteriol* **195**: 5174–5185.
99. Sudarsan N, Lee ER, Weinberg Z, Moy RH, Kim JN, Link KH, Breaker RR (2008) Riboswitches in eubacteria sense the second messenger cyclic di-GMP. *Science* **321**: 411–413.
100. Soutourina OA, Monot M, Boudry P, Saujet L, Pichon C, Sismeiro O, Semenova E, Severinov K, Le Bouguenec C, Coppée JY, et al. (2013) Genome-Wide Identification of Regulatory RNAs in the Human Pathogen *Clostridium difficile*. *PLoS Genet* **9**:
101. Karaolis DKR, Means TK, Yang D, Takahashi M, Yoshimura T, Muraille E, Philpott D, Schroeder JT, Hyodo M, Hayakawa Y, et al. (2007) Bacterial c-di-GMP is an immunostimulatory molecule. *J Immunol* **178**: 2171–2181.
102. McWhirter SM, Barbalat R, Monroe KM, Fontana MF, Hyodo M, Joncker NT, Ishii KJ, Akira S, Colonna M, Chen ZJ, et al. (2009) A host type I interferon response is induced by cytosolic sensing of the bacterial second messenger cyclic-di-GMP. *J Exp Med* **206**: 1899–1911.
103. Burdette DL, Monroe KM, Sotelo-Troha K, Iwig JS, Eckert B, Hyodo M, Hayakawa Y, Vance RE (2011) STING is a direct innate immune sensor of cyclic di-GMP. *Nature* **478**: 515–518.
104. Huang Y-H, Liu X-Y, Du X-X, Jiang Z-F, Su X-D (2012) The structural basis for the sensing and binding of cyclic di-GMP by STING. *Nat Struct Mol Biol* **19**: 728–730.
105. Shu C, Yi G, Watts T, Kao CC, Li P (2012) Structure of STING bound to cyclic di-GMP reveals the mechanism of cyclic dinucleotide recognition by the immune system. *Nat Struct Mol Biol* **19**: 722–724.
106. Danilchanka O, Mekalanos JJ (2013) Cyclic dinucleotides and the innate immune response. *Cell* **154**: 962–970.
107. Ablasser A, Schmid-Burgk JL, Hemmerling I, Horvath GL, Schmidt T, Latz E, Hornung V (2013) Cell intrinsic immunity spreads to bystander cells via the intercellular transfer of cGAMP. *Nature* **503**: 530–534.
108. Parvatiyar K, Zhang Z, Teles RM, Ouyang S, Jiang Y, Iyer SS, Zaver SA, Schenk M, Zeng S, Zhong W, et al. (2012) The helicase DDX41

recognizes the bacterial secondary messengers cyclic di-GMP and cyclic di-AMP to activate a type I interferon immune response. *Nat Immunol* **13**: 1155–1161.

109. Li W, Cui T, Hu L, Wang Z, Li Z, He Z-G (2015) Cyclic diguanylate monophosphate directly binds to human siderocalin and inhibits its antibacterial activity. *Nat Commun* **6**: 8330.
110. Pruitt RN, Lacy DB (2012) Toward a structural understanding of *Clostridium difficile* toxins A and B. *Front Cell Infect Microbiol* **2**: 1–14.
111. Witte G, Hartung S, Büttner K, Hopfner K-P (2008) Structural biochemistry of a bacterial checkpoint protein reveals diadenylate cyclase activity regulated by DNA recombination intermediates. *Mol Cell* **30**: 167–178.
112. Mehne FMP, Schröder-Tittmann K, Eijlander RT, Herzberg C, Hewitt L, Kaever V, Lewis RJ, Kuipers OP, Tittmann K, Stülke J (2014) Control of the diadenylate cyclase CdaS in *Bacillus subtilis*: An autoinhibitory domain limits cyclic di-AMP production. *J Biol Chem* **289**: 21098–21107.
113. Mehne FMP, Gunka K, Eilers H, Herzberg C, Kaever V, Stülke J (2013) Cyclic Di-AMP Homeostasis in *Bacillus subtilis*: Both lack and high level accumulation of the nucleotide are detrimental for cell growth. *J Biol Chem* **288**: 2004–2017.
114. Rao F, See RY, Zhang D, Toh DC, Ji Q, Liang ZX (2010) YybT is a signaling protein that contains a cyclic dinucleotide phosphodiesterase domain and a GGDEF domain with ATPase activity. *J Biol Chem* **285**: 473–482.
115. Manikandan K, Sabareesh V, Singh N, Saigal K, Mechold U, Sinha KM (2014) Two-step synthesis and hydrolysis of cyclic di-AMP in *Mycobacterium tuberculosis*. *PLoS One* **9**: e86096.
116. Zhang L, Li W, He ZG (2013) DarR, a TetR-like transcriptional factor, is a cyclic di-AMP-responsive repressor in *Mycobacterium smegmatis*. *J Biol Chem* **288**: 3085–3096.
117. Corrigan RM, Campeotto I, Jeganathan T, Roelofs KG, Lee VT, Gründling A (2013) Systematic identification of conserved bacterial c-di-AMP receptor proteins. *Proc Natl Acad Sci* **110**: 9084–9089.
118. Chin K, Liang J-M, Yang J, Shih M, Tu Z, Wang Y, Sun X, Hu N, Liang Z, Dow JM, et al. (2015) Structural Insights into the Distinct Binding Mode of Cyclic di-AMP with SaCpaA-RCK. *Biochemistry* **54**: 4936–4951.
119. Kim H, Youn S-J, Kim SO, Ko J, Lee J-O, Choi B-S (2015) Structural

- Studies of Potassium Transport Protein KtrA Regulator of Conductance of K^+ (RCK) C Domain in Complex with Cyclic Diadenosine Monophosphate (c-di-AMP). *J Biol Chem* **290**: 16393–16402.
120. Joana A. Moscoso, Hannah Schramke, Yong Zhang, Tommaso Tosi, Amina Dehbi, Kirsten Jung AG (2016) Binding of Cyclic Di-AMP to the Staphylococcus aureus Sensor Kinase KdpD Occurs via the Universal Stress Protein Domain and Downregulates the Expression of the Kdp Potassium Transporter. *J Bacteriol* **198**: 98–110.
 121. Sureka K, Choi PH, Precit M, Delince M, Pensinger DA, Huynh TN, Jurado AR, Goo YA, Sadilek M, Iavarone AT, et al. (2014) The Cyclic Dinucleotide c-di-AMP Is an Allosteric Regulator of Metabolic Enzyme Function. *Cell* **158**: 1389–1401.
 122. Davies BW, Bogard RW, Young TS, Mekalanos JJ (2012) Coordinated Regulation of Accessory Genetic Elements Produces Cyclic Dinucleotides for *V. cholerae* Virulence. *Cell* **149**: 358–370.
 123. Ablasser A, Goldeck M, Cavlar T, Deimling T, Witte G, Röhl I, Hopfner K-P, Ludwig J, Hornung V (2013) cGAS produces a 2'-5'-linked cyclic dinucleotide second messenger that activates STING. *Nature* **498**: 380–384.
 124. Kato K, Ishii R, Hirano S, Ishitani R, Nureki O (2015) Structural Basis for the Catalytic Mechanism of DncV, Bacterial Homolog of Cyclic GMP-AMP Synthase. *Structure* **23**: 843–850.
 125. Kellenberger C., Wilson SC, Hickey SF, Gonzalez TL, Su Y, Hallberg ZF, Brewer TF, Iavarone AT, Carlson HK, Hsieh Y-F, et al. (2015) GEMM-I riboswitches from Geobacter sense the bacterial second messenger cyclic AMP-GMP. *Proc Natl Acad Sci* **112**: 5383–5388.
 126. Nelson JW, Sudarsan N, Phillips GE, Stav S, Lünse CE, McCown PJ, Breaker RR (2015) Control of bacterial exoelectrogenesis by c-AMP-GMP. *Proc Natl Acad Sci* **112**: 5389–5394.
 127. Diner EJ, Burdette DL, Wilson SC, Monroe KM, Kellenberger C a., Hyodo M, Hayakawa Y, Hammond MC, Vance RE (2013) The Innate Immune DNA Sensor cGAS Produces a Noncanonical Cyclic Dinucleotide that Activates Human STING. *Cell Rep* **3**: 1355–1361.
 128. Li X, Shu C, Yi G, Chaton CT, Shelton CL, Diao J, Zuo X, Kao CC, Herr AB, Li P (2013) Cyclic GMP-AMP synthase is activated by double-stranded DNA-induced oligomerization. *Immunity* **39**: 1019–1031.
 129. Civril F, Deimling T, de Oliveira Mann CC, Ablasser A, Moldt M, Witte G, Hornung V, Hopfner K-P (2013) Structural mechanism of cytosolic

DNA sensing by cGAS. *Nature* **498**: 332–337.

130. Kasper CA, Sorg I, Schmutz C, Tschon T, Wischnewski H, Kim ML, Arrieumerlou C (2010) Cell-cell propagation of NF- κ B transcription factor and MAP kinase activation amplifies innate immunity against bacterial infection. *Immunity* **33**: 804–816.
131. Gentili M, Kowal J, Tkach M, Satoh T, Lahaye X, Conrad C, Boyron M, Lombard B, Durand S, Kroemer G, et al. (2015) Transmission of innate immune signaling by packaging of cGAMP in viral particles. *Science (80-)* **349**: 1232–1236.
132. Bridgeman A, Maelfait J, Davenne T, Partridge T, Peng Y, Mayer A, Dong T, Kaever V, Borrow P, Rehwinkel J (2015) Viruses transfer the antiviral second messenger cGAMP between cells. *Science (80-)* **349**: 19–23.
133. Kranzusch PJ, Wilson SC, Lee ASY, Berger JM, Doudna JA, Vance RE (2015) Ancient Origin of cGAS-STING Reveals Mechanism of Universal 2',3' cGAMP Signaling. *Mol Cell* **59**: 891–903.
134. Nesper J, Reinders A, Glatter T, Schmidt A, Jenal U (2012) A novel capture compound for the identification and analysis of cyclic di-GMP binding proteins. *J Proteomics* **75**: 4874–4878.
135. Laventie B-J, Nesper J, Ahrné E, Glatter T, Schmidt A, Jenal U (2015) Capture Compound Mass Spectrometry - A Powerful Tool to Identify Novel c-di-GMP Effector Proteins. *J Vis Exp* 1–11.
136. Düvel J, Bertinetti D, Möller S, Schwede F, Morr M, Wissing J, Radamm L, Zimmermann B, Genieser HG, Jänsch L, et al. (2012) A chemical proteomics approach to identify c-di-GMP binding proteins in *Pseudomonas aeruginosa*. *J Microbiol Methods* **88**: 229–236.
137. Düvel J, Bense S, Möller S, Bertinetti D, Schwede F, Morr M, Eckweiler D, Genieser H-G, Jänsch L, Herberg FW, et al. (2015) Application of synthetic peptide arrays to uncover c-di-GMP binding motifs. *J Bacteriol* **198**: 138–146.
138. Rotem O, Nesper J, Borovok I, Gorovits R, Kolot M, Pasternak Z, Shin I, Glatter T, Pietrokovski S, Jenal U, et al. (2015) An extended cyclic di-GMP network in the predatory bacterium *Bedellovibrio bacteriovorus*. *J Bacteriol* **198**: JB.00422–15.
139. Roelofs KG, Wang J, Sintim HO, Lee VT (2011) Differential radial capillary action of ligand assay for high-throughput detection of protein-metabolite interactions. *Proc Natl Acad Sci* **108**: 15528–15533.

140. Corrigan RM, Abbott JC, Burhenne H, Kaeffer V, Gründling A (2011) c-di-AMP Is a New Second Messenger in *Staphylococcus aureus* with a Role in Controlling Cell Size and Envelope Stress. *PLoS Pathog* **7**: e1002217.
141. Roelofs KG, Jones CJ, Helman SR, Shang X, Orr MW, Goodson JR, Galperin MY, Yildiz FH, Lee VT (2015) Systematic Identification of Cyclic-di-GMP Binding Proteins in *Vibrio cholerae* Reveals a Novel Class of Cyclic-di-GMP-Binding ATPases Associated with Type II Secretion Systems. *PLoS Pathog* **11**: e1005232.
142. Hickman JW, Harwood CS (2008) Identification of FleQ from *Pseudomonas aeruginosa* as a c-di-GMP-responsive transcription factor. *Mol Microbiol* **69**: 376–389.
143. Matsuyama BY, Krasteva P V., Baraquet C, Harwood CS, Sondermann H, Navarro MVAS (2015) Mechanistic insights into c-di-GMP-dependent control of the biofilm regulator FleQ from *Pseudomonas aeruginosa*. *Proc Natl Acad Sci* 201523148.
144. Yamada S, Shiro Y (2008) Structural Basis of the Signal Transduction in the Two-Component Signal output. *Adv Exp Med Biol* **2**: 22–39.
145. Perry J, Koteva K, Wright G (2011) Receptor domains of two-component signal transduction systems. *Mol Biosyst* **7**: 1388–1398.
146. Galperin MY (2010) Diversity of structure and function of response regulator output domains. *Curr Opin Microbiol* **13**: 150–159.
147. Krell T, Lacal J, Busch A, Silva-Jiménez H, Guazzaroni M-E, Ramos JL (2010) Bacterial sensor kinases: diversity in the recognition of environmental signals. *Annu Rev Microbiol* **64**: 539–559.
148. Newton A, Hecht GB, Newton A (1995) Identification of a novel response regulator required for the swarmer-to-stalked-cell transition in *Caulobacter crescentus*. *J Bacteriol* **177**: 6223–6229.
149. Jenal U, Galperin MY (2009) Single domain response regulators: molecular switches with emerging roles in cell organization and dynamics. *Curr Opin Microbiol* **12**: 152–160.
150. Capra EJ, Laub MT (2012) Evolution of two-component signal transduction systems. *Annu Rev Microbiol* **66**: 325–347.
151. Stock AM, Mottonen JM, Stock JB, Schutt CE (1989) Three-dimensional structure of CheY, the response regulator of bacterial chemotaxis. *Nature* **337**: 745–749.

152. Silversmith RE, Bourret RB (1999) Throwing the switch in bacterial chemotaxis. *Trends Microbiol* **7**: 16–22.
153. Willett JW, Herrou J, Briegel A, Rotskoff G, Crosson S (2015) Structural asymmetry in a conserved signaling system that regulates division, replication, and virulence of an intracellular pathogen. *Proc Natl Acad Sci* **201503118**.
154. Xu Q, Carlton D, Miller MD, Elsliger MA, Krishna SS, Abdubek P, Astakhova T, Burra P, Chiu HJ, Clayton T, et al. (2009) Crystal Structure of Histidine Phosphotransfer Protein ShpA, an Essential Regulator of Stalk Biogenesis in *Caulobacter crescentus*. *J Mol Biol* **390**: 686–698.
155. Marina A, Waldburger CD, Hendrickson WA (2005) Structure of the entire cytoplasmic portion of a sensor histidine-kinase protein. *EMBO J* **24**: 4247–4259.
156. Marina A, Mott C, Auyzenberg A, Hendrickson WA, Waldburger CD (2001) Structural and Mutational Analysis of the PhoQ Histidine Kinase Catalytic Domain: Insight into the Mechanism. *J Biol Chem* **276**: 41182–41190.
157. Tomomori C, Tanaka T, Dutta R, Park H, Saha SK, Zhu Y, Ishima R, Liu D, Tong KI, Kurokawa H, et al. (1999) Solution structure of the homodimeric core domain of *Escherichia coli* histidine kinase EnvZ. *Nat Struct Biol* **6**: 729–734.
158. Yamada S, Sugimoto H, Kobayashi M, Ohno A, Nakamura H, Shiro Y (2009) Structure of PAS-Linked Histidine Kinase and the Response Regulator Complex. *Structure* **17**: 1333–1344.
159. Ashenberg O, Keating AE, Laub MT (2013) Helix Bundle Loops Determine Whether Histidine Kinases Autophosphorylate in cis or in trans. *J Mol Biol* **425**: 1198–1209.
160. Podgornaia AI, Casino P, Marina A, Laub MT (2013) Structural Basis of a Rationally Rewired Protein-Protein Interface Critical to Bacterial Signaling. *Structure* **21**: 1636–1647.
161. Podgornaia AI, Laub MT (2013) Determinants of specificity in two-component signal transduction. *Curr Opin Microbiol* **16**: 156–162.
162. Salazar ME, Laub MT (2015) Temporal and evolutionary dynamics of two-component signaling pathways. *Curr Opin Microbiol* **24**: 7–14.
163. Rowland MA, Deeds EJ (2014) Correction for Rowland and Deeds., Crosstalk and the evolution of specificity in two-component signaling. *Proc Natl Acad Sci* **111**: 9325–9325.

164. Podgornaia AI, Laub MT (2015) Pervasive degeneracy and epistasis in a protein-protein interface. *Science* (80-) **347**: 673–677.
165. Casino P, Miguel-Romero L, Marina A (2014) Visualizing autophosphorylation in histidine kinases. *Nat Commun* **5**: 1–11.
166. Casino P, Rubio V, Marina A (2009) Structural Insight into Partner Specificity and Phosphoryl Transfer in Two-Component Signal Transduction. *Cell* **139**: 325–336.
167. Dutta R, Inouye M (1996) Reverse Phosphotransfer from OmpR to EnvZ in a Kinase / Phosphatase Mutant of EnvZ(EnvZN347D), a bifunctional signal Transducer of Escherichia coli. *J Biol Chem* **271**: 1424–1429.
168. Huynh TN, Noriega CE, Stewart V (2010) Conserved mechanism for sensor phosphatase control of two-component signaling revealed in the nitrate sensor NarX. *Proc Natl Acad Sci U S A* **107**: 21140–21145.
169. Yang Y, Inouye M (1993) Requirement of both kinase and phosphatase activities of an Escherichia coli receptor (Taz1) for ligand-dependent signal transduction. *J Mol Biol* **231(2)**: 335–342.
170. Chen YE, Tsokos CG, Biondi EG, Perchuk BS, Laub MT (2009) Dynamics of Two Phosphorelays Controlling Cell Cycle Progression in *Caulobacter crescentus*. *J Bacteriol* **191**: 7417–7429.
171. Qin L, Dutta R, Kurokawa H, Ikura M, Inouye M (2000) A monomeric histidine kinase derived from EnvZ, an Escherichia coli osmosensor. *Mol Microbiol* **36**: 24–32.
172. Willett JW, Kirby JR (2012) Genetic and biochemical dissection of a HisKA domain identifies residues required exclusively for kinase and phosphatase activities. *PLoS Genet* **8**: e1003084.
173. Khambaty FM, Ely B (1992) Molecular genetics of the flgI region and its role in flagellum biosynthesis in *Caulobacter crescentus*. *J Bacteriol* **174**: 4101–4109.
174. Wortinger M, Sackett MJ, Brun Y V (2000) CtrA mediates a DNA replication checkpoint that prevents cell division in *Caulobacter crescentus*. *EMBO J* **19**: 4503–4512.
175. Kirkpatrick CL, Viollier PH (2012) Decoding *Caulobacter* development. *FEMS Microbiol Rev* **36**: 193–205.
176. Umbarger MA, Toro E, Wright MA, Porreca GJ, Baù D, Hong S-H, Fero MJ, Zhu LJ, Marti-Renom MA, McAdams HH, et al. (2011) The

Three-Dimensional Architecture of a Bacterial Genome and Its Alteration by Genetic Perturbation. *Mol Cell* **44**: 252–264.

177. Le TBK, Imakaev M V, Mirny LA, Laub MT (2013) High-resolution mapping of the spatial organization of a bacterial chromosome. *Science* **342**: 731–734.
178. Quon KC, Yang B, Domian IJ, Shapiro L, Marczyński GT (1998) Negative control of bacterial DNA replication by a cell cycle regulatory protein that binds at the chromosome origin. *Proc Natl Acad Sci U S A* **95**: 120–125.
179. Siam R, Marczyński GT (2000) Cell cycle regulator phosphorylation stimulates two distinct modes of binding at a chromosome replication origin. *EMBO J* **19**: 1138–1147.
180. Laub MT, Chen SL, Shapiro L, McAdams HH (2002) Genes directly controlled by CtrA, a master regulator of the *Caulobacter* cell cycle. *Proc Natl Acad Sci U S A* **99**: 4632–4637.
181. Jacobs-Wagner C (2004) Regulatory proteins with a sense of direction: cell cycle signalling network in *Caulobacter*. *Mol Microbiol* **51**: 7–13.
182. Laub MT, McAdams HH, Feldblyum T, Fraser CM, Shapiro L (2000) Global analysis of the genetic network controlling a bacterial cell cycle. *Science* **290**: 2144–2148.
183. Ryan KR, Judd EM, Shapiro L (2002) The CtrA response regulator essential for *Caulobacter crescentus* cell-cycle progression requires a bipartite degradation signal for temporally controlled proteolysis. *J Mol Biol* **324**: 443–455.
184. Iniesta AA, Shapiro L (2008) A bacterial control circuit integrates polar localization and proteolysis of key regulatory proteins with a phospho-signaling cascade. *Proc Natl Acad Sci U S A* **105**: 16602–16607.
185. Grünenfelder B, Tawfilis S, Gehrig S, Østerås M, Eglin D, Jenal U (2004) Identification of the protease and the turnover signal responsible for cell cycle-dependent degradation of the *Caulobacter* FliF motor protein. *J Bacteriol* **186**: 4960–4971.
186. Biondi EG, Reisinger SJ, Skerker JM, Arif M, Perchuk BS, Ryan KR, Laub MT (2006) Regulation of the bacterial cell cycle by an integrated genetic circuit. *Nature* **444**: 899–904.
187. Jacobs C, Domian IJ, Maddock JR, Shapiro L (1999) Cell cycle-dependent polar localization of an essential bacterial histidine kinase that controls DNA replication and cell division. *Cell* **97**: 111–120.

188. Fioravanti A, Clantin B, Dewitte F, Lens Z, Verger A, Biondi EG, Villeret V (2012) Structural insights into ChpT, an essential dimeric histidine phosphotransferase regulating the cell cycle in *Caulobacter crescentus*. *Acta Crystallogr Sect F Struct Biol Cryst Commun* **68**: 1025–1029.
189. Iniesta AA, McGrath PT, Reisenauer A, McAdams HH, Shapiro L (2006) A phospho-signaling pathway controls the localization and activity of a protease complex critical for bacterial cell cycle progression. *Proc Natl Acad Sci U S A* **103**: 10935–10940.
190. Iniesta AA, Hillson NJ, Shapiro L (2010) Cell pole-specific activation of a critical bacterial cell cycle kinase. *Proc Natl Acad Sci U S A* **107**: 7012–7017.
191. Angelastro PS, Sliusarenko O, Jacobs-Wagner C (2010) Polar localization of the CckA histidine kinase and cell cycle periodicity of the essential master regulator CtrA in *Caulobacter crescentus*. *J Bacteriol* **192**: 539–552.
192. Chen YE, Tropini C, Jonas K, Tsokos CG, Huang KC, Laub MT (2011) Spatial gradient of protein phosphorylation underlies replicative asymmetry in a bacterium. *Proc Natl Acad Sci U S A* **108**: 1052–1057.
193. Tsokos CG, Perchuk BS, Laub MT (2011) Article A Dynamic Complex of Signaling Proteins Uses Polar Localization to Regulate Cell-Fate Asymmetry in *Caulobacter crescentus*. *Dev Cell* **20**: 329–341.
194. Childers WS, Xu Q, Mann TH, Mathews II, Blair JA, Deacon AM, Shapiro L (2014) Cell fate regulation governed by a repurposed bacterial histidine kinase. *PLoS Biol* **12**: 1–15.
195. Reisinger SJ, Huntwork S, Viollier PH, Ryan KR (2007) DivL performs critical cell cycle functions in *Caulobacter crescentus* independent of kinase activity. *J Bacteriol* **189**: 8308–8320.
196. Christen B, Abeliuk E, Collier JM, Kalogeraki VS, Passarelli B, Collier JA, Fero MJ, McAdams HH, Shapiro L (2014) The essential genome of a bacterium. *Mol Syst Biol* **7**: 528–528.
197. Subramanian K, Paul MR, Tyson JJ (2015) Dynamical Localization of DivL and PleC in the Asymmetric Division Cycle of *Caulobacter crescentus*: A Theoretical Investigation of Alternative Models. *PLoS Comput Biol* **11**: e1004348.
198. Sciochetti SA, Lane T, Ohta N, Newton A (2002) Protein Sequences and Cellular Factors Required for Polar Localization of a Histidine Kinase in *Caulobacter crescentus* Protein Sequences and Cellular Factors Required for Polar Localization of a Histidine Kinase in

Caulobacter crescentus. *J Bacteriol* **184**: 6037–6049.

199. Lam H, Matroule J, Jacobs-Wagner C, Haven N (2003) The Asymmetric Spatial Distribution of Bacterial Signal Transduction Proteins Coordinates Cell Cycle Events. *Cell* **5**: 149–159.
200. Paul R, Abel S, Wassmann P, Beck A, Heerklotz H, Jenal U (2007) Activation of the diguanylate cyclase PleD by phosphorylation-mediated dimerization. *J Biol Chem* **282**: 29170–29177.
201. Paul R, Weiser S, Amiot NC, Chan C, Schirmer T, Giese B, Jenal U (2004) Cell cycle-dependent dynamic localization of a bacterial response regulator with a novel di-guanylate cyclase output domain. *Genes Dev* **18**: 715–727.
202. Foreman R, Fiebig A, Crosson S (2012) The lovK-lovR two-component system is a regulator of the general stress pathway in *Caulobacter crescentus*. *J Bacteriol* **194**: 3038–3049.
203. Herrou J, Foreman R, Fiebig A, Crosson S (2010) A structural model of anti-anti-sigma inhibition by a two-component receiver domain: The PhyR stress response regulator mmi. *Mol Microbiol* **78**: 290–304.
204. Herrou J, Willett JW, Crosson J (2015) Structured and Dynamic Disordered Domains Regulate the Activity of a Multifunctional Anti-Factor. *MBio* **6**: 1–11.
205. Kaczmarczyk A, Hochstrasser R, Vorholt JA, Francez-Charlot A (2014) Complex two-component signaling regulates the general stress response in Alphaproteobacteria. *Proc Natl Acad Sci U S A* **111**: E5196–E5204.
206. Herrou J, Rotskoff G, Luo Y, Roux B, Crosson S (2012) Structural basis of a protein partner switch that regulates the general stress response of γ -proteobacteria. *Proc Natl Acad Sci* **109**: E1415–E1423.
207. Lourenço RF, Kohler C, Gomes SL (2011) A two-component system, an anti-sigma factor and two paralogous ECF sigma factors are involved in the control of general stress response in *Caulobacter crescentus*. *Mol Microbiol* **80**: 1598–1612.
208. Francez-Charlot A, Kaczmarczyk A, Fischer H-M, Vorholt J a (2015) The general stress response in Alphaproteobacteria. *Trends Microbiol* **23**: 1–8.
209. Kim HS, Caswell CC, Foreman R, Roop RM, Crosson S (2013) The *Brucella abortus* general stress response system regulates chronic mammalian infection and is controlled by phosphorylation and proteolysis. *J Biol Chem* **288**: 13906–13916.

210. Kaczmarczyk A, Hochstrasser R, Vorholt JA, Francez-Charlot A (2015) Two-Tiered Histidine Kinase Pathway Involved in Heat Shock and Salt Sensing in the General Stress Response of *Sphingomonas melonis* Fr1. *J Bacteriol* **197**: 1466–1477.
211. Purcell EB, Siegal-Gaskins D, Rawling DC, Fiebig A, Crosson S (2007) A photosensory two-component system regulates bacterial cell attachment. *Proc Natl Acad Sci* **104**: 18241–18246.
212. Alexandre MTA, Purcell EB, Van Grondelle R, Robert B, Kennis JTM, Crosson S (2010) Electronic and protein structural dynamics of a photosensory histidine kinase. *Biochemistry* **49**: 4752–4759.
213. Purcell EB, McDonald CA, Palfey BA, Crosson S (2008) An analysis of solution structure and signaling mechanism of LovK, a sensor histidine kinase integrating light and redox signals. *Biochemistry* **141**: 520–529.
214. Nunes-Alves C (2015) Bacterial physiology: Linking cell differentiation and growth. *Nat Rev Microbiol* **13**: 398–399.
215. VanHook AM (2015) Cyclin-like function of bacterial c-di-GMP. *Sci Signal* **8**: 195.
216. Malumbres M (2014) Cyclin-dependent kinases. *Genome Biol* **15**: 122.
217. Blanpain C, Simons BD (2013) Unravelling stem cell dynamics by lineage tracing. *Nat Rev Mol Cell Biol* **14**: 489–502.
218. Ishidate T, Elewa A, Kim S, Mello CC, Shirayama M (2014) Divide and differentiate: CDK/Cyclins and the art of development. *Cell Cycle* **13**: 1384–1391.
219. Morgan D (1997) Cyclin-dependent kinases : Engines , clocks , and microprocessors. *Annu Rev Cell Dev Biol* **13**: 261–291.
220. Paul R, Weiser S, Amiot NC, Chan C, Schirmer T, Giese B, Jenal U (2004) Cell cycle-dependent dynamic localization of a bacterial response regulator with a novel di-guanylate cyclase output domain. *Genes Dev* **18**: 715–727.
221. Biondi EG, Reisinger SJ, Skerker JM, Arif M, Perchuk BS, Ryan KR, Laub MT (2006) Regulation of the bacterial cell cycle by an integrated genetic circuit. *Nature* **444**: 899–904.
222. Kim J, Heindl JE, Fuqua C (2013) Coordination of division and development influences complex multicellular behavior in *Agrobacterium tumefaciens*. *PLoS One* **8**: 1–13.
223. Wheeler RT, Shapiro L (1999) Differential localization of two histidine

- kinases controlling bacterial cell differentiation. *Mol Cell* **4**: 683–694.
224. Choi YJ, Anders L (2014) Signaling through cyclin D-dependent kinases. *Oncogene* **33**: 1890–1903.
225. Hochegger H, Takeda S, Hunt T (2008) Cyclin-dependent kinases and cell-cycle transitions: does one fit all. *Nat Rev Mol Cell Biol* **9**: 910–916.
226. Robinett CC, Straight A, Li G, Willhelm C, Sudlow G, Murray A, Belmont AS (1996) In vivo localization of DNA sequences and visualization of large-scale chromatin organization using lac operator/repressor recognition. *J Cell Biol* **135**: 1685–1700.
227. Capra EJ, Perchuk BS, Lubin EA, Ashenberg O, Skerker JM, Laub MT (2010) Systematic dissection and trajectory-scanning mutagenesis of the molecular interface that ensures specificity of two-component signaling pathways. *PLoS Genet* **6**: 1–14.
228. Brillì M, Fondi M, Fani R, Mengoni A, Ferri L, Bazzicalupo M, Biondi EG (2010) The diversity and evolution of cell cycle regulation in alpha-proteobacteria: a comparative genomic analysis. *BMC Syst Biol* **4**: 52.
229. Arellano BH, Ortiz JD, Manzano J, Chen JC (2010) Identification of a dehydrogenase required for lactose metabolism in *caulobacter crescentus*. *Appl Environ Microbiol* **76**: 3004–3014.
230. Hung DY, Shapiro L (2002) A signal transduction protein cues proteolytic events critical to *Caulobacter* cell cycle progression. *Proc Natl Acad Sci U S A* **99**: 13160–13165.
231. Kjaergaard M, Poulsen FM (2011) Sequence correction of random coil chemical shifts: correlation between neighbor correction factors and changes in the Ramachandran distribution. *J Biomol NMR* **50**: 157–165.
232. Hildebrand A, Remmert M, Biegert A, Söding J (2009) Fast and accurate automatic structure prediction with HHpred. *Proteins Struct Funct Bioinforma* **77**: 128–132.
233. Šali A, Blundell TL (1993) Comparative Protein Modelling by Satisfaction of Spatial Restraints. *J Mol Biol* **234**: 779–815.
234. Viollier PH, Thanbichler M, McGrath PT, West L, Meewan M, McAdams HH, Shapiro L (2004) Rapid and sequential movement of individual chromosomal loci to specific subcellular locations during bacterial DNA replication. *Proc Natl Acad Sci U S A* **101**: 9257–9262.
235. Ely B (1991) Genetics of *Caulobacter crescentus*. *Methods Enzymol* **204**: 372–384.

236. Thanbichler M, Shapiro L, Iniesta AA (2007) A comprehensive set of plasmids for vanillate- and xylose-inducible gene expression in *Caulobacter crescentus*. *Nucleic Acids Res* **35**: 1–15.
237. Bernhardt TG, de Boer PAJ (2004) Screening for synthetic lethal mutants in *Escherichia coli* and identification of EnvC (YibP) as a periplasmic septal ring factor with murein hydrolase activity. *Mol Microbiol* **52**: 1255–1269.
238. Navarre WW, Zou SB, Roy H, Xie JL, Savchenko A, Singer A, Edvokimova E, Prost LR, Kumar R, Ibba M, et al. (2010) PoxA, yjeK, and elongation factor P coordinately modulate virulence and drug resistance in *Salmonella enterica*. *Mol Cell* **39**: 209–221.
239. Skerker JM, Prasol MS, Perchuk BS, Biondi EG, Laub MT (2005) Two-Component Signal Transduction Pathways Regulating Growth and Cell Cycle Progression in a Bacterium: A System-Level Analysis. *PLoS Biol* **3**: 1771–1788.
240. Christen M, Christen B, Allan MG, Folcher M, Jenö P, Grzesiek S, Jenal U (2007) DgrA is a member of a new family of cyclic diguanosine monophosphate receptors and controls flagellar motor function in *Caulobacter crescentus*. *Proc Natl Acad Sci U S A* **104**: 4112–4117.
241. Pervushin K, Riek R, Wider G, Wüthrich K (1997) Attenuated T2 relaxation by mutual cancellation of dipole-dipole coupling and chemical shift anisotropy indicates an avenue to NMR structures of very large biological macromolecules in solution. *Proc Natl Acad Sci U S A* **94**: 12366–12371.
242. Salzmann M, Pervushin K, Wider G, Senn H, Wüthrich K (1998) TROSY in triple-resonance experiments: new perspectives for sequential NMR assignment of large proteins. *Proc Natl Acad Sci U S A* **95**: 13585–13590.
243. Zuiderweg ER, Fesik SW (1989) Heteronuclear three-dimensional NMR spectroscopy of the inflammatory protein C5a. *Biochemistry* **6**: 2387–2391.
244. Quisel JD, Lin DC, Grossman AD (1999) Control of development by altered localization of a transcription factor in *B. subtilis*. *Mol Cell* **4**: 665–672.
245. Taylor JA, Ouimet M-C, Wargachuk R, Marczynski GT (2011) The *Caulobacter crescentus* chromosome replication origin evolved two classes of weak DnaA binding sites. *Mol Microbiol* **82**: 312–326.
246. Evinger M, Agabian N (1977) Envelope-associated nucleoid from

- Caulobacter crescentus stalked and swarmer cells. *J Bacteriol* **132**: 294–301.
247. Aldridge P, Jenal U (1999) Cell cycle-dependent degradation of a flagellar motor component requires a novel-type response regulator. *Mol Microbiol* **32**: 379–391.
248. Woodcock DM, Crowther PJ, Doherty J, Jefferson S, DeCruz E, Noyer-Weidner M, Smith SS, Michael MZ (1989) Quantitative evaluation of Escherichia coli host strains for tolerance to cytosine methylation in plasmid and phage recombinants. *Nucleic Acids Res* **17**: 3469–3478.
249. Simon R, Priefer U, Pühler A (1983) A Broad Host Range Mobilization System for In Vivo Genetic Engineering: Transposon Mutagenesis in Gram Negative Bacteria. *Bio/Technology* **1**: 784–791.
250. Vargas C, Tegos G, Vartholomatos G, Drainas C, Ventosa A, Nieto JJ (1999) Genetic organization of the mobilization region of the plasmid pHE1 from Halomonas elongata. *Syst Appl Microbiol* **22**: 520–529.
251. Bartels S, Lori M, Mbengue M, Verk M Van, Klauser D, Hander T, Böni R, Robatzek S, Boller T (2013) The family of peps and their precursors in arabidopsis: Differential expression and localization but similar induction of pattern-Triggered immune responses. *J Exp Bot* **64**: 5309–5321.
252. Roberts RC, Toochinda C, Avedissian M, Baldini RL, Gomes SL, Shapiro L (1996) Identification of a Caulobacter crescentus operon encoding hrcA, involved in negatively regulating heat-inducible transcription, and the chaperone gene grpE. *J Bacteriol* **178**: 1829–1841.
253. Casino P, Rubio V, Marina A (2010) The mechanism of signal transduction by two-component systems. *Curr Opin Struct Biol* **20**: 763–771.
254. Möglich A, Ayers RA, Moffat K (2009) Design and Signaling Mechanism of Light-Regulated Histidine Kinases. *J Mol Biol* **385**: 1433–1444.
255. Diensthuber RP, Bommer M, Gleichmann T, Mo A (2013) Article Full-Length Structure of a Sensor Histidine Kinase Pinpoints Coaxial Coiled Coils as Signal Transducers and Modulators. 1127–1136.
256. Bhate MP, Molnar KS, Goulian M, DeGrado WF (2015) Signal Transduction in Histidine Kinases: Insights from New Structures. *Structure*.
257. Batchelor E, Goulian M (2003) Robustness and the cycle of

- phosphorylation and dephosphorylation in a two-component regulatory system. *Proc Natl Acad Sci U S A* **100**: 691–696.
258. Hart Y, Alon U (2013) The Utility of Paradoxical Components in Biological Circuits. *Mol Cell* **49**: 213–221.
 259. Gao R, Stock AAM (2013) Probing kinase and phosphatase activities of two-component systems in vivo with concentration-dependent phosphorylation profiling. *Proc Natl Acad Sci U S A* **110**: 672–677.
 260. Mechaly AE, Sassoon N, Betton JM, Alzari PM (2014) Segmental Helical Motions and Dynamical Asymmetry Modulate Histidine Kinase Autophosphorylation. *PLoS Biol* **12**.
 261. Wang C, Sang J, Wang J, Su M, Downey JS, Wu Q, Wang S, Cai Y, Xu X, Wu J, et al. (2013) Mechanistic Insights Revealed by the Crystal Structure of a Histidine Kinase with Signal Transducer and Sensor Domains. *PLoS Biol* **11**.
 262. Chou S-H, Galperin MY (2015) Diversity of c-di-GMP-binding proteins and mechanisms. *J Bacteriol* JB.00333–15.
 263. Zhu Y, Qin L, Yoshida T, Inouye M (2000) Phosphatase activity of histidine kinase EnvZ without kinase catalytic domain. *Proc Natl Acad Sci U S A* **97**: 7808–7813.
 264. Sanowar S, Le Moual H (2005) Functional reconstitution of the Salmonella typhimurium PhoQ histidine kinase sensor in proteoliposomes. *Biochem J* **390**: 769–776.
 265. Yeo WS, Zwir I, Huang H V., Shin D, Kato A, Groisman EA (2012) Intrinsic Negative Feedback Governs Activation Surge in Two-Component Regulatory Systems. *Mol Cell* **45**: 409–421.
 266. Duerig A, Abel S, Folcher M, Nicollier M, Schwede T, Amiot N (2009) Second messenger-mediated spatiotemporal control of protein degradation regulates bacterial cell cycle progression. 93–104.
 267. Chakrabarti P, Pal D (2001) The interrelationships of side-chain and main-chain conformations in proteins. *Prog Biophys Mol Biol* **76**: 1–102.
 268. Straube R (2014) Reciprocal Regulation as a Source of Ultrasensitivity in Two-Component Systems with a Bifunctional Sensor Kinase. *PLoS Comput Biol* **10**.
 269. Leslie AGW, Powell HR (2007) *Processing diffraction data with MOSFLM*.
 270. Kabsch W (2010) Software XDS for image rotation, recognition and crystal symmetry assignment. *Acta Crystallogr, Sect D Biol Crystallogr* **66**:

125–132.

271. Potterton E, Briggs P, Turkenburg M, Dodson E (2003) A graphical user interface to the CCP4 program suite. *Acta Crystallogr - Sect D Biol Crystallogr* **59**: 1131–1137.
272. Emsley P, Lohkamp B, Scott WG, Cowtan K (2010) Features and development of Coot. *Acta Crystallogr Sect D Biol Crystallogr* **66**: 486–501.
273. Valdar WSJ (2002) Scoring residue conservation. *Proteins Struct Funct Genet* **48**: 227–241.
274. Hoops S, Gauges R, Lee C, Pahle J, Simus N, Singhal M, Xu L, Mendes P, Kummer U (2006) COPASI - A COmplex PATHway SIMulator. *Bioinformatics* **22**: 3067–3074.
275. Francez-Charlot A, Kaczmarczyk A, Fischer H-M, Vorholt JA (2015) The general stress response in Alphaproteobacteria. *Trends Microbiol* **23**: 1–8.
276. Galperin MY (2006) Structural classification of bacterial response regulators: Diversity of output domains and domain combinations. *J Bacteriol* **188**: 4169–4182.
277. Radhakrishnan SK, Thanbichler M, Viollier PH (2008) The dynamic interplay between a cell fate determinant and a lysozyme homolog drives the asymmetric division cycle of *Caulobacter crescentus*. *Genes Dev* **22**: 212–225.
278. Ryan KR, Huntwork S, Shapiro L (2004) Recruitment of a cytoplasmic response regulator to the cell pole is linked to its cell cycle-regulated proteolysis. *Proc Natl Acad Sci* **101**: 7415–7420.
279. Kern D, Volkman BF, Luginbühl P, Nohaile MJ, Kustu S, Wemmer DE (1999) Structure of a transiently phosphorylated switch in bacterial signal transduction. *Nature* **402**: 894–898.
280. Volkman BF, Lipson D, Wemmer DE, Kern D (2001) Two-state allosteric behavior in a single-domain signaling protein. *Science* **291**: 2429–2433.
281. Gao R, Mack TR, Stock AM (2007) Bacterial response regulators: versatile regulatory strategies from common domains. *Trends Biochem Sci* **32**: 225–234.
282. Tsokos CG, Laub MT (2012) Polarity and cell fate asymmetry in *Caulobacter crescentus*. *Curr Opin Microbiol* **15**: 744–750.
283. Jenal U, Malone J (2006) Mechanisms of Cyclic-di-GMP Signaling in

- Bacteria. *Annu Rev Genet* 385–407.
284. James P, Halladay J, Craig EA (1996) Genomic libraries and a host strain designed for highly efficient two-hybrid selection in yeast. *Genetics* **144**: 1425–1436.
 285. Alvarez-Martinez CE, Lourenço RF, Baldini RL, Laub MT, Gomes SL (2007) The ECF sigma factor sigma(T) is involved in osmotic and oxidative stress responses in *Caulobacter crescentus*. *Mol Microbiol* **66**: 1240–1255.
 286. Britos L, Abeliuk E, Taverner T, Lipton M, McAdams H, Shapiro L (2011) Regulatory response to carbon starvation in *Caulobacter crescentus*. *PLoS One* **6**: e18179.
 287. Sycz G, Carrica MC, Tseng T-S, Bogomolni RA, Briggs WR, Goldbaum FA, Paris G (2015) LOV Histidine Kinase Modulates the General Stress Response System and Affects the *virB* Operon Expression in *Brucella abortus*. *PLoS One* **10**: e0124058.
 288. Correa F, Ko WH, Ocasio V, Bogomolni RA, Gardner KH (2013) Blue light regulated two-component systems: Enzymatic and functional analyses of light-oxygen-voltage (LOV)-histidine kinases and downstream response regulators. *Biochemistry* **52**: 4656–4666.
 289. Karimova G, Pidoux J, Ullmann A, Ladant D (1998) A bacterial two-hybrid system based on a reconstituted signal transduction pathway. *Proc Natl Acad Sci U S A* **95**: 5752–5756.
 290. Tsai JW, Alley MRK (2000) Proteolysis of the McpA chemoreceptor does not require the *Caulobacter* major chemotaxis operon. *J Bacteriol* **182**: 504–507.
 291. Khan SR, Gaines J, Roop RM, Farrand SK (2008) Broad-Host-Range Expression Vectors with Tightly Regulated Promoters and Their Use To Examine the Influence of TraR and TraM Expression on Ti Plasmid Quorum Sensing. *Appl Environ Microbiol* **74**: 5053–5062.
 292. Gober JW, Shapiro L (1992) A developmentally regulated *Caulobacter* flagellar promoter is activated by 3' enhancer and IHF binding elements. *Mol Biol Cell* **3**: 913–926.
 293. Kovach ME, Elzer PH, Hill DS, Robertson GT, Farris MA, Roop RM, Peterson KM (1995) Four new derivatives of the broad-host-range cloning vector pBBR1MCS, carrying different antibiotic-resistance cassettes. *Gene* **166**: 175–176.
 294. Sambrook J, Fritsch EF, Maniatis T (1964) Molecular Cloning: a

Laboratory Manual. *Cold Spring Harb Lab.*

295. Fumeaux C, Radhakrishnan SK, Ardisson S, Théraulaz L, Frandi A, Martins D, Nesper J, Abel S, Jenal U, Viollier PH (2014) Cell cycle transition from S-phase to G1 in *Caulobacter* is mediated by ancestral virulence regulators. *Nat Commun* **5**:
296. Pini F, De Nisco NJ, Ferri L, Penterman J, Fioravanti A, Brillì M, Mengoni A, Bazzicalupo M, Viollier PH, Walker GC, et al. (2015) Cell Cycle Control by the Master Regulator CtrA in *Sinorhizobium meliloti*. *PLOS Genet* **11**: e1005232.

Curriculum vitae

Personal details:

Name: Christian Lori

Date of Birth: 6 July 1987

Address: Terrassenstrasse 2, 4144 Arlesheim

Hometown: Malans (GR)

Nationality: Swiss

Education:

2007-2010: B. Sc. in Molecular Biology, Biozentrum, University of Basel

2010-2012: M .Sc. in Microbiology, Group of Prof. Urs Jenal, Biozentrum, University of Basel. Topic: *C-di-GMP-mediated control of the Pga exopolysaccharide secretion machinery in Escherichia coli.*

2012-2016: PhD studies in Microbiology, Group of Prof. Urs Jenal, Biozentrum, University of Basel. Topic: *C-di-GMP acts as a cell cycle oscillator to drive chromosome replication.*

Published articles:

Steiner S, Lori C, Boehm A, Jenal U (2013) Allosteric activation of exopolysaccharide synthesis through cyclic di-GMP-stimulated protein-protein interaction. *EMBO J* **32**: 354–368.

Lori C, Ozaki S, Steiner S, Böhm R, Abel S, Dubey BN, Schirmer T, Hiller S, Jenal U (2015) Cyclic di-GMP acts as a cell cycle oscillator to drive chromosome replication. *Nature* **523**: 236–239.

